

**GENETICS OF GOLGI APPARATUS REGULATION  
IN MAMMALIAN CELLS**

**CHIA ZHI HUI JOANNE**

*(B. Sc. (Hons), NUS)*

**A THESIS SUBMITTED FOR THE DEGREE OF  
DOCTOR OF PHILOSOPHY  
DEPARTMENT OF BIOCHEMISTRY  
NATIONAL UNIVERSITY OF SINGAPORE**

**2013**

## **DECLARATION**

I hereby declare that this thesis is my original work and it has been written by me in its entirety. I have duly acknowledged all the sources of information which have been used in the thesis.

This thesis has also not been submitted for any degree in any university previously.

---

Chia Zhi Hui Joanne

29<sup>th</sup> November 2013

## **Acknowledgements**

I would like to extend my heartfelt gratitude to my supervisor Dr Frederic Bard for his mentorship, encouragement, guidance, and advice over the years. I will also like to thank Professor Pernille Rørth, Associate Professor Tang Bor Luen, Dr Song Zhi Wei for their advice and critical feedback during the thesis advisory committee meeting.

Special thanks to all the wonderful co-workers from FB laboratory, especially Dr. Germaine Goh, Dr. Samuel Wang, Dr. Alexandre Chaumet, Dr. Wong Hui Hui, Dr. Violette Lee, Dr. David Gill, Dr. Pankaj Kumar, Dr. Ahn Tuan Ngyuen, Jasmine Tham and Sze Hwee for their help, advice, friendship and encouragement.

I would also like to thank IMCB (A\*STAR) for awarding me the research scholarship under the Scientific Staff Development Scheme.

This work would not have been possible without the unfailing support of my family – my parents, grandmother and siblings Jason and Jiahui.

## TABLE OF CONTENTS

SUMMARY .....	vii
LIST OF TABLES .....	ix
LIST OF FIGURES .....	x
LIST OF ABBREVIATIONS.....	xv
PUBLICATIONS.....	xix
CHAPTER ONE: LITERATURE REVIEW OF GOLGI ORGANIZATION AND GLYCOSYLATION.....	1
1.1 OVERVIEW OF THE SECRETORY APPARATUS .....	2
1.2 THE GOLGI APPARATUS: STRUCTURE .....	5
1.2.1 Cisternal organization of the Golgi .....	5
1.2.2 Cisternal stacking of the Golgi .....	6
1.2.3 Golgi ribbon formation.....	11
1.3 GLYCOSYLATION FUNCTION OF THE GOLGI.....	25
1.3.1 Glycan diversity in mammals .....	26
1.3.2 Biological roles of glycans .....	29
1.3.3 The glycosylation machinery in the cell.....	32
1.3.4 Glycosylation reactions in the Golgi .....	37
1.3.5 Regulation of mammalian glycosylation.....	49
1.4 OBJECTIVES .....	55
CHAPTER TWO: MATERIALS AND METHODS .....	58
2.1 MATERIALS .....	59
2.1.1 General reagents and chemicals .....	59
2.1.2 Enzymes.....	60
2.1.3 Antibodies.....	60
2.1.4 siRNAs .....	61
2.1.5 Drugs and recombinant proteins.....	61
2.1.6 Lectins .....	62
2.2 CELLS AND VIRUSES .....	62
2.2.1 Cell culture .....	62
2.2.2 Producing lentivirus in HEK293T cells.....	63

2.2.3	Generating stable cell lines using lentiviral transfection.....	64
2.3	MOLECULAR CLONING.....	64
2.3.1	Preparation of competent cells.....	64
2.3.2	Polymerase chain reaction.....	65
2.3.3	DNA agarose gel electrophoresis.....	66
2.3.4	Gel purification.....	66
2.3.5	Plasmids and plasmid constructions.....	66
2.3.6	Plasmid purification.....	69
2.3.7	DNA sequencing.....	69
2.4	SIRNA SCREENING.....	70
2.4.1	siRNA plate preparation and transfection.....	70
2.4.2	Immunofluorescence staining.....	71
2.4.3	Automated image acquisition and processing.....	71
2.4.4	Selection of primary and validated hits.....	71
2.4.5	Bioinformatics analysis.....	72
2.4.6	Lectin secondary screen.....	72
2.4.7	Secondary Met-Luc secretion screen.....	75
2.4.8	VSVG secretion assay.....	76
2.5	HIGH RESOLUTION FLUORESCENCE MICROSCOPY.....	76
2.6	PROTEIN EXPRESSIONS AND ANALYSIS.....	77
2.6.1	Transient expression of plasmid DNA in mammalian cells.....	77
2.6.2	Western blot analysis.....	77
2.6.3	ER-trapped GalNAc-T activity reporter assay.....	78
2.7	GROWTH FACTOR AND DRUG TREATMENTS.....	79
2.8	SCRATCH WOUND ASSAY.....	80
2.9	HUMAN FROZEN TISSUE ARRAY ANALYSIS.....	80
2.9.1	Tissue array staining.....	80
2.9.2	Tissue array imaging and quantification.....	81
CHAPTER THREE: RNAI SCREENING REVEALS A LARGE SIGNALING NETWORK CONTROLLING THE GOLGI APPARATUS IN HUMAN CELLS.....		82

3.1 INTRODUCTION.....	83
3.2 RESULTS: RNAi screening reveals molecular regulators of Golgi organization and functions. ....	86
3.2.1 Identification of screening conditions .....	86
3.2.2 A pilot siRNA screen on membrane trafficking regulators revealed three main Golgi morphologies. ....	88
3.2.3 Golgi phenotypes can be automatically classified using nine phenotypic features.....	92
3.2.4 159 signaling genes regulate Golgi organisation.....	96
3.2.5 Golgi phenotypes from the signaling screen were diverse. ....	98
3.2.6 A large signaling network regulates Golgi apparatus organisation. ....	103
3.2.7 Specific sub-networks further reveal Golgi regulatory mechanisms..	107
3.2.8 Growth factors and cell surface receptors signal to the Golgi apparatus .....	118
3.2.9 110 Golgi organisation regulators also affect general secretion.....	120
3.2.10 146 Golgi organisation regulators also affect glycan biosynthesis ..	125
3.2.11 A complex interaction between signaling genes and the regulation of glycosylation.....	131
3.4 DISCUSSION .....	153
CHAPTER FOUR: ERK8 IS A NEGATIVE REGULATOR OF O-GALNAC GLYCOSYLATION AND CELL MIGRATION .....	159
4.1 INTRODUCTION.....	160
4.2 RESULTS: RNAi screening identifies ERK8 as a negative regulator of O-GalNAc glycosylation and cell migration. ....	163
4.2.1 RNAi screening identifies 12 signaling genes negatively regulating Tn levels.....	163
4.2.2 Negative regulators of Tn expression are not required for O-glycan extension.....	170
4.2.3 Tn levels depend on GalNAc-Ts subcellular localization. ....	171
4.2.4 Bioinformatics analyses reveal a putative complex network of Tn regulators acting at the Golgi apparatus. ....	175
4.2.5 ERK8 kinase activity is required for O-glycosylation regulation. ....	177
4.2.6 ERK8 inhibitor induces a rapid and reversible increase in Tn levels.	178

4.2.7 O-glycosylation is initiated in the ER and several proteins are hyper glycosylated when ERK8 is inhibited. ....	181
4.2.8 ERK8 localizes at the Golgi and is displaced upon growth factor stimulation. ....	183
4.2.8 ERK8 regulates COPI-dependent GalNAc-Ts traffic. ....	187
4.2.9 ER relocation of GalNAc-Ts in ERK8 depletion is dependent on tyrosine phosphorylation of Golgi proteins. ....	191
4.2.10 ERK8 regulates cell migratory ability through control of O-glycosylation. ....	194
4.2.11 ERK8 expression is frequently downregulated in breast and lung carcinoma. ....	197
4.3 DISCUSSION .....	204
CHAPTER FIVE: CONCLUSIONS AND FUTURE DIRECTIONS .....	212
5.1 RNAI SCREENING REVEALS A LARGE SIGNALING NETWORK CONTROLLING THE GOLGI APPARATUS IN HUMAN CELLS .....	213
5.1.1 Main conclusions .....	213
5.1.2 Future directions: towards better Golgi morphological classification	213
5.2 ERK8 IS A NEGATIVE REGULATOR OF O-GALNAC GLYCOSYLATION AND CELL MIGRATION.....	216
5.2.1 Main conclusions .....	216
5.2.2 Future directions: more in-depth studies of the regulatory mechanisms of GalNAc-T localisation .....	217
5.3 THE GOLGI: A HIGHLY REGULATED SORTING AND PROCESSING MACHINE .....	219
5.4 FINAL REMARKS.....	229
BIBLIOGRAPHY .....	231

## SUMMARY

The mammalian Golgi apparatus plays many important physiological functions, including protein glycosylation. Glycosylation involves the addition of glycans, or complex polymers of sugar and is one of the most abundant post-translational modification of proteins. Glycans can have a profound effect on protein structure and functions, hence regulating numerous biological processes. While it is known that glycan expression is variable with different physiological and pathological conditions, their regulatory mechanisms remain poorly understood. Most glycans are synthesized by a series of sequential biosynthetic reactions in the Golgi where they diversify and become complex structures. Thus, they intimately depend on the intricate and compartmentalized organization of the Golgi. However, the regulation of Golgi organization is not completely known and how it affects glycosylation remain poorly understood.

In this dissertation, I studied the mechanisms that control Golgi organization and its glycosylation function. To investigate organizational regulation, I have developed a quantitative morphological assay using three different Golgi compartment markers and quantitative image analysis, and performed a kinome- and phosphatome-wide RNAi screen in HeLa cells to identify molecular regulators. Depletion of 159 signaling genes, nearly 20% of genes assayed, induced strong and varied perturbations in Golgi morphology. Using bioinformatics data, a large regulatory network could be constructed. Specific sub-networks involving phosphoinositides regulation, acto-myosin dynamics and MAPK signaling provided further insights to Golgi regulatory mechanisms. Several cell surface receptors and their corresponding growth factor treatment strongly affected Golgi organization, indicating direct impact of extracellular signals on Golgi physiology. Secondary screens with different lectins revealed that most of these gene depletions also affected glycan biosynthesis, suggesting that signaling cascades can control glycosylation through Golgi organizational remodeling. Collectively, these results provide a genetic overview of the signaling



pathways that control the organization and functions of Golgi apparatus in human cells.

In the subsequent part of the thesis, I focused on the regulation of O-GalNAc glycosylation initiation. Our previous report demonstrated that the process can be induced in the ER through the relocalisation of GalNAc glycosyltransferases (GalNAc-Ts) from the Golgi and drives upregulated expression of the Tn antigen, prevalent tumor-associated glycan. The process markedly stimulates cell migration and was found to be constitutively activated in various carcinomas. To examine the regulatory mechanisms of Tn expression in cancer, I have identified 12 negative regulators through an RNAi screen on signaling genes. All 12 proteins were found to regulate Tn expression by controlling GalNAc-T subcellular localisation. Atypical MAPK ERK8 appeared as a potent regulator whose inhibition rapidly induced ER O-glycosylation initiation. ERK8 is partially localized at the Golgi where its high basal kinase activity constitutively inhibits COPI-dependent retrograde traffic of GalNAc-Ts. This, in turn, inhibits cell motility. In human breast and lung carcinomas, ERK8 expression is frequently downregulated while O-glycosylation initiation is hyperactivated. Thus, ERK8 appears as a constitutive brake on GalNAc-T relocation and loss of its expression could drive cancer aggressivity through increased cell motility. (475 words)

## LIST OF TABLES

- Table 1.1:** Consensus motifs and enzymes responsible for various glycosylation reactions occurring in vertebrates
- Table 2.1:** List of general reagents and chemicals
- Table 2.2:** List of primary and secondary antibodies
- Table 2.3:** List of drugs and recombinant proteins
- Table 2.4:** List of primers for polymerase chain reactions
- Table 2.5:** List of primers used for mutagenesis
- Table 2.6:** List of drug and concentrations used
- Table 3.1:** List of drug and gene siRNA treatments (Reference morphological phenotypes) for training the SVM
- Table 3.2.** List of 181 primary hits of Golgi morphology screen

## LIST OF FIGURES

- Figure 1-1:** Schematic of the organization of the secretory apparatus and intracellular transport pathways
- Figure 1-2:** A model for the formation of Golgi stack
- Figure 1-3:** Model of Golgi ribbon assembly
- Figure 1-4:** The Golgi ribbon is required for cell polarization and directed secretion in a migrating cell
- Figure 1-5:** The representative symbols of the ten monosaccharides used in mammals
- Figure 1-6:** Structure of a typical Golgi glycosyltransferase
- Figure 1-7:** Schematic of the N-glycosylation pathway
- Figure 1-8:** Schematic of the O-glycosylation pathway
- Figure 3-1:** An imaging-based screen to identify Golgi organisation phenotypes
- Figure 3-2:** A pilot screen of membrane trafficking regulators revealed three Golgi phenotypes
- Figure 3-3:** An automated image analysis method for Golgi phenotypic classification
- Figure 3-4:** A large proportion of signaling genes regulate Golgi structure.

- Figure 3-5:** A diversity of Golgi phenotypes could be observed from signaling gene depletions
- Figure 3-6:** Diffuse Golgi morphology is likely due to relocation of marker to the ER
- Figure 3-7:** A map of 111 hit kinases on the phylogenetic tree of kinases reveals Golgi regulation by all kinase families
- Figure 3-8:** Protein network analysis of hits reveals multiple connections between signaling molecules and Golgi proteins
- Figure 3-9:** Phosphatidylinositol (PI) network regulators identified in the screen
- Figure 3-10:** Regulators of the actomyosin machinery control Golgi organization
- Figure 3-11:** A possible link between cell-cycle kinases and trans Golgi-plasma membrane trafficking
- Figure 3-12:** MAPKs from all four signaling cascades regulate Golgi organization
- Figure 3-13:** Golgi fragmentation by depletion of DUSPs requires ERK1/2 activation
- Figure 3-14:** Condensed Golgi from MECOM depletion is likely due to JNK activation
- Figure 3-15:** Cell surface receptors control Golgi organization
- Figure 3-16:** 110 Golgi organisation regulators also regulate constitutive secretion

- Figure 3-17:** Most Met-Luc secretion hits also affect ER to Golgi trafficking of VSVG-tsO45G protein
- Figure 3-18:** Eight fluorescent lectins that display different glycan specificities were chosen probe N- and O-glycan expression patterns
- Figure 3-19:** Most signaling proteins regulate Golgi morphology and glycans expression
- Figure 3-20:** A high diversity of glycophenotypes could be observed in signaling gene depletions
- Figure 3-21:** The variety of glycophenotypes of the Golgi hits is illustrated by glycan profiles
- Figure 3-22:** A model of Golgi organisation and glycosylation regulation
- Figure 4-1:** RNAi screening revealed 12 negative regulators of Tn expression
- Figure 4-2:** Depletion of ERK8 results in dramatic increase in Tn levels
- Figure 4-3:** Upregulation of Tn in ERK8 depletion and most hits is conserved across cell lines
- Figure 4-4:** Tn increases are predominantly due to GalNAc-T1 and -T2 activity
- Figure 4-5:** The identified Tn regulators do not control O-glycan extension
- Figure 4-6:** Tn regulators control Tn expression through GalNAc-T subcellular localisation

- Figure 4-7:** A potential regulatory network of signaling proteins regulating GalNAc-T localisation at the Golgi apparatus
- Figure 4-8:** Kinase activity of ERK8 is required to block Tn expression
- Figure 4-9:** ERK8 inhibition led to rapid and reversible changes in Tn expression
- Figure 4-10:** Tn increase in ERK8 inhibition was not due to expression changes in the O-glycoproteins and O-glycosylation machinery
- Figure 4-11:** ERK8 inhibited cells displayed increased ER- localized O-glycosylation
- Figure 4-12:** Endogenous ERK8 is enriched at the Golgi
- Figure 4-13:** ERK8 is dynamically localized at the Golgi
- Figure 4-14:** COPI machinery is required for GalNAc-T relocation in ERK8 depleted cells
- Figure 4-15:** ERK8 regulates the formation of COPI transport carriers
- Figure 4-16:** ERK8 regulates Golgi-localized phosphotyrosine levels
- Figure 4-17:** Loss of ERK8 result in spindle-shaped cells
- Figure 4-18:** ERK8 regulates cell migration through ER O-glycosylation
- Figure 4-19:** Quantification of ERK8 and Tn expression levels in human breast carcinomas

- Figure 4-20:** ERK8 is downregulated in human breast carcinomas
- Figure 4-21:** ERK8 is downregulated in human lung carcinomas
- Figure 4-22:** A model illustrating signaling regulation of O-glycosylation initiation at the Golgi that influences cellular motility and cancer invasiveness
- Figure 5-1:** Schematic of the involvement of the Golgi apparatus in mitosis
- Figure 5-2:** Schematic of the involvement of the Golgi apparatus in cell migration
- Figure 5-3:** Schematic of the regulatory mechanisms of secretion at the Golgi
- Figure 5-4:** Schematics of Golgi organization and glycosylation regulation
- Figure 5-5:** Schematic of the regulation of O-glycosylation initiation

## LIST OF ABBREVIATIONS

ARF	ADP-ribosylation factor
$\beta$ 4GalT	$\beta$ 1-4galactosyltransferase
BFA	Brefeldin A
BSA	Bovine serum albumin
C1GalT1	$\beta$ 1-3 galactosyltransferase
C2GnT	Core 2 $\beta$ 1-6 N-acetylglucosaminyltransferase
C3GnT	Core 3 $\beta$ 1-3 N-acetylglucosaminyltransferase
CDG	Congenital disorders of glycosylation
CMP	Cytidine-5'-monophosphate
COP	Coat protein complex
DMEM	Dulbecco's Modified Eagle medium
DMSO	Dimethyl sulfoxide
DNA	Deoxyribonucleic acid
dNTP	Deoxynucleotide triphosphate
DTT	1,4-dithiothreitol
EDTA	Ethylenediaminetetraacetic acid



eGFP	Enhanced GFP
EndoH	Endoglycosidase H
ER	Endoplasmic reticulum
ERGIC	ER-Golgi intermediate compartment
FBS	Fetal bovine serum
FITC	Fluorescein isothiocyanate
FucT	Fucosyltransferase
GalNAc-T	Polypeptide N-acetylgalactosaminyltransferase
GDP	Guanosine diphosphate
GFP	Green fluorescent protein
GlcNAc-T	N-acetylglucosamine transferase
GM130	Golgi matrix protein of 130 kDa
GRASPs	Golgi reassembly stacking proteins
GTP	Guanosine-5'-triphosphate
GTPase	Guanosine triphosphatase
IF	Immunofluorescence
IGF-1	Insulin-like Growth Factor 1
IgG	Immunoglobulin G

IP	Immunoprecipitation
kDa	kiloDalton
LPAT	Lysophospholipid acyltransferase
LPL	Lysophospholipid
MPCC	Mean Pearson's correlation coefficient
PBS	Phosphate buffered saline
PCR	Polymerase chain reaction
PI4P	Phosphatidylinositol-4- phosphate
PI4,5P2	Phosphatidylinositol 4,5-bisphosphate
PI3,4,5P3	Phosphatidylinositol 3,4,5-triphosphate
PLA	Phospholipase A
TGF-B1	Transforming Growth Factor B1
RNAi	RNA interference
SDS	Sodium dodecyl sulfate
SDS-PAGE	Sodium dodecyl sulfate-polyacrylamide gel electrophoresis
shRNA	Short hairpin RNA
SiaT	Sialyltransferase
siRNA	small interfering RNA

VSVG Vesicular stomatitis virus (VSV) glycoprotein G

UDP Uridine diphosphate

## PUBLICATIONS

1. **Chia J.**, Tham K.M., Gill D.J., Bard-Chapeau E., Bard F. (2014) ERK8 is a negative regulator of O-GalNAc glycosylation and cell migration. (Manuscript in preparation)
2. Gill D.J., Tham K.M., **Chia J.**, Wang SC, Steentoft C, Clausen H, Bard-Chapeau EA, Bard F. (2013) Initiation of GalNAc-type O-glycosylation in the endoplasmic reticulum promotes cancer cell invasiveness. *Proc Natl Acad Sci U S A.* 110(34):E3152-61.
3. **Chia J.**, Goh G., Racine V., Ng S., Kumar P., Bard F. (2012) RNAi screening reveals a large signaling network controlling the Golgi apparatus in human cells. *Mol Syst Biol.* 2012; 8:629
4. Gill D.J., **Chia J.**, Senewiratne J., Bard F. (2010). Regulation of O-glycosylation through Golgi-to-ER relocation of initiation enzymes. *J Cell Biol.*;189(5):843-58.

**CHAPTER ONE: LITERATURE REVIEW OF GOLGI ORGANIZATION  
AND GLYCOSYLATION**

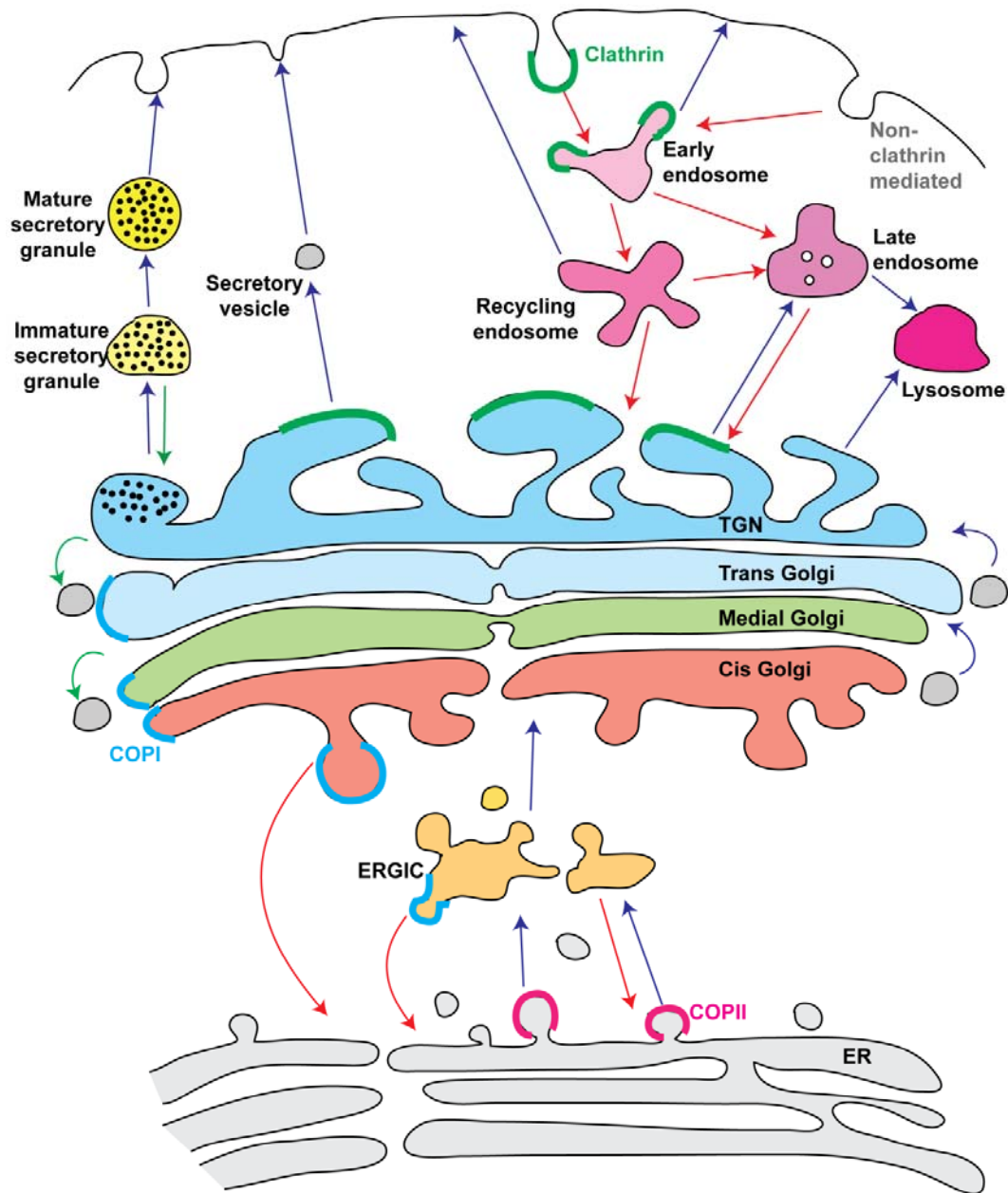
## 1.1 OVERVIEW OF THE SECRETORY APPARATUS

The cellular evolution of prokaryotes to eukaryotes is undoubtedly one of the transcendent transitions in life. This step took four times longer than the transition from insentient matter to life as highlighted by fossil records [1]. Unlike prokaryotic cells that only has a plasma membrane barrier to separate the cell from the environment, the cytoplasm of eukaryotic cells is further compartmentalized into discrete membrane-bound structures known as organelles. Compartmentalization results in membrane expansion that enabled the development of larger cells (1000-10,000 fold increase in volume) and allowed more efficient division of cellular functions. Separation into discrete organelles creates microenvironments for specific sets of concentrated and essential biochemical reactions, hence, enabling specialization and conferring evolvability to the system [2].

Although performing different functions, there's a need for communication between different organelles, as well as with the environment, so as to regulate organellar microenvironment and maintain cellular homeostasis. A major process of communication between the compartments that link the cell with the environment is mediated by the intracellular vesicular transport pathways. The process involves membrane-bound transport intermediates including small vesicles or larger carriers and tubules [3, 4] which enable macromolecules such as proteins to be ferried between organelles and to the cell surface.

The intracellular transport system is an extensive and complicated network. In general, the system is divided into two major pathways: the endocytic and exocytic/ secretory pathways. In the exocytic/ secretory pathway, newly synthesized proteins and lipids from the endoplasmic reticulum (ER) are shuttled to the Golgi apparatus which eventually sorts them to various destinations either within the cell or secreted to the exterior. Reverse to this, in the endocytic pathway, extracellular materials are internalized from the environment into cells

via endocytosis which is mediated by a set of endosomes, early and late, to the lysosomes or the Golgi. In addition, retrieval processes are also essential to regulate the trafficking along both pathways. A schematic of the intracellular vesicular transport pathways is illustrated in Figure 1-1. At the crossroads of all these complex membrane trafficking events is the Golgi apparatus which is the focus of the subsequent sections of this chapter.



**Figure 1-1: Schematic of the organization of the secretory apparatus and intracellular transport pathways.** The scheme demonstrates the extensive and complicated network of the endocytic and exocytic/ secretory pathways. Retrograde transport steps are indicated by red arrows and anterograde transport steps are indicated by blue arrows. Clathrin coats are in green, COPI in blue and COPII in pink. The major organelles of the secretory apparatus consists of the endoplasmic reticulum (ER), ER-Golgi intermediate compartment (ERGIC), Golgi apparatus, early endosome, the late endosome, body, recycling endosome, lysosome and the plasma membrane. Situated central to this busy traffic of intracellular transport pathway is the Golgi apparatus.



## 1.2 THE GOLGI APPARATUS: STRUCTURE

Situated at the heart of the secretory pathway, the Golgi apparatus is perhaps the most suitable model to illustrate intracellular compartmentalization. First visualized and described in 1898 as an intracellular reticular apparatus by Camillo Golgi [5], the Golgi has since been studied intensely on its morphology. No other cell compartment or organelle has been so thoroughly investigated in morphology as the Golgi. Efforts to define the Golgi biochemically have been hampered by the fact that the organelle is highly integrated within the cellular endomembrane system, thus sharing similar biochemical characteristics with the ER and plasma membrane. Hence, it remains till today that morphology is the main criterion by which the Golgi apparatus is defined. The intriguingly complex structure of the Golgi has spurred the use of various techniques in ultrastructural research, ranging from standard electron microscopy to the recent correlative light and electron microscopy (CLEM), to visualize and understand the mechanisms behind its architecture [6]. Indeed, it is one of the most photographed organelles in the cell.

### 1.2.1 Cisternal organization of the Golgi

Based on these numerous studies, the consensus view of the Golgi is the composition of a series of flattened, disk-shaped membrane bound compartments known as cisternae, which form the basic structural unit of the Golgi. This unique cisternal architecture is conserved throughout eukaryotic evolution as it was apparent even in one of the earliest branching extant eukaryotes, the diplomonad *Giardia lamblia* [7]. In most organisms, apart from the budding yeast *Saccharomyces cerevisiae* [8, 9] and some protists, the cisternae are piled up to form a stacked structure. Cisternae membranes are smooth due to the lack of ribosomes and they are usually curved. Depending on the cell type and position in the stack, different cisternae differ in their architectural detail. For instance, the diameter of the cisternae between distinct organisms can range from 0.7 to 1.1  $\mu\text{m}$  [10, 11]. The central part of a cisterna is usually quite narrow with a width of 10

to 20nm while the edges or rims are more dilated. These rims are perforated with gaps or fenestrae of up to 100nm in diameter. Increased number and size of fenestrae were found at the exterior cisternae of the Golgi stacks [12]. The presence of fenestrates is thought to add surface area to cisternae and introduces more curvature to the membranes. This might be essential to the vesicle formation and segregation of proteins and lipids [13]. Continuous with the fenestrae is a complex system of tubules and coated vesicles for inter-stack connections and intracellular transport.

### **1.2.2 Cisternal stacking of the Golgi**

Perhaps the most striking structural feature of the Golgi is cisternal stacking. With the exception of the budding yeast and a few protists, in which the Golgi consists of several scattered cisternae, Golgi stacks are conserved throughout eukaryotic evolution. The number of cisternae in a stack depends on cell type, ranging from four to eleven in a typical mammalian Golgi [14] and more than twenty in scale-secreting algae [15]. Plants and animal cells can have 500 or more stacks and can reach over 25,000 stacks in algal rhizoids.

#### *The polarized Golgi stack*

Golgi stacks are polarized structures and are generally divided into three main compartments: cis, medial and trans Golgi. Both cis and trans Golgi are largely fenestrated tubular-reticular networks (also known as cis Golgi and trans Golgi networks) that form the two external faces of the Golgi and flank the medial-Golgi. Proximal to the ER is the cis-Golgi which receives and exchanges proteins and lipids from the ER whereas the cargo exits and gets sorted from the trans-Golgi network to different cellular destinations [16]. The cargo traverses through the Golgi stack in a cis-to-trans fashion where it gets increasingly post-translationally modified, although the mechanism of how it is transported is still disputed [17].

Although morphologically indistinguishable, these different compartments differ biochemically and functionally. The distinct polarity of the compartments was already apparent from early electron microscopy studies. Cisternae from the cis-Golgi preferentially reduced osmium and appeared blacken while the trans cisternae is stained preferentially for acid phosphatase and thiamine pyrophosphatase [18, 19], demonstrating distinct compositions. Interestingly, several gradients can be found in a Golgi stack: in cisterna fenestration and thickness, membrane thickness, pH, resident protein and lipid compositions.

The sizes of fenestraes appear to decrease from the cis to medial cisternae and increase again at the trans while the cisterna thickness decreases from cis to trans Golgi [12]. This is correlated with the amount of transport events taking place. Conversely, membrane thickness was found to increase from the cis to trans face [20, 21]. For instance, in the rat liver, trans cisterna membrane is 8nm thick compared to the cis cisterna at 6.5nm. This is comparable to the thickness of both plasma membrane and ER respectively. This difference in thickness is thought to be due to the difference in lipid composition as the concentration of cholesterol is higher at the trans-side of the stack and particularly high in the endosomes [22-24]. The presence of cholesterol fills the space between the two leaflets of the lipid bilayer, hence expanding the membrane width. Given that the plasma membrane is highly enriched in cholesterol, it can be inferred that the cis-Golgi membranes resemble the ER while the trans' are similar to that of the plasma membrane. Differential membrane thickness is thought to be the mechanism for the retention of Golgi resident proteins as Golgi proteins have shorter transmembrane segments (~15 amino acids) compared to plasma membrane proteins (20-25 amino acids) [25]. The luminal pH levels decreases across the progression of the secretory pathway by two units, from neutral pH at the ER (7.2) to acidic levels at the trans Golgi (6.0) and secretory granules (5.2). Across the Golgi stacks, the pH drops by 0.7 units [26]. pH changes are fundamental for correct processing and sorting of secreted cargo [27, 28] as well as the correct

targeting of resident Golgi proteins such as TGN46 and furin [29]. Finally, each Golgi cisternae is studded with distinct sets of resident Golgi proteins. This includes the glycosidases, nucleotides sugar transporters, and at least 250 different glycosyltransferases, which are arrayed in the order which they function. Enzymes involved in the early and late stages of glycosylation are predominantly localized at the cis and trans sides respectively [30]. For instance, polypeptide N-acetylgalactosaminyltransferase (ppGalNAc-T) and GlcNAc-phosphotransferase are associated with the cis Golgi, while GlcNAc transferase I, mannosidase I and II and phosphodiesterase are localized at the medial Golgi, and  $\beta$ -1,4-galactosyltransferase and  $\alpha$ -2,6-sialyltransferase at the trans side [31]. This allows sequential action on the modified glycoprotein as it traverses across the compartments. Further elaborations of the glycosylation process will be made in the subsequent sections. In addition, proteins that are associated with Golgi function, including the matrix proteins, Rabs, SNARE, also exhibit polarized distribution. It should be noted that the polarity across the stack is not strict and occurs as a gradient-like distribution because the Golgi is in dynamic equilibrium with the rest of the secretory apparatus.

#### *Functions of cisternal stacking*

The assembly of cisternae into stacks is thought to promote fidelity and efficiencies of these biosynthetic processes by spatially separating the enzymatic reactions. By concentrating and localizing the enzymes to specific cisternae also increases the enzyme-to-substrate ratio. Furthermore, the duration of cargo presentation to the enzymes is lengthened with stacking transport vesicle budding is confined at the cisternal rims. It was observed that once the cisternae unstack, the rate of vesicle budding and transport through the Golgi increases due to more accessible membrane areas [32]. Overall, this improves the yield and accuracy of the processes. In line with this, some species without Golgi stacks have been reported to have fewer glycosylases which suggests that stacking is required for cells with more extensive glycosylation processes [33]. Conversely, the rate of

cargo trafficking is improved with Golgi stacking. As the stacked cisternae are in close proximity, it minimizes the distance travelled by transport vesicles, ensuring their efficient movement between cisternae. The efficiency is further promoted with tethering complexes, such as the COG complex for intra- Golgi trafficking [34], that directly connect the budding vesicles to the target compartment. In addition, tubular connections between the proximal heterologous cisternae within the stack can be formed at times of increased cargo load, allowing the rapid transfer of cargo. This has been observed in spermatids and Sertoli cells [14] and more recently, other cell types such as normal rat kidney (NRK) and pancreatic  $\beta$  cells [35, 36]. Interestingly, these tubules are only observed in mammalian cells, possibly an advanced feature added to cisternal stacking in mammalian evolution. In other organisms such as plants where the polarized Golgi stacks are highly itinerant, stacking ensures efficient cargo processing and inter-cisternal trafficking as the stacks move [37, 38].

Yet, Golgi stacks do not exist in some lower eukaryotes such as the budding yeast *S. cerevisiae* and some developmental stages of *D. melanogaster* but consists of scattered cisternae [8] and clusters of vesicles or tubules [39] respectively. The scattered cisternae of the yeast can still be subdivided into cis, medial and trans Golgi [40] and efficient secretion is still supported in both organisms [39]. In addition, phylogenetic studies revealed that multiple Golgi proteins are highly conserved across eukaryotic evolution [41], implying that stacking is not an absolute requirement for the basic functioning of the Golgi but serves to increase complexity of Golgi functions.

#### *Golgi matrix proteins in cisternal stacking*

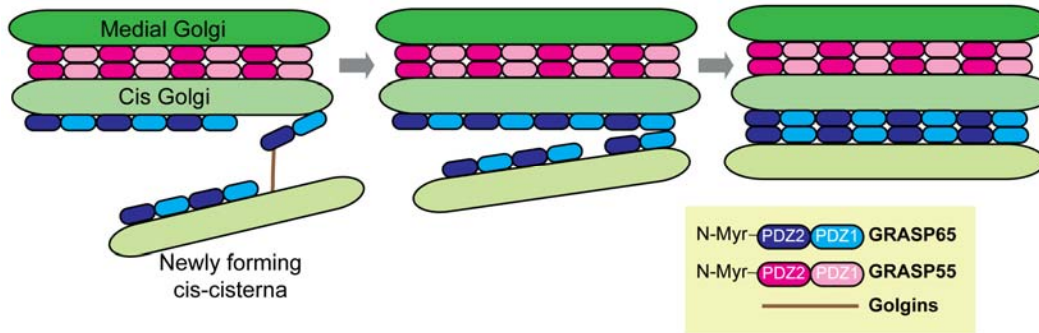
Despite of its central position in the secretory pathway where extensive membrane flux exchanges occur (Figure 1-1) and its highly dynamic nature in physiological and experimental conditions, how the elegant stacked structure of the Golgi is maintained remain contentious. Based on early morphological and

biochemical studies, the Golgi stacks were found to be held by proteinaceous cross-links between adjacent Golgi cisternae [42-44]. These proteinaceous links were later isolated in a detergent and salt-resistant fraction termed as the “Golgi matrix” [45]. The Golgi matrix forms a ribosome-free area surrounding the cisternae. Numerous proteins were found to compose the Golgi matrix whereby the Golgi reassembly stacking proteins (GRASPs) and golgins form the two major groups (Baringa- rementeria, 2009). These proteins are very dynamic and cycle between membrane and cytoplasm. The cycling process are usually effected by modification such phosphorylation. In addition to Golgi structural maintenance, matrix proteins are involved in membrane trafficking and more recently, in novel roles such as signaling, microtubule organization and apoptosis [46].

The GRASPs were first identified as the Golgi stacking factors [47, 48]. Both GRASPs in mammals, GRASP65 and GRASP55, appear to have redundant roles in Golgi stacking as depletion of either one of them resulted in minor effects on stacking [49-51], while depletion of both proteins profoundly abolishes stack formation [52]. However, loss of the single GRASP in lower eukaryotes such as the fly *D. melanogaster* [53] and *T. brucei* [54] did not massively perturb stacking. On the other hand, GRASP is also present in organisms without Golgi stacks [39, 55, 56] while plants have stacked Golgi but lack of a GRASP [57, 58]. This suggests that other factors are involved in stack formation and the GRASPs have additional functions.

Mechanistically, the GRASPs are capable of trans-oligomerizing, mediated by their N-terminal PDZ domains, hence are proposed to tether and cross-link Golgi cisternal membranes for stacking [59, 60] (Figure 1-2). In line with this, the trans-oligomerization domain appears to be absent in organisms with no stacks [61]. GRASPs are anchored to Golgi membranes via N-terminal myristoylation site and its interaction with the elongated coiled-coil golgins, whereby GM130 interacts with GRASP65 [47, 62] while Golgin45 with GRASP55 [63]. Extending out of Golgi membranes alike tentacles, golgins could mediate long-range tethering of

newly generated Golgi cisterna during cisternal maturation, before the homo-dimerization of GRASPs for Golgi stacking [64]. This is coherent with their participation in several membrane tethering events [65] and GM130 appear to act before GRASP65 in cisternal stacking during Golgi assembly [66].



**Figure 1-2: A model for the formation of Golgi stack.** During Golgi assembly or cisternal maturation of newly formed cisternae, the cisterna is first tethered to the cis-Golgi through a long-range golgin-mediated attachment. When the cisterna are in close proximity, this allows GRASP65 on both Golgi cisterna to interact via PDZ1-mediated trans-oligomerization, resulting in cross-linking and stacking of the Golgi cisterna. GRASP55 oligomerization is required to cross-linking cisternae in the stack. The model is modified from [64].

### 1.2.3 Golgi ribbon formation

Unlike in cells of lower organisms, such as protozoa, some fungi and insects, where the Golgi exists as discrete stacks scattered in the cytoplasm, the Golgi in vertebrates exhibit more complex organization. A typical vertebrate Golgi comprise of multiple stacks that are interconnected to form a continuous ribbon-like structure and is localized in the perinuclear and usually pericentriolar region [67]. Ultrastructural analysis revealed that the compact stacks are laterally linked by a reticulated network of branching and rejoining tubules, also known as the non-compact zone [12]. These ~30nm diameter tubules can sometimes stretch over several micrometers to bridge the adjacent stacks and can also project backwards to the same cisterna that they emanate from or to other structures such

as the vesicular tubular structures (VTCs) from the cis- and medial-cisternae [12-14]. These tubules can not only link heterologous cisternae of similar positions in the adjacent stacks but sometimes also connect cisternae at different levels of the stacks [14]. Although the significance behind perinuclear ribbon organization of the vertebrate Golgi is not completely comprehended, various factors involved in the ribbon formation have been studied and will be elaborated in the subsequent paragraphs.

#### *Microtubules in Golgi ribbon formation*

Intimately linked to the feature of structural continuity between stacks is the perinuclear localisation next to the centrosomes. Loss of structural continuity of the ribbon often correlates with dispersion from perinuclear positioning. This suggests a functional association with the microtubule cytoskeleton. As the major microtubule-organizing centre (MTOC) of the cell, the centrosomes emanate a polarized radial array of microtubule filaments that gathers Golgi stacks in close proximity at the perinuclear region for ribbon biogenesis. This assembly and clustering is mediated by the motor protein dynein, that transports the stacks along microtubules towards the centrosome [68] (Figure 1-3). Interestingly, although the centrosomes are the main MTOC, it is dispensable for Golgi ribbon formation. This is evidenced by the ability of dispersed Golgi membranes to self-organize into a continuous structure without the presence of centrosomes [69, 70].

Indeed, the Golgi itself can also form an MTOC that locally nucleate and polymerize microtubules, forming an asymmetric network (Figure 1-3) [71, 72]. Golgi-nucleated microtubules is dependent on  $\gamma$ -tubulin ring complex ( $\gamma$ -TuRC) which anchors on Golgi membranes based on association with various Golgi proteins such as GMAP210 [73], GCC185 [72] and GM130 [74]. Distinct mechanisms are involved in microtubule formation at different Golgi compartments. While microtubules at the trans Golgi are controlled by microtubule-stabilizing protein CLASP associated with golgin GCC185 [72],



those nucleated at the cis Golgi require GMAP210 and  $\gamma$ -tubulin-interacting proteins AKAP450 via GM130 binding [73, 74].

Thus, microtubules are essential for ribbon biogenesis whereby two sets of independently nucleated microtubule arrays from the centrosomes and Golgi act in concert for the assembly and positioning of the ribbon structure. Perturbations of microtubule integrity such as depolymerization of microtubules with nocodazole or loss of dynein function scatters the ribbon into separate stacks throughout the cytoplasm [75-79]. Upon nocodazole washout, the dispersed Golgi stacks were found to cluster locally at the cell periphery by Golgi-derived microtubules and subsequently moved along the centrosome-derived microtubules towards the perinuclear region [68, 80]. Ribbon assembly would not be possible if either step is perturbed, subsequently affecting Golgi functions such as polarized secretion and directional cell migration [81].

#### *Golgi matrix proteins in Golgi ribbon formation*

Once the Golgi stacks are clustered at the perinuclear region, they are laterally tethered together and linked to form a continuous ribbon (Figure 1-3). Formation of lateral connections between homotypic cisternae between stacks is assisted by Golgi structural proteins and also presumably by the Golgi-derived microtubules. It is speculated that both factors also confer specificity to allow linking between homotypic cisterna. For instance, microtubules from both cis and trans sides of the Golgi could confer geometric constraints to stacks which promotes ribbon formation [72, 74].

Golgi structural proteins such as the GRASPs were initially shown to mediate stacking between heterotypic cisternae, having complementary roles with each other [42, 43, 82]. More recently, they were found to participate in the lateral linking between stacks by tethering homotypic cisterna but in a non-redundant fashion, as single depletions resulted in ribbon unlinking [50, 51]. While the role

of GRASP55 in ribbon formation is not completely confirmed [83], GRASP65 appears to be convincingly involved in ribbon formation. Conferred with the ability to trans-oligomerise, GRASP65 was proposed to mediate ribbon formation by forming homo-oligomers to tether homotypic cisternae in close proximity [44, 84]. Other Golgi structural proteins such as the golgins, were also found to be involved in Golgi ribbon maintenance and seem to cooperate with the GRASPs in the process [45, 50, 85-89]. As golgins are extended proteins, they could provide long-range tethering for lateral linking between Golgi stacks before the trans-oligomerization of the GRASPs [64].

Although the mechanisms remain speculative, it has been proposed that the matrix proteins are essential for Golgi ribbon biogenesis and confer its identity. This is highlighted by experiments using laser microsurgical removal of Golgi membranes [90] or dominant negative Sar1 microinjection after Brefeldin A (BFA) drug washout [91] which demonstrated the appearance of the matrix proteins in a continuous ribbon structure before the resident Golgi enzymes. However, the results have been contested by other reports that show redistribution of the matrix proteins to the ER at higher at higher Sar1 mutant expression [92, 93]. More recent reports show that these proteins are highly dynamic and the Golgi-like remnants after BFA treatment [94, 95] and mitosis [96] are argued to be ER exit sites based on colocalisation with ERES markers. Collectively, while it is known that Golgi matrix proteins are important for Golgi organization, whether it serves as a stable template to confer Golgi identity or the Golgi forms *de novo* remains to be further proven.

#### *Lateral linking of the Golgi ribbon*

Lateral links between homotypic cisternae are formed by tubuloreticular structures (Figure 1-3). While the processes and molecular machinery that lead to this lateral fusion event remain obscure, recent results suggest that tubules

emanating from the Golgi play a major role and appear to be regulated by the phospholipid remodeling enzymes: phospholipase A (PLA) and lysophospholipid acyltransferases (LPATs); both exhibiting antagonistic roles. While PLA promotes tubulation through the formation of lysophospholipid (LPLs) [97], LPATs revert LPLs back to phospholipids and block tubule formation [98]. Mechanistically, tubular formation by PLA could arise from the conversion of cylindrically-shaped phospholipids to conically-shaped LPLs at specific sections of a single leaflet of the lipid bilayer, inducing membrane curvature [99]. Conversely, LPATs transfer fatty acids from acyl-CoA donors to LPLs, reforming phospholipids and inhibiting membrane curvature.

This phospholipid interconversion was recently discovered to influence Golgi structure and function. The precise mechanisms are still not known but several possibilities have been proposed. Firstly, the lipid conversion generates membrane curvature for tubules and/ or vesicular carriers that could be involved in lateral linking between Golgi cisternae and membrane trafficking events [99-101]. Secondly, a concentration gradient of lipid species could be formed that recruits effector proteins, such as vesicular coat machinery [102, 103], to Golgi membranes. The generated LPLs and fatty acids could also influence signal transduction and metabolic pathways.

To date, four cytoplasmic PLA (PAFAH1b, cPLA<sub>2</sub> $\alpha$ , PLA2G6 and iPLA<sub>1</sub> $\gamma$ ) and an integral membrane LPAT (AGPAT3/LPAAT3) enzyme have been implicated in membrane trafficking processes and Golgi structural regulation, although the combination of PLA<sub>2</sub> and LPAT enzymes involved remains to be unraveled [97, 104]. Lateral links in Golgi ribbon are thought to be mediated primarily by the PAFAH1b enzymes, which could act in concert with dynein and microtubules to facilitate the coalescence of Golgi stacks at the peri-centrosome region [105]. The dynamic balance of membrane fluxes at the Golgi that is mediated by the membrane trafficking activities of PAFAH1b and other PLA enzymes could also be a critical influence on ribbon maintenance. For instance, PAFAH1b influences

trafficking at the TGN and endosomes [106] and cPLA<sub>2</sub>α facilitates intra-Golgi trafficking [107].

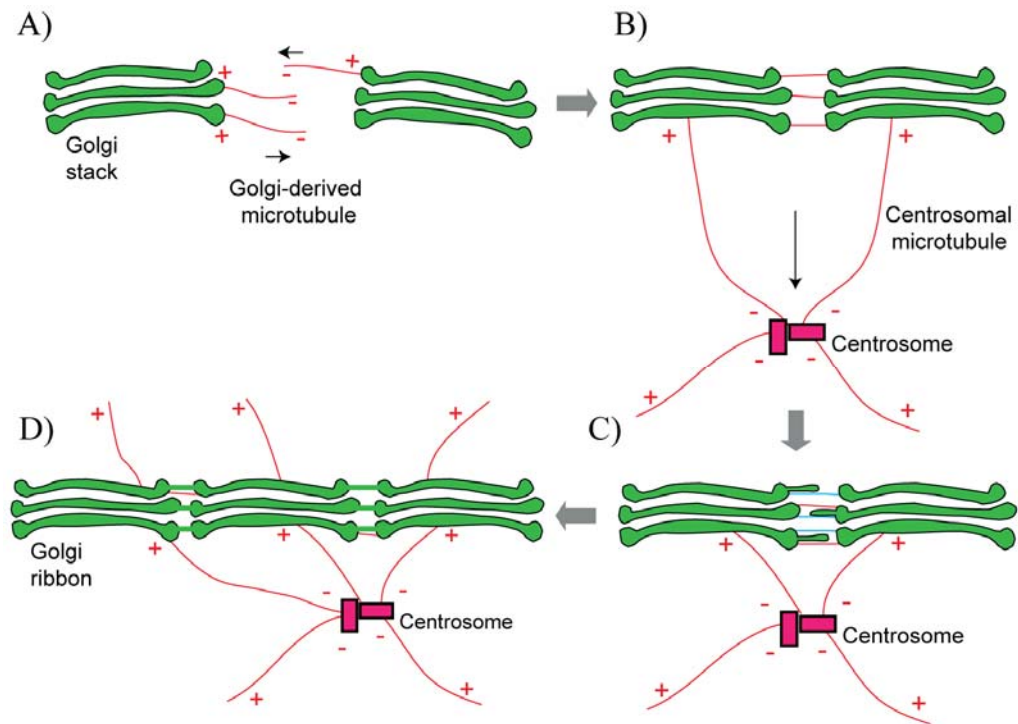
Another question revolves around the mechanisms and molecular machinery that initiate tubule formation. Recent findings identified the involvement of the COPI coat in driving membrane bud formation at Golgi and tubule or vesicle formation depends on the relative activities of cPLA<sub>2</sub>α and LPAAT3(γ) [108]. This led to speculations that the COPI coat machinery could be involved. Yet, conversely, BFA treatment also evokes tubule formation from the Golgi. BFA acts by inhibiting COPI regulators ARF GEFs which causes dissociation of the COPI coat from Golgi membranes. In other words, BFA-induced Golgi tubules are independent of the COPI coat. It is possible that both COPI-dependent and COPI-independent mechanisms are involved in controlling tubule formation at the Golgi.

The mechanisms involving extension of the tubules from the initiating Golgi membrane protrusions also remain to be characterized. This requires directed force to pull membranes into tubules, hence actin- and microtubule-associated molecular motors are ideal candidates for this process. Indeed, it is clear that these cellular motors are essential for the intracellular movement of Golgi stacks; actin-based myosins are required for the plants and fungi while microtubule-associated motors in vertebrates. It was found that tubules induced by BFA appear to require microtubule plus-end directed kinesin motors. Formation of BFA-induced tubules was prevented when dominant negative inactive mutant of KIF1C was expressed [109]. Supporting this, Golgi-nucleated microtubules are involved in gathering Golgi stacks for ribbon formation. It is thus possible that interstack tubules are elongated by kinesin activity along these local microtubules.

In addition, actin-associated myosins might also contribute to tubule formation (Figure 1-3). A recent report suggests that unconventional myosin MYO18A interacts with Golgi phosphoprotein (GOLPH3), which is recruited to the Golgi

through phosphoinositol-4-phosphate binding. This interaction provides the tensile force for tubulation and allowing extension of the Golgi ribbon [110]. In addition, actin polymerisation at the Golgi region can be induced through the activation of formin mDia via LPL-induced Rho activation. This was found to induce Golgi dispersal in a mechanism involving myosin-II activity [111]. Mentioned previously, LPL promotes tubule formation, this suggests that the coordination of Rho activity by LPL might link membrane buds to myosin and actin filaments, which pulls the buds to form tubules. The formation of tubules for lateral linking might involve the concerted action of actin and microtubules. Indeed, Golgi protein WHAMM (WASP homology associated with actin, membrane, and microtubules) binds to microtubules and activates Arp2/3 complex-mediated actin polymerisation which promotes tubule formation from the Golgi [112]

Based on these various studies, while it is clear that tubules are required for coupling Golgi stacks to form a continuous ribbon, the mechanisms of how the tubules are initiated, extended and fuse with homotypic cisternae of different stacks would require more in-depth characterization.



**Figure 1-3: Model of Golgi ribbon assembly.** (A) Microtubules (*red lines*) that are nucleated and polymerized at the Golgi emulate to contact other Golgi stacks in the vicinity. The Golgi stacks are then clustered together by moving along microtubules towards the minus ends. (B) The clustered stacks then move along centrosomal nucleated microtubules by dynein motor towards the perinuclear region next to the centrosomes. (C) and (D) Tubular structures elongate on microtubules (*red lines*) and/or actin filaments (*blue lines*) further link the clustered stacks to form a continuous ribbon.

### *Functions of the Golgi ribbon*

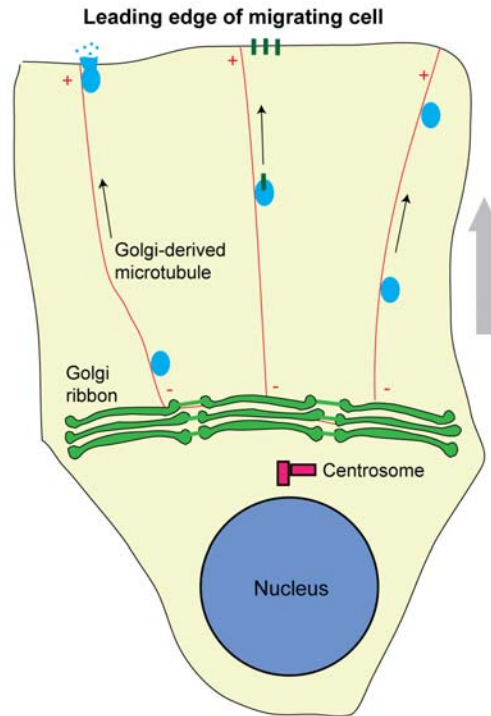
The Golgi ribbon is only found in vertebrates. This is intriguing as such a sophisticated structure would pose a challenge for processes particularly mitosis that requires even partitioning between the two progeny cells. To ensure faithful inheritance to the daughter cells, the Golgi ribbon would have to undergo multiple steps: disassembly and vesiculation, division and reassembly. This involves a non-trivial effort in terms of coordination and energy. This, hence suggest that natural selection favors ribbon structure in higher organisms and there must be exclusive reasons and advantages for its maintenance and inheritance. The ribbon structure could serve to broaden the repertoire of Golgi functions in vertebrates.

Interestingly, the primary function of the Golgi, membrane trafficking, does not rely on the ribbon structure. Disruptions in the ribbon structure minimally affected intra-Golgi trafficking and general secretion to the plasma membrane [36, 50, 75, 113]. It has been proposed that a continuous ribbon is required for uniform glycosylation of cargo, by allowing lateral diffusion of glycosylation enzymes between Golgi stacks. This is highlighted in the loss of golgin GM130 and GRASP65 which reduced to Golgi into ministacks and led to changes in glycan patterns [50] while others have observed changes in diffusion rate of glycosylating enzymes [52, 68, 114]. However, opposing results were also observed [115], making it hard to conclude. This may be due to differences in experimental conditions and tested glycosylation enzymes and cargo. Thus, it warrants a systematic analysis of Golgi ribbon integrity and glycosylation function to better address this.

In contrast, formation of the Golgi ribbon is clearly required for advanced functions of cell polarization and directed secretion. The orientation of the Golgi in the cell is in particular importance to specialized functions including cell migration [116, 117], polarized secretion of lytic granules in cytotoxic T cells [118], distinguishing apical-basal epithelia axis [119] and regulated dendritic

growth in neurons [120]. For instance, during cell migration, the Golgi has to remodel and reposition at the leading edge of the cell to mediate delivery of new membrane and secretory cargo to the cell periphery (Figure 1-4). Disrupting the Golgi integrity would impair cell polarization and directed cell migration [116, 121, 122]. In addition, the ribbon structure also substantially increased the total volume of the Golgi and this is important for specialized secretory cells. It was found that while insulin producing  $\beta$  cells of mice are  $3.7\text{-}5.8\mu\text{m}^3$ , the Golgi stack comprised of  $3.1\text{-}3.6\mu\text{m}^3$  [123]. Finally, unlinking of the ribbon is an intrinsic G2/M checkpoint requirement before mitosis [124-126]. Although the reasons and the mechanistic basis of how morphology is sensed are not known, it suggests that the Golgi ribbon is closely linked to cell events and cell fate. Indeed, the Golgi ribbon appeared unlinked and fragmented in many diseases including neurological diseases such as Parkinson's disease and cancer.





**Figure 1-4: The Golgi ribbon is required for cell polarization and directed secretion in a migrating cell.** The Golgi ribbon orientates towards the leading edge of the migrating cell. Golgi-derived microtubules extend to the cell periphery and allow delivery of transport carriers containing secretory cargo such as cell adhesion factors as well as new membrane to the leading edge of the cell. The model is modified from [64].

#### *Signaling regulation on the Golgi apparatus*

As highlighted in Figure 1.1, the cell transports a large amount of proteins and lipids in the secretory pathway and this is essential for its growth, survival, communication and homeostasis. Conversely, the secretory pathway also needs to accommodate and respond to internal and external stimuli in order for the cell to adapt to the surrounding environment and varying endogenous contexts. Signal transduction detects and converts the stimulus on the cell into a specific cell response. It usually starts with a signal to receptor and ends with a effect in cell function. It is now well documented that the secretory pathway is responsive to signaling cascades.

In particular, the Golgi is centrally located in the secretory pathway and bears the responsibility of modifying and sorting of proteins and lipids that are trafficked in the secretory pathway. It, hence, needs to be able to sense and integrate endogenous and exogenous signals from various sources to maintain cellular homeostasis. Indeed, over the last ten years, several signaling molecules localise to Golgi membranes. These proteins were found to phosphorylate key Golgi proteins that resulted in modulation of Golgi organization or its functions in response to intracellular and extracellular cues [127-129]. Hence, the Golgi is highly responsive to endogenous and exogenous stimuli and its functional organization is deeply integrated to various signaling events in order to accommodate cellular requirements.

The most well-established and best studied to date is the mitotic kinase cascade. During mitosis, the Golgi apparatus progressively disperses to allow correct partitioning into the two daughter cells at metaphase. Several signaling players including CDK1, RAF, MEK1, ERK1c, Plk1 and Plk3 [130-135] have been identified to participate in the process and they phosphorylated various Golgi proteins including GRASPs and golgins to mediate Golgi fragmentation. Surprisingly, the unlinking of the Golgi at the G2/M phase is required for mitotic entry, suggesting the existence of a novel 'Golgi mitotic checkpoint' [126, 136]. How this checkpoint occurs remains elusive at the moment but it suggests that the unlinking of Golgi membranes might trigger a set of signaling cascades to regulate mitotic entry.

In addition to endogenous stimuli as observed with mitosis, it is now emerging that the Golgi and the secretory pathway also responds to signaling cascades induced by exogenous stimuli such as hormones, nutrients or growth factors. This modifies various aspects of its functional organization in response to the qualitative and quantitative demands required for cell growth, survival and homeostasis. For instance, general secretion is increasingly found to be regulated at the Golgi level in addition to our current understanding of regulation at the ER.

Several molecules such as protein kinase D (PKD) [137], PI4 kinases [138], p38 MAPK [138-141] and protein kinase A (PKA) activation [142, 143] were found to remodel the Golgi structure and facilitate cargo flux from the TGN. For instance, PKD is present at the TGN where it activates PI4KIII $\beta$  which generates lipid PI4P for the formation of post-Golgi carriers. PI4P is able to recruit various membrane trafficking effectors important for various aspects of vesicle budding and fission [144]. This is supported by the finding that in situations when secretion is inhibited, such as serum and nutrient starvation, phosphoinositide phosphatase Sac1 is recruited to the Golgi where it locally depletes PI4P levels and reduces export from the Golgi [141]. Stimulation of mitogens in serum starved cells led to redistribution of Sac1 back to the ER in a p38/MAPK-dependent manner, rescuing reduced secretion. This elegantly demonstrates the nutrient sensing ability of the Golgi that allows the modulation its secretion according to the changing cell environment and needs. The Golgi also generates its own signaling in response to variable cargo load to modulate its own functional organization. Local activation of SFKs at the Golgi was observed upon increase in incoming secretory cargo [145]. This appears to be mediated by the binding of KDEL receptor with incoming luminal chaperones entering the Golgi. Subsequently, SFK activation promotes secretion and facilitates intra-Golgi trafficking to adapt to the cargo flow.

Another clear example of a cellular process influencing Golgi function in response to external cues is during directional cell migration. When cells migrate towards a chemoattractant, the Golgi has to remodel and reorientate towards the leading edge of the cell [121]. This is required to establish cell polarity and ensure delivery of new membrane and secretory cargo to the leading cell periphery. Phosphorylation of GRASP65 at serine residue 277 by ERK has been shown to be crucial to mediate this process [116]. Strikingly, the same residue on GRASP65 was also reported to be phosphorylated by CDK1 during mitosis that allows the disassembly of the Golgi [146], further substantiating the importance of GRASP65 in regulating Golgi integrity. Nevertheless, how cell polarity and

specific trafficking of material to the leading edge is regulated remains to be discovered. Like in the regulation of secretion, the Golgi also generates signaling for its own reorientation during cell migration. It was found that germinal-centre kinases III (GCKIII), MST4 and YSK1, are recruited to the Golgi by GM130 which promotes their activation [147]. Unlike GRASP65, GM130 is not phosphorylated by these kinases but appears to serve as a scaffold at the Golgi. Given that GCKIII also phosphorylate polypeptide 14-3-3 $\zeta$ , it might help recruit the Par complex to the Golgi. The Par complex is a master regulator of cell polarity [148]. Furthermore, Cdc42, a well-known activator of Par complex, was also found to be recruited via dynamin-binding protein DBMBP, by GM130 [149]. Altogether, these findings demonstrate that there is a polarity complex localised on Golgi membranes that is recruited by GM130. Hence, GM130 is likely to play a central role in cell migration.

The Golgi also serves as a platform for localised signaling and this spatially organizes signaling cascades, allowing differential signaling outputs. Signaling molecules, particularly the Ras proteins [150, 151] and members to the Raf-MEK-ERK signaling cascade, are associated to Golgi membranes by palmitoylation or by scaffold proteins. It was found that both H-Ras and N-Ras are palmitoylated on Golgi membranes [152]. Remarkably, targeting Ras to the ER elevated survival and proliferation rates of NIH3T3 fibroblasts while control fibroblasts expressing Ras at the plasma membrane die after two to three days [153], further indicating differential results with signaling from different locations. Similarly, Ras targeted to Golgi membranes can also activate downstream signaling molecules [153, 154]. Downstream of Ras is the Raf-MEK-ERK signaling cascade which was found to be spatially organized by scaffold proteins. Interleukin-17 receptor D (IL17RD/ Sef) localises MEK and ERK to the Golgi [155] and sequesters them from translocating into the nucleus upon activation. Golgi localised peptidyl-tRNA hydrolase 2 (PTRH2/BIT1) also binds to ERK1/2 which blocks its activity [156] and promotes apoptosis.

Collectively, these various examples highlight the importance of signaling cascades regulating Golgi structure and functions. Although the mechanistic details still remain poorly understood, future work will have to focus on the regulation of the machineries involved. While it is well-established that the Ras-MEK-ERK pathway regulates many aspects of the secretory pathway, many other signaling molecules are likely involved that remains undiscovered. To further grasp the extent of the regulatory mechanisms on the Golgi, systems biology would be an appropriate tool to study the regulation in a systematic and unbiased genome-wide manner. This would greatly advance our understanding in the interplay between signaling and the secretory pathway which aid further insights to how the secretory pathway can act in a processive and precise system.

### **1.3 GLYCOSYLATION FUNCTION OF THE GOLGI**

Central to the secretory pathway in all eukaryotic cells, the Golgi apparatus is well-established for its role as a processing, membrane trafficking and sorting center in the transport of secretory proteins and lipids to their appropriate destinations. Among the most common processes occurring at the Golgi is glycosylation and this will be reviewed in the subsequent sections.

Glycosylation is the enzymatic process involving covalent attachment of carbohydrate moieties, also known as glycans, on luminal and transmembrane proteins and lipids that passage through the secretory pathway. This process is probably as ancient as life itself as all life-forms ranging from unicellular archaea and eubacteria to multicellular vertebrates depend on glycans for cell viability and functioning [157-160].

### 1.3.1 Glycan diversity in mammals

Unlike other biopolymers such as nucleic acids and amino acids, glycan synthesis is not template-driven. The result is a vastly large diversity of glycan structures that could be generated. Mature glycans may range from a single sugar molecule to a complex polymer of more than 200 sugars and could be potentially further modified with sulphate, phosphate, acetate or phosphorylcholine. Glycans are also often branched. For example, a complex N-glycan structure could encompass up to six branches or antennae with each antenna made up of multiple repeating disaccharide units.

In mammals, glycan structures are assembled from ten monosaccharides: fucose (Fuc), galactose (Gal), glucose (Glc), N-acetylglucosamine (GlcNAc), N-acetylgalactosamine (GalNAc), glucuronic acid (GlcA), iduronic acid (IdoA), sialic acid (Sia), mannose (Man) and xylose (Xyl) (Figure 1-5) [161-163]. The combination of these different monosaccharides with differences in their anomeric state ( $\alpha$  versus  $\beta$ ), glycosidic linkages (1–3 versus 1–4, etc.), branching, length and their substituted components (phosphate, sulfate, etc.) adds to the diversity of glycans that can be generated. Glycan addition to substrate proteins and lipids also creates different subsets of glycoconjugates. Glycans can be added to proteins through amide linkages to asparagine residues (N-glycosylation, through glycosidic linkages to serine and threonine side chains (O-glycosylation) [164, 165], hydroxylysine (collagen) or Tyr (glycogenin) or through carbon-carbon linkages to the C2 position of tryptophan (C-mannosylation). The former two glycosylation subtypes are the main processes occurring in the cell.

Fucose (Fuc)	▲	Glucuronic acid (GlcA)	◊
Galactose (Gal)	●	Iduronic acid (IdoA)	◊
Glucose (Glc)	●	Sialic acid (Sia)	◆
N-acetylglucosamine (GlcNAc)	■	Mannose (Man)	●
N-acetyl-galactosamine (GalNAc)	■	Xylose (Xyl)	★

**Figure 1-5: The representative symbols of the ten monosaccharides used in mammals.**

Furthermore, glycans can be attached between glycosylphosphatidylinositol [166] anchors and proteins, serving as a bridge [167]. Within the O-glycans, there are at least six different types of attachments in vertebrates (Table 1.1). Many are branched except glycosaminoglycans which are linear glycans, that are often sulphated, and involve a different mechanism [168]. On the other hand, lipid glycosylation generates glycolipids (glycosphingolipids), including sialic acid-bearing gangliosides [169]. In addition, there are unique glycans that are unattached to any substrates and this includes hyaluronan that is secreted into extracellular regions [170]. In contrast, the yeast only utilises four monosaccharides for glycan formation: Man, GlcNAc, Glc and Gal and the most common glycans are usually a simple structure of branching repeats of Man sugar or oligomannose structure with fewer forms of glycosidic linkages [171, 172].

Type	Linkage	Enzyme	Consensus sequence	Domain	Examples
N-glycosylation	GlcNAc- $\beta$ -Asn	OST	N-X(S/T)(standard sequons) N-X-C, N-G, N-X-V (non-standard sequons)		Nascent polypeptides
O-glycosylation	GalNAc- $\alpha$ -Ser/Thr	ppGalNAc-Ts	Isoform specific		Mucins
	GlcNAc- $\beta$ -Ser/Thr	OGT	No set consensus		Cytosolic, nuclear proteins
	GlcNAc- $\beta$ -Ser/Thr	EOGT	Unknown	EGF	Notch, Dumpy
	Xyl- $\beta$ -Ser	XYLT1, XYLT2	a-a-a-a-G-S-G-a-(a/G)-a (‘a’ represents Asp or Glu)		Heparin, proteoglycan core proteins
	Fuc- $\alpha$ -Ser/Thr	POFUT2	C-X-X(S/T)-C-X-X-G	TSR	Thrombospondin, ADAMTS family
		POFUT1	C-X-X-X(S/T)-C	EGF	Notch, clotting factors
	Glc- $\beta$ -Ser	POGLUT1	C-X-S-X(A/P)-C	EGF	Notch, clotting factors
	Man- $\alpha$ -Ser/Thr	POMT1, POMT2	I-X-P-T(P/X)-T-X-P-X-X-X-P-T-X(T/X)-X-X		$\alpha$ -dystroglycan
		GLT25D1, GLT25D2	X-Hyl-Gly (collagen repeats)		Collagen, adiponectin
	Glc- $\alpha$ -Tyr	GYG	Tyr194 of GYG		GYG (autoglycosylation during glycogen formation)
C-mannosylation	Man- $\alpha$ -Trp	Unknown	W-X-X-W	TSR	Thrombospondin, ADAMTS family
Glypiation	Pr-C(O)EthN-6-P-Man	Transamidase	No set consensus		THY1, NCAM1

**Table 1.1: Consensus motifs and enzymes responsible for various glycosylation reactions occurring in vertebrates.** The table is modified from [173].

Therefore, the mammalian glycan repertoire, also known as the glycome, is theoretically tremendously vast and diverse. Although the actual number of the entire glycome is not known, due to the limited existing knowledge of glycan determination, it was predicted to be 10-10,000 larger than the proteome [174]. However, constraints are also provided by the synthesis and regulatory mechanisms. The glycosylation machinery in the cell encompasses an array of several hundreds of glycosylating enzymes and nucleotide sugar transporters, altogether spanning about 1% to 2% of the genome [175]. This magnitude of genomic commitment further stresses the central role of glycoconjugate biosynthesis in humans. Further supporting this is the abundance of glycoproteins generated in the cell which forms about 50% of the proteome. Hence, as the most common post-translational modification process for proteins, the process has a broad impact on metazoans.

Glycan addition is important for the functionality of the final glycoprotein product and this is essential for its activity, stability and localization. The incorporation of



glycan structures also creates structural and functional diversity to proteins. In fact, glycans carry much more finely tuned information that could not be accomplished by a simpler polypeptide modification. This is highlighted by differences in *in vivo* serum half lives and potencies of peptide hormone erythropoietin with different glycan structures [176]. Therefore, by conferring additional information at the molecular and cellular level that expands the simple genome-encoded protein functions, glycans introduce biological complexity to eukaryotes [177].

### **1.3.2 Biological roles of glycans**

Glycans are prominent in the intracellular, cell surface and secreted proteins. They influence a wide range of important biological functions including structural roles, protein maturation and turnover, cell adhesion, receptor function and cell signaling, molecular trafficking and clearance, self-recognition, immune surveillance and pathogen invasion and some of these appear to be conserved in evolution of multicellular vertebrates [159].

#### *Protective role of glycans*

It is without doubt that glycans play many protective, organizing and stabilizing roles in the cell. Every eukaryotic and various prokaryotic cells are coated with a layer of polysaccharide coat known as the glycocalyx which can represent a substantial physical barrier. The attachment of glycans, such as proteoglycans, to extracellular matrix molecules are required for maintaining tissue structure, integrity and porosity and can also, in turn, contribute to matrix organization. In addition, the orientation of glycans in the extracellular regions prevents the attached underlying proteins to be targeted by proteases and antibodies [178]. For instance, mucins, large glycoproteins that are heavily O-glycosylated, line the surfaces of epithelial cells and goblet or mucous cells of the tracheobronchial, gastrointestinal, and genitourinary tracts. In the gastrointestinal tract, mucins

constitute the mucosal layer to protect the tissue from gastric proteases [179]. Another structural role of glycans is the involvement as an insulating warehouse for biologically important molecules. For example, glycosaminoglycan chains of the extracellular matrix in the basement membrane of epithelial and endothelial cells were found to contain many heparin-binding growth factors. This serves to prevent the factors from diffusing away from the localized region, inhibit their degradation, maintain their activities and allow them to be released under stimulated conditions [180, 181].

#### *Role of glycans in cell-cell interaction*

Glycans at the cell surface modulate cell-cell and cell-matrix interactions by providing ligands for cell adhesion, macromolecule interactions and pathogenic invasion [157, 182]. This is often mediated by specific lectin-glycan binding and is best exemplified in the interactions between selectins and the sialyl-Lewis X oligosaccharide ligand in various cell adhesion systems. In particular, the process is important for the tethering and rolling of the circulating leukocytes on the endothelium of the vasculature to allow infiltration of the leukocytes into the surrounding tissues to execute inflammation and maintain immune system homeostasis [183]. Glycan-lectin interaction is also required for fertilization of mammalian embryos and loss of some glycans was found to block the process [184-186].

Glycans also affect cells' sensitivity to extracellular signals by modulating interactions between cell surface receptors and their ligands. This, in turn, alters the downstream signal transduction events in the cell. This could occur by regulating signaling thresholds of the receptors. For instance, glycan heterogeneity on cytokine and adhesion receptors modifies ligand occupancy thresholds for intracellular signaling at different cell physiological states [187]. The glycan expressed could also determine the receptor residency duration at the cell surface by preventing its endocytosis or by organizing them in membrane

microdomains, thus modulating the time and magnitude of the signaling. For example, modifications of N-glycan structure by GlcNAc-transferase V (GlcNAcT-V) on epidermal growth factor, transforming growth factor- $\beta$  and cytokine receptors delays removal by endocytosis via galectin interaction [188].

#### *Role of glycans in intracellular processes*

Apart from cell surface and extracellular events, glycan are also essential for various intracellular processes. Glycan structures on newly translated glycoproteins are critical for proper protein folding, ER-localised protein quality control and the subsequent maintenance of protein solubility and conformation which is required for passage and selective protein targeting across the secretory apparatus [189, 190]. For instance, the targeting and transport of hydrolases to the lysosomes relies on the recognition of mannose-6-phosphate residues by specific mannose-6-phosphate receptors [190].

#### *Glycan variations in different physiological settings*

Glycan structures can vary greatly between cell and tissue types and physiological states. This is observed during maturation and activation of dendritic cells which alter lectin recognition by other immune cells [191]. Glycan chains at the cell surface were also reported to be more branched in high nutrient conditions and this is likely to favor cell growth and subsequently differentiation [192]. Furthermore, we have shown that growth factor stimulation promotes relocation of pp-GalNAc-Ts from the Golgi to the ER, which, in turn, increases expression of short O-glycans and promotes cell migration [193, 194]. Distinct glycan structures have biologically significant roles in the specific cell/tissue type. Distinct glycan structures are utilized by different cells in the alteration of the rates of cell surface glycoprotein endocytosis. For instance, cell surface maintenance of glucose transporter 2 in pancreatic  $\beta$  cells requires the

construction of a specific N-glycan that is recognized by pancreatic lectin receptors. The mechanism, in contrast, does not exist in hepatocytes [195].

Altered glycan structures are observed in a broad spectrum of pathological situations such as cancer [196, 197], immune disorders [198], diabetes [159] and genetic diseases like congenital disorders of glycosylation (CDG) [174] and cystic fibrosis [199]. Although the mechanistic links in cancer and diabetes are less clear than for genetic disorders at the moment, alterations in the glycan profiles can be observed during many malignant transformations [200] and there is an emerging link between cancer metastasis and glycosylation. Interestingly, there is a general tendency for tumor cells to express immature and usually short or truncated cell surface glycans, usually with alterations in density and patterns which are rarely found in normal tissues. These altered glycans was proposed to confer proliferative, survival, antigenic and adhesive properties to the cancer cells and increase their metastatic potential and invasiveness by reducing contact inhibition between cells. For instance, it was observed in mammary cancer cells that express the short O-glycans sialyl-Tn, there were increased growth and migration rates in mammary cancer cell lines and expression is associated with poor prognosis in breast cancer patients [197, 201]. These aberrant glycans can serve as a source for diagnosis, prognosis, monitoring disease progression and developing therapies and immunization against cancer [202-204].

### **1.3.3 The glycosylation machinery in the cell**

Glycans are constructed by the combined action of an intricate array of glycosyltransferases and glycosidases, collectively termed as glycosylating enzymes, as well as nucleotide sugar transporters that are localized in the secretory apparatus. It is estimated that approximately 700 proteins are involved in the glycan synthesis in mammals, whereby most of them reside at the Golgi. Although the initiation of glycosylation usually occurs in the ER, the subsequent addition or trimming of different sugars and branching, i.e. the construction of

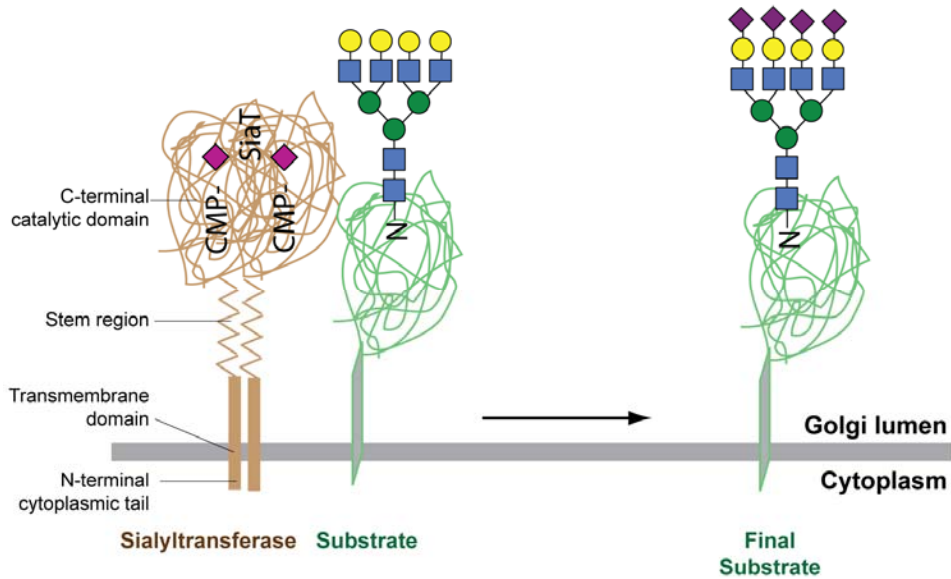
complex oligosaccharide chains to generate a mature glycoprotein/glycolipid, is accomplished in the Golgi. Hence, emphasis will be placed on glycosylation at the Golgi in the subsequent sections.

The primary determinants of glycan structure at the Golgi are the glycosyltransferases which catalyze the transfer and glycosidic linkage of a monosaccharide molecule from a simple nucleotide sugar donor substrate (for example, UDP-GalNAc, GDP-Fuc, or CMP-Sia) to an acceptor substrate (sugar of a glycan chain or protein/lipid). Some glycosyltransferases could also catalyze the transfer of two different sugars, usually to generate a string of repeating units such as the proteoglycans. Currently, there are more than 250 glycosyltransferases known to reside at the Golgi in mammals. This number is huge in mammals possibly because of the increased number of enzyme isoforms that catalyze the same reactions. For instance, while there are 20 mammalian sialyltransferases [205], *Drosophila* and yeast have one and none respectively [206]. Similarly, there are 20 ppGalNAc-Ts in humans and much fewer in the *Drosophila* (12) and *C. elegans* (9) [207]. In contrast, only a few glycan biosynthetic enzymes at the Golgi are glycosidases which remove monosaccharides to form intermediates that are subsequently acted on by glycosyltransferases. This is particularly relevant to N-glycan formation which involves the trimming of mannose residues as an intermediate step to generate complex and hybrid-type chains.

#### *Structure of Golgi glycosyltransferases*

The similarity shared by Golgi glycosyltransferases is their secondary structure. Golgi glycosyltransferases are mostly type II transmembrane proteins with transmembrane domain flanked by a short amino-terminal cytoplasmic tail and a long carboxy-terminal domain that comprises of a stalk-like stem region followed by a globular catalytic domain (Figure 1-6). In contrast, ER glycosyltransferases are mainly multitransmembrane proteins span the ER membrane. The carboxy-terminal domain of Golgi glycosyltransferases extends within the lumen of the

Golgi in order to act on glycosylated substrates that passage through the organelle. Only a few exceptions to this configuration include GlcNAc-phosphotransferase (a multisubunit complex) and the GlcNAc-1-phosphodiester  $\alpha$ -N-acetylglucosaminidase (type I membrane-spanning) that are involved in the synthesis of the mannose-6-phosphate targeting signal of newly synthesized lysosomal hydrolases. Interestingly, some glycosyltransferases contain more functional domains in addition to the catalytic domain. For example, ppGalNAc-Ts have a lectin domain that binds to existing GalNAc on substrates. Glycosyltransferases are often glycosylated by other glycosyltransferases or sometimes, they can auto-glycosylate. This glycosylation event is required for proper folding and functioning of the enzyme. Some glycosyltransferases may also be cleaved in their stem region at the Golgi to be secreted in the cell surface or extracellular region [208, 209]. The reasons and the range of enzymes involved are not clear but it may serve as a mechanism to regulate their activities.



**Figure 1-6: Structure of a typical Golgi glycosyltransferase.** The Golgi glycosyltransferase is typically a type II transmembrane protein (shown in brown: a sialyltransferase). The glycosyltransferase comprise of a short cytoplasmic tail, transmembrane domain, extended stem region and a globular catalytic domain that is shown binding CMP-Sia from which it transfers Sia to Gal on a complex N-glycan on a glycoprotein (*green*).

#### *Golgi localisation and retention of glycosylating enzymes*

Biochemical and ultrastructural studies indicate glycosylating enzymes are exquisitely distributed to distinct Golgi cisternae and organized in the order which enzymes function. While early acting core glycan forming enzymes are enriched in the early cis- and medial-Golgi compartments, late acting capping enzymes are localized predominantly in trans Golgi compartment [30]. This localization segregation spatially organizes different enzymatic reactions to ensure the sequential construction of the growing glycan chain as it traverses across the successive cisternae. However, it does not mean that the glycosylating enzymes are rigidly confined in the Golgi compartment. As mentioned in the previous sections, the Golgi is a highly dynamic organelle central to the multiple membrane exchanges in the secretory pathway. Various Golgi trafficking models have been proposed for proteins that may influence cellular glycan expression.

According to the prevailing cisternal maturation model for membrane transport in the Golgi, Golgi resident proteins such as the glycosylating enzymes retain their steady-state Golgi localization by retrieval back to the “newer” cisternae. In contrast, the vesicular transport model proposes the existence of stable Golgi cisterna containing glycosyltransferase while the cargo traffics from cis to trans Golgi via vesicular transport. Thus, the mechanisms involved in how glycosyltransferases retain Golgi compartmental segregation are extensively explored.

Various factors have been identified including sequence motifs in the cytosolic, transmembrane or stem regions of the enzyme, formation of an enzyme complex, length of transmembrane domain and association with a localization or activity chaperone. Sequence motifs on the enzymes could lead to homo-oligomerisation and retention as observed with sialyltransferases (Colley et al. 1992; Fenteany and Colley 2005). Enzymes that participate sequentially in a common glycosylation pathway may also form a complex by a mechanism known as the kin recognition. For example, GlcNAcT-I interacts with  $\alpha$ -mannosidase II and GlcNAcT-II which all act chronologically in the synthesis of N-glycans [85, 210-212]. These enzyme aggregates may reach a size that can be excluded from transport vesicles. This is in support of the vesicular transport model but not the cisternal maturation model which involves movement of glycosylating enzymes in vesicles. It has been proposed that Golgi glycosyltransferases generally have a shorter transmembrane domain than proteins that span the plasma membrane which promotes Golgi retention (Munro 1995). This correlates with the membrane thickness of the secretory system and the plasma membrane whereby the latter is thicker. Golgi glycosyltransferases could interact with a protein chaperone that is required for its localization or activity. For instance, a number of glycosyltransferases in the yeast contain a sequence motif at the N-terminus that binds to peripheral sorting protein Vps74p. Vps74p interacts with COPI vesicles and mediates their Golgi retention [213, 214]. Additionally, the *Drosophila* glycosaminoglycans enzyme pipe, requires another protein known as “windbeutel” to localize to the Golgi [215].



Furthermore, T-synthase/ C1GalT1 needs to form a complex with a chaperone COSMC in the ER in order to constitute an active enzyme in the Golgi [216, 217].

### **1.3.4 Glycosylation reactions in the Golgi**

As illustrated in Table 1.1, a variety of glycosylation reactions on proteins has been identified and among the most prevailing processes occurring at the Golgi are N-glycosylation and O-glycosylation. Here we describe the current understanding of their general structure, common biosynthesis and processing steps and biological functions.

#### **1.3.4.1 N-glycosylation**

##### *N-glycosylation initiation*

N-glycans are covalently attached to asparagines residues of the polypeptide chain by an amide linkage [218]. The process is initiated on the cytoplasmic face of the ER which begins with the transfer of a GlcNAc sugar to dolichol phosphate (Dol-P), a polyisoprenol lipid, to generate the dolichol pyrophosphate N-acetylglucosamine (Dol-P-P-GlcNAc) precursor (Figure 1-7). The subsequent steps involve the stepwise construction of the N-glycan with 14 sugars of mannose and glucose, along with the flipping of the Dol-P precursor into the lumen of the ER, to generate the mature N-glycan precursor  $\text{Glc}_3\text{Man}_9\text{GlcNAc}_2\text{-P-P-Dol}$  (also known as the lipid-linked oligosaccharide precursor) that is ready for transfer to the asparagines of nascent proteins during translation [219]. The transfer requires the multisubunit oligosaccharyltransferase (OST) complex on the luminal face of the ER [220]. Subsequent to the polypeptide transfer, the three glucose sugars of the N-glycan are removed to generate the  $\text{Man}_9\text{GlcNAc}_2\text{Asn}$  structure for lectin chaperone calnexin and calreticulin to prevent hydrophobic aggregation and disulphide bonding during folding and to increase the ER retention time for proper protein folding [221]. In addition, removal of the

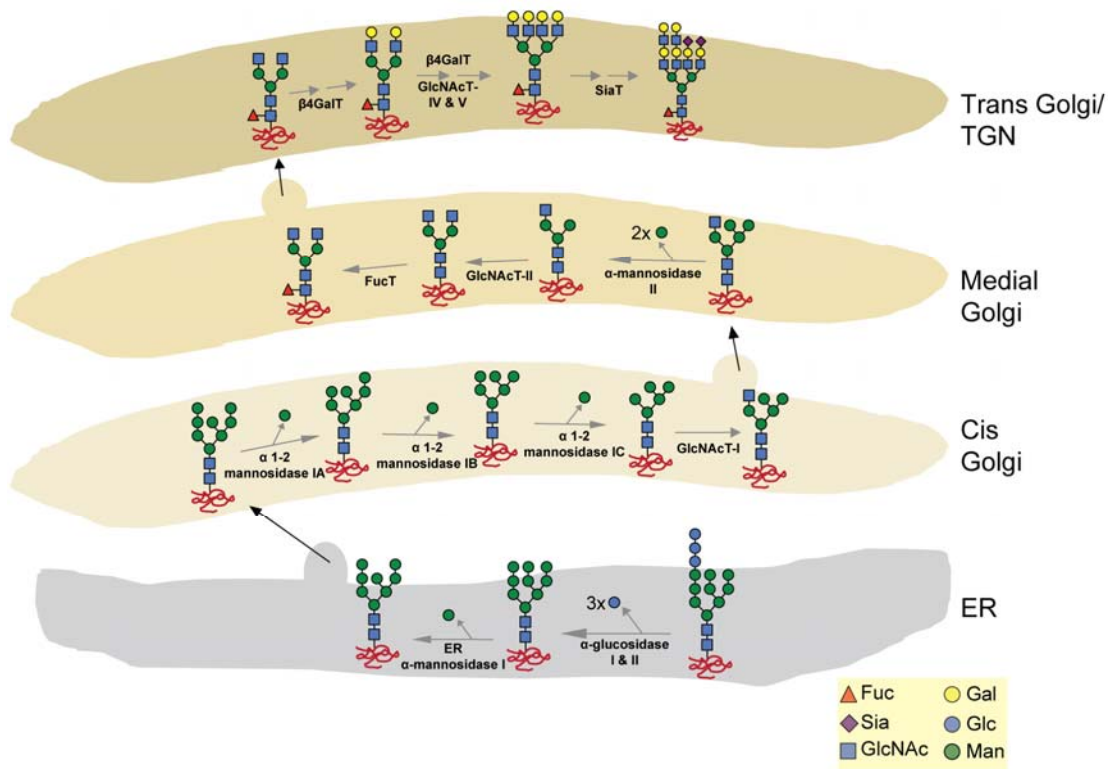
terminal  $\alpha$ 1-2 mannose targets misfolded glycoprotein for proteasomal degradation in a process termed as the ER-associated degradation (ERAD) for protein quality control [221, 222]. This initial step in the ER is conserved in all eukaryotes and has major influence in protein folding and quality control before exiting the ER.

#### *N-glycosylation in the Golgi: Formation of complex N-glycans*

Upon entry at the cis Golgi, N-glycans normally carry eight or nine mannose residues (Figure 1-7). In some vertebrate cell types, a few 'high-mannose' glycans can reach the cell surface [223]. However, almost all N-glycans on glycoproteins are subjected to trimming and extension on their passage through the Golgi. The cis Golgi contains  $\alpha$ 1-2 mannosidases IA, IB and IC which further trims additional mannose residues and generates the  $\text{Man}_5\text{GlcNAc}_2\text{Asn}$  intermediate. This intermediate forms the substrate for the synthesis of hybrid and complex N-glycans by medial Golgi glycosyltransferase GlcNAcT-I that transfers the GlcNAc to  $\text{Man}_5\text{GlcNAc}_2\text{Asn}$ . Incompletely processed N-glycans that did not achieve  $\text{Man}_5\text{GlcNAc}_2\text{Asn}$  configuration cannot undergo further remodeling into hybrid and complex structures. Hybrid N-glycans are formed with the elongation of the GlcNAc arm with galactose and sialic acid while maintaining the remaining five mannose residues.

The majority of N-glycans are complex structure. Complex N-glycans are formed firstly, by the action of  $\alpha$ -mannosidase II at the medial Golgi on  $\text{GlcNAcMan}_5\text{GlcNAc}_2\text{Asn}$  which trims the two mannose residues terminal  $\alpha$ 1-3 mannose and  $\alpha$ 1-6 mannose to form  $\text{GlcNAcMan}_3\text{GlcNAc}_2$  (Figure 1-7). A second GlcNAc is then added to C-2 of the mannose  $\alpha$ 1-6 in the core by GlcNAcT-II to generate the precursor for all biantennary, complex N-glycans. This comprises of two antennae or branches. More branches can be initiated with the addition of GlcNAc to C-4 of the core mannose  $\alpha$ 1-3 by GlcNAcT-IV and C-6 of the core mannose  $\alpha$ 1-6 by GlcNAcT-V to yield tri- and tetra-antennary N-

glycans. The fifth branch can be initiated at C-6 of the core mannose  $\alpha$ 1-3 by GlcNAc-IX. Lastly, another branch can begin at the C-4 of the core mannose  $\alpha$ 1-3 by GlcNAcT-VI. Hence, the resulting biantennary N-glycan can be branched up to six times and subsequently, each branch is extended by the addition of different sugars including galactose, GlcNAc, GalNAc, sialic acid and disaccharide units [224]. These further sugar additions occur mostly at the trans Golgi which expands the array of mature, complex N-glycans. A galactose is often added after GlcNAc and the branch is usually lengthened by tandem repeats of galactose and GlcNAc known as poly-N-acetyllactosamine or polyLacNAc. In addition, fucose can be added in a  $\alpha$ 1-6 linkage to the GlcNAc adjacent to the asparagines in the core. Finally, the “capping” of the glycan chain usually involves the  $\alpha$ -linking of sialic acid residue which protrudes away from the  $\beta$ -linked polyLacNAc structure, allowing these terminal sugars to be presented to glycan binding proteins such as lectins and antibodies to facilitate biological processes.



**Figure 1-7: Schematic of the N-glycosylation pathway.** GlcNAc-T refers to N-acetylglucosamine transferase; FucT refers to fucosyltransferase; SiaT refers to Sialyltransferase; β4GalT refers to β1-4galactosyltransferase.

The processing steps described above occur in predominantly in vertebrates. In contrast, this final hybrid and complex N-glycan structure is not found in lower organisms such as the yeast and *Drosophila*. The yeast do not truncate the  $\text{Man}_8\text{GlcNAc}_2\text{Asn}$  that enter the cis Golgi, but further add mannose residues to produce the oligomannose with many branched mannose residues known as the yeast mannan [171]. Most *Drosophila* N-glycoproteins contains high mannose N-glycans that sensitive to cleavage by endoglycosidase H (EndoH) [225, 226]. Although complex N-glycans can be found, they have fewer sugars compared to the vertebrates'. Similarly, the N-glycans of *C. elegans* comprise of high mannose

and complex structures but with fewer sugars and may include phosphorylcholine attachment to GlcNac [227].

#### *N-glycans in health and disease*

Mutant cells or organisms with perturbations in N-glycosylation have shed light to biological functions of N-glycans, their effects on the biochemistry of glycoproteins and on how the glycosylation pathway operates. For instance, defects in N-glycosylation have been linked to a group of human diseases termed as the congenital disorders of glycosylation (CDG) [174]. Mouse mutants of the N-glycosylating machinery in particular have shed huge insights on the functions of N-glycans. For example, the deletion of the *Mgat1* gene that encodes GlcNAcT-I inhibits the formation of complex and hybrid N-glycans. While this deletion in *Lec1* cultured cells does not affect viability and growth, mice with this deletion die early during embryonic development, suggesting the relevance of the complex N-glycans in growth and development of an organism. Indeed, complex N-glycans are required to retain the growth factor and cytokine receptors at the cell surface as those lacking of branches of complex N-glycans have shorter cell surface residence time and attenuated signaling. In addition, mice lacking of sialyltransferases, fucosyltransferases, or branching N-GlcNAcTs that produce complex N-glycans suffer from defects in immunity or neuronal cell migration, inflammation or lung emphysema. Furthermore, increased branching of N-glycans has been observed during cancer formation and progression, which has been found to be attributed to increased transcriptional expression of GlcNAcT-V (*Mgat5*). Thus, the N-glycosylation machinery have been studied as a target for the design of cancer therapeutics [228].

#### **1.3.4.2 O-glycosylation**

O-glycosylation is defined by the addition of glycan sugars onto serine (Ser) and threonine (Thr) residues of glycoproteins. Several sugar types can be added to the

Ser/Thr to yield different classes of O-linked glycans, such as  $\alpha$ -linked O-GalNAc,  $\alpha$  or  $\beta$ -linked O-galactose,  $\alpha$  or  $\beta$ -linked O-glucose,  $\alpha$ -linked O-fucose,  $\alpha$ -linked O-mannose,  $\beta$ -linked O-GlcNAc and  $\beta$ -linked O-xylose [229-232]. Among these, O-GalNAc glycans is the most abundant type whereby O-GalNAc glycosylation is found in more than 10% of human glycoproteins and more than 50% of the glycoproteins passing through the secretory pathway. Interestingly, this process only occurs in eumetazoans while N-glycosylation is present in lower eukaryotes [233]. Traditionally considered as the classical O-GalNAc glycoproteins are mucins and mucin-like proteins that contain PTS (Pro, Thr and Ser) repeats carrying dense clusters of O-glycans in a heterogeneous manner [234, 235]. Hence, O-GalNAc glycosylation are often termed as mucin O-glycosylation. However, recently, it is increasingly evident that O-GalNAc glycans are widely distributed in regions of many different proteins that do not have mucin-like features [236-239].

#### *O-glycosylation initiation is mediated by ppGalNAc-Ts*

The initial step O-GalNAc glycosylation involves the transfer of GalNAc sugar from UDP-GalNAc to the hydroxyl of Ser/Thr residues  $\alpha$ -linked with an O-glycosidic bond which is catalyzed by a ppGalNAc-T (Figure 1-8). In humans, up to 20 different ppGalNAc-T isoforms are localised in the Golgi with distinct but partially overlapping substrate specificities [240-242]. ppGalNAc-Ts are evolutionary conserved in all eukaryotes with numbers appear to increase across evolution: *C. elegans*, *Drosophila* and humans have 9, 12 and 20 GalNAc-T isoforms respectively [207, 243, 244]. This is in contrast to other types of protein O-glycosylation which usually involves only one or two isoenzymes. Hence, O-GalNAc glycosylation is arguably the most complex form of protein glycosylation because of the incomparable cell- and protein-specific regulation of the O-GalNAc glycan attachment sites and eventually, the nature of the O-glycoproteome [241].

Deciphering the specificities of each of the 20 GalNAc-T isoforms is an arduous task. At current status, the defined amino acid sequences for GalNAc addition remain unknown although it is characterized that proline residues near the sites of addition are usually promote GalNAc addition, possibly by increasing exposure of Ser/Thr residues in a  $\beta$ -turn conformation [240]. In addition, unique to other glycosyltransferases, it has an additional lectin-like domain at the carboxyl terminus that binds existing GalNAc residues on glycoproteins [245]. This influences the further GalNAc addition by other GalNAc-Ts in the glycosylated protein substrate. Phylogenetic analysis allowed the classification of GalNAc-Ts into subfamilies of similar functions [243, 246]. Subfamily members may have similar substrate selectivity but generally show tissue specific expression, resulting in partial functional redundancy. The catalytic sites of GalNAc-Ts appear to be the driver for substrate selectivity as these residues are conserved within isoforms of different organisms while there is poor conservation between isoforms. This suggests that during evolution, orthologous GalNAc-Ts maintain similar substrate repertoire and newly evolved GalNAc-Ts acquire new substrate preferences, allowing a diverse range of substrates to be O-glycosylated. It also means that through the differential control of the GalNAc-Ts present, it provides an effective mechanism select for the repertoire of proteins to be O-glycosylated in the cell. The localisation of the GalNAc-Ts is also critical for O-glycan synthesis. It was found that different GalNAc-T isoforms have been found to be located throughout the Golgi in HeLa cells [247].

Only recently, *in vivo* isoform-specific O-glycosylation has been identified for some proteins. For instance, GalNAc-T3 is essential to glycosylate a specific site in Fibroblast growth factor 23 (FGF23) and prevent inactivation by proprotein convertase in humans. Loss of GalNAc-T3 function leads to Familial tumoral calcinosis [248]. Similarly, GalNAc-T2 is required for site-specific O-glycosylation of angiopoietin-like protein 3 to prevent proprotein convertase inhibition [249]. In mice, GalNAc-T1 is important for O-glycosylation of Osteopontin and Bone sialoprotein [250]. However, for most of the other O-

GalNAc glycosylated proteins, the specific sites and ppGalNAc-T enzymes that act on it remains elusive. It was predicted that over 700 proteins could be potentially regulated by site-specific O-glycosylation and proprotein convertase processing (Gram Schjoldager et al, 2011). Thus, there are obviously many undiscovered site-specific O-glycans with important biological roles that awaits to be uncovered.

### *The Tn antigen*

GalNAc addition to glycoproteins generates the Tn antigen (GalNAc $\alpha$ 1-Ser/Thr), which in the terminal form represents the simplest structure of O-GalNAc glycan (Figure 1-8). The Tn antigen is normally not expressed in normal tissues as it is rapidly modified by downstream glycosyltransferases upon GalNAc addition. Thus, the glycan is antigenic. Tn expression is associated with a number of human disorders and diseases such as cancer, Tn syndrome and immunoglobulin A (IgA) nephropathy [251]. In particular, the high prevalence of Tn in cancers of multiple tissue types led to its classification as a tumor-associated cancer antigen. More than 70-90% of cancers of the breast, colon, lung, bladder, cervix, ovary, stomach, and prostate exhibit Tn expression [252-254]. Tn expression also correlates with metastatic potential and poor prognosis of cancer patients, suggesting its significant influence on tumor progression [251]. This led to extensive investigations as a cancer biomarker [252-254]. The mechanisms of how Tn expression links to cancer progression are not well understood at the moment. It has been suggested that Tn antigen present on Mucin1 may lead to immunosuppressive effects by binding to macrophage galactose type lectin (MGL) on immature and tolerogenic dendritic cells, hence allowing the tumor to avoid immunosurveillance [255]. Furthermore, various cell surface receptors such as low-density lipoprotein (LDL) receptor [256, 257], transferrin receptor [258], P-selectin glycoprotein ligand-1 (PSGL-1) [259] and dystroglycan [260] have been observed to exhibit Tn expression or incomplete O-glycosylation, it is postulated that Tn expression perturbs cell surface protein expression and/or



biological activity, hence affecting cell proliferation or adhesive/ migratory properties of cancer cells. Indeed, our group has recently found that increased Tn expression promotes adhesion and migration in cells [194].

### *Synthesis of O-GalNAc glycan Core structures*

The transfer of the initiating O-GalNAc to the protein forms the branchpoint of O-GalNAc glycosylation. The initiating GalNAc can serve as an acceptor of at least three other glycosyltransferases which adds a galactose, GlcNAc or sialic acid and generating the Core 1, Core 3 and sialyl-Tn antigen respectively. The first two occurs in normal cells while the sialyl-Tn (Sia $\alpha$ 2-6GalNAc $\alpha$ Ser/Thr) structure, like Tn antigen, is prevalent in diseases and often observed in cancers [261-263]. In normal cells, including the previously mentioned Core 1 and 3, a total of eight different core structures could subsequently be derived by the action of different core forming enzymes, whereby Core 1 through 4 constitute the more common structures. It is of note that in contrast to other glycosylation reactions such as N-glycosylation (Section 1.3.4.1) or O-mannosylation, no lipid-linked intermediates are involved in O-GalNAc glycan biosynthesis and unlike N-glycosylation, the initiating process normally occurs at the cis Golgi instead of the ER. Lastly, in the subsequent processing steps of O-GalNAc glycans in the Golgi do not encompass any glycosidase trimming of the glycan chain.

Core 1 (Gal $\beta$ 1-3GalNAc-Ser/Thr) structure is generated by the addition of galactose by a Core 1  $\beta$ 1-3 galactosyltransferase (also known as C1GalT1 or T-synthase) and it forms the precursor for Core 2 O-glycan. This is in contrast to Core 3 structure (GlcNAc $\beta$ 1-3GalNAc-Ser/Thr) which forms the precursor for Core 4 O-glycan. Core 1 synthesis is most common occurring as it is generated in most cell types due to the ubiquitous expression of C1GalT1 [264], thus is essential for organism's functioning. Indeed, the disruption of C1GalT1 in mice is embryonic lethal, highlighting its importance in organism development [265].

The activity of C1GalT1 requires a specific molecular chaperone termed as Cosmc, an ER protein that mediates proper folding of C1GalT1 and preventing its ubiquitin degradation in the ER [266]. Absence of functionality of either cosmc or C1GalT1 results in defects in Core 1 synthesis and high expression of Tn antigen. Indeed, loss of Cosmc is associated with Tn-related human diseases including IgA nephropathy and a rare condition called the Tn syndrome [251]. Although it was proposed that loss of Cosmc could explain high Tn expression in neoplasm [267], it could not explain all incidences [194]. Core 1 O-glycan in its terminal form is known as the T antigen. Like the Tn antigen, its expression is uncommon in normal tissues and observed in cancer and inflammatory bowel disease [254]. However, it is rare that the T antigen is exposed without further substitution but usually substituted by sialic acid at the C-3 of galactose and then C-6 of GalNAc, forming sialyl-T antigen and disialyl-T antigen (DiSia<sub>3,6</sub>Core 1) respectively [268]. The addition of sialic acid also prevents further modification of Core 1 by adding a negative charge to the glycan. Sialyl-Core 1 glycans are often observed on the cell surfaces of many leukemia and tumor cells [197].

Normally in many tissues including the intestinal mucosa, Core 1 is branched by the addition of GlcNAc to GalNAc of the Core 1 structure by Core 2  $\beta$ 1-6 N-acetylglucosaminyltransferase or  $\beta$ 6-GlcNAcT/C2GnT to yield the Core 2 O-glycans (GlcNAc $\beta$ 1-6(Gal $\beta$ 1-3)GalNAc $\alpha$ Ser/Thr) [269]. Alternatively, the Core 1 structure can be elongated to form extended Core 1 O-glycans by GlcNAc addition to the galactose of Core 1 by  $\beta$ 3-GlcNAcT-3. This prevents further substitution by C2GnT as the enzyme is highly specific to unmodified Core 1 structure. There are at least three isoforms of C2GnT: C2GnT1-3 and they can be subcategorized into two major types: leukocyte-type/L-type comprising of C2GnT-1 and -3 and mucin-type/M-type comprising of C2GnT-2. The L-type enzymes synthesize only the Core 2 structure while the M-type is also involved in Core 4 synthesis and other GlcNAc $\beta$ 1-6-linked branches. Both isoforms subtypes also show differential tissue expression whereby the L-type is ubiquitous in many tissue types particularly in the bone marrow and thymus tissues (including

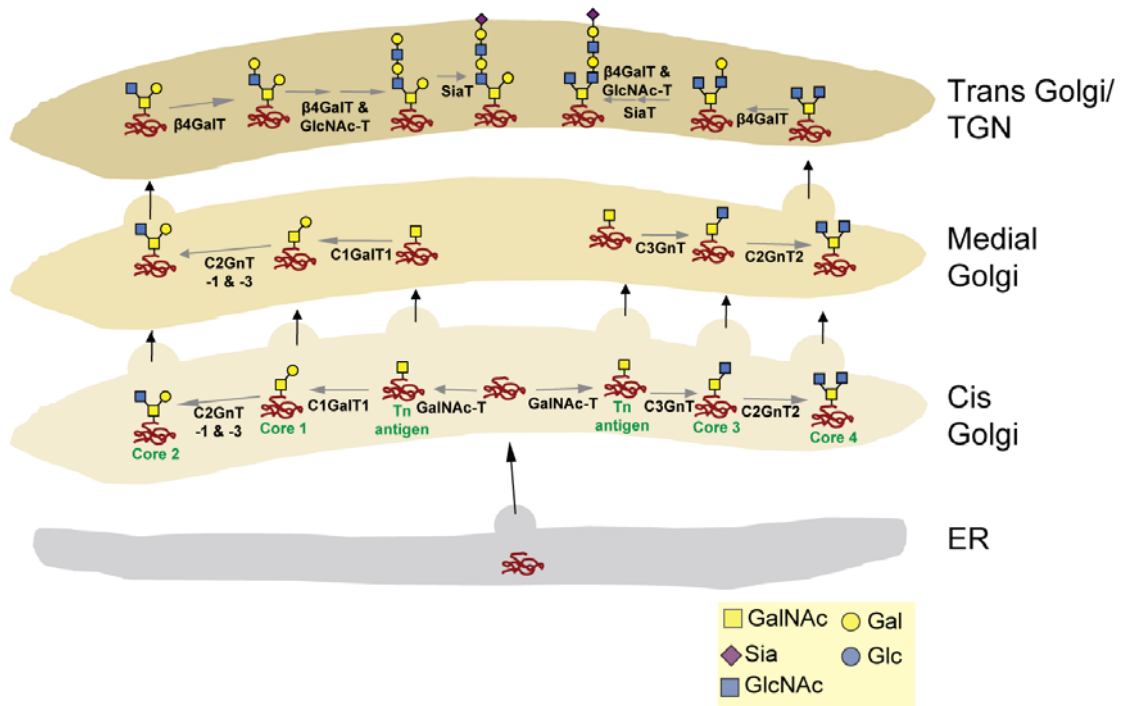
product B- and T-cells) while the M-type is restricted only in mucin-secreting cell types such as the gastrointestinal tissues. The synthesis of Core 2 glycans was found important for immune system physiology. Its expression is regulated during lymphocyte activation and cytokine stimulation [270, 271]. Core 2 glycan expression is also correlated with tumor progression whereby leukemia and other cancer types exhibit abnormally upregulated Core 2 levels [272]. It is proposed that the branched nature of Core 2 glycan can shield the exposure of mucin peptide epitopes. Interestingly, HIV also upregulates Core 2 formation in T-cells through C2GnT-1 expression to induce Galectin-1 mediated T-cell death [273].

Unlike Core 1 and 2 which is generated in most tissue types, Core 3 O-GalNAc glycans (GlcNAc $\beta$ 1-3GalNAc $\alpha$ Ser/Thr) appears to be synthesized in the mucous epithelia of the gastrointestinal and respiratory tracts as well as the salivary glands. This is due to the high expression of Core 3  $\beta$ 1-3 GlcNAc-T (also known as C3GnT) in these tissues [274, 275]. Loss of C3GnT expression in gastrointestinal cancers have been proposed to upregulate sialyl-Tn antigen and Core 1 O-glycans and this switch serves as a good biomarker for colonic and rectal cancers [276, 277]. C3GnT catalyses the addition of GlcNAc to the initiating GalNAc sugar. Generally, unmodified Core 3 is subsequently branched by C2GnT-2 to form Core 4 (GlcNAc $\beta$ 1-6(GlcNAc $\beta$ 1-3)GalNAc $\alpha$ Ser/Thr) and extended to complex chains. Core 3 may also be substituted with sialic acid in a  $\alpha$ 2-6 linkage to the GalNAc sugar or with galactose in  $\beta$ 1-4 linkage to GlcNAc of the Core 3 structure.

#### *Synthesis of complex O-GalNAc glycans*

Beyond the Core glycan formation involves primarily elongation steps. The galactose residue of the Core 1 glycan and both galactose and GlcNAc branches of the Core 2 structure may be extended by elongation GlcNAc-Ts and galactosyltransferases to form repeating units of GlcNAc $\beta$ 1-3Gal $\beta$ 1-4 (poly-N-acetylglucosamine) sequences. Elongation reactions can also encompass the formation of GalNAc $\beta$ 1-4GlcNAc- (LacdiNAc) and Gal $\beta$ 1-3GlcNAc- sequences

that are less common. The terminating structures of the O-glycan chains are commonly blood group A (GalNAc $\alpha$ 1-3(Fuc $\alpha$ 1-2)Gal-), blood group B (Gal $\alpha$ 1-3(Fuc $\alpha$ 1-2)Gal-), blood group O (Fuc $\alpha$ 1-2Gal-), Lewis antigens (Gal $\beta$ 1-3(Fuc $\alpha$ 1-4)GlcNAc-, Gal $\beta$ 1-4(Fuc $\alpha$ 1-3)GlcNAc-, Sia $\alpha$ 2-3Gal $\beta$ 1-4(Fuc $\alpha$ 1-3)GlcNAc-, Fuc $\alpha$ 1-2Gal $\beta$ 1-4(Fuc $\alpha$ 1-3)GlcNAc-) as well as sialic acids, fucose and sulphate.



**Figure 1-8: Schematic of the O-glycosylation pathway.** Biosynthesis of core 1 and 2 O-glycans which occurs in most tissues is shown in the left. Biosynthesis of core 3 and 4 O-glycans that is restricted to mucous epithelia is shown on the right. GalNAc-T refers to polypeptide N-acetyl galactosamine transferase; C1GalT1 refers to  $\beta$ 1-3 galactosyltransferase; C2GnT refers to Core 2  $\beta$ 1-6 N-acetylglucosaminyltransferase; C3GnT refers to Core 3  $\beta$ 1-3 N-acetylglucosaminyltransferase; GlcNAc-T refers to N-acetylglucosaminyltransferase; SiaT refers to Sialyltransferase;  $\beta$ 4GalT refers to  $\beta$ 1-4-galactosyltransferase.

### *Functions of O-glycans*

O-GalNAc glycosylation is an essential process particularly to eumetazoans because of its importance in the formation of cell surface and secreted mucins in mucous of the ocular, gastrointestinal, respiratory, genitourinary tracts. The O-GalNAc glycans of the mucous glycoproteins generates barrier that is essential for tissue lubrication, protection from physical and chemical damage, and preventing pathogen infection [235, 278]. This is due to the hydrophilic and negatively charged nature of O-glycans, which promote water and salt binding, contributing to the viscosity and adhesiveness of mucous. The viscosity also allows bacteria and particles to be trapped and removed easily. High density O-glycan addition could also shield the underlying protein epitopes from recognition by antibodies and proteases. For instance, more than 80% of the molecular weight of the mucin glycoprotein comprise of O-glycans and this protects from protease degradation in the gut [279]. O-glycans on cell surface receptors are also important for regulating receptor stability and expression levels [280]. O-GalNAc glycans are particularly important for the functioning of the immune system. For instance, the attachment of leukocytes to the capillary endothelium during lymphocyte homing or extravasation of leukocytes to the surrounding tissues during inflammation is mediated by the interaction of P-selectin with sialyl-Lewis<sup>X</sup> attached on Core 2 O-glycans. Loss of C2GnT-1 expression, which generates the Core 2 glycan, in mice severely disrupts the functioning of the immune system [281]. This system is taken advantage by cancer cells for metastasis. They commonly express sialyl-Lewis<sup>X</sup> and use selectin-binding as a mechanism to invade tissues [282].

#### **1.3.5 Regulation of mammalian glycosylation**

Although the biological functions of glycans are well studied, the mechanisms regulating the glycan structure variation are still yet to be fully understood [159]. Unlike other biopolymers such as nucleic acids and amino acids, glycan synthesis is not template-driven [177] but constructed by the combined and sequential

action of the numerous glycosyltransferases and glycosidases in the secretory apparatus. Although generally one enzyme catalyses one saccharide linkage applies to almost all the steps in glycan biosynthesis, the existence of numerous enzyme isoforms as well as hierarchical and competing relationships between the enzymes further increases the complexity and heterogeneity of glycan formation in different cell types and physiological processes.

Given the dynamic nature of glycosylation in the secretory pathway, multiple mechanisms have been proposed to regulate glycan formation. Gene expression of glycosylating enzymes appears to have a major impact on glycan construction. This is reflected by differences in RNA expression signatures of the glycosylation machinery in different cell types and developmental stages [283]. However, gene transcription cannot fully explain all glycan variations in different physiological conditions such as the rapid cell surface glycan changes of differentiating stem cells [284] and cell-cell and cell-matrix changes during cell migration [159].

Glycan expression can be regulated at the post-transcriptional and post-translational levels. For instance, some glycosyltransferases require to be glycosylated or interaction with molecular chaperones to be active, suggest a possible mechanism for glycan regulation. Mentioned previously, the activity of C1GalT1 requires the presence of its molecular chaperone Cosmc and loss of Cosmc leads to failure of Core 1 O-glycan formation [266]. The conditions of the enzymatic environment such as pH could also have some effects on activity [240, 285]. A potential mechanism proposes the phosphorylation of the glycosylating enzymes and modulating their trafficking and substrate access. However, they are mostly type II transmembrane proteins and have a short cytoplasmic tail, the likelihood of a phosphorylation motif in this short protein sequence is low. Another putative mechanism involves the cleavage of the glycosylating enzymes from their membrane anchored locations and abolish their glycan forming activities. This hypothesis is supported by the findings of catalytic domain fragments of glycosyltransferases in most body fluids which appears to be

upregulated during physiological settings such as inflammation [286]. However, it remains elusive the range of enzymes affected and the exact purpose of the extracellular release given that the concentrations of extracellular nucleotide sugar donors are too low for enzyme substrate binding affinities.

Most glycosylation reactions take place in the Golgi and the majority of the glycosylation machinery in the cell resides there. The Golgi is known to host more than 250 glycosyltransferases, glycosidases and nucleotide sugar transporters. With such an astonishing number of proteins in a confined space in addition to the competitive nature of various glycosyltransferases, it is remarkable that the Golgi can synthesize the various glycan structures with precision and speed even without a direct quality control system as in the ER. There must be multiple systems to correctly coordinate and control the glycan outcome. Spatial compartmentalization by Golgi cisternae allow the concerted action of the glycosylating enzymes and provide the optimal environment for them to function, and thus plays a major role in glycan formation [287]. Hence, the factors that affect the structure and organization of Golgi membranes as well as the luminal Golgi environment are likely to execute a major influence on glycan synthesis.

pH changes in the Golgi lumen was found to alter glycosylation by affecting the localisation and trafficking of glycosyltransferases [288, 289], the activity of the enzymes [285], the formation of functional heteromeric complexes [290] and substrate and sugar transport [291-293]. pH disruption also often result in perturbed Golgi morphology [291, 292], which could also affect glycan synthesis by physically segregating the enzymes from the substrates or from each other. In the first case, pH increases in the Golgi lumen was found to induce mislocalisation of the  $\alpha(2,3)$ -sialyltransferase from the trans Golgi into endosomal compartments and led to inhibition of terminal  $\alpha(2,3)$ -sialylation [289]. It was postulated to be due to the impairment of enzyme retrieval to their correct compartments. Enzyme activity also depends on the optimal pH of the environment. This is not surprising given that there is a 0.7 unit pH reduction

from cis to trans Golgi and glycosylating enzymes involved in different steps of glycan processing are localised separately. It was observed that by increasing pH from 6.5, the optimal pH for  $\beta$ 1-4-galactosyltransferase and  $\alpha$ 2,3-sialyltransferase, to pH7.0-7.2, their activities reduced significantly by 50-60% [285]. Heteromeric complex formation of glycosylating enzymes participating in common pathways is required for efficient glycan synthesis and it was found recently that defective acidification inhibits complex formation [290]. An anion channel named Golgi pH regulator (GPHR) was recently identified to regulate Golgi pH. Mutant cells lacking of GPHR exhibit retarded transport of glycoproteins, coupled with the expression of truncated glycoproteins and glycolipids [291, 292]. Disrupted Golgi luminal pH has been observed in numerous cancer cell types and it correlates with perturbed glycosylation [294], suggesting that aberrant glycosylation in cancer cells are partially due to Golgi pH changes.

Other factors in the Golgi lumen that is vital for proper glycan formation includes the biosynthesis and availability of nucleotide sugar donors. This depends on the expression levels and efficiencies of the nucleotide sugar transporters and pyrophosphorylases that work in concert for the import of nucleotide sugar diphosphates into the lumen [295]. Inhibition of either protein can abolish the addition of specific sugar types onto glycan structures [296, 297]. Interestingly, loss of sugar transporters also slow down cargo passage through the Golgi and accumulate glycoproteins with shortened glycans in the Golgi which do not proceed to the cell surface. This was observed when sialic acid and fucose transporters were depleted or mutated in Lec2 CHO cells. Eventually, ER stress pathways were also activated, possibly to prevent further accumulation of proteins [298]. Unlike the pH of the Golgi, the impact of this augmented form of glycosylation on mammalian physiology is not known. Nevertheless, it remains an avenue for which glycans are modulated.

Glycosyltransferases are mostly constitutively active in nature; hence direct modulation of their activities in the Golgi lumen would also alter glycan



expression. Recent discoveries identified inhibitors of glycosyltransferase activities. An example is the GlcNAcT-I Inhibitory Protein (GnT1IP) which is a testis-specific glycoprotein that binds and blocks the activity of GlcNAcT-I. GlcNAcT-I is required to initiate the branching of N-glycans to form complex and hybrid structure. The interaction of GnT1IP blocks this pathway and also mislocalises GlcNAcT-I from its medial Golgi position to earlier compartments, finally leading to increased expression of high mannose glycans [299]. High mannose N-glycan increases cell adhesive properties and hence was speculated to facilitate Sertoli-germ cell attachment during spermatogenesis. Another example is the transmembrane BAX inhibitor motif-containing family (TMBIM) of proteins which inhibit Gb3 synthase which synthesizes glycolipid Gb3, receptor of Shiga toxin [300].

Maintenance of the Golgi structure and organization is a major aspect in glycan regulation. A main highlight of this is found in the mutations in the conserved oligomeric Golgi (COG) complex. The COG complex comprises of eight subunits which are essential for vesicle tethering of retrograde carriers and scaffolding for the Golgi structure. Mutations of members in the COG complex resulted in glycan changes [301]. For instance, mutation in COG1 member was identified in a CHO mutant IdIC which has multiple glycosylation defects in N- and O-glycoproteins as well as glycolipids [302]. More importantly, defective glycosylation that result from COG mutations are the cause of genetic diseases known as the congenital disorders of glycosylation [303-306].

Both the network and cisternal organization of the Golgi are essential for proper glycan formation. In the former, loss of lateral linking between Golgi stacks led to variable levels of glycosylating enzymes among the fragmented mini-stacks which was due to reduced lateral motility of the enzymes [50]. On the other hand, cisternal unstacking was observed to induce N-glycosylation defects in Fms, an M-CSF cytokine receptor for maintaining macrophages in an anti-inflammatory state. Hypo-N-glycosylated Fms remains in the immature form and accumulates

at the Golgi. This impacts macrophage functioning and was proposed as a mechanism utilised by HIV to induce immunodeficiency (Hiyoshi M et al, 2011). Changes in cisternal levels of specific glycosyltransferases by relocation also impacts glycan output. We have reported that a number of O-glycosylation initiation enzymes ppGalNAc-Ts are rapidly re-localized from the cis Golgi to ER upon the growth factor stimulation and Src activation [193]. The process is mediated by COPI vesicles. Relocation to the ER resulted in marked increase in O-glycosylation initiation, leading to high densities of O-GalNAc added to the O-glycoproteins and hence promotes the expression of the terminal O-GalNAc or Tn antigen. The process has implications in metastasis and invasion in cancer as it promotes cell adhesion and migratory properties. Indeed, this relocation event is observed quite frequently in at least 60% of breast carcinomas and various cancer cell lines [194].

## 1.4 OBJECTIVES

From the above mentioned indications, protein glycosylation modifies multiple proteins and can have a profound effect on protein structure and functions. The process ultimately influences multiple biological processes that are important for the cell and organism physiology. The bulk of glycan synthesis occurs at the Golgi where they diversify and become complex structures. As glycans are constructed in a series of sequential glycosylation reactions at the Golgi, it is without doubt that the Golgi organization is critical for proper glycan construction.

Despite of its complex structure, the mammalian Golgi is actually highly dynamic and its morphology changes under different physiological settings. Several regulatory mechanisms that control Golgi organization and functions have recently been discovered. For instance, ERK controls the Golgi re-modeling and re-orientation to the leading edge of the cell for cell migration [116] while PKD controls cargo flux out of the TGN [139, 140]. This suggests that the complex Golgi organization is likely to be under the influence of multiple regulators. However, the molecular regulators of Golgi organisation have not been completely identified and how they affect glycosylation remains poorly understood. Identification of these regulators would provide further understanding to the mechanisms involved in controlling Golgi organization and glycosylation in health and disease. Ultimately, it has implications in guiding the design and development of therapeutics for diseases associated with aberrant Golgi morphology and function [307, 308]. Finally, the data could also aid in the study of the long-standing question of Golgi structure-function relationship. Therefore, the objectives of this study encompass:

( I ) Identification of the genetic basis of Golgi organization and glycosylation function using RNAi screening.

Current studies on Golgi regulation often centered on a few genes and most did not attempt to characterize their role in glycosylation. Here I aim to understand Golgi regulation under the influence of multiple genes in the genome. To fulfill this objective, RNAi screening is the method of choice as it offers the possibility of systematically probing the loss-of-function effects of a large number of genes in the genome. In this study, a kinome- and phosphatome-wide siRNA screen was employed given that signaling proteins are the main pivots for most regulatory events in the cell. The screen involved individual silencing of 948 known and putative human signaling genes and analysing their impact on the Golgi morphology from markers of three different compartments of the Golgi. Automated machine learning, known as support vector machine learning (SVM), was used to classify and quantify the various Golgi morphological phenotypes. Genes that affect any of the markers significantly were identified as regulator of Golgi organization and further tested in secondary assays for their effects on glycosylation. Secondary assays involved the use of several lectins that recognize different glycan structures to characterize glycan changes.

( II ) Characterization of the regulatory mechanisms of O-GalNAc glycosylation initiation in cancer.

The second part of the thesis sought to further understand the regulatory mechanisms of a particular glycosylation event. O-glycosylation initiation normally occurs at the Golgi and is mediated by the GalNAc glycosyltransferases GalNAc-Ts. Our previous report demonstrated that O-glycosylation initiation can take place in the ER when GalNAc-Ts are induced to relocate from the Golgi (Gill, 2010). The process promotes the expression of the aberrant glycan, Tn antigen, that is prevalent in tumors of multiple tissue types. How this process is activated remains unclear. Hence, identification of the molecular players with

RNAi screening would gain further insights to the regulation of this process and eventually could provide potential targets for Tn-related cancer therapy. A potent regulator of this pathway was characterized in detail to understand the regulatory mechanisms leading to GalNAc-T relocation and its role in cancer progression.

## **CHAPTER TWO: MATERIALS AND METHODS**

## 2.1 MATERIALS

### 2.1.1 General reagents and chemicals

The general reagents and chemicals used in this study and their corresponding sources are listed in alphabetical order in Table 2.1.

**Table 2.1: List of general reagents and chemicals**

<b>Reagent/Chemical</b>	<b>Source</b>
<b>Agarose</b>	Bio- Rad
<b>Ampicillin</b>	Sigma Aldrich
<b>β-mercaptoethanol</b>	Merck
<b>Dulbecco's Modified Eagle Medium (DMEM)</b>	Gibco
<b>Dithiothreitol (DTT)</b>	Sigma-Aldrich
<b>DNA ladder – 100bp</b>	New England Biolabs
<b>DNA ladder – 1kb</b>	New England Biolabs
<b>Deoxyribonucleotides (dNTPs)</b>	New England Biolabs
<b>Ethidium bromide</b>	Bio-rad
<b>Fetal bovine serum (FBS)</b>	Hyclone
<b>Formaldehyde</b>	Sigma Aldrich
<b>GelRed™ Nuclei Acid Gel Stain</b>	Biotium
<b>Geneticin ® Reagent (G418)</b>	Invitrogen
<b>HiPerfect transfection reagent</b>	Qiagen
<b>Hoescht 33342</b>	Invitrogen
<b>Kanamycin</b>	Sigma Aldrich
<b>Luria Broth (LB) medium</b>	Biopolis Shared Facilities (A*STAR)
<b>NP-40 Alternative</b>	Sigma Aldrich
<b>OptiMEM</b>	Invitrogen
<b>Penicillin-Streptomycin stock solution (100x)</b>	Invitrogen
<b>Phosphate saline buffer</b>	Biopolis Shared Facilities (A*STAR)
<b>Phosphatase inhibitor cocktail tablets (Phos-STOP)</b>	Roche
<b>Poly L- lysine</b>	Sigma Aldrich
<b>Protein Ladder (Precision Plus Protein™ Dual Color)</b>	Biorad
<b>Protease inhibitor cocktail tablets (Complete EDTA free)</b>	Roche
<b>Sodium Dodecyl Sulfate (SDS)</b>	Biorad
<b>Sodium Fluoride</b>	Sigma Aldrich
<b>Sodium orthovanadate</b>	Sigma Aldrich

<b>TRIS- Base</b>	Sigma Aldrich
<b>TRIS- HCL</b>	Sigma Aldrich
<b>Triton ® X-100</b>	Merck
<b>Trypsin</b>	Biopolis Shared Facilities (A*STAR)
<b>Tryptone-yeast extract broth (TY) medium</b>	Biopolis Shared Facilities (A*STAR)
<b>Tween ® 20</b>	Sigma Aldrich

### 2.1.2 Enzymes

All restriction enzymes were purchased from New England Biolabs. KOD DNA polymerase was purchased from Calbiochem. Reverse transcriptase SuperScript-III, BP Clonase II and LR Clonase II were purchased from Invitrogen.

### 2.1.3 Antibodies

Table 2.2 shows the list of primary and secondary antibodies used in this study.

**Table 2.2: List of primary and secondary antibodies**

<b>Primary Antibody</b>	<b>Source</b>
<b>Actin monoclonal antibody (mouse)</b>	Abcam
<b>Arf1 polyclonal antibody (mouse)</b>	Novus Biologicals
<b>Beta COP polyclonal antibody (rabbit)</b>	Abcam
<b>Cosmc polyclonal antibody (rabbit)</b>	Abcam
<b>C2GNT1 polyclonal antibody (rabbit)</b>	Abcam
<b>ERK8 polyclonal antibody (rabbit)</b>	Sigma Aldrich
<b>FLAG monoclonal antibody (mouse)</b>	Sigma Aldrich
<b>GFP polyclonal antibody (rabbit)</b>	Abcam
<b>Giantin polyclonal antibody (rabbit)</b>	Abcam
<b>PY20 monoclonal antibody (mouse)</b>	Abcam
<b>TGN46 polyclonal antibody (sheep)</b>	AbD Serotec
<b>Tubulin monoclonal antibody (mouse)</b>	Abcam



<b>GalNAc-T1 monoclonal antibody (mouse)</b>	U. Mendel and H. Clausen (University of Copenhagen, Copenhagen, Denmark)
<b>GalNAc-T2 monoclonal antibody (mouse)</b>	
<b>Tn monoclonal antibody (mouse)</b>	
<b>Secondary Antibody</b>	<b>Source</b>
<b>AlexaFluor® 488 anti-rabbit</b>	Invitrogen
<b>AlexaFluor® 488 anti-mouse</b>	Invitrogen
<b>AlexaFluor® 594 anti-rabbit</b>	Invitrogen
<b>AlexaFluor® 594 anti-mouse</b>	Invitrogen
<b>AlexaFluor® 594 anti-sheep</b>	Invitrogen
<b>AlexaFluor® 594 Streptavidin</b>	Invitrogen
<b>AlexaFluor® 647 anti-rabbit</b>	Invitrogen
<b>AlexaFluor® 647 anti-mouse</b>	Invitrogen
<b>Anti-rabbit IgG, peroxidase-linked antibody</b>	GE Healthcare
<b>Anti-mouse IgG, peroxidase-linked antibody</b>	GE Healthcare

#### 2.1.4 siRNAs

All siRNAs used in this study were obtained from Dharmacon, now Thermo Fisher.

#### 2.1.5 Drugs and recombinant proteins

Table 2.3 shows the list of drugs and recombinant proteins used in this study.

**Table 2.3: List of drugs and recombinant proteins**

<b>Drugs</b>	<b>Source</b>
<b><math>\alpha</math>-armanitin</b>	Tocris Bioscience
<b>Brefeldin A (BFA)</b>	Merck
<b>FR180204</b>	Tocris Bioscience
<b>Golgicide A (GCA)</b>	Sigma Aldrich
<b>Imidazole</b>	Sigma Aldrich
<b>IPA3</b>	Tocris Bioscience
<b>Latrunculin B</b>	Sigma Aldrich
<b>Monensin</b>	Sigma Aldrich
<b>Nocodazole</b>	Sigma Aldrich
<b>Ro31-8220</b>	Calbiochem
<b>SP600125</b>	Tocris Bioscience
<b>Recombinant proteins</b>	<b>Source</b>
<b>Platelet-derived growth factor (PDGF)</b>	R & D systems
<b>Epidermal growth factor (EGF)</b>	R & D systems
<b>Insulin growth factor (IGF-1)</b>	R & D systems
<b>Transforming growth factor beta (TGF-B)</b>	R & D systems

### **2.1.6 Lectins**

*Helix Pomatia* lectin (HPL) conjugated with 647nm fluorophore was purchased from Invitrogen. All other lectins PNA, ConA, LCA, PHA-L and MAL-II that are conjugated with 594nm fluorophore as well as ECA and DSL that are conjugated with 488nm fluorophore and were purchased from Vector Labs.

## **2.2 CELLS AND VIRUSES**

### **2.2.1 Cell culture**

Wildtype HeLa (human cervical epithelial cells) and HeLa-MannII-GFP (HeLa cells expressing GFP-tagged Mannosidase II) cell lines were obtained from V. Malhotra's laboratory (Centre for Genomic Regulation, Barcelona, Spain).

HEK293T (human kidney epithelial cells constitutively expressing simian virus 40 (SV40) large T antigen) cell line was a gift from V. Tergaonkar (IMCB, Singapore). Skov3 (human ovarian epithelial cells) was a gift from E. Bard (IMCB, Singapore).

All cells were grown at 37°C in a 10% CO<sub>2</sub> humidified incubator. HeLa cells were grown in high glucose DMEM supplemented with 10% FBS. HEK293T cells were grown in high glucose DMEM supplemented with 15% FBS.

Cells were routinely subcultured or passaged in accordance to the following procedure: after media aspiration, the cells were first washed with PBS to remove residual medium, then dislodged from the culture flask by incubating the cells in trypsin (0.25% w/v, Ca<sup>2+</sup>- and Mg<sup>2+</sup>-free) for 3 minutes at 37°C. The dislodged cells were resuspended in fresh media supplemented with 10% FBS and seeded onto new culture flasks or assay plates.

### **2.2.2 Producing lentivirus in HEK293T cells**

HEK293T cells were seeded onto three poly-L-lysine-coated T175 culture flasks and incubated at 37°C in a 10% CO<sub>2</sub> humidified incubator for 6 hours. The cells were transfected with packaging plasmids (pLp1, pLp2, pVSVG) and pLenti expression plasmid containing a fluorophore- tagged protein using calcium phosphate transfection method. Briefly, the plasmids were first mixed in BBS solution and calcium phosphate was added to the mixture dropwise. The mixture was vortexed for 20 seconds before incubating at room temperature for 20 minutes for the formation of transfection complexes. The transfection complexes were added to the HEK293T cells and incubated at 37°C for 24 hours. The culture medium was then aspirated and replaced with fresh DMEM supplemented with 15% FBS. The cells were incubated for an additional 24 hours before the supernatant was collected for virus harvesting. Viral supernatant was filtered using 0.45µm syringe to remove cell debris and centrifuged at 18,000 rpm for 3 hours at 4°C. The virus pellet was resuspended in PBS supplemented with 20%

sucrose. The resuspended virus was then distributed to 100µl aliquots and snap-frozen using liquid nitrogen before stored at –80°C.

### **2.2.3 Generating stable cell lines using lentiviral transfection**

HeLa cells were seeded at 30,000 cells per well of a 24-well plate and allowed to settle overnight at 37°C in a 10% CO<sub>2</sub> humidified incubator. The lentiviral stock was then added to the cells the following day and incubated overnight at 37°C. Cells were monitored under fluorescence microscope on the subsequent days to check for infection. To ensure homogenous expression in the cell line, cells expressing the fluorophore- tagged protein were sorted using fluorescent-activated cell sorting (FACS). The sorted cells were then further propagated and cell stocks were stored in liquid nitrogen.

## **2.3 MOLECULAR CLONING**

### **2.3.1 Preparation of competent cells**

*Escherichia coli* (E. coli) strain One Shot® TOP10 from Invitrogen was streaked onto a LB agar plate (1% bactotryptone, 0.5% bacto-yeast extract, 1% NaCl and 1.5% agar, pH7.0) and incubated overnight at 37°C. A single colony was then picked and inoculated in 200ml of 2X TY broth. Culture was allowed to grow overnight at 37°C with aeration by shaking at 220rpm. An inoculum of the overnight culture was diluted 100 times in 600ml of 2X TY medium and incubated at 37°C with shaking until a reading of 0.6-0.8 was attained for the absorbance at 660nm (A660). This was followed by chilling the culture on ice for 1 hour before they are pelleted by centrifugation at 3,000g for 15 minutes at 4°C. The pellet was re-suspended in 100ml pre-chilled CCMB80 solution and incubated on ice for a further 30 minutes. The process of centrifugation was repeated and cells were re-suspended in 5ml pre-chilled CCMB80 buffer with a

further incubation on ice for 30 minutes. The competent cells were then aliquoted (50µl) on ice and stored at -80°C.

### 2.3.2 Polymerase chain reaction

The PCR reaction mix is typically prepared using the recipe below:

Sterile Water	variable
10x KOD hotstart Buffer	5 µl
MgSO <sub>4</sub> (25mM)	4 µl
dNTPs (2mM)	5 µl
DMSO	2.5 µl
cDNA template	variable (10-100ng)
KOD hotstart polymerase	1 µl
Forward Primer (10uM )	2 µl
Reverse Primer (10uM)	2 µl
<hr/>	
Total	50 µl

PCR reactions were typically carried out by 1 cycle of denaturation at 94°C for 2 minutes, followed by 30-40 cycles of polymerase chain reaction consisting of denaturation at 94°C for 20 seconds, primer annealing for 20 seconds at 50-60°C (depending on primer melting temperatures) and DNA extension at 70°C. Duration for DNA extension at 70°C depends on the length of amplicon and was calculated according to the polymerase's extension rate of approximately 25 base pairs (bp) per second. The primers and the optimised annealing temperature used in this study are listed below:

**Table 2.4: List of primers for polymerase chain reactions**

Primer	Sequence	Annealing Temperature (°C)
<b>ERK8 forward + AttB1 + kozak</b>	GGGGACAAGTTTGTACAAAAA AGCAGGCTCCacc <b>ATGTGCACCG</b> <b>TAGTGGACCC</b>	56
<b>ERK8 reverse + attB2 + STOP</b>	GGGGACCACTTTGTACAAGAAA GCTGGGTCC <b>CACATGGTGCCCT</b> <b>CCAGC</b>	57

### 2.3.3 DNA agarose gel electrophoresis

6X DNA loading buffer (0.25% (w/v) bromophenol blue and 0.25% (w/v) xylene cyanol FF and 20% (w/v) glycerol) was added to DNA samples prior to their separation by electrophoresis in 1.0-1.5% (w/v) agarose in TAE buffer (40mM Tris-acetate and 2mM EDTA) supplemented with 1:10000 GelRed™, at constant voltage of approximately 100-120V. DNA bands were visualised with UV illumination.

### 2.3.4 Gel purification

Purification of DNA fragments following gel electrophoresis was performed using QIAquick™ Gel Extraction Kit (Promega) according to manufacturer's protocol, except that elution of DNA from silica columns were deionized water (ddH<sub>2</sub>O). DNA products obtained were quantitated using NanoDrop™ 1000 Spectrophotometer to establish its concentration and purity levels.

### 2.3.5 Plasmids and plasmid constructions

Plasmids encoding N-terminus eGFP-tagged full-length wildtype Arf, N-terminus eGFP-tagged Arf with point mutant Q71L (Arf (Q71L)), N-terminus eGFP-tagged Muc-PTS and C-terminus eGFP-tagged ER-2Lec were a gift from D.J. Gill (IMCB, Singapore). C-terminus mCherry-tagged Src with point mutant 8A7F and

6N7F (Src(8A7F) and Src(6N7F)) were a gift from S.Wang (IMCB, Singapore). VSVG-tsO45 plasmid was a gift from V. Malhotra's laboratory (Centre for Genomic Regulation, Barcelona, Spain). VSVG-tsO45 was subsequently cloned into pLenti6.3\_CmChe\_DEST to generate a C-terminal mcherry tagged version. cDNA encoding full-length ERK8 (GenBank/EMBL/DDBJ accession no. NM\_139021) purchased from OriGene Technologies, Inc. ERK8 full-length wildtype and mutants were subsequently cloned into pcDNA6.2\_NmChe\_DEST and pLenti6.3\_NmChe\_DEST gateway vectors to generate N-terminal mCherry tagged versions. cDNA encoding Metridia Luciferase was purchased from Clontech and subsequently cloned into pLenti6.3\_V5\_DEST gateway vector. Construction of all wild-type and mutant plasmids used in this study is described below:

cDNA from the original plasmids were PCR amplified using attB-containing primers (described in Section 2.3.2) and cloned using Gateway® Technology (Invitrogen). The attB-flanked PCR products were cloned into an attP-containing donor vector (pDONR221) using BP-clonase II (Invitrogen) to generate an entry clone. The BP reaction mix was prepared as follows:

attB-PCR product	150ng
pDONR221	150ng
5X BP Clonase II	0.5 µl
TE buffer pH8.0	variable
<hr/> Total	<hr/> 10 µl

The reaction mix was incubated overnight at 25°C. The following day, 1µl of 2µg/µl Proteinase K solution was added to the reaction and incubated at 37°C for 10 minutes. For bacteria transformation, 1µl of the reaction mix was added to 50µl of competent One Shot® TOP10 E. coli (see Section 2.3.1) and incubated on ice for 30 minutes. The mixture was then heat shocked at 42°C for 1 minute and chilled on ice for another 2 minutes. Competent cells were resuspended in 200µl 2X TY buffer and recovered on shaker at 37°C for 30 minutes before plating on an LB agar plate containing 35µg/ml kanamycin for selection of successful

transformants. Single colonies were picked, amplified in 2X TY buffer and screened for incorporation of DNA insert through restriction digest using appropriate enzymes and DNA sequencing (Section 2.3.7).

All point mutants were introduced into pDONR221 entry clone by PCR using overlapping mutagenic primers and KOD polymerase. The entry clones were then subcloned into gateway destination vectors using LR-clonase II (Invitrogen). The LR reaction mix was prepared using the recipe below:

Entry clone	150ng
Destination vector	150ng
5X BP Clonase II	0.5 $\mu$ l
TE buffer pH8.0	variable
<hr/> Total	<hr/> 10 $\mu$ l

The subsequent procedures are similar to the BP reaction as described above, with the exceptions that the competent cells were plated on an LB agar plate containing 100 $\mu$ g/ml ampicillin for selection of successful transformants, and all constructs were verified by restriction digest using appropriate enzymes and DNA sequencing (Section 2.3.7) before use. The primers used for mutagenesis in this study are listed below:



**Table 2.5: List of primers used for mutagenesis**

Primer	Sequence
<b>siRNA-resistant ERK8 forward</b>	gggggcctatggTatCgtgtggaaggcagtgg
<b>siRNA-resistant ERK8 reverse</b>	ccactgcctccacacGatAccataggccccc
<b>ERK8 T175A+Y177F forward</b>	ccagggccgtgGcagagtTcgtggccacac
<b>ERK8 T175A+Y177F reverse</b>	gtgtggccacgAactctgCcacggcctgg

### 2.3.6 Plasmid purification

The Nucleobond® Plasmid DNA purification kit (Macherey-Nagel) was utilised for large-scale extraction of plasmids from E. coli cells. Briefly, a single colony was picked after antibiotic selection and scaled up into a 200ml culture by shaking overnight at 37°C. Bacteria cells were pelleted by centrifugation at 4,000g for 15 minutes and resuspended in Buffer S1 in the presence of RNase A (100mg/ml). This was followed by cell lysis with the addition of Buffer S2 for 5 minutes and neutralisation with Buffer S3. The precipitates were clarified using an equilibrated Nucleobond® column. After two rounds of washing with the wash buffer solution provided, plasmid was eluted with 15ml elution buffer N5. The eluted plasmid DNA was precipitated with isopropanol, washed and dried with 70% ethanol, and reconstituted with 500-1000µl ddH<sub>2</sub>O. Plasmid yield and quality was determined using NanoDrop™ 1000 Spectrophotometer.

### 2.3.7 DNA sequencing

Plasmid DNA (200-500ng) was added to a sequencing mix comprising of 1X Big Dye termination mix (1st Base), 3.2pmol of appropriate primer topped up to 10ul with ddH<sub>2</sub>O. Thermal cycling was carried out by 25 cycles of denaturation at 95°C for 10 seconds, annealing at 55°C for 10 seconds, and extension at 60°C for 4 minutes. The reaction products were precipitated by addition of 2 volumes of

100% ethanol with 0.1 volume of 3M sodium acetate (pH5.2), incubation on ice for 10 minutes and finally centrifugation at 14,000 rpm. The pellet was washed with 70% ethanol, air-dried and sequenced by an automatic DNA sequencer (Applied Biosystems, Model 3730XL). Sequencing data obtained were analyzed by Chromas program.

## **2.4 SIRNA SCREENING**

### **2.4.1 siRNA plate preparation and transfection**

The primary siRNA screen to identify signaling regulators of Golgi morphology was performed using a commercial genomic siRNA library (Dharmacon siGenome) (Thermo-Fisher) in 384 well format. The RNAi library consisted of pools of 4 distinct siRNAs targeting each of the known 948 human kinases, phosphatases and related genes. 2.5  $\mu$ l of 500nM siRNA was printed into blackwalled 384-well plates (384-well black  $\mu$ clear, Greiner) with Velocity 11. The pilot screen plate that consist of membrane trafficking regulators were assembled manually into 384-well plates (384-well V-bottom plates, Greiner). siRNA plates for secondary screens were prepared by assembling cherry picked siRNA tubes. Deconvoluted siRNAs were custom-ordered from Thermo-Fisher. The pilot membrane trafficking, cherry-picked and deconvoluted siRNA libraries were robotically printed onto 384-well plates as for the primary screen.

Reverse siRNA transfection was performed by pre-mixing 0.25 ml of Hiperfect (Qiagen) with 7.25 ml of Optimem (per well) for 5 minutes, then adding the mixture to the siRNA for complexation for 20 minutes, followed by addition of 2000 HeLa MannII-GFP cells per well with the Multidrop combi (Thermo-Fisher). In the pilot membrane trafficking plate, some wells without siRNA were treated with 10  $\mu$ g/ml BFA, 6  $\mu$ g/ml nocodazole, 1  $\mu$ g/ml monensin, or 1  $\mu$ g/ml latrunculin B for 1 hour before fixation.

### **2.4.2 Immunofluorescence staining**

After 3 days of siRNA knockdown, the cells were fixed with 4% paraformaldehyde in D-PBS for 10 minutes, washed with D-PBS and permeabilized with 0.2% Triton X-100 for a further 10 minutes. The cells were then stained with primary antibody diluted in 2% FBS in D-PBS for 2 hours at room temperature or overnight at 4°C. Cells were subsequently washed three times for 5 minutes with 2% FBS in D-PBS and stained for 20 minutes with secondary antibodies (Alexa Fluor, Invitrogen), HPL and Hoechst 33342 diluted in 2% FBS in D-PBS. The cells were then washed three times for 5 min with D-PBS before high-throughput confocal imaging. siRNA plates were performed in duplicates.

### **2.4.3 Automated image acquisition and processing**

During automated image acquisition, four sites per well (each imaged at four excitation wavelengths of 405, 488, 561 and 635 nm) were acquired sequentially with a 20x Plan Apo 0.75 NA objective on a laser scanning confocal high throughput microscope (ImageXpress Ultra, MDS Analytical Technologies). For the analysis of Golgi morphology, a web application was created to access links and meta-information on the proprietary database provided with the acquisition software (MDCStore, MDS) and to launch a dedicated image analysis application called HCSU (high content screening unit) which performs image segmentation and feature extraction. HCSU is composed of a set of optimized algorithms written in C and C++. On a single computer dedicated to image processing, a java application manages the parallelization of HCSU on multiple CPUs. Implementations of the algorithms are homemade.

### **2.4.4 Selection of primary and validated hits**

To select for primary hits in the Golgi morphology screen, threshold determination was performed for each phenotypic score using the derivative

method [309]. Specifically, this corresponds to cutoff phenotypic scores of 0.44 (cis diffuse), 0.43 (cis fragmented), 0.33 (cis condensed), 0.21 (medial diffuse), 0.4 (medial fragmented), 0.43 (medial condensed), 0.44 (trans diffuse), 0.4 (trans fragmented) and 0.35 (trans condensed). Each of the scores corresponds to a z-score of >2. Genes with one or more phenotypic scores above the cutoff values were selected as hits. Thresholds for the deconvoluted siRNA validation screen were defined as 50% of the primary screen cutoff scores.

#### **2.4.5 Bioinformatics analysis**

For the hierarchical clustering of Golgi morphology phenotypes, the ‘Agglomerative Hierarchical Clustering’ method was applied using ‘Euclidean Distance’ as distance metric and ‘Complete Linkage’ as the linkage criteria. The clusters were picked manually by visual analysis of the heatmap which identified six major groups of genes. Annotation information for each gene was gathered from Gene Ontology, GeneCards ([www.genecards.org](http://www.genecards.org)), NCBI (<http://www.ncbi.nlm.nih.gov/gene>) and Phosphosite (<http://www.phosphosite.org/>). Gene enrichment was analysed using DAVIDS bioinformatics (<http://david.abcc.ncifcrf.gov/>). Protein networks were created using data from STRING (<http://stringdb.org/>), Pathway studio and Human Protein Reference Database (HPRD) (<http://www.hprd.org/>) which are imported into Cytoscape software (<http://www.cytoscape.org/>) for network arrangements.

#### **2.4.6 Lectin secondary screen**

##### **2.4.6.1 Transfection and fluorescent staining**

siRNA transfection on HeLa cells was performed as in the primary screen (Section 2.4.1) and fixed with 4% paraformaldehyde in PBS for 10 minutes, washed with PBS, then incubated for 1–2 hours at room temperature with the respective fluorescently labeled lectins (20 mg/ml) in D-PBS containing 2% FBS. Cells were then washed three times for 10 minutes each with 2% FBS in D-PBS,

incubated with Hoechst 33342 in PBS for 10 minutes to stain nuclei, and washed another two times for 10 minutes each with PBS. For biotin-conjugated lectins, the Hoechst staining was preceded by 1 hour incubation with streptavidin-FITC or streptavidin-Alexa594 (2 mg/ml) in 2% FBS/D-PBS. Cells were then imaged using the high-throughput ImageXpress Ultra with 2–4 sites imaged per well. Each lectin was assayed at least in duplicate.

#### 2.4.6.2 Image analysis

Images of cells were analysed using MetaXpress software (Molecular Devices). The Transflour HT module was used to quantify the lectin intensity and cell number for each site, and the average intensity per cell obtained for each well. It was observed that for most lectins, there was a correlation between lectin intensity per cell and cell number, hence for each plate of 181 genes, a plot of intensity per cell vs cell number was fit to a log equation ( $y = y_0 + a \log x$ , where  $y_0$  and  $a$  are constants) to obtain the expected intensity per cell for no siRNA knockdown (red solid curve). The same fit was performed on the control transfection reagent-treated wells (TR) in the same plate (black solid curve), and the mean absolute deviation of the TR wells ( $\text{mean } |d_{tr}| = \text{mean } |I_{tr} - I_{x,tr}|$ , where  $I_{tr}$  is the intensity per cell for the given well, and  $I_{x,tr}$  is the expected intensity per cell for the cell count of the given well) was calculated as a measure of the experimental variation in the assay. The deviation of each gene's intensity per cell from the expected value at its given cell number was then calculated ( $d_i = I_i - I_{x,i}$ , where  $I_i$  is the intensity per cell for the given gene, and  $I_{x,i}$  is the expected intensity per cell for the cell count of the given gene), and expressed in terms of the mean absolute deviation of the TR wells, which we then call the “normalized lectin signal”. Finally, we defined significant perturbation of lectin staining as a normalized lectin signal of at  $>4$  or  $<-4$  (solid black lines in Glycan Profiles).

### 2.4.7 Validation of lectin specificities

PNA and HPL: Peanut Agglutinin and *Helix Pomatia* lectin and are highly specific for O- glycans. PNA recognizes terminal core 1 O-glycans (T antigen) or Gal- $\beta$ 1,3-GalNAc- $\alpha$ 1-Ser/Thr [310]. HPL is specific for terminal  $\alpha$ -linked O-GalNAc glycans. Knockdown [311] of C1GALT1, the Core 1 galactosyltransferase that generates the core 1 glycan structure recognized by PNA, abolishes the already-low PNA staining while increasing HPL staining because of the increase in terminal O-GalNAc. Similarly, loss of C1GALTC1 (cosmc), a molecular chaperone required for C1GALT1 activity [216], also led to reduced PNA and increased HPL stainings.

ConA: Concanavalin A binds mainly  $\alpha$ -D-mannosyl and  $\alpha$ -D-glucosyl groups, having a high affinity for the N-glycan trimannosyl core, thus it tends to reveal high mannose N-glycans [312]. KD of MGAT1 (mannosyl  $\alpha$ 1,3-glycoprotein  $\beta$ 1,2-N-acetylglucosaminyltransferase) which transfers the first GlcNAc residue onto the mannosyl core of N- glycans and is thus essential for the conversion of high-mannose to hybrid and complex N-glycans. Its absence prevents further trimming of the oligomannose structure, promoting more high-mannose glycan structures, and its KD indeed increased ConA staining relative to a GFP KD control.

LCA: *Lens culinaris* agglutinin- A has high affinity for Fuc- $\alpha$ 1,6-GlcNAc-N-Asn containing N-glycans [312]. As a control, we knocked down FUT8 (fucosyl transferase 8) which catalyzes the addition of fucose in  $\alpha$ 1,6 linkage to the first, Asn-linked GlcNAc residue of N-glycans. Its absence prevents the formation of this core fucose structure and its KD indeed decreased LCA staining.

PHA-L: *Phaseolus vulgaris* leucoagglutinin has specificity for tri- and tetra-antennary N-glycans, binding preferentially to GlcNAc in a  $\beta$ 1,6 linkage with the trimannosyl core [313, 314]. To impair N-glycan synthesis, we co-knocked down

STT3A and STT3B, subunits of the oligosaccharyltransferase complex which initiates N-glycosylation by catalyzing the transfer of a lipid-linked high mannose oligosaccharide to an asparagine residue on nascent polypeptide chains, and the KD inhibits PHA-L binding.

ECA: *Erythrina cristagalli* lectin has a preference for the disaccharide galactosyl- $\beta$ 1,4-N-acetylglucosamine, therefore recognizing mostly extended complex N- and O-glycans that are not capped by a sialic acid [315]. KD of SLC35A3 (Golgi UDP-GlcNAc transporter) reduces the availability of UDP-GlcNAc substrate necessary for the addition of GlcNAc to extend both N- and O-glycans; KD of MGAT1 or C1GALT1 inhibits the extension of N-glycans or O-glycans, respectively, and thus Gal- $\beta$ 1,4-GlcNAc structures. Thus KD of any of the three genes led to a reduction in ECA staining.

DSL: *Datura stramonium* lectin has a relatively broad specificity for poly-LacNAc extended N- and O-glycans as well as tri- and tetra-antennary N-glycans [316, 317]. Like PHA-L, co-KD of STT3A and STT3B decreases the initiation of N-glycosylation which hence inhibits DSL binding.

MAL-II: *Maackia amurensis* lectin II binds preferentially to O-linked glycans containing the trisaccharide Sia- $\alpha$ 2,3-Gal- $\beta$ 1,3-GalNAc [318]. Sialidase treatment reduces MAL-II staining.

#### **2.4.7 Secondary Met-Luc secretion screen**

HeLa cells were stably transfected to express secreted Metridia Luciferase (Clontech) using lentivirus transduction (HeLa Met-Luc). siRNA transfection of HeLa Met-Luc cells was performed as in the primary screen (Section 2.4.1). After 3 days, the cells were washed once with PBS and fresh media was added to allow Met-Luc secretion. In some wells without siRNA, media containing either 10  $\mu$ g/ml BFA, 6  $\mu$ g/ml nocodazole, 1  $\mu$ g/ml monensin, or 1  $\mu$ g/ml latrunculin B was

added instead. 25µl of supernatant per well was extracted after 4 hours, and the amount of secreted Met-Luc quantified using the Ready-to-Glow secreted luciferase reporter assay (Clontech). The raw signals were divided by the cell number (quantified by DAPI staining and imaging), logged, and then normalized to the mean of the control transfection reagent-treated (TR) wells. We used the standard deviation (SD) of TR wells as a measure of assay variation, and defined significant perturbation of Met-Luc secretion as a deviation of more than 3 SDs from the TR mean. This corresponded to normalized secretion values of about 0.95 and 1.05.

#### **2.4.8 VSVG secretion assay**

HeLa cells were stably transfected to express the temperature sensitive mutant of VSVG protein (VSVG-tsO45) tagged with mcherry at the C-terminus. siRNA transfection of HeLa-VSVG cells was performed as in the primary screen. Two days after siRNA transfection, the cells were transferred to 40°C and incubated for 16 hours to allow accumulation of VSVG in the ER. The cells were then incubated at 32°C for 15 minutes in the presence of 100 µg/ml of cycloheximide before fixation.

### **2.5 HIGH RESOLUTION FLUORESCENCE MICROSCOPY**

Cells were seeded onto glass coverslips in 24-well dishes (Nunc). After the respective treatments, cells were fixed with 4% PFA-4% sucrose in D-PBS, permeabilised with 0.2% Triton-X for 10 minutes and stained with the appropriate markers using the same procedure performed in the primary siRNA screen. To effectively observe ERK8 localisation at the Golgi, the cells were permeabilised with 0.2% Triton-X for 2 hours and stained with anti-ERK8 antibody diluted in 2% FBS in D-PBS overnight. For Beta COP staining, cells were permeabilised with 0.05% NP40 for 5 minutes twice, washed with D-PBS twice for 5 minutes, blocked with 2% bovine serum albumin (BSA) for 1 hour at room temperature,



followed by staining with anti-Beta COP antibody diluted in 2% FBS in D-PBS overnight.

After staining, cells were mounted onto glass slides using FluorSave and imaged at room temperature using an inverted confocal microscope (Olympus IX81) coupled with a CCD camera (model FVII) either with a 60x objective (U Plan Super Apochromatic [UPLSAPO]; NA 1.35) or 100x objective (UPLSAPO; NA 1.40) under Immersol oil. Images were acquired and processed using Olympus FV10-ASW software.

## **2.6 PROTEIN EXPRESSIONS AND ANALYSIS**

### **2.6.1 Transient expression of plasmid DNA in mammalian cells**

Plasmids were transfected into HeLa cells using FuGENE® HD (Promega) transfection reagent. Cells were seeded a day before transfection in DMEM supplemented with 10% FBS. On the day of transfection, plasmid DNA and FuGENE® HD were added to Opti-MEM and incubated for 15 minutes at room temperature. The transfection complex was added to each well containing cells seeded at 90% confluency and incubated at 37°C in a 10% CO<sub>2</sub> humidified incubator for 16 hours before harvesting for further analysis.

HEK293T cells were transfected using a calcium phosphate method. HEK293T cells were seeded 8–24 hours before addition of transfection complex to obtain an optimal confluency (80–90%) for transfection. On the day of transfection, 1ml transfection complexes composed of 10–30 µg of DNA diluted in 250 mM calcium phosphate and mixed with BBS buffer (140 mM sodium chloride, 0.7 mM disodium hydrogen phosphate, and 25 mM N,N-Bis(2-hydroxyethyl)-2-aminoethanesulfonic acid [BES], pH 6.95 [20°C]) by vortex were incubated at room temperature for 15 minutes before addition to cells.

### **2.6.2 Western blot analysis**

Cells were washed twice using ice-cold D-PBS before scraping in D-PBS. Cells were centrifuged at 300g for 5 min at 4°C and were lysed using lysis buffer (containing 0.5% NP-40 Alternative (Calbiochem), 200mM NaCl and 50mM Tris buffer, pH 8.0) in the presence of protease (Roche) and phosphatase (Roche) inhibitors at 4°C on a 20rpm shaker for 30 minutes. Lysates were clarified by centrifugation at 14,000g for 10 minutes at 4°C and the supernatant was collected. Clarified lysate protein concentrations were determined using Bradford reagent (Bio-Rad Laboratories, Hercules, CA) before sample normalisation. Samples were diluted in lysis buffer with 4x SDS loading buffer and boiling at 95°C for 2 minutes. They were then resolved by SDS-PAGE electrophoresis using bis-tris NuPage gels as per manufacturer's instructions (Invitrogen) and transferred to PVDF membranes which was blocked using 3% BSA dissolved in TBST (50 mM Tris [pH 8.0, 4°C], 150 mM NaCl, and 0.1% Tween 20) for 2 hours at room temperature. Membranes were washed to remove traces of BSA before incubation with antibodies as per manufacturer's instructions. Membranes were washed 5 times with TBST before incubation with secondary HRP-conjugated antibodies (GE Healthcare). Membranes were further washed 5 times with TBST before ECL exposure.

### **2.6.3 ER-trapped GalNAc-T activity reporter assay**

HEK293T cells were seeded into 10-cm petri dishes 24 hours before transfection and were transfected with the ER-trapped mucin construct (GFP-MUC5-PTS) using the calcium phosphate method. The growth media was then replaced the following day and the cells were further incubated for 24–48 hours before ERK8 inhibitor treatment for 4 hours. Cells were harvested and lysed as previously mentioned. All subsequent steps were performed either on ice or at 4°C. Immunoprecipitation (IP) samples were incubated with 1–2 µg of HPL-conjugated agarose (Sigma-Aldrich) overnight at 4°C. The next day, IP samples were washed for 5 times with 1 ml of IP wash buffer (50 mM Tris [pH 8.0, 4°C], 100 mM NaCl, 0.5% NP-40 alternative, 1 mM DTT, and complete protease

inhibitor [Roche]). Samples were diluted in IP wash buffer and 4× SDS loading buffer before boiling at 95°C for 2 minutes. Samples were then resolved by SDS-PAGE electrophoresis as mentioned above.

#### **2.6.4 GalNAz metabolic labeling**

HeLa cells were treated with siRNA for 3 days before metabolically labelling with 20 µM GalNAz for 6 hours. Ro-31-8220 was added to cells during GalNAz metabolic labelling for 4 hours treatment before harvesting. Cells were harvested, lysed and measured for protein concentration as previously mentioned. 50µg of protein lysate was added with 500µM of FLAG- phosphine to label GalNAz-incorporated proteins and the samples were incubated overnight under constant agitation. The next day, the samples were diluted in lysis buffer with 4x SDS loading buffer and boiling at 95°C for 2 minutes and resolved by SDS-PAGE electrophoresis. Membranes were incubated with anti-FLAG antibody overnight to visualize GalNAz incorporation.

### **2.7 GROWTH FACTOR AND DRUG TREATMENTS**

For growth factor stimulation, cells were seeded overnight and serum-starved for 16 hours before incubation with EGF (100 ng/ml), PDGF (50 ng/ml), IGF1 (100 ng/ml) or TGF-B1 (2 ng/ml) in serum-free DMEM for various durations before fixing.

For drug treatments, cells were seeded and incubated with the drugs of different concentrations for various durations before harvesting for further analysis.

**Table 2.6: List of drug and concentrations used.**

<b>Drugs</b>	<b>Concentration used</b>
<b><math>\alpha</math>-armanitin</b>	10 $\mu$ g/ml
<b>Brefeldin A (BFA)</b>	2 $\mu$ g/ml
<b>FR180204</b>	100 $\mu$ M
<b>Golgicide A (GCA)</b>	50nM
<b>Imidazole</b>	5mM
<b>IPA3</b>	10 $\mu$ M
<b>Latrunculin B</b>	1 $\mu$ g/ml
<b>Monensin</b>	1 $\mu$ g/ml
<b>Nocodazole</b>	6 $\mu$ g/ml
<b>Ro31-8220</b>	5 $\mu$ M
<b>SP600125</b>	50 $\mu$ M

## **2.8 SCRATCH WOUND ASSAY**

Cells were seeded onto fibronectin-coated 35-mm plastic tissue culture dishes (Ibidi GmbH) and grown to confluence for 16–24 hours. A wound was manually generated using micropipette tip before washing to remove cell debris. Live phase contrast imaging was performed at 37°C using a Zeiss Axiovert microscope (model 200M; Zeiss Microimaging; Thornwood, NY) equipped with a CCD camera (AxioCam HRc) with a 20 $\times$  objective (LD Plan-NEOFLUAR; 20 $\times$ ; N.A. 0.4). Frames were acquired at 5-minute intervals for at least 7 hours. The rates of wound closure were calculated by extracting images of the movie every hour and measuring the wound area ( $\mu\text{m}^2$ ) using ImageJ (National Institutes of Health).

## **2.9 HUMAN FROZEN TISSUE ARRAY ANALYSIS**

### **2.9.1 Tissue array staining**

Frozen human tumour microarrays FBN406a, FMC407 and BRF404 were purchased from US Biomax, Inc., United States. The slides were dried and fixed in chilled 1:1 acetone:methanol for 10 minutes at room temperature. Subsequently, the slides were washed 3 times with TBST and blocked with 10%

goat serum-PBS for 30 minutes. Subsequent staining with ERK8 (0.9 µg/ml), VVL-biotin (4 µg/ml) and Hoescht (1:10,000) was performed overnight before staining with secondary antibody anti-rabbit Alexa Fluor 488 (1:1000) and Streptavidin-Alexa 594 (1:400) for 30 minutes. Slides were counterstained with DAPI and then mounted (Vectashield).

## **2.9.2 Tissue array imaging and quantification**

The arrays were first automatically imaged (using constant acquisition parameters) using a 10× objective (LD Plan-NEOFLUAR; 10×; N.A. 0.4) on a motorized stage coupled to a Zeiss inverted confocal microscope equipped with a CCD camera (AxioCam HRc). Images of the cores were exported as from Zeiss Zen2011 software to enable quantification of ERK8 and VVL staining in tumour cores.

To quantify the levels of ERK8 or Tn (VVL) expression in a tissue core, the images were first converted to 8-bit images on ImageJ. The area above the threshold set for background staining (Threshold for ERK8 and VVL was 30 and DAPI was 40) then quantified. Area of ERK8 and VVL was normalised to the total area of the core represented by nuclei (DAPI) staining. The values of each core was then normalised to the average area of the normal tissue cores.

**CHAPTER THREE: RNAI SCREENING REVEALS A LARGE  
SIGNALING NETWORK CONTROLLING THE GOLGI APPARATUS IN  
HUMAN CELLS**

## **CHAPTER THREE: RNAI SCREENING REVEALS A LARGE SIGNALING NETWORK CONTROLLING THE GOLGI APPARATUS IN HUMAN CELLS**

### **3.1 INTRODUCTION**

Central to the secretory pathway in all eukaryotic cells, the Golgi apparatus is pivotal for post-translational modifications, in particular glycosylation, of lipids, luminal and membrane-associated proteins and sorting of these secretory cargos to their appropriate destinations. In addition to these well established ‘classical’ functions of the Golgi, there has been mounting evidences of numerous other functions that converge at the mammalian Golgi. These neo-functions of the Golgi include mitosis [319], cell migration [116, 121], apoptosis [320, 321], cytoskeletal organization [68, 322], calcium storage and release [323, 324] and signal transduction [127, 128]. For all these functions, the Golgi organization is important.

In spite of uncovering these diverse and unprecedented functions of the Golgi, the mechanisms controlling Golgi organization and its functions are not completely known. In recent years, various signaling mechanisms that control Golgi organization and function have increasingly been discovered [127, 129]. For example, ERK controls remodeling and re-orientation of the Golgi towards the leading edge for cell migration [116]. On the other hand, mitogen-activated protein kinases (MAPKs) MEK and ERK as well as various signaling proteins act to fragment the Golgi in preparation for mitosis [130-135] and the resulting Golgi fragmentation, in turn, forms a G2 mitotic checkpoint [124, 125, 319, 325]. Furthermore, the flux of secretory cargo release from the TGN was found to be regulated by protein kinase D (PKD) and p38 MAPK [138-141].

Interestingly, the Golgi also senses and responds to endogenous signals, generating signaling cascades to modulate its own organisation and function. This is highlighted by the local activation of Src family kinases (SFKs) by the Golgi in response to variable amounts of membranes and cargo [145]. SFK activation, in turn, promotes intra-Golgi trafficking and secretion, likely through Golgi structure remodeling. In addition to responding to external cues for cell migration [116], the Golgi also generates signaling for its own re-orientation, as observed by the local activation of the germinal centre kinases III (GCKIII) upon Golgi recruitment [117, 326]. Activation of GCKIII kinases, in turn, phosphorylates 14-3-3 $\zeta$  protein which could recruit the cell polarity regulator, the Par complex, to the Golgi to mediate its orientation [148]. Notably, the Golgi also serves as a platform for spatially localising signaling cascades where they propagate differential signaling outcome and hence, different cellular responses. A well-known example is the specific localisation of Ras GTPases at the Golgi [153, 154] that spatiotemporally activate the signaling cascades. It was proposed that the Raf-MEK-ERK cascade is activated downstream of Golgi-localised Ras, resulting in differential MAPK outputs [150, 151] and establish different physiological outcomes [327, 328]. In line with this, ERK is tethered to Golgi membranes where it is directed to different substrates [155, 156, 329].

By contrast, the regulation of glycosylation at the Golgi remains poorly understood. Our recent report highlights that O-GalNAc glycan synthesis can be regulated by re-localisation of O-glycosylating enzymes from the Golgi to the ER. This relocation event is stimulated by growth factors and mediated by signaling of tyrosine kinase Src [193, 240].

Collectively, these examples suggest that the organisation and functions of the mammalian Golgi are likely under multiple regulatory controls. Current studies commonly examine Golgi regulation by one or a few genes and different studies have variations in experimental setups. Furthermore, their effects on glycosylation are frequently not explored. Given the highly integrated and dynamic nature of



the Golgi, modifying a single aspect could also affect others. Thus, this calls for systematic evaluation of Golgi phenotypes so as to obtain a system's view of Golgi regulation. In mammalian cells, RNAi screening is a method of choice to study Golgi regulation in a coordinated and unbiased fashion. In this chapter, I describe the use of an RNAi screen to identify the genetic basis of Golgi regulation. The screen involved a systematic analysis of the signaling complement of the genome: kinases, phosphatases and related genes to uncover signaling regulation on the mammalian Golgi organisation. Subsequently, I explored the roles of the identified regulators in Golgi functions glycosylation and secretion.

## **3.2 RESULTS: RNAi screening reveals molecular regulators of Golgi organization and functions.**

### **3.2.1 Identification of screening conditions**

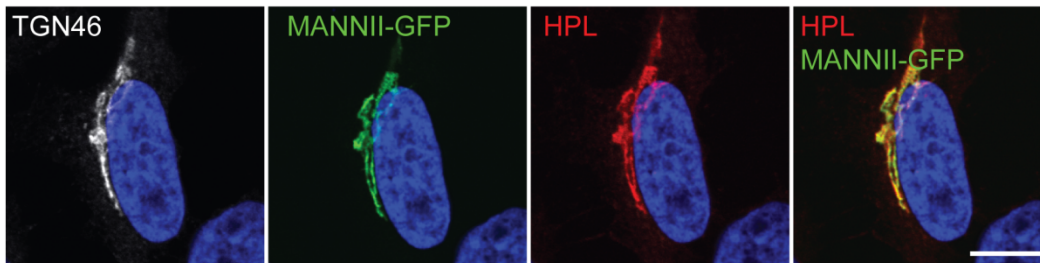
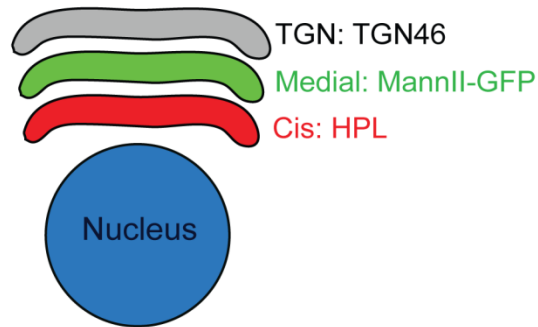
To assess Golgi organisation in mammalian cells, I chose to fluorescently label each of the three Golgi compartments (cis, medial and trans) with their specific markers. This would allow us to assess cisternal stacking and overcome the resolution limits of conventional microscopy. Adjacent Golgi cisternae can be as close as 50 nm apart and the cis-to-trans dimension of Golgi stacks range between 200 and 400 nm [330]. By simultaneous imaging and pattern comparison between markers, this enables us to detect compartment specific effects. Although they appear morphologically indistinguishable under normal conditions, the compartments can be segregated when perturbed [331-333]. Furthermore, Golgi compartments are known to differ greatly both biochemically and functionally such as their biosynthetic tasks, resident protein and lipid composition, pH and membrane trafficking events involved [26, 334-336]. Labeling all three compartments would map the influence of a gene to the specific compartment and membrane trafficking process. Hence, this serves to better dissect the regulation of Golgi organisation.

I have selected human cervical carcinoma HeLa cells for their elaborate Golgi ribbon morphology. HeLa cells have been commonly used in studies to dissect regulatory mechanisms of Golgi organisation [211, 337-339]. In addition, their high amenability to siRNA transfection [340] further substantiated their use in the RNAi screen.

The cis compartment was represented with *Helix pomatia* lectin (HPL) staining. HPL binds specifically terminal GalNAc residues added to cargo proteins by GalNAc-Ts, the O-GalNAc glycosylation initiation enzymes [341]. As GalNAc is rapidly modified by the downstream galactosyltransferase C1GalT in subsequent

Golgi compartments, HPL staining has been shown to be restricted to the cis Golgi [342]. Furthermore, the staining intensity of HPL reflects the expression levels of terminal O-GalNAc (also known as the Tn antigen), a well-known tumor associated carbohydrate marker. Hence, it provides another aspect that could be derived from this high-content screen which is in the dissection of Tn regulation. This will be further discussed in Chapter 4 of this dissertation. Technically, the use of fluorophore conjugated HPL would add ease and speed to the high throughput cell staining procedure and the staining is strongly detectable on the automated confocal microscope. Altogether, these further supported HPL as a convenient readout for the cis Golgi integrity. The medial Golgi was marked by GFP tagged Mannosidase II (MannII-GFP) that was stably expressed in the HeLa cells. The only concern of the stable expression was to obtain a homogenous level of expression for imaging. This was circumvented by flow cytometry sorting for high expressing cells for the screen. To reveal the trans Golgi network, I have selected a specific antibody staining for TGN46 protein. Finally, nuclear DNA staining was used to identify individual cells and to demarcate the cell boundaries in our automated image analysis software.

Under physiological conditions, all three markers colocalize significantly at the immunofluorescence level using a 100X objective. This is consistent with the resolution limit of conventional microscopy, which is unable to distinguish between cisternae (Figure 3-1). However, despite this colocalisation in normal cells, the three proteins have, in fact, different dynamics and compartmental distributions. On the cis side of the Golgi complex, HPL reveals the activity of GalNAc-Ts, which cycle to the ER independently of other Golgi enzymes [193]. While MannII-GFP is a medial Golgi marker expected to cycle at a slow rate between the Golgi complex and the ER [343], TGN46 is distributed to the TGN compartment and has been reported to traffic continuously between the plasma membrane and the endosomes [344].



**Figure 3-1: An imaging-based screen to identify Golgi organisation phenotypes.** HeLa MannII-GFP (medial Golgi) cells were stained with cis Golgi marker HPL and trans Golgi network (TGN) marker TGN46. Compartments co-localized extensively even at x 100 magnification (UPLSAPO; NA 1.40). Scale bar: 10 $\mu$ m.

### 3.2.2 A pilot siRNA screen on membrane trafficking regulators revealed three main Golgi morphologies.

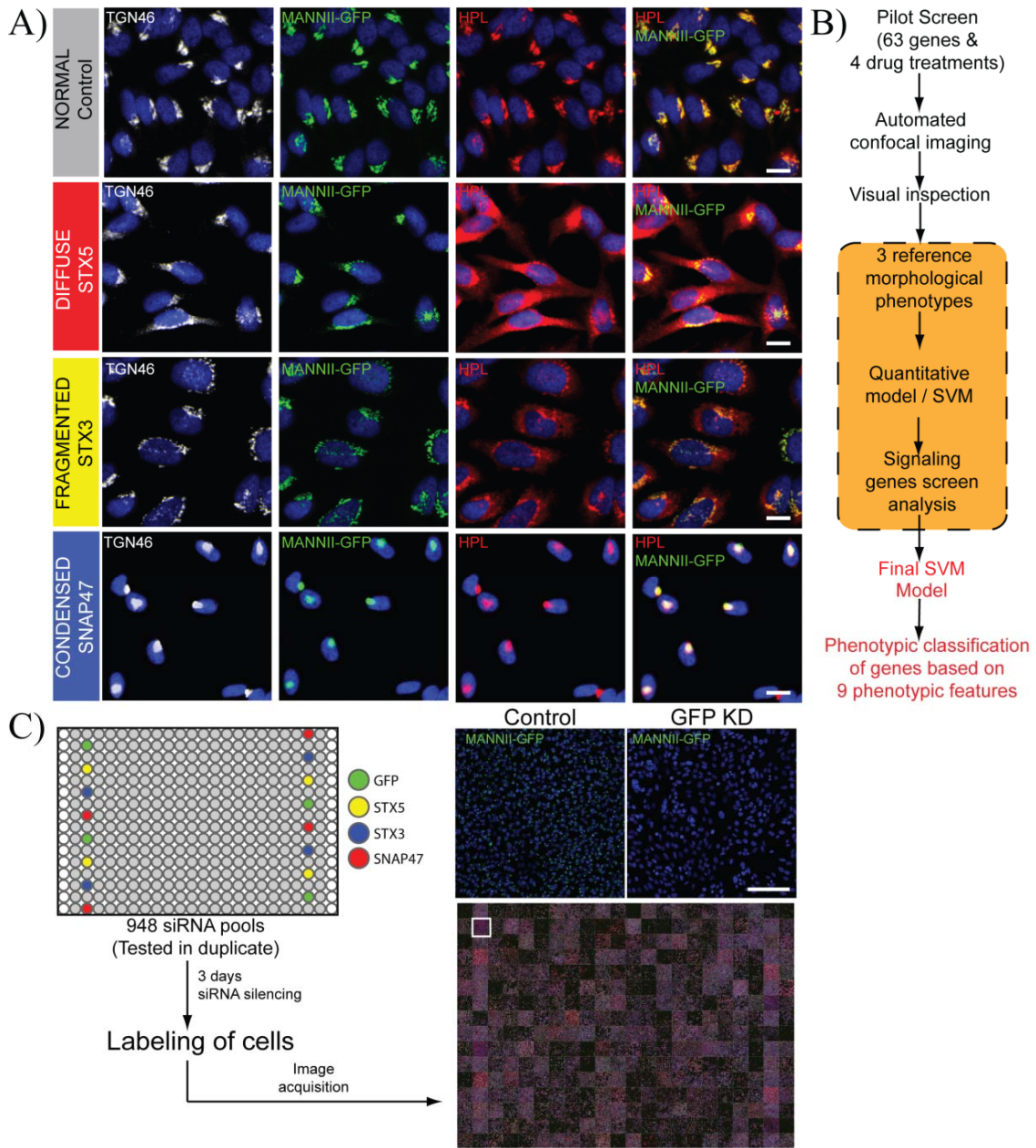
In order to explore the range of Golgi phenotypes that could be observed, I screened a custom-designed set of 63 known regulators of membrane traffic. These regulators, including SNAREs and Rabs, participate in vesicle budding and fusion [345, 346]. I have also tested drugs such as brefeldin A (BFA), nocodazole, monensin and latrunculin B, which are known to perturb the Golgi in different ways [347]. For each perturbation, 2000 cells were reverse transfected with siRNAs spotted in 384-well imaging plates. 72 hours after siRNA transfection, some untransfected wells were treated with the drugs for one hour before fixing and staining for the nucleus, cis and trans Golgi compartments. The cells were then imaged using high throughput confocal microscopy.

Visual inspections on each treatment revealed that depletion of several of these genes perturbed Golgi morphology. Through this exercise, I defined three major classes of perturbed Golgi morphology that were visually identifiable and labeled them “diffuse”, “fragmented” and “condensed” (Figure 3-2A and B). Diffuse Golgi morphology is typically observed after Brefeldin A treatment. This morphology usually reflects the relocation of Golgi markers to the ER. With a fragmented Golgi, granular structures are still visible, but they appear no longer connected in a perinuclear half-moon shape. Fragmentation has been reported in multiple studies and occurs for example after nocodazole or monensin treatment [347, 348]. Fragmentation is sometimes attributed to a loss of the connections between Golgi stacks [349, 350]. The condensed Golgi usually appears compact and rounded in a perinuclear location. This morphology has been previously reported to occur upon latrunculin treatment [351] and upon various genetic perturbations [352, 353].

Cellular images of selected gene depletions that resulted in strong Golgi phenotypes were used to train our automated image classification tool to recognize and classify Golgi phenotypes for each Golgi marker (Figure 3-2B). This image classification tool involved support vector machine (SVM) learning and will be further discussed in Section 3.2.3. The initial SVM trained with the pilot screen set was further refined with more examples from the subsequent signaling genes screen, altogether constituting the set of “Reference morphological phenotypes”, (Figure 3-2B and Table 3.1) to achieve a final SVM model for phenotypic readout.

The dramatic Golgi phenotypes observed from the depletions of membrane trafficking genes validated the screening protocol and assay method. In addition, the screen also identified controls for our subsequent screens. Three SNAREs were, hence, selected based on their prototypical effects on the Golgi apparatus: Syntaxin 3 (STX3) with a fragmented morphology, SNAP47 with a condensed

morphology and Syntaxin 5 (STX5) with a marked diffuse distribution for the cis marker HPL but almost unaffected MannII-GFP and TGN46 stainings (Figure 3-2A). Diffuse HPL staining in STX5 knockdown is accompanied with intensity increases (see Chapter 4). The siRNA transfections were verified to be efficient given that more than 80% of cells showed reduction in MannII-GFP levels when treated with GFP siRNA and increased HPL staining in STX5 depleted cells (Figure 3-2C). With an optimized screen workflow, I proceeded with the subsequent screens.



**Figure 3-2: A pilot screen of membrane trafficking regulators revealed three Golgi phenotypes.** (A) Examples of the three identified Golgi phenotypes. STX5 knockdown induced a diffuse phenotype specifically for the cis Golgi while STX3 and SNAP47 knockdown induced a fragmented and condensed Golgi in all three compartments respectively. Scale bar: 30 $\mu$ m. (B) Schematic overview of the screening process. The pilot screen was imaged using x20 objective and visually screened for changes in Golgi organisation. Three Golgi phenotypes were identified and used to train a preliminary Support Vector Machine (SVM) for quantitative scoring of treatments. Images of selected genes from the signaling genes screen (Table 3.1) were used to refine SVM training and obtain a final score. (C) Workflow of the siRNA screen. Screen plates were loaded with

controls for the three phenotypes for quality control in each plate. Non targeting siRNA (NT siRNA) knockdown using GFP siRNA and STX5 knockdown demonstrate homogeneous gene depletions in all wells seeded with the siRNAs. Scale bar: 200  $\mu$ m.

Golgi compartment	Cis				Medial				Trans			
Phenotype	Diffuse	Fragmented	Condensed	Normal	Diffuse	Fragmented	Condensed	Normal	Diffuse	Fragmented	Condensed	Normal
Drug and siRNA treatments	BFA	Monensin Nocodazole SEC22L3 ITPKB SYBL1 EPHA1 TSKS STX4A MAPK12	AP1M1 CLK1 MKNK1 GCK CDC2L2 RIPK2 Latrunculin B MGC42105	Control	BFA	IKBKE NSF Monensin Nocodazole SYBL1 KHK EPHA1 EPHA1 TSKS STX4A MAPK12	AP1M1 ARF1 CLK1 MKNK1 CDC2L2 RIPK2 GAP43 SNAP47 SRMS Latrunculin B PKM2 MGC42105	Control	BFA	Monensin Nocodazole ITPKB KHK DMPK TSKS STX4A MAPK12	CLK1 MKNK1 GCK CDC2L2 RIPK2 MYO3A Latrunculin B MGC42105	Control

**Table 3.1 List of drug and gene siRNA treatments (Reference morphological phenotypes) for training the SVM.**

### 3.2.3 Golgi phenotypes can be automatically classified using nine phenotypic features.

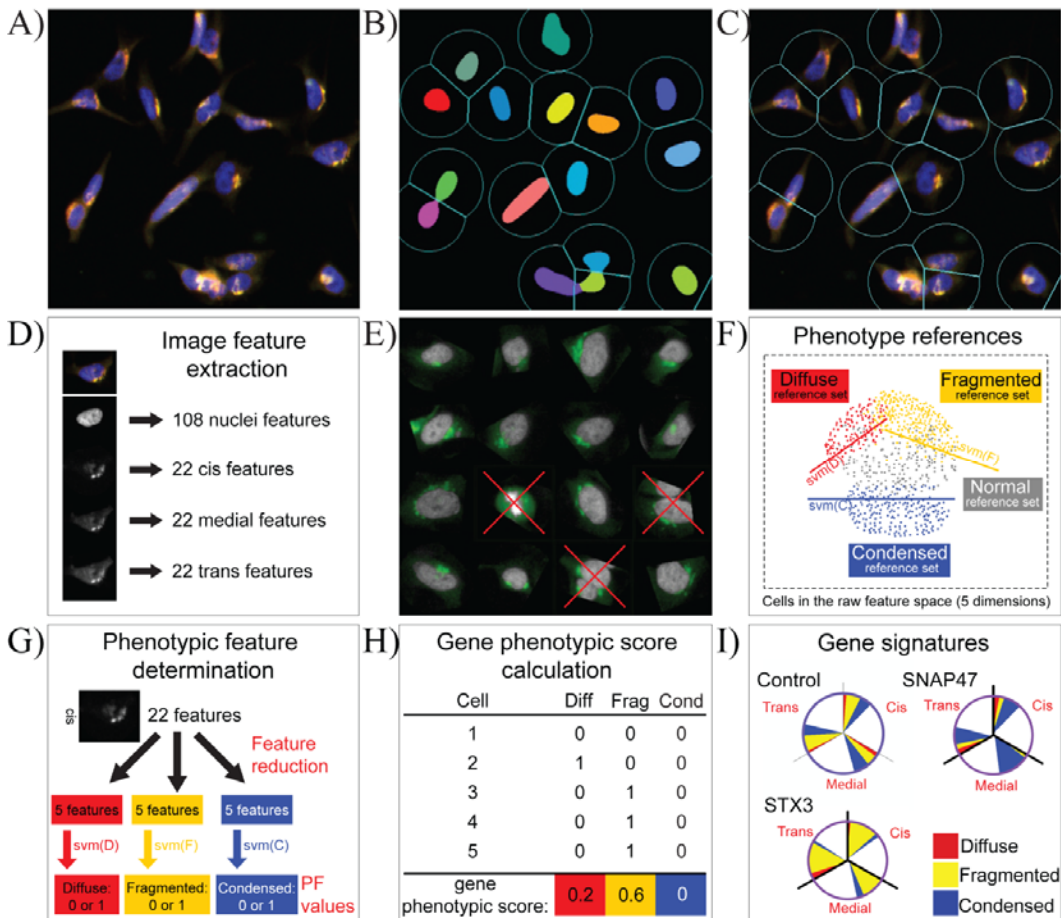
In order to quantify and classify the various Golgi phenotypes induced by gene knockdown, we have developed an automated image analysis and classification approach. The work was performed in collaboration with Dr. Victor Racine. To obtain phenotypic analysis at the individual cell level, nuclei were segmented based on DNA staining (Figure 3-3A). A cell territory was defined around the mass center of each nucleus (Figure 3-3B). Cell image features were then extracted for the nucleus (108 features) and the three Golgi markers' staining (22 features) (Figure 3-3C and D). The features ranged from intensity-based, segmentation-based and colocalisation analyses [354]. We found that a single image feature is insufficient to capture nuclei or Golgi phenotypes. Therefore, we used Support Vector Machine (SVM) machine learning [355] to find combinations of image features that could discriminate phenotypes.



A first SVM was trained to recognize and exclude out-of-focus, badly segmented and mitotic cells (Figure 3-3E). Another SVM was thereafter trained to recognize the three types of morphology, diffuse, fragmented and condensed, using reference phenotypes that were visually detected in the pilot screen (Figure 3-3F and Table 3.1). The five most discriminative image features from the pool of 22 computed Golgi features were selected for each of the three phenotypes. Image feature scores from the reference phenotypes defined the cutoff boundaries in the five-dimensional feature space. For instance, one of the image features that was selected to define cutoff for the fragmented phenotype is the number of granular structures (Obj[1].nbSubstructures) and axis length after ellipse fitting for the condensed Golgi (Obj[2].sigma.y). We found that this method provided better phenotypic discrimination (Figure 3-3F and G). The cutoff boundaries of the SVM were further refined and reinforced with cell images from the signaling genes screen (“Reference morphological phenotypes”) (Figure 3-2B and Table 3.1). The Golgi morphology of individual cells was described by the SVM classifier as a set of nine binary phenotypic features (PFs), ranging from Cis-Condensed to Trans-Diffuse (Figure 3-3G). To elaborate, the Golgi compartment of a cell was assigned as either displaying one of the three phenotypes or unaffected (normal). All three Golgi compartments were evaluated exclusively, giving rise to nine PFs (Figure 3-3G). At the gene level, the percentage of analyzed cells positive for each of the nine PFs was computed (Figure 3-3H). This is reflective of the extent of Golgi perturbations. For example, BFA treatment, which led to extensive diffused Golgi phenotype, scored significantly higher than SNAP23 depletion that has a moderate phenotype. Hence, the phenotype of each gene knockdown or cell treatment condition was assigned a signature with nine phenotypic scores. This signature is represented in a graphical manner by a colour-coded pie chart (Figure 3-3I). Correlation analysis of the screens’ phenotypes indicated that the nine scores are non-redundant (Figure 3-5D).

The performance of the SVM classifier was bench-marked against three individuals at the cellular level with a representative set of 300 cells and found to

be comparable to human classification. At the gene level, we compared SVM and experimenter classification with 120 wells displaying different phenotypes and found more than 90% agreement, indicating that our automated image analysis faithfully reproduces a human expert evaluation with the added benefit of quantification.



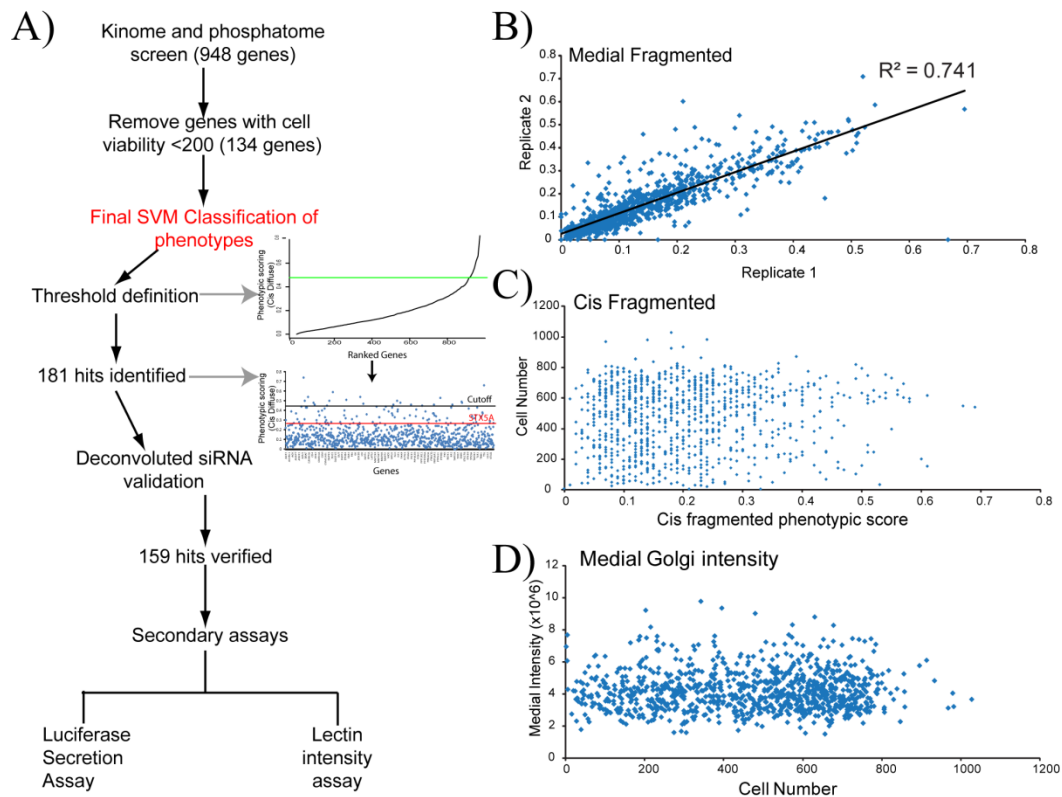
**Figure 3-3: An automated image analysis method for Golgi phenotypic classification.** (A) Cells were stained for the nucleus and Golgi compartments and (B) identified based on their nuclear staining (colored masks). (C) Cell boundaries were defined from the centers of mass of the nuclei. (D) Multiple image features for each channel of each cell were extracted. (E) Mitotic, apoptotic or closely apposed cells were detected by a specific SVM and discarded from further analysis. (F) During SVM training, reference images for each phenotypic feature (PF) (Table 3.1) were used to select the five most discriminative image features to derive SVM functions that define phenotypic boundaries in this five-dimensional space. (G) To quantify Golgi phenotypes in test images, the three SVM functions

were applied to each of the three Golgi staining: cis (shown), medial and trans, to determine PFs. These features are binary (1=yes or 0=no) for individual cells and exclusive within one channel. For instance, the cis Golgi of one cell can only be fragmented, diffuse, condensed or normal. Individual cells were eventually attributed nine binary PFs, three for each of the three channels. (H) Illustration of phenotypic score calculation for a gene. Each of the nine phenotypic scores for a gene corresponds to the fraction of analyzed cells with the particular PF. (I) The nine morphological scores constitute a phenotypic signature displayed in a colour-coded pie-chart. White sectors represent cells with normal Golgi morphology.

### **3.2.4 159 signaling genes regulate Golgi organisation.**

To probe Golgi regulatory mechanisms, I next screened 948 siRNAs targeting kinases, phosphatases and related genes (Figure 3-4A). The morphological analysis gave highly reproducible results between the two replicates, suggesting low experimental variations (Figure 3-4B). To avoid quantifying effects associated with apoptosis or cell necrosis, I discarded genes with a significant effect on cell number. Based on the average number of nuclei for all treatments in the screen, I eliminated those that resulted in less than 200 nuclei detected (Figure 3-4A). Furthermore, I found no correlation between any of the phenotypic scores with cell number, arguing against any bias induced by cell viability issues (Figure 3-4C). Similarly, a lack of correlation between the intensities of Golgi compartments and cell counts indicated cell number did not affect intensities (Figure 3-4D).

Subsequently, I determined significance thresholds for each of the nine morphological features based on the first derivative of ranked data as described in [356]. Each threshold corresponds to a z-score of two or more. A gene was classified as a hit when at least one Golgi compartment was significantly perturbed, hence identifying 181 primary hits (Figure 3-4A). I further confirmed the hits by examining individual images to ensure that the knockdowns induced visually significant perturbations on the Golgi. To remove false-positive hits due to off-target effects, I next tested if the phenotypes scored could be reproduced by at least two independent siRNAs out of the four (deconvoluted siRNA) used in the original pools in the screen. This validated 159 hits for which the possibility of off-target effect is greatly reduced (Table 3.2). This represents about 20% of the signaling genes tested, which is a surprisingly large proportion. I, in collaboration with Dr Germaine Goh, further screened the validated hits for effects on Golgi functions: secretion (Section 3.2.9) and glycosylation (Section 3.2.10).



**Figure 3-4: A large proportion of signaling genes regulate Golgi structure.**

(A) Schematic workflow of the signaling genes screen. Gene knockdowns having a total cell number of more than 200 were excluded from the final SVM classification. Thresholds for primary hit identification were defined using the derivative method for each of the nine PFs, resulting in 181 primary hits. The primary hits were re-tested with the four individual siRNAs present in the pool (deconvoluted siRNA) of the primary screen and 159 hits were validated (Table 3.2). These validated hits were then further screened for glycosylation (lectin intensity assay; Figure 3-19) and secretion (Met-luc secretion assay; Figure 3-16) changes. (B) A scatter plot demonstrating reproducibility in the phenotypic scores between the two screen replicates in the medial fragmented scores. Good reproducibility between replicates was observed in the scores of all nine PFs. (C) Plot of total cell count versus phenotypic scores reveals absence of correlation between cell number and Golgi phenotype. All nine PFs demonstrated absence of correlation with cell number. (D) Plots comparing the intensities of Golgi compartments with cell count also show lack of correlation.

### **3.2.5 Golgi phenotypes from the signaling screen were diverse.**

The primary screen revealed that numerous signaling genes are essential for the maintenance of normal Golgi organisation (Table 3.2). With our analysis method, the relative intensities of morphological perturbations are encoded in the percentage of cells classified as perturbed. Comparing the data from the membrane traffic and signaling genes screen, it is apparent that depletions of several signaling genes have an effect on the Golgi more pronounced than most well known regulators such as the SNAREs (Figure 3-5A). Using the significance thresholds from the signaling screen, I could find only 10% (6 out of 63) of membrane trafficking regulators, as opposed to 20% in the signaling genes, resulted in equally significant Golgi perturbations. This suggests that these signaling hits could regulate Golgi organisation in multiple ways.

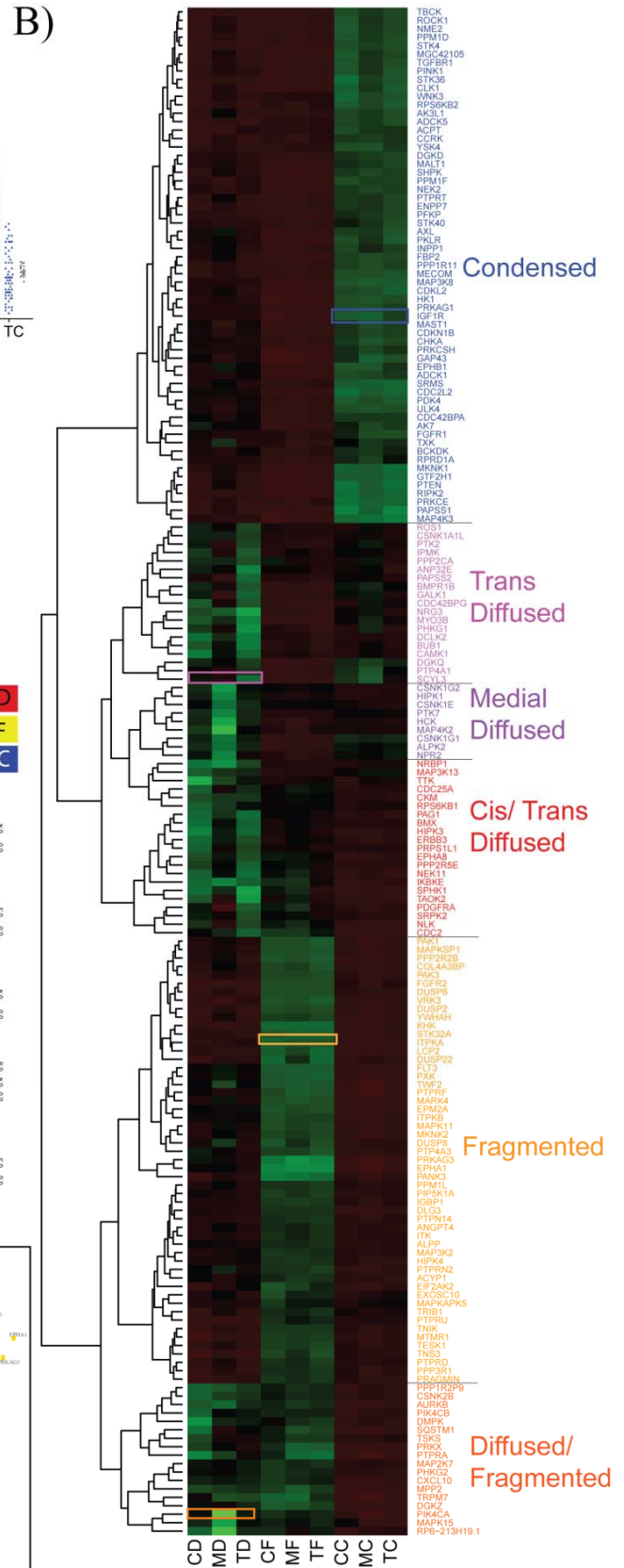
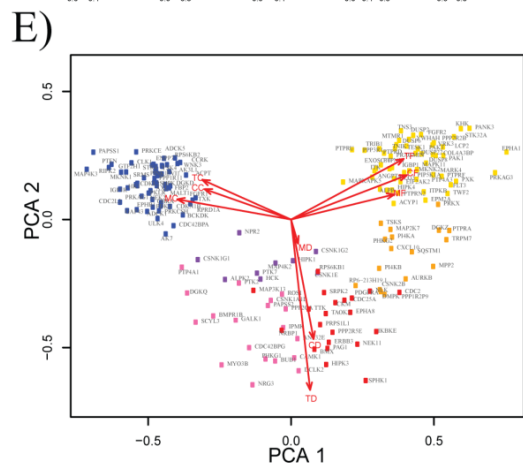
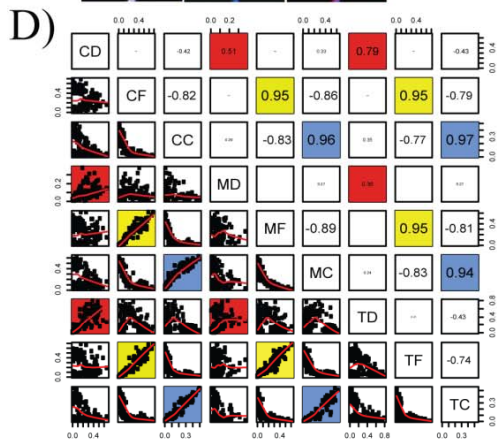
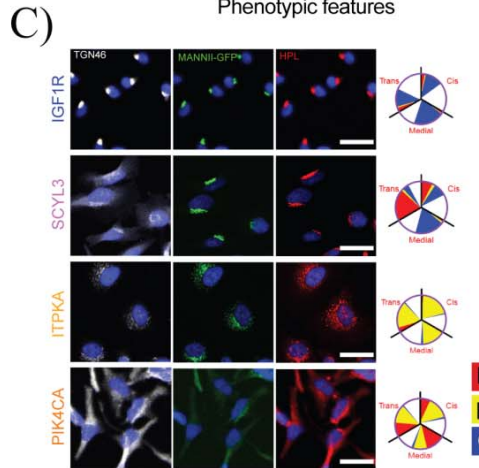
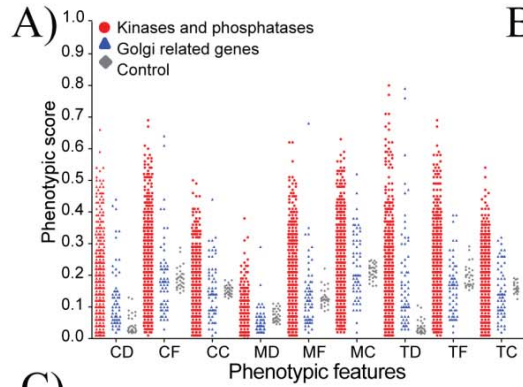
The perturbations of Golgi phenotypes observed were diverse, ranging from perturbations specific for one cisternal marker (SCYL3, trans Golgi) to perturbations affecting all three markers with either a condensed (IGF1R), fragmented (ITPKA) or diffuse (PIK4CA) appearance (Figure 3-5B and C). Consistent with results in the pilot screen, the morphological scores for each of the three Golgi markers were highly correlated with each other in the fragmented or condensed phenotypes (for example Cis-fragmented and Medial-fragmented: correlation coefficient of 0.95) (Figure 3-5D). By contrast, the scores of the Golgi markers did not correlate well between each other for the diffuse morphology (Figure 3-5D).

The diffuse Golgi morphology is reminiscent of an ER pattern, suggesting that the marker displaying this morphology has been relocalized at least partially to the ER. When I co-stained some of the diffuse cis-Golgi hits with the ER marker calreticulin, I could observe and quantify significant increase in colocalisation between calreticulin and HPL (Figure 3-6A and B). This indicates that the glycosylation enzymes GalNAc-Ts, whose activities are revealed by HPL, have

been relocated to the ER. Interestingly, depletions of several genes induced specifically GalNAc-Ts but not MannII-GFP ER relocation (Figure 3-5B). This is consistent with the notion that the trafficking of different Golgi enzymes is independently regulated as our group has previously reported [193].

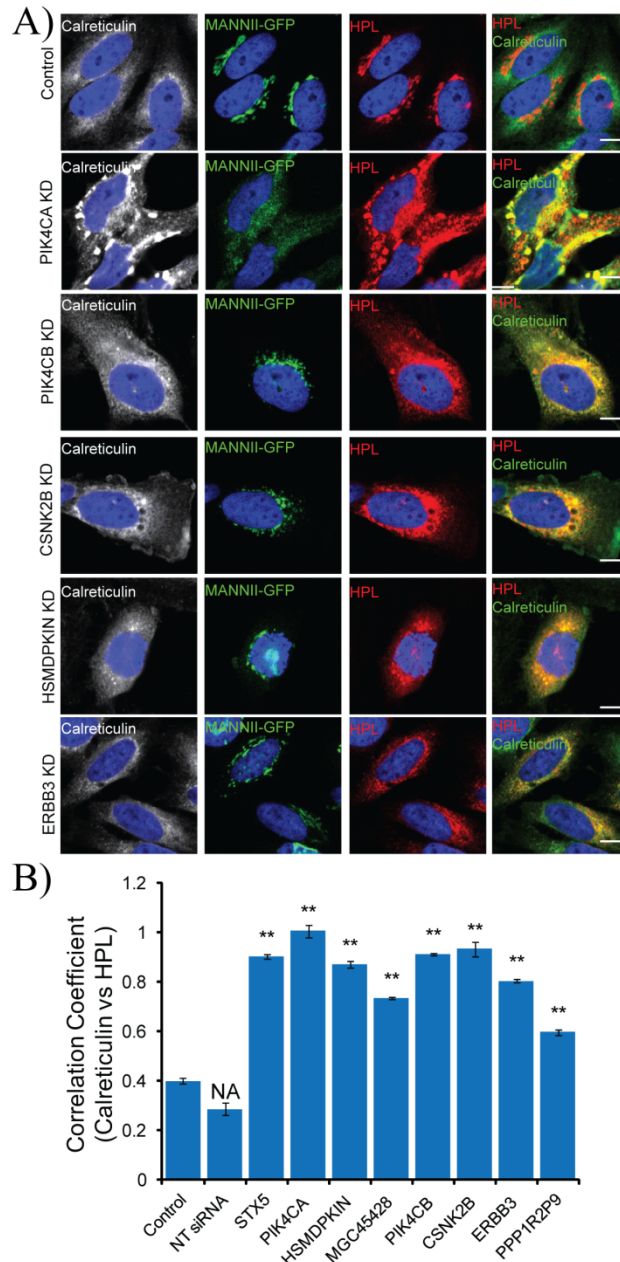
Hierarchical clustering using the scores of nine PFs revealed six major morphological groups (Figure 3-5B). The two dominant groups are those that display condensed Golgi (61 genes) or fragmented Golgi (53 genes) for all markers (Figure 3-5B). For these phenotypes, the three markers colocalize extensively, as much as in untreated cells, either in fragments or in a perinuclear condensed structure (Figure 3-5D). A reduction of the nine morphological features in two dimensions by principal component analysis (PCA) resulted in these two groups appearing relatively compact and well-separated (Figure 3-5E, yellow and blue dots). The separation also indicated that these two Golgi morphologies occur mutually exclusive of each other, suggesting antagonistic effects of the two groups of genes on the Golgi. In the other four groups (67 genes in total), the phenotypes were at least partially diffuse and were more heterogeneous. Most genes presented a varied mix of fragmented and diffuse phenotypes, consequently they appeared more spread in the two dimensional PCA phenotypic space (Figure 3-5E, pink, purple, red and orange dots). For these phenotypic groups, staining of the three Golgi markers are generally less well colocalized than in the control (see example SCYL3 in Figure 3-5C).

Because each marker is specific for different Golgi compartments, the partially diffused phenotypes suggest a perturbation of cisternal organisation. By contrast, condensed and fragmented phenotypes imply an alteration of the network organisation of the Golgi stacks, within which cisternal organisation is maintained. By extension, the large number of genes in these two groups suggests that many signaling pathways affect the overall network structure of the Golgi rather than its cisternal organisation.





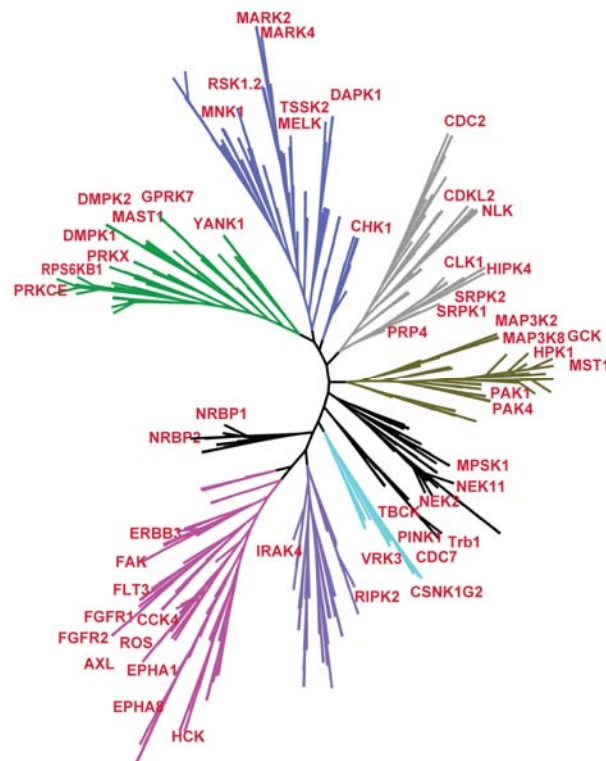
**Figure 3-5: A diversity of Golgi phenotypes could be observed from signaling gene depletions.** (A) Morphological scores of signaling genes (*red dots*) compared with membrane trafficking genes (*blue dots*) and control wells (*gray dots*). CD, MD, TD, CF, MF, TF, CC, MC and TC refer to cis diffuse, medial diffuse, trans diffuse, cis fragmented, medial fragmented, trans fragmented, cis condensed, medial condensed, and trans condensed, respectively. (B) Hierarchical clustering of 181 primary hits using the nine PFs. The range of phenotypic scores is represented by green (high score) to red (low score) in the heatmap. Six major morphological groups were identified and color-coded: condensed (*blue words*), trans diffuse (*pink*), medial diffuse (*purple*), cis and trans diffuse (*red*), fragmented (*yellow*), diffuse and fragmented (*orange*). (C) Corresponding images of the genes highlighted in colored rectangles in (B). IGF1R depletion (*blue label*) resulted in all Golgi compartments condensed; SCYL3 (*pink*) in strongly diffuse trans compartment; ITPKA (*yellow*) in all Golgi compartments fragmented; PIK4CA (*orange*) in a mix of diffuse and fragmented for all compartments. Scale bar: 30  $\mu\text{m}$ . (D) Correlation plots of the nine phenotypic features. (E) Principal component analysis (PCA) of the nine phenotypic features revealed the distributions of the six morphological groups. Color coding corresponds to the six morphological groups defined in (C).



**Figure 3-6: Diffuse Golgi morphology is likely due to relocation of marker to the ER.** (A) Genes that exhibited a cis diffuse Golgi upon depletion show extensive colocalisation between cis Golgi marker HPL and ER marker calreticulin. Images were acquired with 60x magnification. Scale bar: 10  $\mu$ m. (B) Colocalisation between the cis Golgi and ER markers was measured using Pearson's correlation coefficient of the two markers' staining. Cells were analyzed using MetaeXpress Translocation-Enhanced analysis module. Values on graphs indicate the mean  $\pm$  SEM. \*\* $p < 0.0001$ , \* $p < 0.05$  by two-tailed unpaired t-test, relative to untransfected control cells.

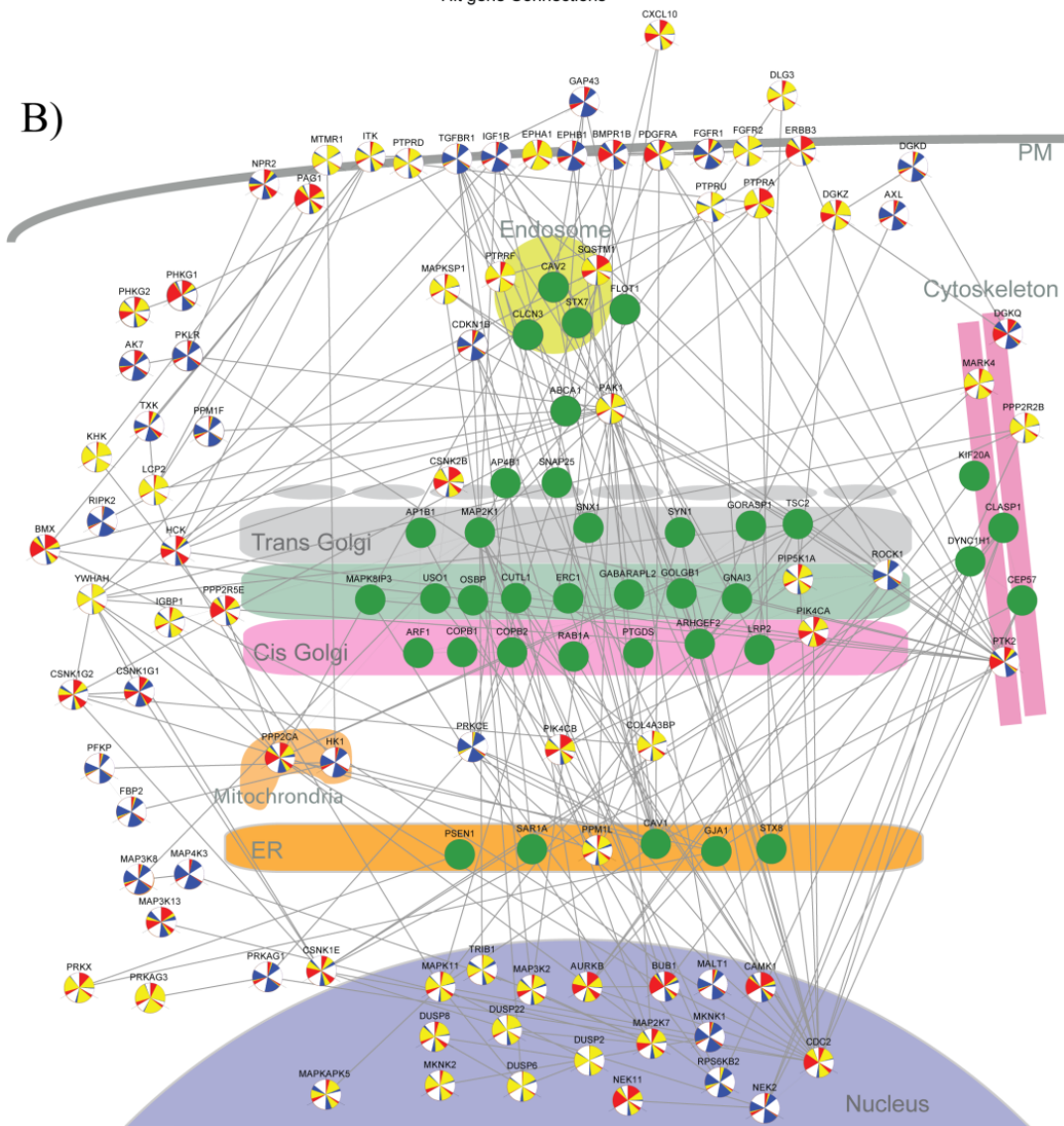
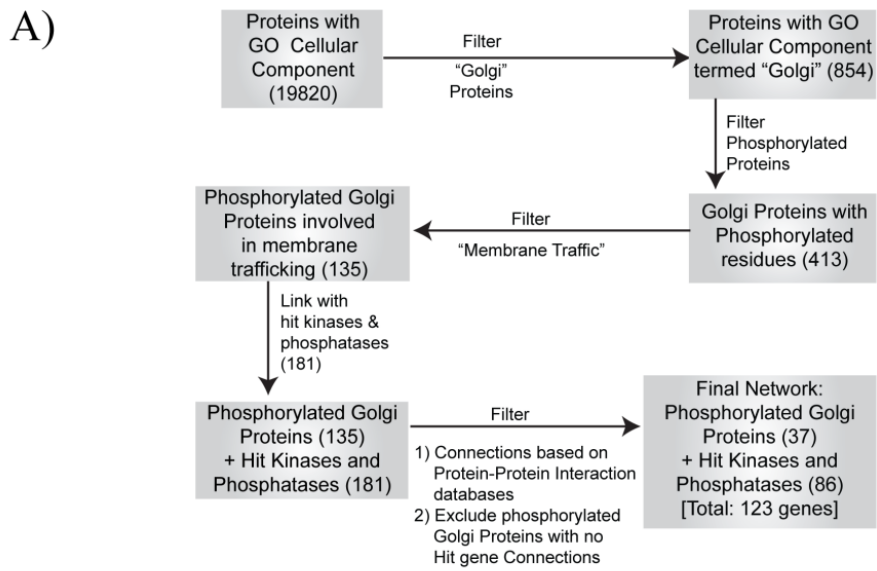
### 3.2.6 A large signaling network regulates Golgi apparatus organisation.

The number of signaling gene depletions affecting Golgi organisation is large. To further understand the nature of signaling regulation on the Golgi, in collaboration with Dr Pankaj Kumar, I mapped the 111 hit kinases (out of 181 primary hits) from the screen on a phylogenetic tree of kinases [357]. This reveals that all the major families are involved in Golgi regulation (Figure 3-7). By extension, this suggests that signaling regulation on the Golgi is an evolutionary conserved event.



**Figure 3-7: A map of 111 hit kinases on the phylogenetic tree of kinases reveals Golgi regulation by all kinase families.** Hit kinases are labeled in red words. Seven main kinase families are indicated in different color branches: Calcium/calmodulin-dependent protein kinase (CAMK) family in blue, Containing CDK, MAPK, GSK3, CLK families (CMGC) in grey, Homologs of Yeast Sterile kinases (STE) in brown, Casein kinase 1 (CK1) family in aqua, Tyrosine kinase- like (TKL) in purple and Tyrosine kinase (TK) in pink.

If these enzymes act directly on the organelle, one could expect a high number of phosphoproteins associated with Golgi membranes. To test this, we conducted a systematic search for proteins with a Gene Ontology (GO) Cellular Component (CC) containing the term “Golgi” and found 854 proteins. In the PhosphositePlus database, almost half (413) of these Golgi associated proteins were found to carry at least one phosphorylated residue (Figure 3-8A). Additionally, to ensure that the network generated would be as stringent as possible, the additional filter of “membrane trafficking” GO Biological Process (BP) term was applied, resulting in 135 out of 413 proteins being retained. Hence, 135 proteins are annotated in databases to be localized at the Golgi, phosphorylated and regulate membrane traffic. We next evaluated how our screen hits could be associated with these 135 Golgi phosphoproteins. Using only experimental-based evidences in the STRING database, 37 Golgi phosphoproteins were found to interact with 86 of our screen hits. We used these interactions and the available GO Cellular Compartment annotations to draw a map of the Golgi regulatory network (Figure 3-8B). These results suggest that the effects that are observed are likely due to direct regulation through phosphorylation of Golgi-associated proteins.



**Figure 3-8: Protein network analysis of hits reveals multiple connections between signaling molecules and Golgi proteins.** (A) Step-wise construction of the Golgi regulatory network. 413 of the 854 proteins localized at the Golgi in the Gene ontology (GO) database were also found in the Phosphosite plus database. A functional filter using Biological Process GO yielded 135 phosphorylated proteins present at the Golgi and functioning in membrane trafficking. Using protein-protein interaction information from three databases (String, Pathway Studio and HPRD), 37 of these curated phosphorylated Golgi proteins were reported to have a direct interaction with 86 hits. (B) A preliminary map of the Golgi regulatory network arranged based on available Cellular Compartment GO for all 123 genes. Signaling hits are represented in their gene signatures while dark green nodes represent membrane trafficking annotated Golgi phosphoproteins.

### **3.2.7 Specific sub-networks further reveal Golgi regulatory mechanisms.**

To better understand the relationships between Golgi proteins and the screen hits, I probed further in the Golgi regulatory network and incorporated in-depth literature searches to reconcile the Golgi phenotypes observed with the regulatory mechanisms involved. The sub-networks are reviewed in the following sections:

#### **3.2.7.1 New players in the Golgi phosphoinositide regulatory network**

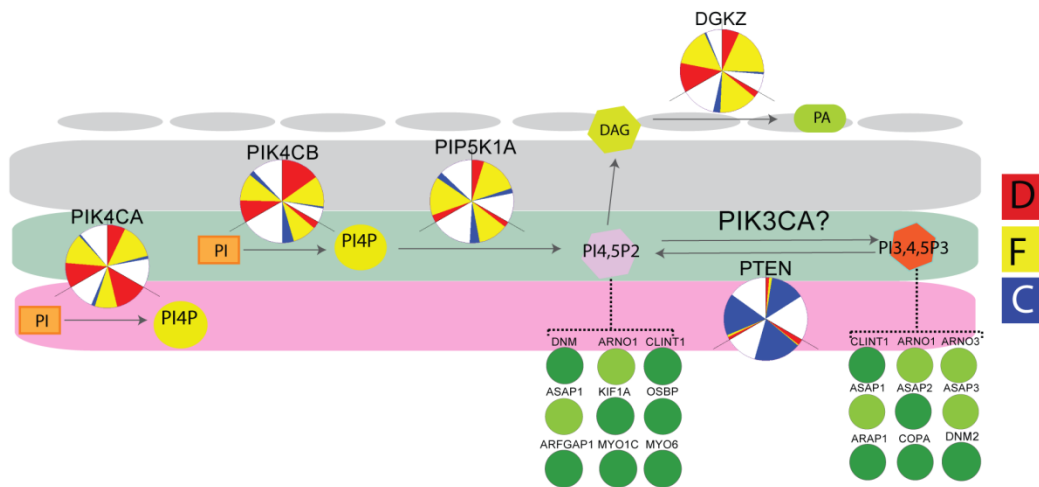
Phosphoinositides are known to regulate membrane dynamics at the Golgi level [358]. Phosphatidylinositol 4-phosphate (PI4P) in particular is enriched in Golgi membranes and is known to regulate multiple molecular events [358] (Figure 3-9). Depletion of both PI4P kinases PIK4CA and PIK4CB, which phosphorylate PI, resulted in strong perturbations of Golgi organisation. The lack of compensation and differences in phenotype suggest that both kinases regulate different pools of PI4P as previously suggested [359, 360]. Specifically, PIK4CA appears to regulate PI4P at the level of ER exit sites as recently shown [361], while PIK4CB appears to function at the Golgi itself [362].

PIP4 can be phosphorylated into PI4,5P2 and it has been suggested that PI4,5P2 may play an important role in Golgi membrane dynamics, but the kinase responsible has remained unknown [363-365]. Here, I found that depletion of PIP5K1A, which produces PI4,5P2, also resulted in a significant fragmentation of the Golgi (Figure 3-9).

I also observed a condensed Golgi phenotype upon depletion of PTEN, a phosphatase with specificity for the position 3 of PI3,4,5P3 (Figure 3-9), consistent with a previous report that localized PTEN2 at the Golgi [366]. Previous reports have also suggested a role for PI3,4,5P3 at the Golgi, identifying multiple possible effectors [367-369]. A class I PI3 kinase, PIK3CA, has recently been found to localize at the TGN in macrophages and to be important for the

release of cytokine-containing carriers at the TGN [370]. Depletion of the same kinase PIK3CA in my screen induced mild Golgi fragmentation, albeit below my cutoff threshold, suggesting that its role at the TGN is not limited to macrophages.

Finally, I have also integrated in this sub-network the diacylglycerol (DAG) kinase zeta (DGKZ), which produces a strong phenotype. Indeed, PI4,5P2 can be converted into DAG by the phospholipases C, PLCB2 and PLCE, which both have been localized at the Golgi [371, 372]. These results demonstrate the screen's capacity to identify known players and suggest novel regulators of the PI network operating at the Golgi.



**Figure 3-9: Phosphatidylinositol (PI) network regulators identified in the screen.** Depletion of either PIK4CA or PIK4CB resulted in a highly diffuse and fragmented Golgi. PI4P is possibly converted into PI4,5P2 by PIP5K1A as indicated by fragmentation of the Golgi upon knockdown. Depletion of PTEN, the phosphatase for PI3,4,5P3, exhibited a condensed Golgi phenotype. Diacylglycerol (DAG), a downstream product of PI4,5P2 is converted into phosphatidic acid (PA) by DGKZ whose knockdown resulted in a fragmented Golgi. Different PI species can recruit various membrane trafficking effectors (green nodes). Black arrows indicate non-phosphorylation based activation. Dark green nodes and light green nodes represent phosphorylated Golgi proteins and Golgi proteins, respectively.



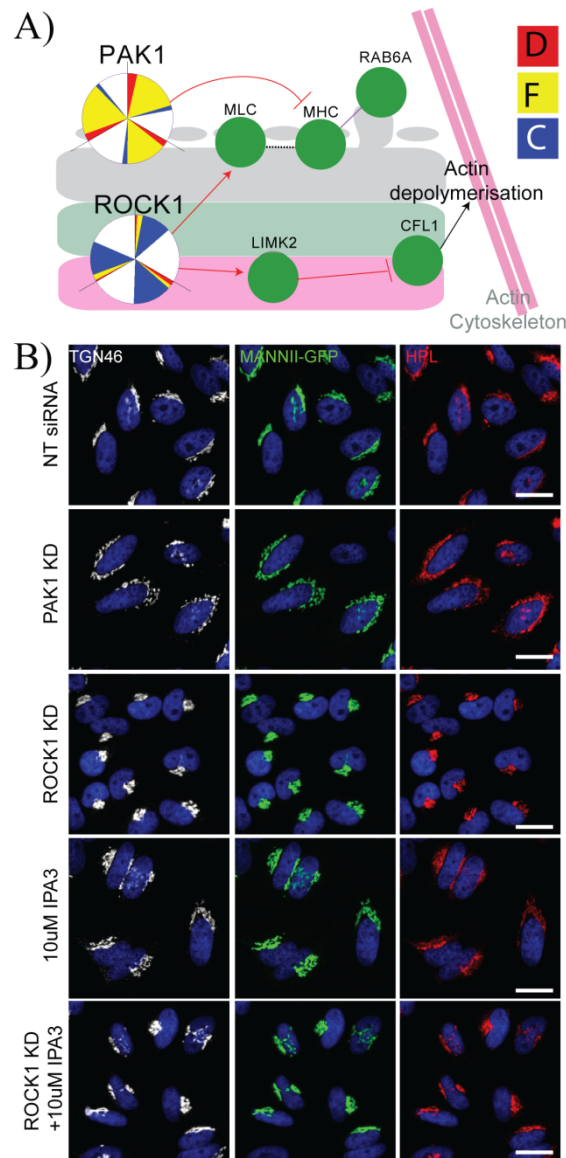
### 3.2.6.2 Regulators of acto-myosin dynamics at the Golgi apparatus

Another network of Golgi regulation appears to revolve around actin dynamics. A condensed Golgi phenotype was induced by depletion of the protein kinase ROCK1 and also, to a lesser extent, of ROCK2 (Figure 3-10A). Consistently, expression of an active form of ROCK1 was previously reported to induce Golgi fragmentation [373]. In non-muscle cells, ROCKs regulate actomyosin contractility in two ways: phosphorylation of the regulatory myosin light chain (MLC) of motor protein myosin II and phosphorylation and activation of the LIMK1 and LIMK2 kinases that, in turn, phosphorylate and inhibit the actin depolymerising protein cofilin (CFL1). Interestingly, all these effectors have been localized at the Golgi complex [374]. It was reported recently that myosin II regulates the fission of transport carriers at the Golgi [375]. Regulation of actin dynamics by cofilin was also reported to regulate Golgi organisation and export from the TGN [376] [377] [378]. Treatment by Latrunculin and other drugs able to block actin polymerization have been reported to induce a compaction of the Golgi apparatus [379].

Surprisingly, I also found that depletion of PAK1 induces a marked fragmented phenotype (Figure 3-10A). This is consistent with previous reports of PAK1 inhibition of actomyosin contractility by inactivation of MLCK [380] and by phosphorylation and inactivation of myosin II heavy chain (MHC) [381]. Treatment of cells with IPA3, a PAK1 inhibitor [382], also induced fragmentation of the Golgi (Figure 3-10B) after six hours of treatment. The effect was dose dependent. In agreement with the model of opposite action of ROCK1 and PAK1 at the Golgi, IPA3 could rescue at least partially the effect of ROCK1 knockdown while having no effect on PAK1 depleted cells (Figure 3-10B).

Together these data suggest that ROCK1 and PAK1 exert antagonistic forces on the structure of the Golgi apparatus through actomyosin processes. These processes are proposed to be required for the generation of transport carriers at the Golgi [375]. Consistent with this model, depletion of ROCK1 induces a

significant reduction of constitutive secretion as measured by a secreted *Metridia* luciferase (Met-Luc) assay (Figure 3-16).



**Figure 3-10: Regulators of the actomyosin machinery control Golgi organisation.** (A) ROCK1 depletion resulted in a compact Golgi while PAK1 depletion resulted in a fragmented Golgi, suggesting antagonistic effects on the Golgi structure through actomyosin processes. Red arrows indicate phosphorylation. Dashed lines indicate recruitment. (B) Treatment of cells with 10µM of PAK inhibitor IPA3 for six hours recapitulated the fragmented Golgi phenotype in PAK1 depletion. ROCK1 depleted cells treated with IPA3 reverted the condensed Golgi phenotype to normal.

### 3.2.6.3 A link between cell cycle regulators and the TGN

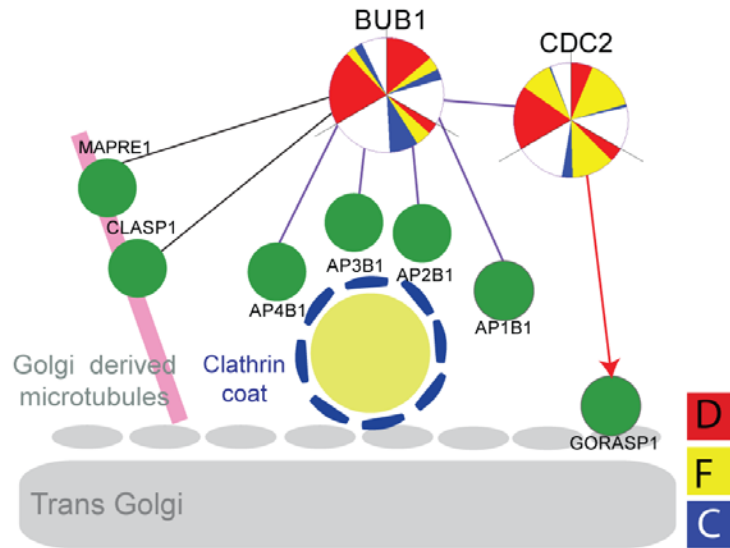
Depletion of the mitotic checkpoint kinase BUB1 resulted in a strong diffuse morphology affecting more specifically the trans Golgi marker. A previous report indicated that BUB1 interacts with the  $\beta$  chains of the 4 heterotrimeric adaptor complexes AP1, AP2, AP3 and AP4 [383]. AP complexes, except AP2, act at the TGN to promote sorting of cargo proteins into clathrin coated transport carriers [384]. Phosphorylation of AP complexes has been proposed to regulate their interaction with clathrin coat and/or sorting signals on cargo proteins [385]. Consistently, the yeast homologue of BUB1, Bub1p, has been found to interact with the human Nexin-1 homolog, Vps5, that is required for trafficking from the prevacuolar/late endosomal compartments back to the Golgi apparatus [386].

Consistent with a direct role of BUB1 at the TGN, two BUB1 interactors [387], the CLIP-associated protein (CLASP) and microtubule associated protein (MAPRE1) are Golgi associated proteins, and have roles in nucleation and stabilization of a subset of microtubules that originate from the TGN [72]. These TGN-derived microtubules are required for maintaining Golgi structure, directional post-Golgi trafficking and cell migration [68].

Another key mitotic kinase, CDC2, alias Cdk1, known to regulate BUB1 [388], also results in a marked perturbation of the TGN. It was therefore hypothesized that both kinases may function together at the TGN. Cdk1 has previously been reported to phosphorylate GRASP65 during mitosis [389]. However, it is not clear whether this is related to the phenotype that was observed in my screen, as GRASP65 is not known to localize at the TGN.

Overall, this sub-network suggests an intriguing link between cell cycle kinases and post-Golgi traffic (Figure 3-11) that may have to do with the dramatic changes in cell morphology and surface-to-volume ratio observed at the onset of mitosis. Whether or not this link is related to the Golgi fragmentation observed

during mitosis is hard to establish at present: judging by their DNA, the cells are not arrested in mitosis and their Golgi phenotype appears different from a mitotic Golgi, which would be clearly fragmented: for BUB1 the phenotype is mostly diffuse cis and trans and for CDC2 it is a mixture of diffuse and fragmented (Figure 3-11).



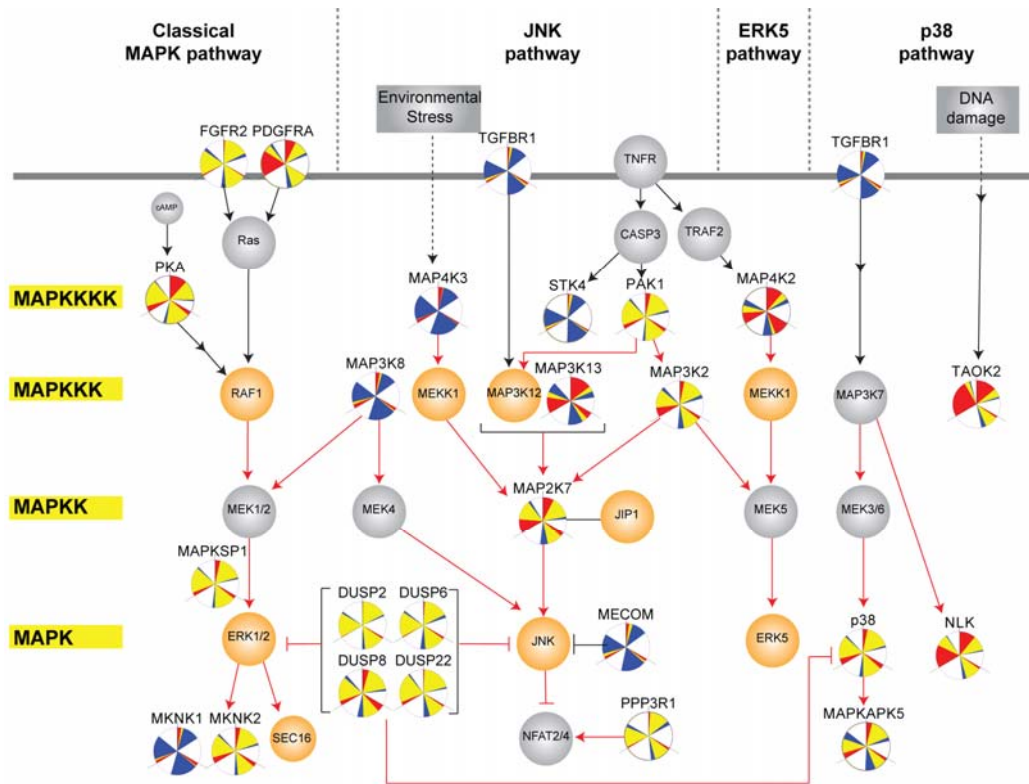
**Figure 3-11: A possible link between cell-cycle kinases and trans Golgi-plasma membrane trafficking.** Knockdown of mitotic checkpoint kinase BUB1 and cell-cycle control kinase CDC2 resulted in a specifically trans diffuse Golgi. Purple lines indicate confirmed protein–protein interaction curated in HPRD database. Red arrows indicate phosphorylation. Black lines indicate protein–protein interaction based on the STRING database.

#### 3.2.6.4 Different MAPKs cascades affect Golgi organisation

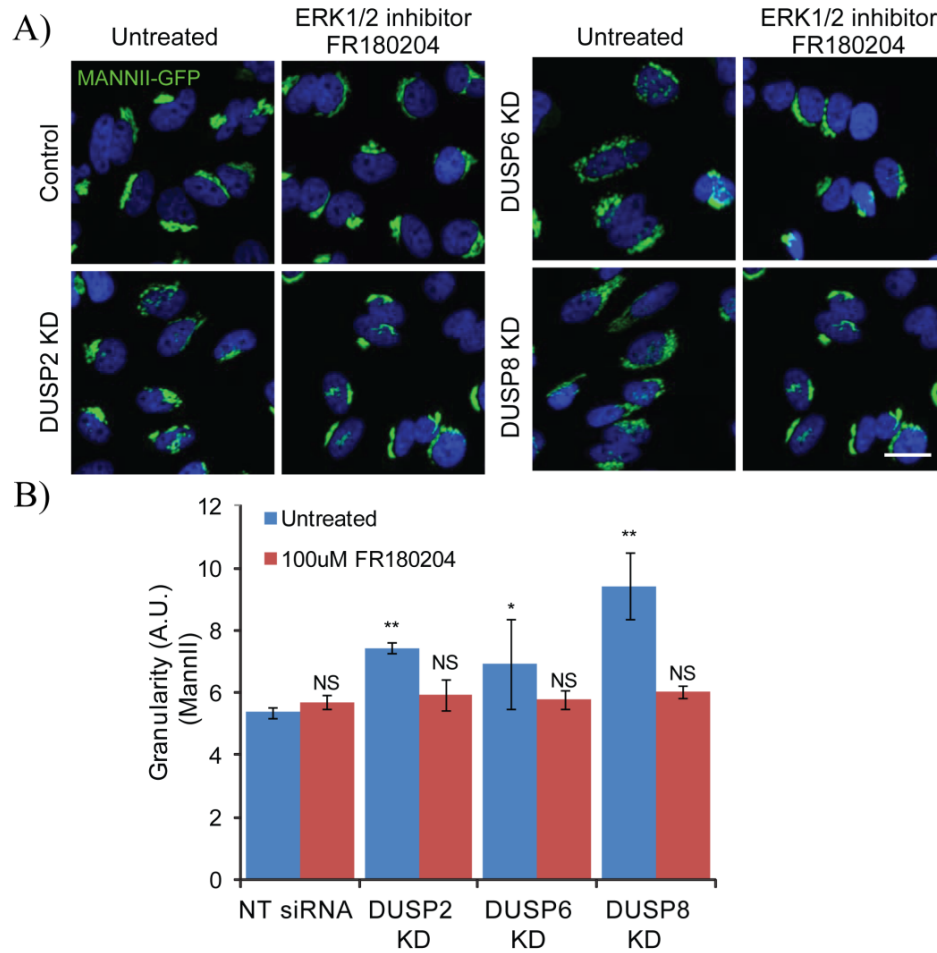
The Mitogen Activated Protein Kinases (MAPK) family include more than 30 different protein kinases that respond to various stimuli [390]. MAPK cascade involves, typically in mammalian cells, three or four levels going from MAP4K to MAPK [391]. My screen results indicate a significant enrichment in the MAPK signaling pathway based on the KEGG pathway database (Enrichment= 9.43, p-value=  $3.7 \times 10^{-10}$ ) This is consistent with the results of two recent screens looking at ER exit sites in mammalian cells and Golgi morphology in *Drosophila* S2 cells [392, 393].

Eight MAPK family kinases and thirteen closely related genes were identified, including four dual specificity phosphatases (DUSP) (Figure 3-12). DUSP are proposed negative regulators of MAPK pathways. I verified that depletion of DUSP2, 6 and especially 8 resulted in up regulated phosphorylation of ERK1/2 based on immunoblotting with phospho-ERK specific antibody. This suggests that fragmentation of the Golgi apparatus results from the activation of ERK. Indeed, treatment of the DUSP2, 6 or 8 depleted cells with the ERK inhibitor FR180204 reverted the Golgi phenotype (Figure 3-13A and B). ERK has been shown to phosphorylate the Golgi structural protein GRASP65 during the orientation of the Golgi towards the leading edge [394]. This phosphorylation event could be one of the underlying mechanisms of the observed Golgi fragmentation.

At present, four main MAPK cascades have been described, the classical pathway, which respond to mitogenic stimulation, the p38 and JNK cascades that tend to be activated by environmental stress and the lesser known ERK5 cascade. Based on results from my screen and previous RNAi screens [392], it appears that all four cascades are involved in the regulation of Golgi organisation.



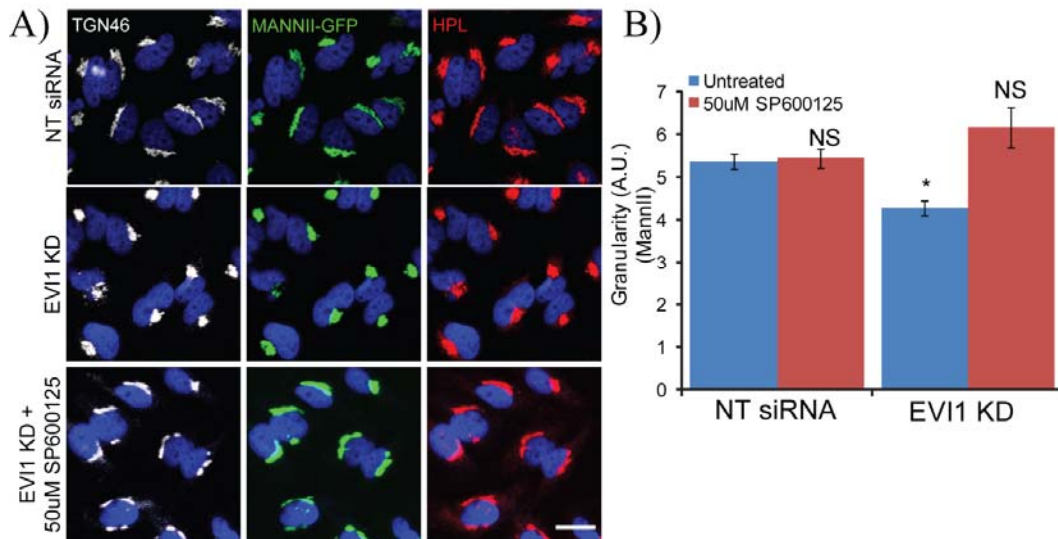
**Figure 3-12: MAPKs from all four signaling cascades regulate Golgi organization.** Multiple players from different tiers of the MAP kinase signaling pathway appear as hits in my screen and the screen by [392], highlighting the importance of MAP kinases in the regulation of the secretory system. Tiers of the MAP kinase pathway are indicated on the left and the four main MAP kinase pathways are indicated at the top. Dark green nodes and light green nodes represent phosphorylated Golgi proteins and Golgi proteins, respectively. Orange nodes represent hit genes from [392]. Grey nodes represent non-hit genes in both screens. Black arrows indicate activation. Red arrows indicate phosphorylation.



**Figure 3-13: Golgi fragmentation by depletion of DUSPs requires ERK1/2 activation.** (A) Treatment of DUSP-depleted cells with 100 $\mu$ M ERK1/2 inhibitor FR180204 for six hours rescue the fragmented Golgi phenotype. Scale bar: 10  $\mu$ m. (B) Quantification of medial Golgi fragmentation in cells with (red bars) and without (blue bars) drug treatments indicate the reversion to normal Golgi by ERK inhibition. Values on graphs indicate the mean  $\pm$  SEM. \*\* $p < 0.0001$ , \* $p < 0.05$  by two-tailed unpaired t-test, relative to untreated control (NT siRNA-treated) cells.

Indeed, one of my screen hits, MECOM, aka Evi1, has been proposed to negatively regulate the JNK by direct binding [392]. JNK has been linked to Golgi associated proteins, such as AKRL1/2 [395] or vesicular trafficking proteins such as JIP1/2/3 [396]. Consistent with the effect of Evi1 depletion being mediated by JNK, I found that treatment of the Evi1 depleted cells with the JNK inhibitor SP600125 reverted the Golgi condensed phenotype (Figure 3-14A and B).

The Golgi proteins that could be mediating these changes of morphology remain relatively few at present. In addition to GRASP65, recent screens have demonstrated that the classical MAPK ERK1/2 and the atypical ERK7 phosphorylates the ER exit site component Sec16 to regulate export from the ER [392]. Given the variability of phenotypes and the number of kinases involved in my screens, it is likely several other substrates are engaged by different pathways.



**Figure 3-14: Condensed Golgi from MECOM depletion is likely due to JNK activation.** (A) The condensed Golgi phenotype in MECOM depleted cells is reverted back to normal after treatment with 50 $\mu$ M of JNK inhibitor SP600125 for six hours. Scale bar: 30 $\mu$ m. (B) Quantification of medial Golgi fragmentation in cells with (red bars) and without (blue bars) drug treatment substantiates that JNK inhibition rescued the condensed Golgi in in EVI1 knockdown. Values on graphs

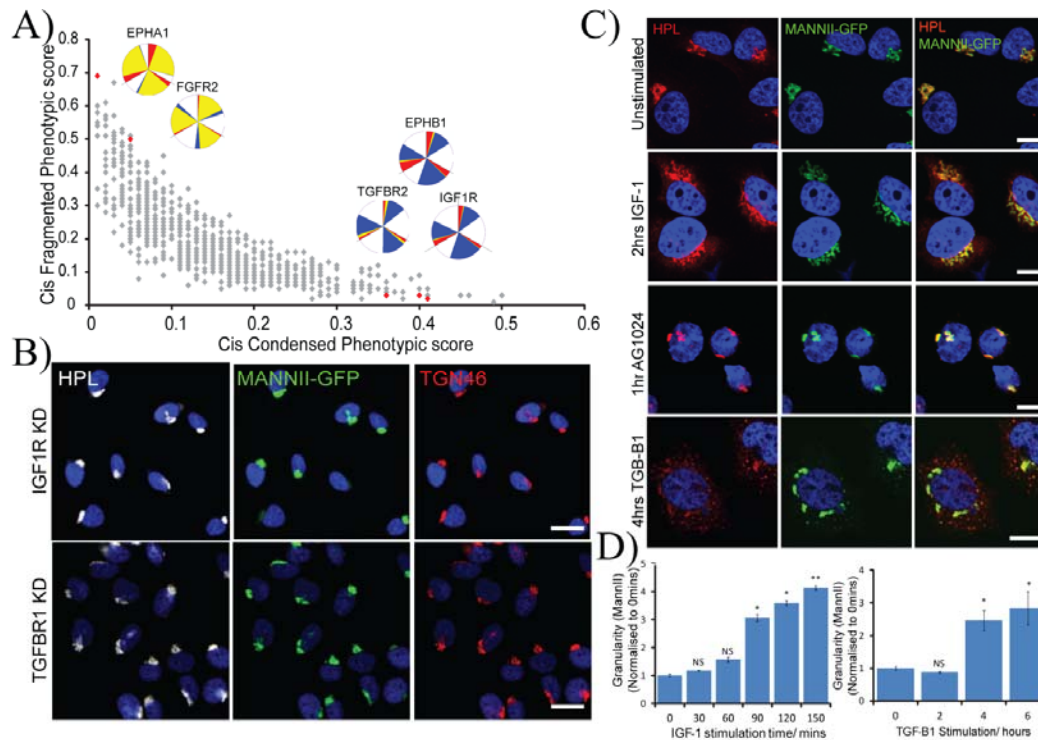


indicate the mean  $\pm$  SEM. \*\* $p < 0.0001$ , \* $p < 0.05$  by two-tailed unpaired t-test, relative to untreated control cells.

### **3.2.8 Growth factors and cell surface receptors signal to the Golgi apparatus**

Among the confirmed gene depletion affecting most significantly Golgi morphology, several cell surface receptors were identified. FGFR2 and IGF1R displayed opposite phenotypes, fragmented and condensed respectively, suggesting that different signaling cascades can balance each other's effects on the Golgi apparatus (Figure 3-15A and B). These Golgi phenotypes imply that cells modulate the secretory pathway in response to ligand binding to these receptors.

To test this, I stimulated cells with Insulin-like Growth Factor 1 (IGF-1) or the Transforming Growth Factor B1 (TGF-B1). Stimulation of serum-starved HeLa cells with 100ng/ml of IGF-1 or 2ng/ml TGF-B1 induced significant fragmentation of the Golgi apparatus as early as one hour and for as long as four hours (Figure 3-15C and D). This relatively short time-course suggests that these cell surface receptors could regulate the secretory pathway relatively directly. This is further supported by the rapidity of response to the IGF1R inhibitor AG1024, which recapitulates IGF1R depletion (condensed Golgi apparatus) as early as one hour after drug addition (Figure 3-15C).



**Figure 3-15: Cell surface receptors control Golgi organisation.** (A) Correlation plot of cis fragmented against cis condensed phenotypic scores from the depletion of signaling genes. (B) Golgi staining of different compartments in the depletion of cell surface receptors IGF1R and TGFBR1 reveals a typical condensed Golgi phenotype. Scale bar: 30µm. (C) Golgi staining after cell stimulation with 100ng/ml IGF1R ligand IGF-1 for two hours (top) and 2ng/ml TGFBR1 ligand TGF-B1 (bottom) for four hours or treatment with the IGF1R inhibitor AG1024 for one hour (middle). Images were acquired at x60 magnification. Scale bar: 10µm. (D) Quantification for Golgi fragmentation in IGF-1 (left) and TGF-B1 stimulation (right) reveal increasing Golgi fragmentation over time of stimulation. Values on graphs indicate the mean ± SEM. \*\*p<0.0001, \*p<0.05 by two-tailed unpaired t-test, relative to unstimulated cells.

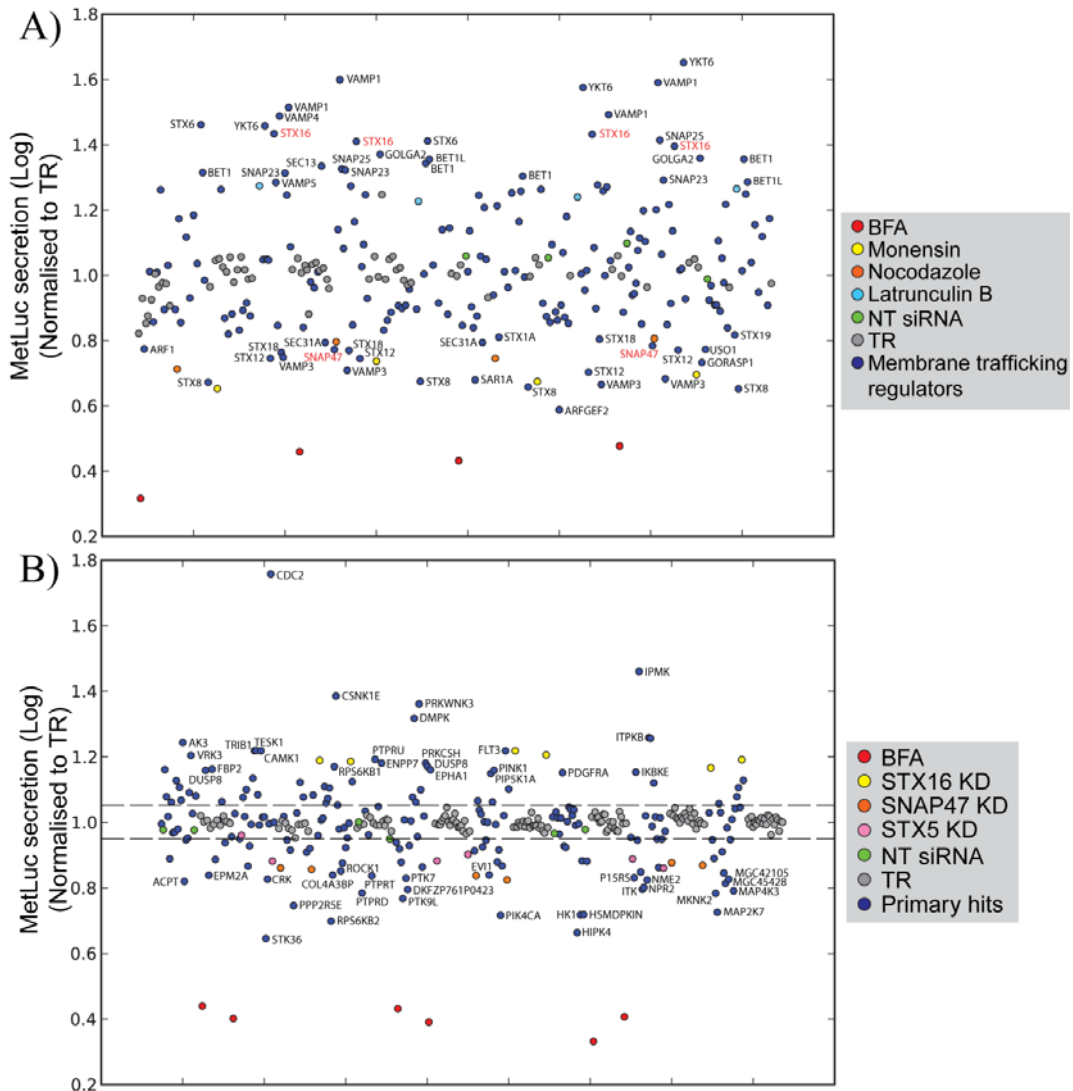
### 3.2.9 110 Golgi organisation regulators also affect general secretion

The Golgi apparatus plays essential roles in protein sorting. To test whether the Golgi regulators that were identified also affect general protein secretion, I have generated a HeLa cell line stably expressing secreted Metridia luciferase (Met-Luc) and the subsequent secretion screens were performed with Dr. Germaine Goh. To test this reporter system, the cell line was subjected to RNAi by the pilot library of membrane trafficking regulators and the drugs known to affect Golgi organisation. Total secretion levels of Met-Luc in the well were measured in the supernatant four hours after media change. To normalize Met-Luc secretion according to the number of cells, the number of cells was counted from imaging nuclei staining.

Not surprisingly, BFA treatment and depletion of several membrane trafficking proteins involved in secretion significantly reduced Met-Luc secretion (Figure 3-16A) which validated our assay. For instance, SAR1A is a GTPase for assembly of COPII coats for ER to Golgi transport [397] while v-SNARE VAMP3 is involved in post- Golgi trafficking for constitutive secretion [398, 399]. SNAP47, that is involved general intracellular membrane trafficking [400], could also regulate secretion by mediating intra-Golgi traffic. On the contrary, we identified loss of several other SNAREs induced an increase in Met-Luc secretion (Figure 3-16A). This relatively surprising result was highly reproducible among replicates of different wells in the same plate and on different plates, verifying that it was not due to experimental variations. A possible explanation is that Met-Luc, being an exogenous substrate, is not secreted at full efficiency but is partially diverted to intracellular compartments such as lysosomes. A defect in the normal sorting machinery would then result in the observed increase in secretion. In support of this hypothesis, Syntaxin 16 depletion resulted in Met-Luc hypersecretion (Figure 3-16A). Syntaxin 16 (STX16) is known to regulate mostly retrograde trafficking from the endosomes to the TGN [401, 402]. Its knockdown could therefore be expected to perturb sorting from Golgi to lysosomes. Hence, we found various

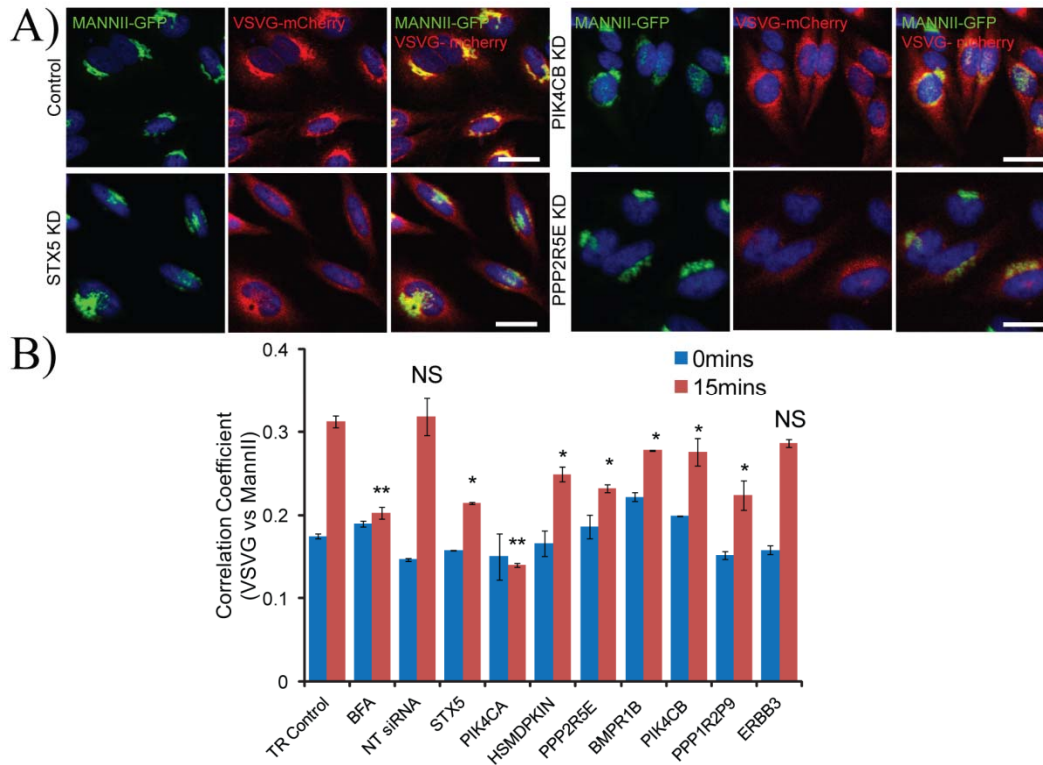
proteins that are involved in different trafficking events to be important for constitutive secretion.

Next, the signaling hits were screened for Met-Luc secretion. Both hypo and hyper secretion phenotypes were again observed and the amplitude of phenotype was comparable to the pilot library results (Figure 3-16B). We found that 62 of the gene depletions caused a significant decrease in Met-Luc secretion, while 58 resulted in increased secretion (Table 3.2). Notably, phosphatidylinositol 4-kinases PIK4CA (and less prominently, PIK4CB) knockdown led to significant inhibition of Met-Luc secretion (Figure 3-16B). This is consistent with their critical role in maintaining functional Golgi membranes through PIP4 production as mentioned in Section 3.2.7.1. Indeed, the phosphatidylinositol 4-kinases have been shown to regulate secretion in cells [138, 403-405]. No clear correlation between morphological phenotype and secretion phenotype could be found, indicating that similar Golgi morphologies can reflect significantly different functional perturbations.



**Figure 3-16: 110 Golgi organisation regulators also regulate constitutive secretion.** Met-Luc secretion (log of luciferin signal per cell and normalized to the average score of transfection reagent-treated control (TR) wells) of (A) genes in the pilot membrane trafficking screen and (B) the primary Golgi morphology hit genes. Control wells are indicated as in the legend. Some genes on the extremes are labeled. Dashed lines in (B) indicate the cutoff values for significant secretion changes.

I then further verified the secretion defect for nine hits, that perturb the cis marker specifically when depleted, using the well-established VSVG-tsO45G transport assay [406]. Briefly, VSVG-tsO45G is a transmembrane protein that contains a mutation that leads to its reversible folding and retention in the ER at 40°C and upon temperature reduction to 32°C, it folds properly and is exported out of the ER and proceeds in the secretory pathway. I have generated HeLa cells stably expressing VSVG-tsO45G-mcherry and MannII-GFP and tested the kinetics of the VSVG release. VSVG was found to accumulate strongly at the Golgi after 15 to 20 minutes of release from the restrictive temperature of 40°C. By probing the colocalisation of VSVG-tsO45G with the Golgi marker MannII-GFP at 15 minutes after release from the restrictive temperature, I was able to assess more specifically and quantitatively the ER to Golgi trafficking step. In agreement with the Met-Luc secretion data, depletion of six genes induced a significant reduction in ER to Golgi traffic (Figure 3-17A and B).



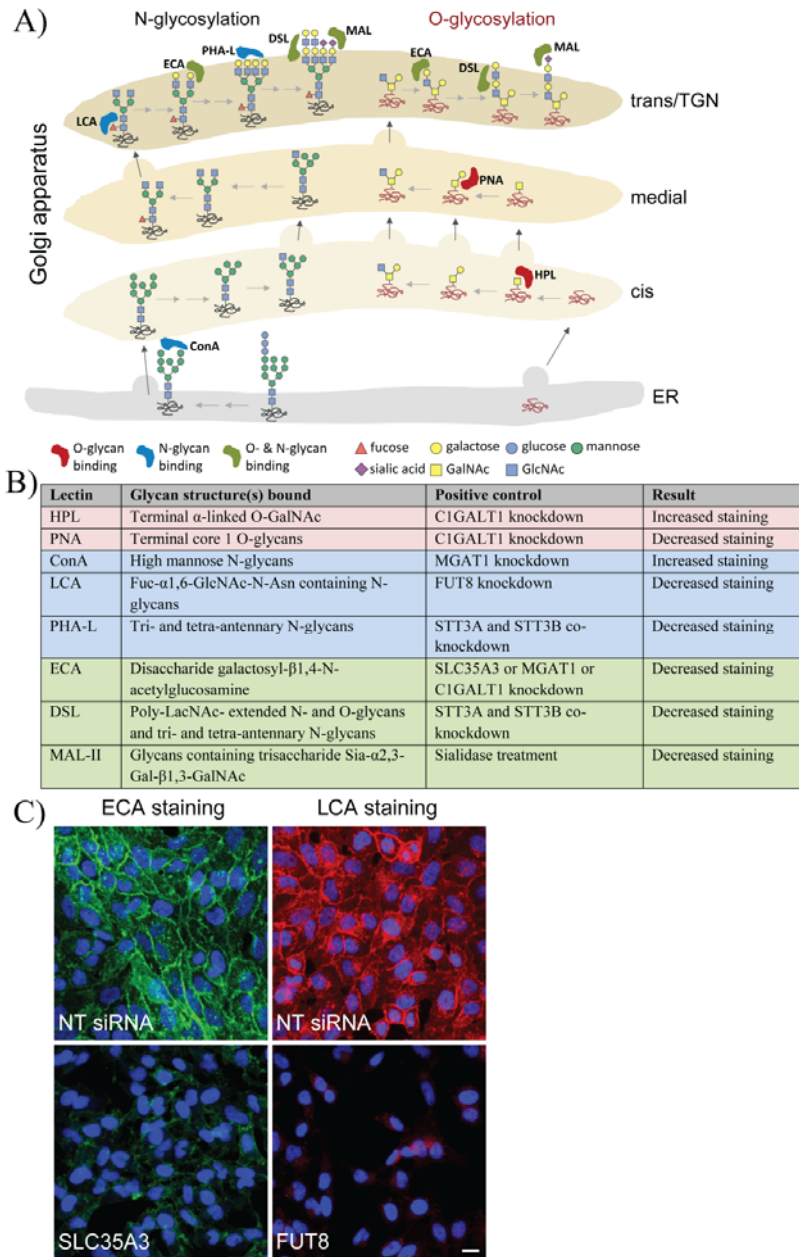
**Figure 3-17: Most Met-Luc secretion hits also affect ER to Golgi trafficking of VSVG-tsO45G protein.** (A) ER to Golgi trafficking of VSVG-tsO45-mcherry is impaired in the depletion of most genes that display both cis diffuse Golgi and reduced Met-Luc secretion phenotypes. (B) Pearson's correlation coefficient of Golgi marker MannII-GFP and VSVG at 0 minutes (blue bars) and 15 minutes (red bars) after change to permissive temperature at 32°C. Cells were analysed using Metaexpress Translocation-Enhanced analysis module. Values on graphs indicate the mean  $\pm$  SEM. \*\* $p < 0.0001$ , \* $p < 0.05$  by two-tailed unpaired t-test, relative to transfection reagent-treated control cells at 15 minutes.



### **3.2.10 146 Golgi organisation regulators also affect glycan biosynthesis**

I, in collaboration with Dr. Germaine Goh, sought to evaluate whether the perturbations in Golgi organisation resulted in changes in cell surface glycan patterns. Cell surface glycans were studied because they are the final products after the passage through the Golgi. Hence, they would reflect glycosylation defects along the biosynthetic pathway. An increase in premature glycan structures and a decrease in end-capping glycans on the cell surface would indicate defects in the early glycan synthesis. The prominent glycans in most cell types are N-glycans and O-GalNAc glycans. Therefore, we selected eight fluorescent lectins with different specificities that are known to bind the main N- and O-glycan structures (Figure 3-18A). We included the intracellular staining intensities of HPL that was used in the primary screen in this analysis.

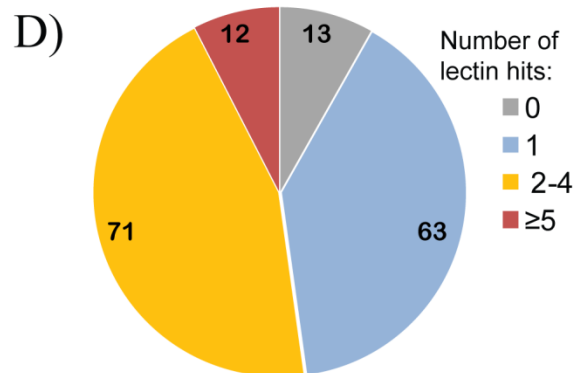
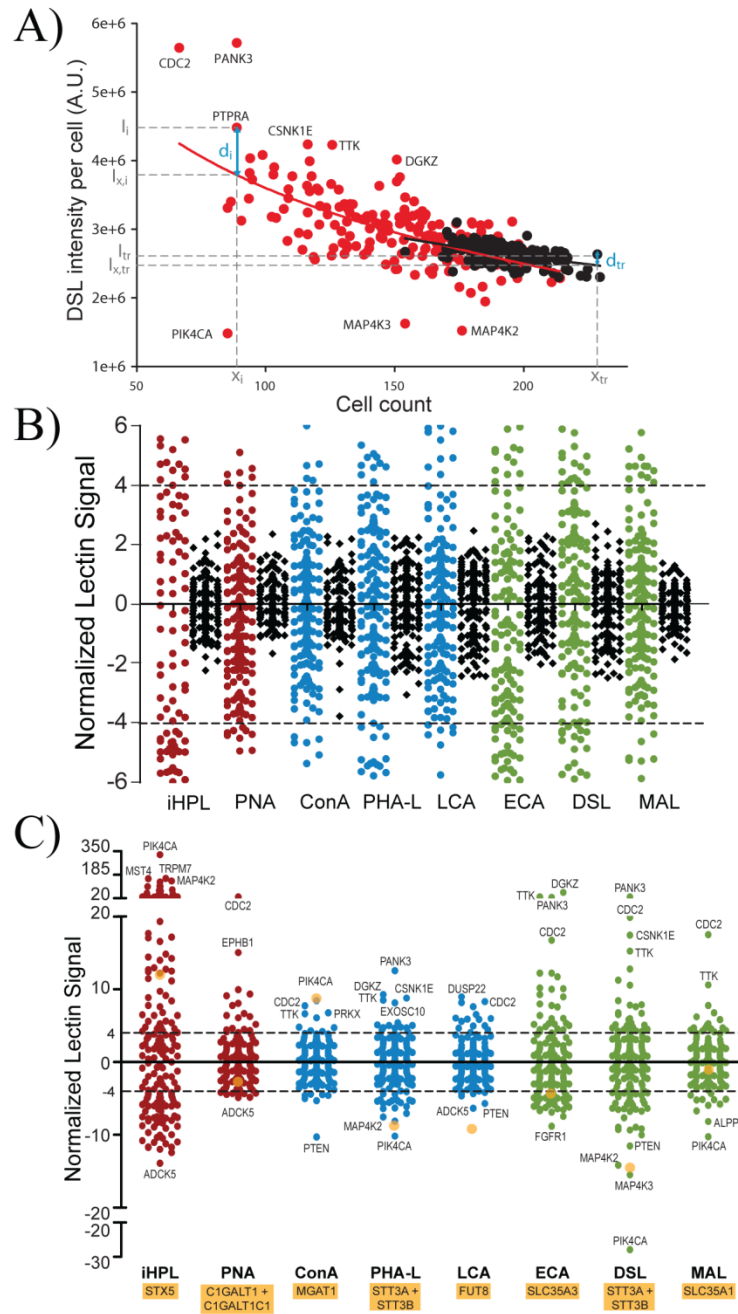
To evaluate the range of lectin staining variation that could be expected and to test the specificities of the lectins, various enzymes and/ or sugar transporters were knocked down and lectin fluorescence signals were quantified. For each lectin, we could obtain significant changes in staining upon depletion of enzymes or transporters involved in the specific glycosylation processes, consistent with their expected specificity (Figure 3-18B and further elaborations are found in Materials section of Chapter 2). For example, depletion of the Golgi-localized UDP-GlcNAc transporter SLC35A3 reduced staining by ECA, which binds mostly the common disaccharide Gal-GlcNAc. Alternatively, knockdown of the fucosyltransferase 8 (FUT8) reduced staining with LCA, a fucosyl-specific lectin (Figure 3-18C). These genes, hence, serve as positive controls for our secondary screen on the hits.



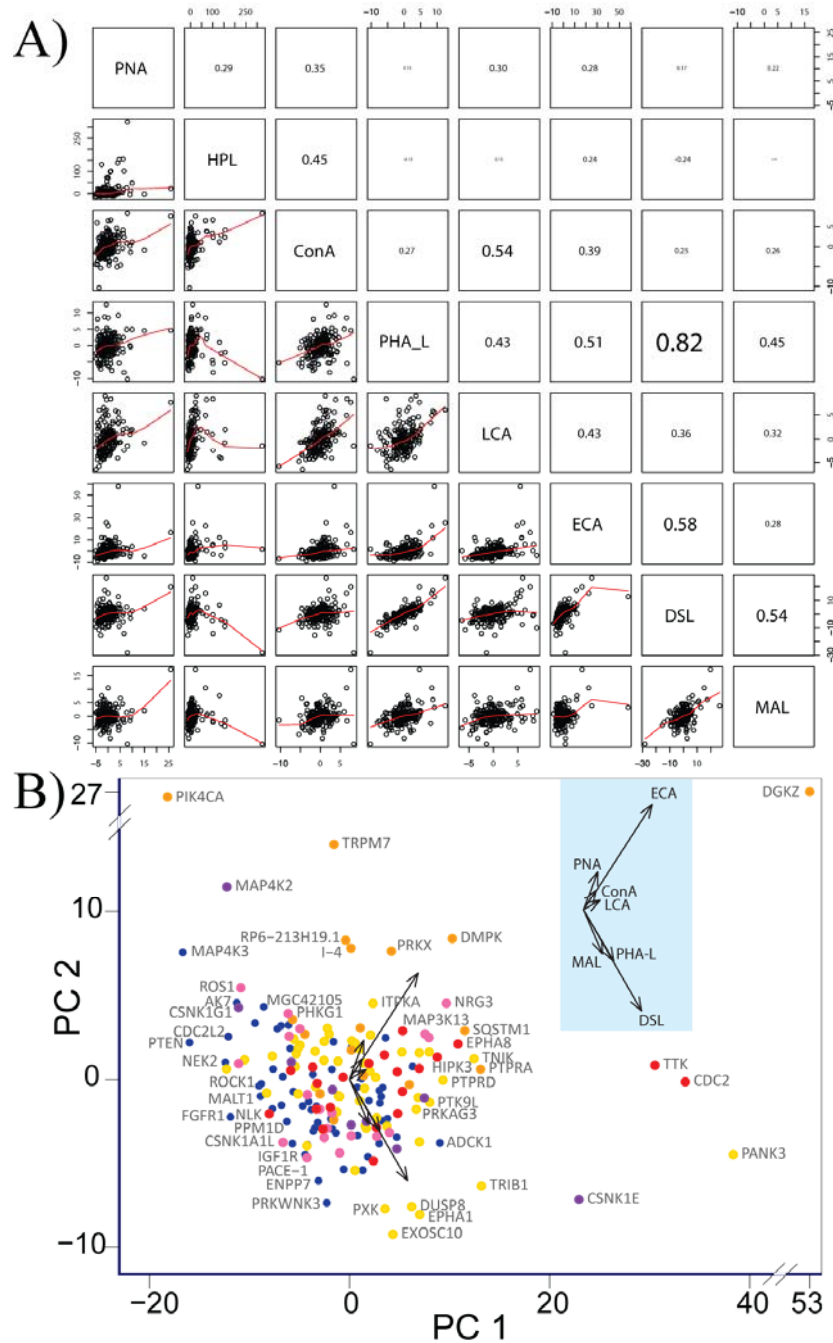
**Figure 3-18: Eight fluorescent lectins that display different glycan specificities were chosen probe N- and O-glycan expression patterns.** (A) A schematic of the main glycan structures recognised by the lectins used in the secondary screening. (B) Overview of the validation of lectin specificities (elaborations found in Material section in Chapter 2). (C) *Erythrina cristagalli* lectin (ECA) and *Lens culinaris* agglutinin-A (LCA) lectin staining were dramatically reduced in cells depleted of Golgi UDP-GlcNAc transporter SLC35A3 and fucosyltransferase FUT8 respectively. Cells were imaged under constant acquisition parameters.

We next proceeded with the secondary screen for the identified 181 primary Golgi morphology hits using the seven lectins on non-permeabilized fixed cells (Table 3.2). For most lectins, we noted a trend of slightly higher staining intensity values per cell in wells with lower cell number (Figure 3-19A). By fitting this systematic shift into a standard curve, followed by measuring the deviation of lectin intensities of each gene depletion from the curve, we derived a “normalized lectin signal” for each gene. This, thus, would eliminate the variability of lectin signals due to cell number (Further elaborated in methods section in Chapter 2).

We found the lectin fluorescence staining highly reproducible in our experimental conditions demonstrated by the tight distribution of the multiple control wells comprising of untransfected cells (Figure 3-19B). High reproducibility between experimental replicates for each lectin staining was also observed (not depicted). Based on the distribution of lectin staining in the control wells, we defined the thresholds of significance as a normalized lectin signal of  $>4$  or  $<-4$  (Figure 3-19B and C). The former indicates significantly increased lectin staining while the latter indicates significantly decreased lectin staining. Strikingly, most (146/159) of the validated Golgi morphology hits resulted in a significant change of intensity for at least one lectin (Figure 3-19D). Interestingly, siRNA knockdown of several signaling genes resulted in lectin staining changes similar to or more pronounced than the respective positive controls. For example, while knockdown of UDP-GlcNAc transporter SLC35A3 induced a ~35% reduction of ECA staining, FGFR1 depletion showed ~40% reduction and DGKZ targeting resulted, conversely, in a dramatic, 3.5-fold increase (Figure 3-19C and 3-21).



**Figure 3-19: Most signaling proteins regulate Golgi morphology and glycans expression.** (A) DSL lectin intensity per cell (arbitrary units) against cell count for each of the hit genes (*red*) and control wells (*black*). Each data set is fit to a log equation and the resulting fits (solid lines) represent the expected intensity under unperturbed conditions. A normalized lectin signal for each gene is then calculated in relation to the mean absolute deviation of control wells, as a measure of extent of perturbation (see Methods section in Chapter 2 for further elaborations). (B) Normalized lectin signals of control wells (*black*) in comparison with signaling genes (colored), for all lectins tested. Dotted lines indicate hit cutoff values of  $<4$  and  $>4$ . (C) Complete zoomed out plot of (B), with some extreme genes labeled. Yellow filled circles represent the normalized lectin signal for control genes (indicated below lectin names). (D) Overview of the distribution of the number of lectin hits per gene. The corresponding numbers of genes are indicated on the chart.



**Figure 3-20: A high diversity of glycophenotypes could be observed in signaling gene depletions.** (A) Plots of pairwise comparisons between the normalized lectin signals for the eight different lectins. Squares on the bottom left of the diagonal are scatter plots of lectin intensities of the primary hits while squares on the top right of the diagonal contain the Pearson's correlation coefficients between the paired lectins. (B) Principal Component Analysis plot of the seven lectin scores (excluding HPL) for each hit gene. Genes are color coded according to the six Golgi morphology groups as indicated. Inset: Eigen vectors with the respective lectins labeled.

Surprisingly, results for most of the lectins across the whole screen did not correlate significantly with each other (Figure 3-20A). Yet, the effects were highly reproducible between replicates. Furthermore, two lectins, DSL and PHA-L, which are both proposed to bind tri and tetra-antennary glycans did correlate well with each other (Figure 3-20A). This indicates that the lack of correlation between lectin staining reflects a real biological phenomenon. It suggests that different signaling genes affect different glycosylation pathways.

This complexity is apparent in the PCA of the lectin staining data (Figure 3-20B). PCA demonstrates consistency with the biology of glycans. Indeed, the Eigen vectors organizing the PCA (black arrows in Figure 3-20B) are aligned in two groups, oriented at 90 degrees from each other. One corresponds roughly to short glycan structures, i.e. ConA, PNA, ECA and LCA lectins and the other to elongated glycan structures, i.e. MAL, PHA-L and DSL lectins. However, in contrast with the PCA of the morphological signatures (Figure 3-5E), the lack of clear groups formed by the signaling genes illustrates that their effects on glycan expression are quite diverse.

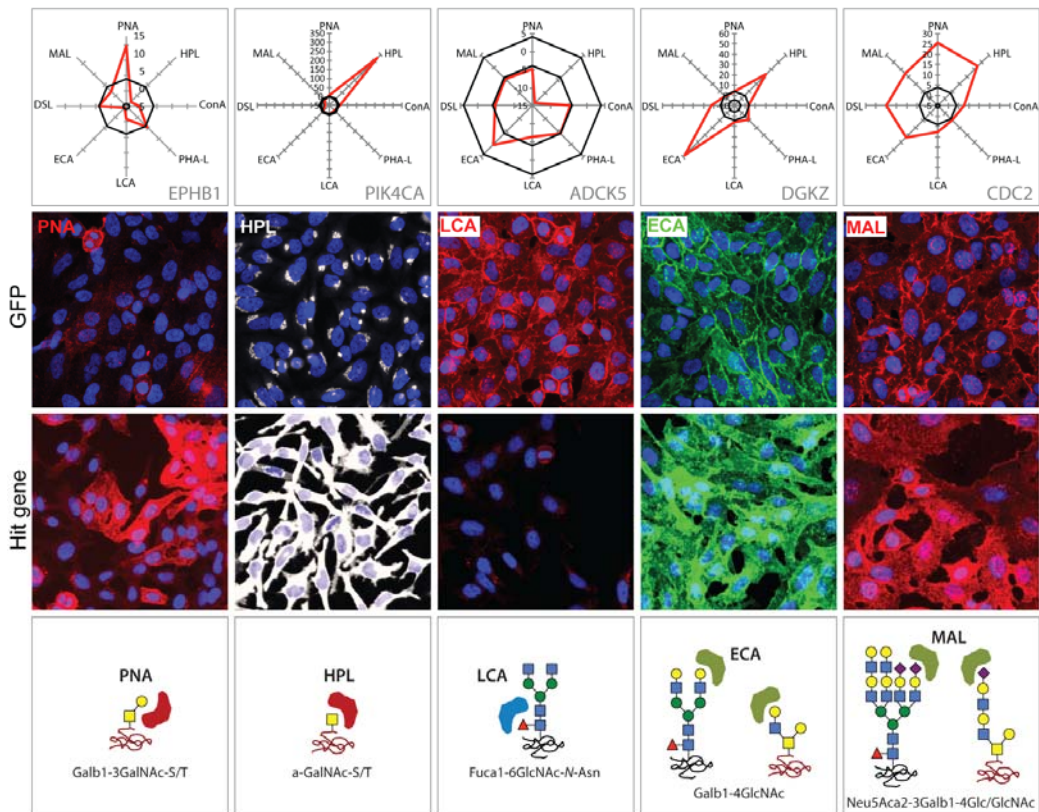
### **3.2.11 A complex interaction between signaling genes and the regulation of glycosylation**

Glycan synthesis in the Golgi apparatus comprises several pathways functioning in parallel, mainly but not exclusively N- and O-GalNAc glycosylation [407]. Even within the N-glycosylation pathway, it is unclear whether different glycosylation reactions such as fucosylation or sialylation are coordinated. Our results indicate that changes in the efficiency of glycosylation reactions can occur relatively independently of each other's.

This variability of effects on glycan expression prompted us to define a glycan profile for each gene by incorporating the data for the eight lectins in one plot,

similar to the Golgi morphology signature (Figure 3-21). Not surprisingly given the diversity of the glyco- and morpho-phenotypes, glycan profiles did not correlate tightly with specific Golgi morphological parameters. However, some general trends surfaced: the glycan profile tends to show a general decrease in lectin intensities when the Golgi adopts a condensed morphology whereas fragmentation tends to yield generally increased lectin intensities (Figure 3-20B).

The variety of glycan profiles is illustrated by some examples with one lectin staining and the overall glycophenotype displayed (Figure 3-21) and the results for every individual gene are available in Table 3.2.



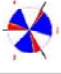















**Figure 3-21: The variety of glycophenotypes of the Golgi hits is illustrated by glycan profiles.** Glycan profiles (top), lectin staining (middle) and the targeted glycan structures (bottom) of representative hit genes. Axis values indicate normalized lectin signals and solid lines delineate cutoff values (-4 or 4) on glycan profiles.























**Table 3.2. 181 primary hits with nine Golgi morphology scores and corresponding phenotypic signature pictogram, deconvolution validation status, 8 lectin-binding scores and corresponding glycan profile pictogram, and Met-Luc secretion score.**





















Gene Symbol	Gene ID	Cell Number	Golgi phenotypic score									Validation by deconvoluted siRNA	Normalized Lectin Signal								Glycan profile	Normalized Met-Luc secretion
			CD	CF	CC	MD	MF	MC	TD	TF	TC		Gene signature	HPL	PNA	ConA	PHA-L	LCA	ECA	DSL		
<a href="#">ACPT</a>	59560	558	0.02	0.1	0.33	0.01	0.08	0.4	0.1	0.11	0.27	YES	-8.3	0.36	-2	0.62	-2.3	0.84	1.36	-1.4		0.820034
<a href="#">ACYP1</a>	97	234	0.2	0.38	0.03	0.04	0.38	0.08	0.19	0.4	0.02	YES	-6.1	0.05	0.72	-1.4	-1.7	0.09	-1.3	0.56		1.067853
<a href="#">ADCK1</a>	57143	518	0.11	0.04	0.37	0.06	0.03	0.49	0.2	0.03	0.32	YES	-2.1	0.64	3.78	4.6	-0.3	3.29	8.36	-0.2		1.127838
<a href="#">ADCK5</a>	203054	468	0.03	0.11	0.34	0.02	0.09	0.42	0.03	0.11	0.36	YES	-14	-5	-4.5	-4	-6.4	0.24	-4.6	-4.4		1.107357
<a href="#">AK3L1</a>	206	667	0.06	0.09	0.34	0.09	0.05	0.41	0.05	0.09	0.35	YES	-5.7	-2.1	0.08	0.17	-2.1	1.4	3.18	-1.8		1.24397
<a href="#">AKZ</a>	122481	464	0.27	0.05	0.23	0.07	0.02	0.48	0.18	0.03	0.32	YES	6.69	-2.1	-0.6	-5.6	1.55	-5	-9.3	-3.4		0.94695
<a href="#">ALPZ</a>	115701	968	0.31	0.07	0.21	0.21	0.06	0.26	0.34	0.07	0.2	YES	-8.4	-1.1	1.34	1.63	0.49	-0.6	2.56	-0.2		0.927981
<a href="#">ALPP</a>	250	211	0.16	0.39	0.04	0.07	0.31	0.09	0.14	0.4	0.05	YES	-8.2	0.9	0.51	0	-3.2	1.9	2.66	-8.3		0.979412
<a href="#">ANGPT4</a>	51378	225	0.09	0.4	0.05	0.08	0.29	0.12	0.13	0.4	0.05	YES	3.98	-3.4	2.42	2.91	-1.2	5.24	4.23	1.3		1.090974
<a href="#">ANP32E</a>	81611	311	0.28	0.23	0.12	0.06	0.17	0.23	0.71	0.11	0.04	NO	14.2	-2.2	-1	0.8	-1.2	-3	2.22	0.55		0.97072

<a href="#">AURKB</a>	9212	229	0.44	0.36	0.02	0.21	0.39	0.03	0.37	0.36	0.02		YES	3.74	0.23	4.21	-1.8	1.35	-4	-1.1	0.48		1.027142
<a href="#">AXL</a>	558	590	0.12	0.05	0.36	0.09	0.03	0.43	0.09	0.04	0.38		YES	-9.8	-1.5	0.2	-2.3	-3.5	-3.2	-0.7	1.19		1.080872
<a href="#">BCKDX</a>	10295	240	0.15	0.08	0.3	0.04	0.04	0.43	0.19	0.09	0.25		YES	-3.8	2.15	0.1	2.43	0.54	1.2	0.89	2.36		1.017487
<a href="#">BMPR1B</a>	658	478	0.31	0.06	0.21	0.07	0.05	0.36	0.54	0.04	0.15		YES	-7.6	-0.8	-2	0.61	-2	-3.5	-0	1.78		0.866552
<a href="#">BMX</a>	660	437	0.5	0.17	0.06	0.09	0.19	0.13	0.59	0.14	0.07		YES	0.81	4.34	1.43	1.58	3.2	1.77	4.19	-3.9		0.99398
<a href="#">BUB1</a>	699	489	0.43	0.11	0.12	0.1	0.13	0.21	0.67	0.07	0.07		YES	-5	0.57	-2	1.14	-3.6	8.86	3.32	1.53		1.084566
<a href="#">CAMKI</a>	8536	235	0.54	0.13	0.06	0.09	0.14	0.17	0.58	0.1	0.07		YES	3.11	0.8	-0.3	-0.6	-1.7	1.03	4.95	3.83		1.218716
<a href="#">CCRK</a>	2952	243	0.02	0.12	0.3	0.04	0.05	0.44	0.04	0.12	0.3		YES	-4.8	-0.9	-2.1	-0.7	-3.6	-4	2.06	-4.6		0.826931
<a href="#">CDCZ</a>	988	251	0.23	0.44	0.02	0.12	0.38	0.06	0.59	0.27	0.01		YES	22.3	25.8	7.64	4.65	7.52	16.6	19.8	17.4		1.75785
<a href="#">CDCZ5A</a>	993	507	0.48	0.23	0.05	0.06	0.26	0.11	0.4	0.24	0.04		NO	12.4	-2.2	2.45	-1	1.22	3.72	1.83	-0.4		1.061662







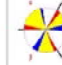





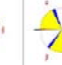

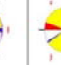


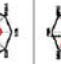
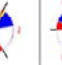

<a href="#">CDC2L2</a>	985	390	0.15	0.03	0.45	0.06	0.02	0.53	0.16	0.02	0.43		NO	-11	-3	-5.4	-5.4	-4.7	-5.1	-6.6	-6.8		0.99998
<a href="#">CDC42BPA</a>	8476	500	0.2	0.06	0.3	0.05	0.05	0.43	0.21	0.06	0.31		YES	-6.1	-2.8	-2.5	0.11	-0.3	-4.2	-6.6	-1.4		1.012931
<a href="#">CDC42BPG</a>	55561	760	0.46	0.08	0.06	0.06	0.03	0.26	0.55	0.03	0.1		YES	1.4	-0.6	-1.3	-4.1	0.64	-1.4	-3.5	-3.3		0.718828
<a href="#">CDKL2</a>	8999	765	0.12	0.04	0.37	0.07	0.03	0.49	0.08	0.04	0.41		YES	-6.1	-1.9	-0.3	-1.1	0.15	1.78	0.83	0.39		1.059352
<a href="#">CDKN1B</a>	1027	341	0.14	0.08	0.29	0.04	0.04	0.44	0.16	0.06	0.33		YES	11.4	0.86	-1.7	2.4	0.03	-2.9	4.02	1.39		1.10536
<a href="#">CHK1</a>	1119	262	0.15	0.07	0.29	0.05	0.05	0.5	0.14	0.06	0.34		YES	0.33	-1.9	-2.6	2	-1.4	1.89	2.02	-5.9		1.078482
<a href="#">CKM</a>	1158	517	0.4	0.23	0.07	0.15	0.23	0.11	0.45	0.22	0.05		YES	6.42	0.56	0.63	-0.4	-0.8	-3.9	-1.6	1.81		0.889
<a href="#">CLK1</a>	1195	603	0.03	0.03	0.41	0.06	0.02	0.44	0.02	0.03	0.42		YES	-12	2.36	-1.3	-2.2	-1.5	0.21	-1.4	-1.4		0.968494
<a href="#">COL4A3BP</a>	10067	794	0.08	0.5	0.03	0.08	0.4	0.06	0.08	0.51	0.03		YES	-8.5	-1.4	-0.5	3.22	-0.2	1.36	3.13	1.23		0.839398
<a href="#">CSNK1A1L</a>	122011	368	0.28	0.14	0.13	0.12	0.1	0.2	0.47	0.1	0.08		NO	6.3	-3.7	-1.8	-0.1	-2.3	-6.2	-2.2	-0.2		1.009401























<a href="#">CSNK1E</a>	1454	717	0.21	0.23	0.08	0.21	0.17	0.13	0.41	0.21	0.06		YES	4.69	-1.4	2.16	8.72	5.76	11.6	17.3	6.11		1.385632
<a href="#">CSNK1G1</a>	59944	576	0.26	0.07	0.28	0.22	0.05	0.34	0.3	0.06	0.26		YES	-6.8	-0.1	-2.9	-6.2	-0.4	-4.8	-9	-1.6		0.979816
<a href="#">CSNK1G2</a>	1455	982	0.3	0.24	0.07	0.25	0.16	0.13	0.24	0.22	0.09		YES	3.6	-0.1	0.83	3.65	0.53	0.42	4.92	1.34		0.87584
<a href="#">CSNK2B</a>	1460	361	0.45	0.3	0.03	0.17	0.33	0.1	0.41	0.35	0.03		YES	12.6	1.91	2.76	-2.9	3.22	1.44	0.06	-1.6		0.923116
<a href="#">CXCL10</a>	3627	743	0.27	0.44	0.03	0.1	0.31	0.05	0.34	0.31	0.02		YES	52.8	-0.5	-0.8	-3.1	-0.1	1.67	0.6	-1.4		0.997692
<a href="#">DCLKZ</a>	166614	837	0.5	0.15	0.06	0.13	0.13	0.15	0.66	0.08	0.05		YES	-5.2	-3.5	-3	-1	-1.7	-2.2	-1.3	-2.8		0.814179
<a href="#">DGKD</a>	8527	677	0.08	0.08	0.29	0.05	0.03	0.44	0.09	0.06	0.34		YES	-0.8	2.34	0.6	0.67	0.25	4.76	3.02	2.98		1.124628
<a href="#">DGKQ</a>	1609	421	0.28	0.05	0.27	0.08	0.04	0.43	0.47	0.04	0.23		YES	-5	-1.3	1.04	3.57	-0.5	-2.1	0.76	0.87		0.878633
<a href="#">DGKZ</a>	8525	622	0.21	0.56	0.02	0.07	0.45	0.05	0.38	0.43	0.01		YES	33.4	4.24	3.5	9.19	5.5	57.8	12.7	3.2		1.00797
<a href="#">DLG3</a>	1741	480	0.14	0.42	0.03	0.05	0.36	0.06	0.11	0.4	0.04		YES	1.47	1.17	-0.4	-0.2	1.09	1.68	0.57	0.21		1.00441

<u>DMPK</u>	1760	459	0.59	0.22	0.03	0.12	0.32	0.06	0.32	0.4	0.03		YES	24.9	3.11	0.73	0.79	5.8	12.1	0.38	-0.3		1.317769
<u>DJSP2</u>	1844	819	0.01	0.49	0.03	0.03	0.4	0.05	0.02	0.47	0.03		YES	2.11	-0.3	0.37	1.81	0.96	0.24	2.99	0.2		0.987178
<u>DJSP22</u>	56940	693	0.06	0.57	0.03	0.06	0.3	0.13	0.12	0.55	0.03		YES	25.2	-1.2	1.25	3.58	8.85	-3.8	-10	1.82		1.130309
<u>DJSP6</u>	1848	543	0.04	0.45	0.04	0.05	0.36	0.08	0.03	0.45	0.04		YES	1.74	-0.4	-0.6	-0.4	-0.4	3.79	0.24	-2		1.007259
<u>DJSP8</u>	1850	602	0.14	0.57	0.02	0.14	0.35	0.09	0.1	0.53	0.04		YES	2.2	-0.5	2.9	5.33	2.87	-1.5	6.68	4.92		1.165005
<u>EIFZAK2</u>	5610	608	0.03	0.53	0.04	0.04	0.4	0.06	0.22	0.33	0.05		YES	-9	-2.2	-2	-3	-0.6	-5.9	-4.3	-1.1		0.86392
<u>EMPPZ</u>	339221	609	0.03	0.05	0.33	0.04	0.03	0.42	0.02	0.05	0.34		YES	-4.5	-1.7	-0.9	1.22	-0.3	-5.9	0.15	4.62		1.180975
<u>EPHA1</u>	2041	540	0.17	0.69	0.01	0.08	0.62	0.02	0.14	0.69	0.01		YES	17.6	-3.4	-0	0.28	-3.3	1.23	10.5	5.2		1.160429
<u>EPHA8</u>	2046	749	0.4	0.31	0.04	0.1	0.24	0.09	0.51	0.19	0.04		YES	17	1.13	0.83	2.54	1.59	9.19	5.28	0.57		1.037985
<u>EPHBI</u>	2047	334	0.12	0.03	0.4	0.1	0.01	0.53	0.18	0.03	0.31		YES	-2.9	14.9	-0.9	4.58	-0.8	-4.4	3.89	2.03		0.925291























<u>EFM2A</u>	7957	650	0.19	0.52	0.04	0.06	0.4	0.08	0.25	0.49	0.02		YES	46.6	9.88	1.11	4.93	1.94	4.1	2.31	2.05		0.83874
<u>ERBB3</u>	2065	683	0.51	0.16	0.05	0.11	0.21	0.08	0.54	0.17	0.04		YES	-1.7	0.96	-0.4	2.44	2.01	1.7	3.79	1.19		0.945981
<u>EVI</u>	2122	467	0.06	0.08	0.3	0.05	0.04	0.49	0.07	0.07	0.36		YES	-11	-3.3	-2.5	3.11	0.24	-0.7	3.78	-0.7		0.839622
<u>EXOSC10</u>	5394	246	0.12	0.52	0.04	0.1	0.31	0.15	0.09	0.35	0.1		NO	3.64	-4.3	-1.8	8.07	3.33	-2.7	7.73	-2.7		1.002314
<u>FBE2</u>	8789	695	0.11	0.06	0.25	0.08	0.02	0.43	0.05	0.05	0.3		YES	-2.7	-0.3	-0.7	1.47	1.57	-1.9	2.4	0.45		1.162342
<u>FGFR1</u>	2260	581	0.15	0.16	0.21	0.06	0.05	0.44	0.12	0.09	0.31		YES	21.3	-4.3	-3.5	-3.1	-0.2	-8.9	-6.9	0.85		1.062487
<u>FGFR2</u>	2263	566	0.03	0.51	0.05	0.03	0.45	0.07	0.04	0.51	0.05		YES	-7.7	-4.2	-1.2	-1.2	2.18	-1.3	-5.4	-1.3		0.993688
<u>FLT3</u>	2322	650	0.17	0.56	0.02	0.1	0.48	0.05	0.21	0.54	0.02		YES	-5.1	-1.6	1.52	-1.2	-0.2	-2.2	1.31	-0.5		1.218855
<u>GALK1</u>	2584	431	0.27	0.08	0.17	0.02	0.05	0.32	0.58	0.06	0.08		YES	-2.4	-4.9	-1.5	-2.4	-1.8	-5.8	-9.4	1.19		1.101845
<u>GAP43</u>	2596	442	0.17	0.02	0.33	0.04	0.01	0.57	0.16	0.01	0.39		YES	-7.6	-0.5	2.45	-2.2	-1.2	-5.2	-4	-1.2		1.014194





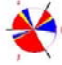







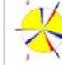









<a href="#">GTF2H1</a>	2965	554	0.06	0.05	0.4	0.05	0.02	0.53	0.06	0.03	0.41		YES	-3.3	-0.7	4.69	0.29	1.46	0.46	3.05	4.33		1.013521
<a href="#">HCK</a>	3065	475	0.27	0.11	0.11	0.27	0.04	0.19	0.33	0.11	0.1		YES	-4.9	9.03	0.16	0	0.95	-4.6	0.4	-1.6		1.002778
<a href="#">HIPK1</a>	204851	1028	0.26	0.18	0.09	0.23	0.13	0.15	0.29	0.17	0.1		YES	-3.7	2.57	1.29	3.68	0.71	3.9	4.72	1.27		1.04034
<a href="#">HIPK3</a>	10114	339	0.54	0.18	0.04	0.1	0.19	0.08	0.62	0.12	0.04		YES	38.3	-0.2	-0.8	4.72	0.35	7.9	3.12	0.64		1.038649
<a href="#">HIPK4</a>	147746	382	0.14	0.42	0.05	0.05	0.38	0.09	0.18	0.4	0.04		YES	-5.7	-1.6	2.31	-2.9	1.82	-3.2	-1.3	0.16		0.663781
<a href="#">HK1</a>	3098	662	0.1	0.02	0.38	0.06	0.01	0.52	0.09	0.02	0.38		YES	-7.8	-1.1	0.11	0.04	-2	-2.2	-0.1	1.73		0.718239
<a href="#">IGBP1</a>	3476	510	0.11	0.43	0.07	0.05	0.39	0.1	0.11	0.44	0.06		YES	-1.3	-3.8	-2.7	-1.7	-3.2	-4.1	0.68	0.15		1.005598
<a href="#">IGFIR</a>	3480	365	0.09	0.02	0.41	0.05	0.01	0.59	0.11	0.02	0.34		YES	0.74	-1.1	-0.8	-1.6	-3.2	-5.6	0.17	2.7		0.881566
<a href="#">KBKE</a>	9641	871	0.47	0.39	0.04	0.23	0.34	0.07	0.57	0.17	0.04		YES	71.8	-0.6	3.82	2.08	8.08	0.27	-1.2	0.1		1.153553
<a href="#">INPP1</a>	3628	706	0.1	0.06	0.34	0.09	0.05	0.36	0.07	0.06	0.34		YES	-8.1	0.14	-0.9	-3.2	-2.6	-3.4	-1.2	1.98		1.063468





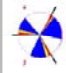

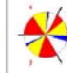




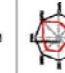
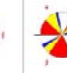

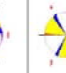
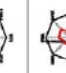
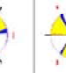

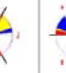

<u>IPMK</u>	253430	531	0.36	0.13	0.12	0.05	0.18	0.19	0.57	0.09	0.08		YES	-0.9	-0.3	0.88	-0.5	0.86	7.66	3.35	1.18		1.46063
<u>ITK</u>	3702	656	0.1	0.43	0.05	0.06	0.3	0.12	0.1	0.39	0.05		YES	3.34	0.01	0.08	2.39	0.04	5.1	2.24	-2		0.795544
<u>ITPKA</u>	3706	597	0.06	0.58	0.01	0.03	0.45	0.04	0.13	0.51	0.02		YES	0.37	3.06	0.13	-0.8	-0.6	4.34	-1	-1		1.019966
<u>ITPKB</u>	3707	615	0.15	0.51	0.01	0.07	0.41	0.04	0.2	0.43	0.02		YES	23.5	-1.1	0.46	-1.1	0.03	2.36	2.22	0.37		1.258502
<u>KHK</u>	3795	616	0.05	0.61	0.02	0.01	0.51	0.03	0.04	0.58	0.02		YES	12.1	9.24	-1.4	-0.4	1.74	-2.2	-3.1	-0.4		0.988023
<u>LCP2</u>	3937	634	0.09	0.54	0.01	0.03	0.41	0.04	0.07	0.58	0.01		YES	14.3	2.42	1.95	-2.6	-0.1	-3.9	-4.6	0.88		0.862439
<u>MALI</u>	10852	651	0.1	0.07	0.25	0.06	0.02	0.43	0.07	0.04	0.33		YES	4.48	-1.3	-0.2	-2.3	-2.1	-7	-4	-3.1		0.972952
<u>MAP2K7</u>	5609	244	0.24	0.44	0.04	0.09	0.32	0.12	0.31	0.4	0.04		YES	2.87	0.35	0.84	-2.1	-1.5	-2	-4.3	-6		0.725815
<u>MAP3K13</u>	9175	418	0.44	0.11	0.14	0.14	0.11	0.25	0.33	0.11	0.18		YES	16.5	6.31	3.36	2.54	3.66	3.14	0.96	-0.9		1.030159
<u>MAP3K2</u>	10746	571	0.1	0.45	0.05	0.06	0.36	0.11	0.21	0.38	0.05		YES	-4.3	-1.5	-3	-3.1	-2.1	-2.3	-3.3	-0.5		0.845681

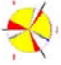



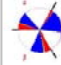

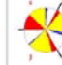




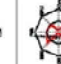


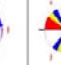


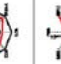

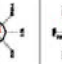
<a href="#">MAP3K3</a>	1326	428	0.09	0.04	0.36	0.05	0.03	0.53	0.1	0.05	0.39		YES	-5	-3.7	-2.2	-1.1	-2.1	-5.6	-3.3	-3		0.983888
<a href="#">MAP4K2</a>	5871	600	0.33	0.14	0.08	0.31	0.07	0.18	0.22	0.15	0.11		NO	101	6.58	2.31	-8.2	-2.4	-2.8	-14	-2.3		0.947697
<a href="#">MAP4K3</a>	8491	594	0.09	0.01	0.49	0.03	0.01	0.63	0.06	0.01	0.51		YES	-12	-3	-1.4	-7.1	-6.3	-16	-3.4		0.791076	
<a href="#">MAPK11</a>	5600	292	0.09	0.51	0.03	0.1	0.39	0.08	0.14	0.47	0.02		YES	3.05	-3.8	-0.3	-3.1	0.11	-0.6	-3.1		1.078687	
<a href="#">MAPK15*</a>	225689	48	0.29	0.35	0.1	0.27	0.23	0.05	0.25	0.34	0.02		YES	18.3	196	7.78	-5.2	3.13	25.5	-9.6	3.84		N.A.
<a href="#">MAPKAPK5</a>	8550	604	0.13	0.45	0.09	0.06	0.25	0.17	0.13	0.29	0.13		YES	1.6	-1.6	-2.4	-2	-0.6	-2.4	-2.7		1.046256	
<a href="#">MAPKSP1</a>	8649	577	0.1	0.52	0.03	0.07	0.43	0.04	0.08	0.52	0.02		YES	-2	0.5	1.27	2.61	2.52	1.09	-0.3	-0.1		0.890065
<a href="#">MARK4</a>	57787	245	0.14	0.51	0.02	0.1	0.45	0.05	0.14	0.49	0.01		YES	5.18	-2	-2.9	-3.7	-4.2	-3.3	-3.5	-5.3		1.106183
<a href="#">MAS11</a>	22983	420	0.15	0.05	0.34	0.03	0.03	0.49	0.16	0.05	0.33		YES	-4.9	0.51	-3.9	1.91	-0.7	-3.1	2.19	-5.2		1.073206
<a href="#">MGCI6169</a>	98627	345	0.04	0.07	0.33	0.03	0.05	0.43	0.03	0.07	0.34		YES	-3.2	-3.4	-0.5	-5.8	-1.3	-2	-5.5	-0.8		1.128729

<u>MGC42105</u>	167359	494	0.05	0.05	0.33	0.07	0.04	0.39	0.04	0.05	0.34		YES	-9.2	-1.5	-1.6	-5.4	-2.4	-2.4	-6.8	-3.1		0.826656
<u>MKNK1</u>	8569	723	0.08	0.05	0.41	0.06	0.02	0.52	0.06	0.03	0.47		YES	1.67	2.76	2.96	4.1	0.79	-0.8	3.2	-0.9		1.057439
<u>MKNK2</u>	2872	602	0.11	0.48	0.04	0.08	0.37	0.07	0.13	0.47	0.04		YES	-8.8	-3.9	2.1	2.8	2.86	-1.4	-2.3	0.54		0.783778
<u>MPP2</u>	4355	454	0.39	0.46	0.02	0.15	0.49	0.04	0.41	0.41	0.03		YES	12.3	-0.4	0.64	-1.5	-0.4	-1.5	-3.9	-3.5		0.944728
<u>MTMR1</u>	8776	604	0.01	0.45	0.04	0.03	0.37	0.06	0.03	0.45	0.04		YES	-5.6	-2.6	-1.6	-0.1	-2.2	2.15	1.82	-0.6		0.938195
<u>MVO3B</u>	140469	717	0.43	0.05	0.16	0.12	0.03	0.35	0.68	0.02	0.14		YES	-6.1	1.6	1.91	1.96	-1.5	-0.9	4.1	0.69		1.014166
<u>NEK1</u>	79858	266	0.46	0.28	0.02	0.1	0.32	0.09	0.62	0.15	0.03		YES	4.75	-2.3	3.28	-1.4	0.78	-4.2	-0.5	3.39		0.949735
<u>NEK2</u>	4751	442	0.12	0.05	0.29	0.03	0.01	0.48	0.12	0.03	0.33		YES	-10	-1.5	-1.8	-4.5	-4.3	-7.6	-6.5	-5.2		1.120654
<u>NLK</u>	51701	291	0.33	0.32	0.04	0.04	0.32	0.06	0.48	0.24	0.02		NO	13.9	-3.2	0.47	-2.6	-0.5	-6.6	-4.9	3.05		1.256322
<u>NMEZ</u>	4831	606	0.03	0.07	0.33	0.06	0.05	0.39	0.02	0.07	0.34		NO	-5.5	-4.4	-3.6	-0.3	-4.4	-3.6	1.15	-2.9		0.824112











<a href="#">NPR2</a>	4882	707	0.22	0.13	0.16	0.23	0.07	0.24	0.17	0.1	0.2		YES	4.69	1.86	-1.4	-1.7	-2.2	-3.5	-4.1	-1		0.801705
<a href="#">NRBP1</a>	29559	980	0.5	0.14	0.09	0.24	0.11	0.19	0.46	0.11	0.11		YES	30	-1.1	-3.3	2.24	-2	-0.4	4.13	2.27		0.848725
<a href="#">NRG3</a>	10718	771	0.39	0.1	0.15	0.19	0.06	0.29	0.8	0.04	0.05		NO	-0.2	2.88	1.26	1.8	-1.1	9.98	3.09	0.26		0.945002
<a href="#">PAG1</a>	58824	390	0.48	0.21	0.06	0.13	0.22	0.14	0.61	0.16	0.04		YES	-3.8	-3.2	-0.7	0.24	-2.6	-1	-2.9	-2.7		0.882869
<a href="#">PAK1</a>	5058	746	0.11	0.51	0.03	0.06	0.44	0.05	0.09	0.55	0.02		YES	-5.7	1.39	0.39	-1.7	0.01	-3.1	-4.5	-1.1		0.995501
<a href="#">PAK3</a>	5063	726	0.05	0.49	0.04	0.05	0.41	0.06	0.07	0.49	0.02		NO	8.32	1.31	-0.2	1.17	0.03	1.39	0.09	-1.1		0.991078
<a href="#">PANK3</a>	79646	548	0.02	0.67	0.03	0.05	0.56	0.06	0.09	0.59	0.04		NO	9.63	-0.7	1.45	12.5	5.98	25.3	26.5	3.82		1.021169
<a href="#">PAPSS1</a>	9061	604	0.04	0.03	0.5	0.04	0.02	0.58	0.02	0.03	0.54		YES	-11	-0.4	0.37	1.35	0.91	2.1	1.93	0.73		1.046888
<a href="#">PAPSS2</a>	9060	577	0.15	0.14	0.13	0.02	0.09	0.19	0.59	0.08	0.07		NO	7.67	0.82	1.55	-1.1	-0.4	-3.1	-0.7	4.08		0.923754
<a href="#">PDGFRA</a>	5156	547	0.24	0.29	0.05	0.01	0.36	0.09	0.56	0.15	0.04		YES	-11	1.46	2.23	-0.3	0.61	-1.5	0.6	-2.9		1.151969




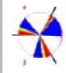
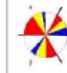


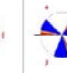
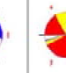
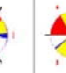
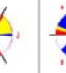
<a href="#">PDK1</a>	5166	681	0.15	0.09	0.35	0.05	0.05	0.48	0.18	0.07	0.35		YES	-4.6	-2	2.85	-0.1	1.12	4.37	0.93	-1.2		0.964513
<a href="#">PFKP</a>	5214	630	0.07	0.06	0.3	0.03	0.04	0.42	0.04	0.04	0.35		YES	-0.3	-1.6	1.97	1.14	-0.3	-4.3	3.16	0.71		1.032123
<a href="#">PHKG1</a>	5260	277	0.35	0.15	0.06	0.06	0.07	0.31	0.71	0.05	0.04		YES	17.1	-3.6	1.32	-1.5	5.9	-2.1	-7.7	-2.1		1.016324
<a href="#">PHKG2</a>	5261	513	0.24	0.43	0.03	0.08	0.32	0.08	0.32	0.31	0.03		YES	2.91	4.05	-1.3	-0.4	3.29	-0.3	1.47	-1		1.020925
<a href="#">PI4KA</a>	5297	305	0.2	0.42	0.02	0.38	0.26	0.03	0.29	0.36	0.02		YES	323	7.99	8.35	-10	-1.4	1.74	-28	-10		0.716836
<a href="#">PI4KB</a>	5298	661	0.46	0.35	0.01	0.08	0.28	0.08	0.29	0.32	0.02		YES	25.4	-1.1	1.19	-1.5	4.9	-3.7	0.7	0.86		0.879445
<a href="#">PINK1</a>	65018	607	0.05	0.04	0.38	0.05	0.03	0.43	0.08	0.04	0.39		YES	-6.9	1.81	-1.2	-1.6	1.15	1.06	-0.6	-0.3		1.158661
<a href="#">PIP5K1A</a>	8394	630	0.15	0.46	0.03	0.05	0.36	0.07	0.1	0.45	0.04		YES	23.2	-1.8	-0.2	1.41	6.46	5.94	3.05	-0.8		1.14957
<a href="#">PKLR</a>	5313	569	0.12	0.04	0.37	0.08	0.03	0.41	0.1	0.03	0.39		YES	-8.9	-0.8	-1.1	-1	-1.3	-4.1	-2.3	0.92		1.000356
<a href="#">PPM1D</a>	8493	637	0.03	0.07	0.36	0.03	0.03	0.43	0.03	0.06	0.35		YES	-7.9	-2.2	0.46	-2.6	-2	-5.7	-2.4	2.11		1.00122





















<u>PPMIF</u>	9647	709	0.07	0.06	0.33	0.02	0.03	0.45	0.1	0.05	0.33		YES	-10	2.16	-0.5	-1.2	-2.1	-3.4	2.14	-1.9		0.956561
<u>PPMIL</u>	151742	599	0.11	0.43	0.06	0.09	0.35	0.1	0.1	0.44	0.05		YES	-2.8	-0.6	1.96	-5.2	2.03	-0.7	-2.1	1.02		1.026901
<u>PPP1R1I</u>	6992	275	0.06	0.06	0.32	0.05	0.03	0.48	0.07	0.06	0.33		YES	-3.5	-1.9	-0.6	0.49	-0.2	-0.4	-1.4	-2.8		1.017964
<u>PPP1R2P9</u>	80316	599	0.45	0.33	0.04	0.18	0.34	0.09	0.44	0.34	0.03		NO	98.6	0.91	3.38	-4.5	0.98	4.92	-4.9	0.93		0.886894
<u>PPP2CA</u>	5515	254	0.32	0.3	0.12	0.12	0.14	0.32	0.55	0.11	0.08		YES	138	3.97	2.84	-2.3	-4.1	-3.8	-4.3	-2.8		0.949888
<u>PPP2R2B</u>	5521	598	0.08	0.54	0.02	0.06	0.42	0.05	0.04	0.53	0.02		YES	3.59	1.28	1.1	0.29	1.89	-1	0.95	1.81		0.915746
<u>PPP2R5E</u>	5529	319	0.39	0.24	0.06	0.08	0.25	0.1	0.6	0.14	0.06		YES	0.51	3.7	-5.1	-0.7	-2.6	-1.9	0.28		0.74632	
<u>PPP3RI</u>	5534	644	0.03	0.4	0.05	0.04	0.32	0.07	0.03	0.41	0.05		YES	-0.1	-0.3	-2.1	-1.2	-0.6	2.38	-0.6	-1.8		1.029219
<u>PRAGMIN</u>	157285	339	0.02	0.45	0.04	0.03	0.33	0.08	0.09	0.42	0.03		YES	2.28	-4.3	-4.6	-5.4	-3.6	-6.5	-6.5	-3.8		0.794859
<u>PRVAGI</u>	5571	368	0.11	0.03	0.36	0.04	0.02	0.5	0.12	0.03	0.33		YES	-4.4	0.14	-0.2	-0.1	0.41	-3.4	0.55	2.82		1.025774





















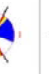

<a href="#">PRKAG3</a>	5963	201	0.27	0.6	0.01	0.07	0.62	0.02	0.15	0.67	0.01		YES	31.6	4.41	0.73	2.77	4.34	1.42	7.5	-5.3		1.065867
<a href="#">PRKCE</a>	5581	640	0.02	0.08	0.39	0.05	0.04	0.54	0.01	0.08	0.41		YES	-3.9	0.42	2.15	-2.8	1.87	-3.2	-5.9	-1.7		0.913564
<a href="#">PRKCSH</a>	5589	245	0.14	0.02	0.27	0.04	0.01	0.46	0.14	0.03	0.28		YES	6.3	5.08	-4.7	1.24	-0.7	0.96	4.03	6.68		1.181042
<a href="#">PRKX</a>	5613	446	0.37	0.4	0.02	0.09	0.49	0.03	0.13	0.54	0.01		YES	101	1.12	6.68	-5.5	8.21	5.87	-0.5	-1.7		1.061314
<a href="#">PRPS1L1</a>	221823	640	0.46	0.2	0.05	0.06	0.19	0.12	0.49	0.14	0.04		YES	20.2	1.23	-1.3	-2.3	-2.5	-3.9	-3	-2.2		0.949315
<a href="#">PTEN</a>	5728	377	0.04	0.03	0.45	0.06	0.01	0.53	0.04	0.02	0.45		NO	-4.6	-3.7	-10	-5.2	-5.8	-6.8	-12	-1.5		1.122621
<a href="#">PTK2</a>	5747	392	0.24	0.13	0.19	0.04	0.07	0.31	0.44	0.09	0.12		YES	5.31	-1.5	-0.9	-1.4	0.21	-2.9	-1.3	2.5		0.929622
<a href="#">PTK7</a>	5754	538	0.29	0.12	0.15	0.23	0.1	0.25	0.33	0.13	0.13		YES	-11	-1.7	0.02	1.82	-2.3	-1.1	1.64	-0.3		0.830101
<a href="#">PTP4A1</a>	7803	218	0.16	0.05	0.27	0.04	0.03	0.51	0.42	0.06	0.15		NO	11	0.76	-3.5	0.45	-0.2	-3.2	-1.2	4.47		1.077327
<a href="#">PTP4A3</a>	11156	699	0.24	0.46	0.04	0.07	0.4	0.08	0.1	0.51	0.04		YES	28.8	-2	0.8	2.47	1.62	2.84	6.45	2.09		0.909142



<a href="#">PTPML4</a>	5784	577	0.1	0.4	0.06	0.04	0.33	0.08	0.07	0.41	0.05		YES	5.54	1.94	-0.1	-1.4	3.68	0.85	-0.7	-0.7	0.92017
<a href="#">PTPRA</a>	5786	395	0.53	0.36	0.02	0.16	0.5	0.02	0.16	0.61	0.01		YES	130	-2.6	1.16	0.99	-3.8	12.1	6.61	7.67	1.083579
<a href="#">PTPRD</a>	5788	696	0.06	0.41	0.04	0.06	0.31	0.08	0.04	0.44	0.05		YES	-5	1.5	1.36	3.05	1.07	6.32	5.75	0.64	0.784632
<a href="#">PTPRF</a>	5792	591	0.18	0.51	0.02	0.06	0.47	0.03	0.14	0.52	0.02		YES	14.7	-3.1	-0.7	1.72	3.95	-3.1	1.98	4.24	1.034419
<a href="#">PTPRN2</a>	5799	693	0.18	0.42	0.03	0.12	0.34	0.07	0.16	0.44	0.04		YES	5.51	6.01	-0.4	-1	1.13	-3.1	-0.8	4.61	0.962146
<a href="#">PTPRI</a>	11122	707	0.08	0.05	0.34	0.08	0.03	0.42	0.07	0.05	0.35		YES	-5.9	0.7	1.72	1.48	-0.4	1.3	2.07	1.64	0.878098
<a href="#">PTPRU</a>	10076	405	0.03	0.43	0.06	0.01	0.25	0.15	0.03	0.34	0.08		YES	-12	-3.6	-2.4	-6.4	-2.5	-5.3	-6.4	-0.1	1.192388
<a href="#">PXK</a>	54889	396	0.17	0.55	0.01	0.1	0.48	0.03	0.19	0.56	0.01		YES	3.29	-4.5	5.98	5.04	0.88	-2.9	5.87	1.68	0.938835
<a href="#">RIPK2</a>	8767	681	0.06	0.03	0.46	0.03	0.02	0.56	0.06	0.03	0.46		YES	-12	-3.1	-3.1	-4.1	-3.6	-5.3	-4	-2.4	0.983898
<a href="#">ROCK1</a>	6093	619	0.03	0.06	0.34	0.04	0.04	0.4	0.02	0.06	0.33		YES	-10	-2.5	-2.7	-2.2	-4.2	-5.1	-5.8	0.04	0.852033

<a href="#">ROSI</a>	6098	320	0.27	0.18	0.07	0.08	0.13	0.25	0.47	0.13	0.08		YES	7.5	0.39	-4.7	-6.5	-3.2	-3.1	-9.2	-2.1		1.05328
<a href="#">RP6-213H19.1</a>	51765	650	0.43	0.39	0.04	0.32	0.15	0.12	0.37	0.29	0.07		NO	156	6.15	4.14	-2	1.95	2.95	-5.7	-1.5	1.029365	
<a href="#">RPRD1A</a>	55167	222	0.1	0.08	0.22	0.06	0.04	0.44	0.13	0.07	0.19		YES	2.24	3.5	4.64	2.49	1.01	-0.7	2.17	1	0.831482	
<a href="#">RP55KB1</a>	6198	686	0.46	0.23	0.06	0.15	0.18	0.17	0.26	0.24	0.1		NO	19.2	-3.6	1.26	-1	2.56	-2.3	-0.5	0.8	1.170245	
<a href="#">RP55KB2</a>	6199	774	0.02	0.11	0.33	0.04	0.06	0.48	0.04	0.11	0.37		YES	-7.7	-0.3	-2.8	-1.1	-0.3	-2.1	-1.8	-2.6	0.698549	
<a href="#">SCYL3</a>	57147	213	0.25	0.06	0.25	0.04	0.04	0.5	0.63	0.04	0.11		YES	12.9	-3.3	-1.2	3.23	-3.9	-5	-0.7	-1	0.954689	
<a href="#">SHPK</a>	23729	784	0.06	0.04	0.32	0.06	0.02	0.45	0.07	0.04	0.31		YES	-2.1	-2.2	-0.8	-2	-0.2	-2.6	-4.4	-3.4	1.016314	
<a href="#">SPHK1</a>	8877	263	0.49	0.3	0.01	0.13	0.33	0.07	0.77	0.11	0.01		NO	1.01	2.09	1.13	3.5	1.71	-1.2	3.4	-1.5	1.109424	
<a href="#">SOSTIM1</a>	8878	290	0.48	0.32	0.02	0.05	0.43	0.03	0.24	0.43	0.01		YES	74.5	0	3.76	3.3	1.45	10.1	4.6	0.76	1.006752	
<a href="#">SRMS</a>	6725	376	0.13	0.09	0.4	0.08	0.05	0.56	0.11	0.08	0.44		YES	2.39	-1.7	0.98	1.78	-2.7	-6.5	-2	-0.5	0.960152	

<u>IRIB1</u>	10221	410	0.04	0.4	0.09	0.06	0.3	0.11	0.04	0.4	0.08		YES	4.16	-2	1.76	4.33	4.59	5.17	11.2	5.75		1.219176
<u>IRPM7</u>	54822	575	0.15	0.58	0.01	0.17	0.51	0.03	0.45	0.38	0.01		NO	154	4.55	2.34	-5.3	-0.8	7.49	-9	-3.8		0.928458
<u>ISKS</u>	60385	488	0.38	0.31	0.06	0.06	0.37	0.1	0.17	0.42	0.05		YES	-0.9	-2.2	1.3	2.71	1.52	4.48	3.36	-0.1		1.099928
<u>ITK</u>	7272	277	0.66	0.16	0.05	0.15	0.15	0.16	0.27	0.19	0.08		NO	67.5	0.06	6.54	8.43	4.87	22.6	15.1	10.5		1.076331
<u>IWF2</u>	11344	753	0.18	0.54	0.01	0.16	0.46	0.04	0.22	0.52	0.01		YES	26.5	7.67	0.89	4.92	2.15	2.5	5.06	1.33		0.767694
<u>IXK</u>	7294	227	0.13	0.12	0.15	0.13	0.03	0.46	0.1	0.08	0.27		YES	8.75	-2.4	1.5	0.04	-1.2	-6.2	-5.7	2.52		0.950375
<u>ULK4</u>	54986	724	0.16	0.05	0.33	0.04	0.04	0.48	0.21	0.05	0.33		YES	-7.5	1.56	-1.8	-7.6	1.32	-5.2	-6	-1.8		0.916236
<u>VRK3</u>	51231	649	0.06	0.52	0.03	0.02	0.44	0.05	0.07	0.53	0.02		YES	-6.2	-1.7	-1.7	0.05	-2.7	-3.1	0.84	-1		1.204446
<u>WVK3</u>	65267	264	0.05	0.12	0.35	0.05	0.11	0.43	0.05	0.11	0.36		YES	4.26	-4.4	-0.6	1.59	-0.7	-5.5	1.58	4.61		1.361775
<u>YSK4</u>	80122	319	0.06	0.09	0.37	0.04	0.06	0.54	0.06	0.1	0.31		YES	-4.7	-3.7	-1	-2.1	-2.9	-4.5	-4.1	2.14		0.867308

<u>TRIB1</u>	10221	410	0.04	0.4	0.09	0.06	0.3	0.11	0.04	0.4	0.08		YES	4.16	-2	1.76	4.33	4.59	5.17	11.2	5.75		1.219176
<u>TRPW7</u>	54822	575	0.15	0.58	0.01	0.17	0.51	0.03	0.45	0.38	0.01		NO	1.54	4.55	2.34	-5.3	-0.8	7.49	-9	-3.8		0.928458
<u>TKS</u>	60385	488	0.38	0.31	0.06	0.06	0.37	0.1	0.17	0.42	0.06		YES	-0.9	-2.2	1.3	2.71	1.52	4.48	3.36	-0.1		1.099928
<u>TK</u>	7272	277	0.66	0.16	0.05	0.15	0.15	0.16	0.27	0.19	0.08		NO	67.5	0.06	6.54	8.43	4.87	22.6	15.1	10.5		1.076331
<u>TWE2</u>	11344	753	0.18	0.54	0.01	0.16	0.46	0.04	0.22	0.52	0.01		YES	26.5	7.67	0.89	4.92	2.16	2.5	5.06	1.33		0.767694
<u>TK</u>	7294	227	0.13	0.12	0.15	0.13	0.03	0.46	0.1	0.08	0.27		YES	8.75	-2.4	1.5	0.04	-1.2	-6.2	-5.7	2.52		0.950375
<u>ULK4</u>	54986	724	0.16	0.05	0.33	0.04	0.04	0.48	0.21	0.05	0.33		YES	-7.5	1.56	-1.8	-7.6	1.32	-5.2	-6	-1.8		0.916236
<u>VRK3</u>	51231	649	0.06	0.52	0.03	0.02	0.44	0.05	0.07	0.53	0.02		YES	-6.2	-1.7	-1.7	0.05	-2.7	-3.1	0.84	-1		1.204446
<u>WVK3</u>	65267	264	0.05	0.12	0.35	0.05	0.11	0.43	0.05	0.11	0.36		YES	4.26	-4.4	-0.6	1.59	-0.7	-5.5	1.58	4.61		1.361775
<u>YSK4</u>	80122	319	0.06	0.09	0.37	0.04	0.06	0.54	0.06	0.1	0.31		YES	-4.7	-3.7	-1	-2.1	-2.9	-4.5	-4.1	2.14		0.867308
<u>YVHAH</u>	7539	617	0.02	0.47	0.03	0.06	0.37	0.04	0.02	0.47	0.03		YES	-4.6	1.3	1.02	-3.1	-0.3	-5	-2.2	1.1		0.952313

Cells colored in yellow or pink indicate score above or below positive and negative thresholds, respectively.

### 3.4 DISCUSSION

My screen results reflect the morphological plasticity of the mammalian Golgi apparatus, as illustrated by the great variety of phenotypes observed. Golgi plasticity was initially revealed through the effect of drugs such as Brefeldin A, which induces a dramatic dispersion of Golgi membranes in a short amount of time [408]. This phenomenon is linked to the highly dynamic nature of this organelle, which is constantly receiving and dispatching membrane material [409].

As shown in the pilot screen, transient depletion of membrane trafficking-related proteins such as SNAREs can drive significant Golgi morphological modifications, presumably through the impairment of specific trafficking events. Indeed, it is known that the Golgi integrity is inextricably linked to the steady state balance of membrane trafficking events and perturbing the rates of trafficking has profound effects on its structure [410]. Although the precise mechanistic links between these protein depletions and the observed phenotypes are not entirely clear at present, some observations were made: proteins acting in specific Golgi trafficking pathways tend to show Golgi compartmental-specific effects and proteins that participate in common pathways often yield similar phenotypes. For instance, depletions of VAMP7 and AP-1 complex that act in trans Golgi trafficking result in trans Golgi specific perturbations. In contrast, knockdown of syntaxin 5 that is involved in ER to Golgi traffic affects predominantly the cis-Golgi. Similar phenotypes were also observed with GS27 and Sec22b that work with syntaxin 5, implying that the observed cis-Golgi effects could be due to an impairment of ER to Golgi traffic. However, it was not obvious for most other SNAREs, presumably because of the promiscuous activity of the SNAREs [411, 412]. It could also be due in part to the difficulty in interpreting Golgi phenotypes. For example, fragmented Golgi phenotypes could reflect changes in the links between stacks and/or their interaction with the underlying cytoskeleton. Yet, it is clear that there are various types of fragmented

phenotypes, which can be detected by a trained human eye. Fragmented phenotypes are also associated with various effects on constitutive secretion and glycan synthesis, suggesting different molecular perturbations at the Golgi level.

Nevertheless, Golgi morphological perturbations can help reveal the genetic regulation of this organelle. The signaling genes screen uncovered that 159 signaling genes, or 20% of the tested set, are implicated in the regulation of the Golgi apparatus. This proportion may appear surprisingly high, however, other evidence support this result. First, in public databases, over 850 different phosphoproteins are associated with Golgi membranes. Second, numerous signaling proteins have been localized on Golgi membranes, and their importance for this organelle is starting to be revealed through various screening approaches [127, 392, 413, 414]. Third, several of my hits or their close homologs are validated by the previous literature. For example, SCYL3 display a clear diffuse trans Golgi phenotype in my screen, suggesting a possible redistribution of TGN46 to the ER. In recent years, it has been well established that a close homolog, SCYL1, binds the COPI coat and regulates both retrograde traffic and Golgi morphology [415, 416]. SCYL2, alias CVAK104, has been proposed to mediate clathrin-coated vesicles formation at the TGN [417]. Together, these data suggest that the SCY-1-like family of catalytically inactive protein kinases have similar roles in regulating membrane traffic. To note, neither SCYL2 nor SCYL3 contains the COPI binding site identified in SCYL1 [416].

The Golgi apparatus is a complex but coordinated structure, which can be conceived as built up of various modules interacting with each other's [418]. The kinases, phosphatases, associated proteins and phosphoproteins that I identified are likely to regulate some of these modules and function to coordinate them. As the Golgi apparatus is relatively constant in shape and function in a given cell population, these signaling molecules acting on the Golgi can be conceived as a large interconnected regulatory network. For the most part, how this network is regulated and what it regulates remains mostly unknown.

An exception is the regulation of the phosphoinositide PIP4 and related lipids in Golgi membranes. PIP4 is known to have multiple effectors in Golgi membranes, its regulation is therefore critical for Golgi physiology [419]. Another exception is the regulation of acto-myosin dynamics, shown to be critical for the formation of transport intermediates both at the TGN and at the CGN [420].

Some of the lipid and protein kinases and phosphatases present in these two subnetworks are known to respond to extracellular stimulations, which could therefore regulate Golgi physiology. Consistently, I also found that several cell surface receptors such as IGFR, TGFBIIR, EGFR or FGFR and their cognate ligands affect strongly Golgi organisation. Cells appear, therefore, to respond to various stimuli by modulating membrane trafficking events at the Golgi level.

Cells also respond to endogenous signals to maintain homeostasis. Endogenous signaling in the secretory pathway has been well described for the unfolded protein response for example [421]. Protein cargo load could also constitute a signal for transport carrier formation that could engage kinases such as PKD [137] or Src [422]. Therefore, it is likely that the large regulatory network that was uncovered from my screen is responsible both for the maintenance of Golgi homeostasis and for adapting Golgi functions to changing extracellular conditions. It has been shown recently that the flux of protein trafficking in the secretory pathway is under the control of a MAPK cascade at the level of the ER exit sites [361, 392, 413]. Additional layers of regulation of secretion probably function at the Golgi level as was shown recently in pancreatic B cells for insulin secretion [423]. This Golgi-localized regulation could possibly act through the modulation of sorting events, as suggested by the hyper-secretion of the Met-Luc reporter. An attractive hypothesis is that not all cargo will be similarly regulated, explaining perhaps partially the complexity of this regulatory network.

In addition, the results suggest that glycosylation is a major target of regulation by signaling networks. Although the precise mechanisms are not known at present, the extensive co-occurrence of perturbations in Golgi morphology and glycan

expression argues that depletion of signaling genes affects glycan expression through Golgi organisation modifications.

Golgi glycosylation is a complex process and signaling could affect multiple mechanisms [424]. For example, luminal pH could be modulated; it has been shown to affect strongly some glycosylation reactions [289]. Alternatively, the organisation of the Golgi stacks in a network could have a critical role in glycosylation, for example by regulating the kinetics of transport and therefore the interaction between substrates and enzymes [50]. Another hypothesis is that glycosylation is regulated through the cisternal distribution of glycosylation enzymes. Indeed, our analysis did detect obvious changes in cisternal organisation. This is exemplified by the dissociation of GalNAc-Ts from Mannosidase II (HPL and MannII-GFP markers) observed in various gene depletions leading to strong cis diffuse but normal medial Golgi.

As shown recently, GalNAc-Ts' activity can be regulated by affecting their intracellular distribution through inducible and specific COPI-dependent transport [193]. By extension, it is possible that other Golgi proteins such as sugar transporters, anion channels or glycosylation enzymes are packaged and redistributed in a specific manner. In favor of this hypothesis, emerging evidence show that Golgi enzymes can be associated with specific adaptors to direct their trafficking [213]. Furthermore, the cytoplasmic tails of different Golgi enzymes have been shown to interact with different cytosolic proteins [425-428], suggesting that they could be differentially trafficked.

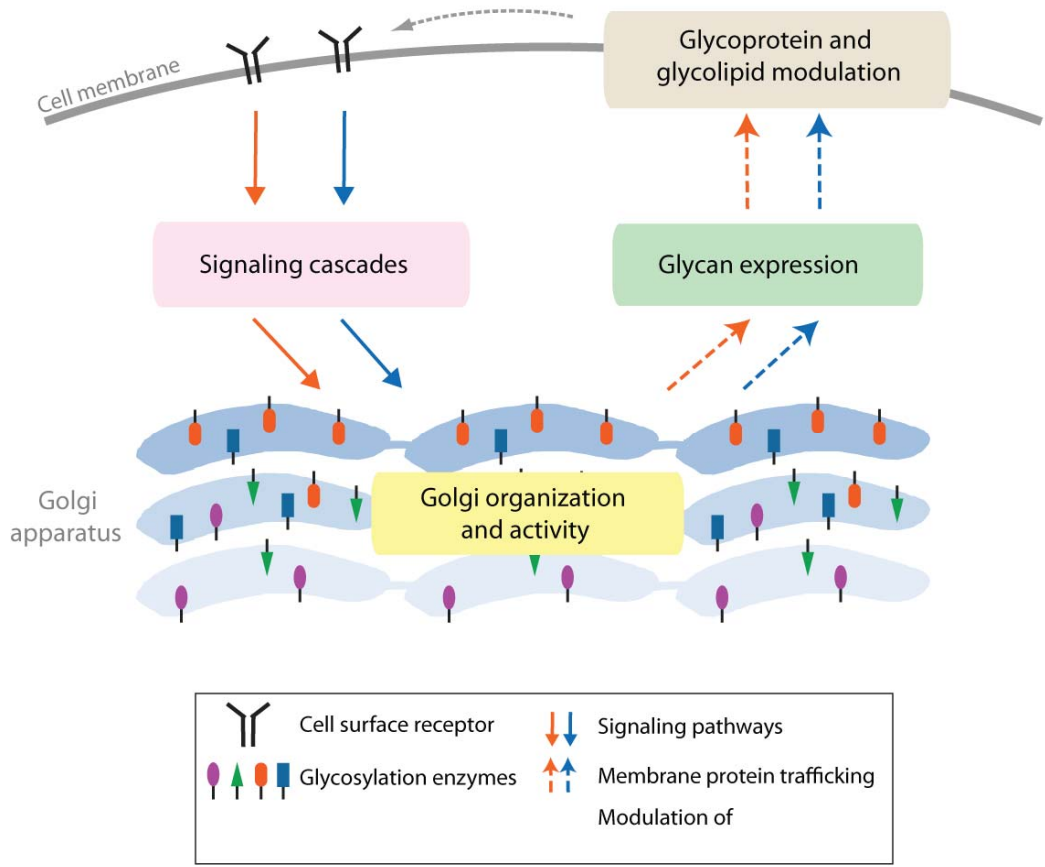
The modulation of glycosylation enzymes expression is arguably the favored mechanism so far to explain changes in glycan expression [283, 429]. Golgi remodeling would represent an alternative, faster mechanism. It could explain the fast changes in glycan expression observed for example during stem cell differentiation programs [430]. Golgi reorganisation would also be an efficient and transient way to regulate cell-cell and cell-matrix adhesion as glycans have been shown to mediate these processes [159]. Furthermore, the cell surface glycan



changes required for apoptotic phases are likely to stem from the Golgi fragmentation that occurs early in apoptosis [431].

As signaling pathways are often modified in cancer cells, our results may help explain some of the abnormal Golgi morphologies commonly observed in cancer cell lines [432]. Alterations in signaling pathways could also potentially explain some of the numerous perturbations of glycoprotein profiles observed in cancer and studied as biomarkers [433, 434]. Overall, our data suggest a complex web of interaction between signaling cascades and the product of Golgi biosynthetic activity, the glycans. There is likely an exquisite regulation of Golgi organisation by different signaling pathways leading to a diversity of glycan expression patterns, each having a unique, distinct role in mediating cellular biology (Figure 3-22). The glycosylation of cell surface receptors is known to affect their stability and signaling potential [435]. Therefore, it is likely that the regulation of glycan expression will, in turn, impact signaling cascades (Figure 3-22).

The cells from complex organisms such as mammals have evolved a capacity to integrate multiple extracellular signal inputs into their physiology, allowing for the coherent behavior of cellular assemblies. Cellular interactions are mainly controlled by cell surface glycoproteins, which are modified and sorted at the Golgi apparatus. Our study highlights that signaling cascades control Golgi physiology and provides a rich data set to further explore this question.



**Figure 3-22: A model of Golgi organisation and glycosylation regulation.** Coloured shapes populating the Golgi illustrate the variety of glycosylation enzymes.

**CHAPTER FOUR: ERK8 IS A NEGATIVE REGULATOR OF O-  
GALNAC GLYCOSYLATION AND CELL MIGRATION**

## **CHAPTER FOUR: ERK8 IS A NEGATIVE REGULATOR OF O-GALNAC GLYCOSYLATION AND CELL MIGRATION**

### **4.1 INTRODUCTION**

GalNAc type O-linked glycans are polysaccharides present on secreted and membrane inserted proteins [242]. Traditionally associated with mucins and mucin-like proteins, recent advances in mass spectrometric analysis have revealed hundreds of different proteins, many do not exhibit mucin-like features, bearing O-glycans [436]. The function of O-glycosylation for most of these proteins is poorly understood but recent results have highlighted examples of its critical role in functional regulation. For instance, O-glycosylation of the growth factor FGF23 regulates its secretion [248, 437] and processing of the lipid homeostatic factor ANGPTL2 is dependent on its glycosylation status [249].

O-glycans are synthesized through the step-wise action of various glycosylation enzymes at the Golgi. Among these are the UDP-N-Acetyl-Alpha-D Galactosamine: Polypeptide N-Acetylgalactosaminyltransferases (GalNAc-Ts, a large family of twenty different isoforms, that catalyzes the initiating sugar residue known as N-Acetylgalactosamine (GalNAc) onto serine and threonine residues of O-glycosylated proteins [241].

GalNAc addition on proteins, in its terminal form, generates the Tn antigen. Earlier work demonstrated that Tn antigen is highly expressed in carcinomas. The high prevalence and specificity of this cancer glycophenotype are remarkable, with corresponding normal tissues and benign tumors expressing much lower levels. Tn increases were also found to correlate with metastatic potential and poor patient prognosis [251] and has been extensively investigated as cancer biomarkers [252-254].

The Tn antigen is specifically detected by antibodies and lectins such as *Helix pomatia* (HPL) and *Vicia Villosa* Lectin (VVL) which have been commonly used to detect Tn levels in carcinoma samples [438, 439]. Antigenicity to Tn is lost upon the addition of further sugar residues, hence, explaining the low Tn levels in normal tissues where GalNAc is rapidly modified by downstream O- GalNAc modifying enzymes.

It has been proposed that increase in Tn levels stem from a block or reduction in the activity of the main O-GalNAc-modifying enzyme, the Core 1 Galactosyl-Transferase (C1GalT) [216, 264, 266, 424]. Loss of C1GalT in the high Tn-expressing T cell leukaemia Jurkat cell line has indeed been reported [267].

Another mechanism was found recently to underlie high Tn levels in cancers. In breast carcinoma and various cancer cell lines, high Tn levels are largely due to the massive relocation of GalNAc-Ts from the Golgi to the endoplasmic reticulum (ER) with Tn staining largely located in the ER [194]. O-glycosylation initiation in the ER in some cancer cells had also been reported earlier by others [440].

Trafficking of GalNAc-Ts to the ER can be stimulated by growth factors such as epidermal growth factor (EGF) and platelet-derived growth factor (PDGF) [193]. GalNAc-Ts are specifically relocated as other glycosylating enzymes are not affected. These enzymes are active in the ER and GalNAc incorporation in proteins increases after relocation [193]. Glycosylation of ER-resident proteins likely explains the observed increase in Tn staining, as several of these proteins bear O-GalNAc in mass spectrometric analyses [436].

Although it is still unclear which specific proteins are modified and how their function might be affected, O-glycosylation in the ER has a marked stimulating effect on cell adhesion and cell migration [194]. This suggests that ER O-glycosylation promotes the invasiveness and metastatic potential of malignant

tumor cells. Tn levels are consistently higher in higher grade, more aggressive breast tumors. Conversely, ER-specific inhibition of O-glycosylation reduced drastically lung metastasis in a mice model [194]. Thus, the precise subcellular location of GalNAc-Ts has important physiological effects.

GalNAc-T transport is stimulated by the Src tyrosine kinases and mediated by COPI- dependent trafficking [193]. COPI transport carrier formation requires the assembly of the COPI coat which is a multimeric protein complex that functions in the retrograde traffic between the Golgi and the ER [441, 442]. The assembly of coat components is regulated by small GTPases of the Arf family and their regulator, the GTP Exchange Factor, GBF1. However, the regulation of COPI-coated carrier formation in response to extracellular signals and how signaling proteins might act to regulate COPI carrier formation are poorly understood. In addition, apart from Src, what are the other signaling proteins regulating Tn expression are not known.

Given that signaling proteins are often modified in cancer, I further explored the role of signaling regulation on Tn expression. In this chapter, I describe the use of RNAi screening to identify signaling regulators of Tn expression. This would help to gain mechanistic insights to Tn expression in cancer and provides potential therapeutic targets for Tn-related cancer therapy.

## **4.2 RESULTS: RNAi screening identifies ERK8 as a negative regulator of O-GalNAc glycosylation and cell migration.**

### **4.2.1 RNAi screening identifies 12 signaling genes negatively regulating Tn levels.**

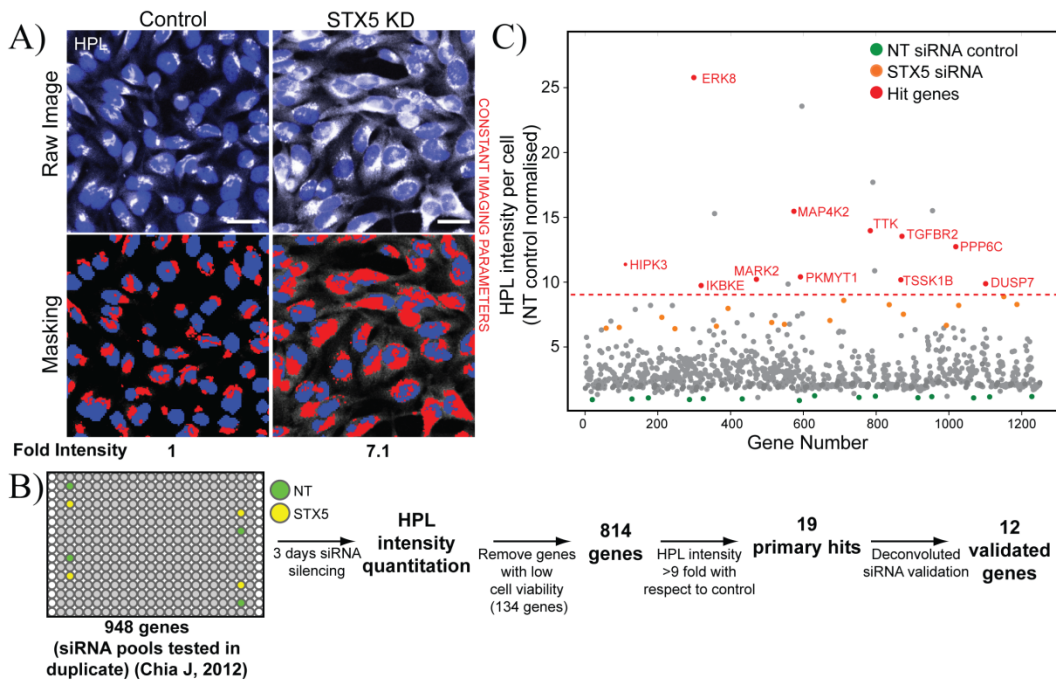
Tn can be detected by glycan binding proteins such as the *Helix Pomatia* Lectin (HPL) [439]. The levels of Tn expression can, hence, be measured from the amount of HPL binding. As described in Chapter 3, I utilized a fluorophore conjugated HPL to mark the Golgi in the primary RNAi screen. Using the same dataset, I quantified the total HPL intensities and the nuclei number to obtain the levels of Tn expression per cell. The automated image analysis module (Transfluor HT) on the MetaXpress software (Molecular Devices) was employed for intensity quantification. The analysis involved setting an intensity threshold to classify the region of measurement for HPL and nuclei staining and the intensity of each pixel within the masking was quantified (Figure 4-1A). The pilot screen with 63 membrane trafficking regulators revealed that knockdown of Syntaxin 5 (STX5) induced a six- to seven-fold increase in HPL intensities relative to a non-targeting control (GFP siRNA) (Figure 4-1A). STX5 and GFP siRNAs were included as controls in the primary screen of 948 signaling genes. In this study, I used them as positive and negative controls respectively to evaluate effects on O-glycosylation. Out of the 948 siRNA pools, 134 that reduced cell number below 20% of average cell number in non-targeting control wells were first excluded from further analysis (Figure 4-1B).

Interestingly, knockdown of several signaling genes was observed to increase HPL levels significantly more than STX5 (Figure 4-1C). The increases were highly reproducible between the two independent replicates, verifying that the phenotypes were not due to experimental variations (not depicted). Staining intensities of the multiple wells of STX5 knockdown were tightly distributed;

further demonstrating reproducibility of the lectin staining and between replicates (Figure 4-1C). The trend was mostly independent of the analysis algorithm used. Quantification by both the MetaXpress software and the HCS analysis algorithm (described in Chapter 3) were highly correlated ( $R^2= 0.93$ ), indicating that the results were consistent across different analysis softwares. The effects observed were not specific to the detection method as a highly consistent pattern could be observed in the staining with VVL, a different lectin specific to Tn antigen (not depicted).

To focus my analysis, I applied a stringent cut-off of nine-fold increase in HPL intensity, significantly above that of STX5 depletion, to select for 19 primary hits (Figure 4-1B and C). To exclude the possibility of off-target effects in these primary hits, I repeated the screen using the four independent siRNAs that were used in the original pools in the primary screen. With the criteria of having significant HPL increases in at least two independent siRNAs, 12 genes were considered validated (Figure 4-1C, red dots and gene names).

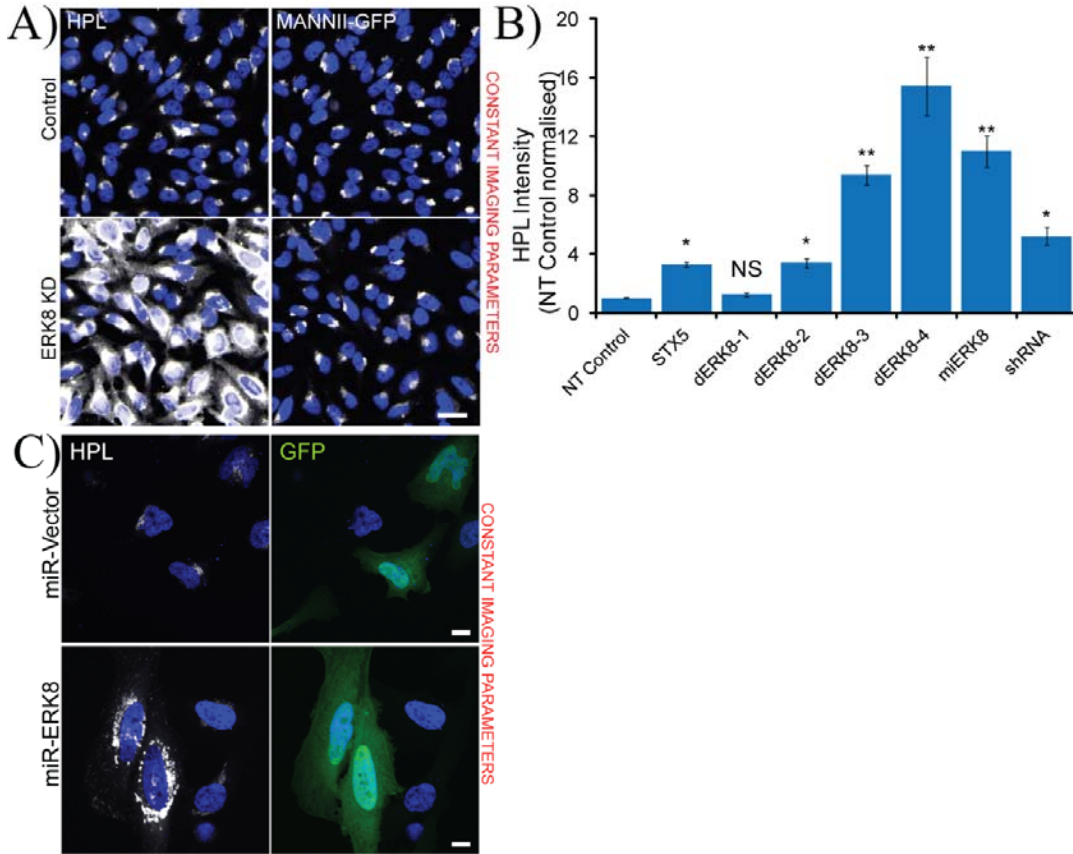




**Figure 4-1: RNAi screening revealed 12 negative regulators of Tn expression.** HeLa cells stained with *Helix pomatia* lectin (HPL) and nuclei (Hoechst) were quantified for HPL intensities using “Transfluor HT” module of MetaXpress software (Molecular Devices). A mask was generated for both HPL and nuclei staining by setting an intensity threshold to classify the regions of measurement (lower panels). Shown here, knockdown of the positive control STX5 (STX5 KD) resulted in seven-fold increase in HPL intensities compared to the non-targeting control. Scale bar: 30µm. (B) A schematic overview of the screening process. HPL and nuclei stained images from the RNAi screen in [443] were quantified for HPL intensities. (C) Plot of fold changes of HPL intensities normalized to non-targeting (NT) siRNA treatment (*green*). A number of genes showed significantly higher HPL increases compared to positive control STX5 (*orange*). 19 primary hits were selected based on a threshold of nine-fold increase (red dashed line) and the 12 deconvoluted siRNA validated genes are labeled red.

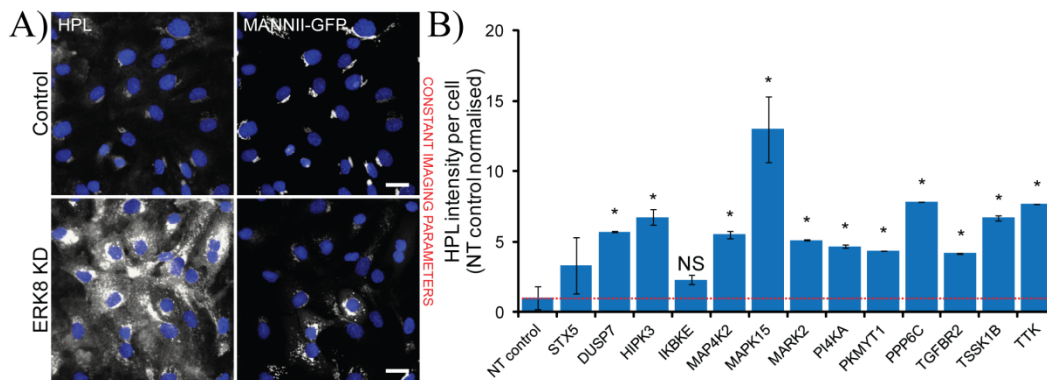
Among the validated hits, I found that depletion of atypical Ser/Thr kinase Mitogen-Activated Protein Kinase 15 (MAPK15, alias ERK8) [444] induced a particularly marked increase in Tn levels (Figure 4-2A). The phenotype was not likely due to an siRNA off-target effect as knockdown with three out of the four single siRNAs (deconvoluted siRNA) from the pool as well as other RNAi

reagents such as short hairpin RNA (shRNA) and microRNA (miR RNA) significantly reproduced Tn increases (Figure 4-2B and C).



**Figure 4-2: Depletion of ERK8 results in dramatic increase in Tn levels.** (A) HPL staining intensities in ERK8 depleted HeLa cells showed pronounced upregulation. The staining appeared diffuse-looking and was not confined to the perinuclear localization observed in untransfected control cells. The general Golgi structure as reflected by Mannosidase II (MannII-GFP) was not affected. Scale bar: 30 $\mu$ m. (B) Knockdown with three out of four single siRNAs (deconvoluted siRNA: dERK8-1 to -4) of the pool or depletion with alternative RNAi methods such as microRNA (BLOCK-iT miR RNAi from Invitrogen) (Illustrated in C) and short hairpin RNA (shRNA) reproduced significant Tn increases, substantiating that the ERK8 depletion phenotype was not likely an off-target effect. Values on graphs indicate mean $\pm$ SEM. \*\* $p$ <0.0001, \* $p$ <0.05 by two-tailed unpaired t-test, relative to NT siRNA-treated cells. (C) Transfection of GFP tagged miR RNAi ERK8 vector (miR-ERK8 bottom panels) induced appreciable Tn increases in cells while those transfected with the empty miR RNA vector (miR-Vector; top panels) had no effect. Scale bar: 10 $\mu$ m.

Tn increase was also apparent when ERK8 was depleted in the ovarian cell line Skov3. Loss of ERK8 led to a diffused, cytoplasmic HPL staining as compared to the predominantly perinuclear staining in untransfected control or non-target siRNA treated cells (Figure 4-3A). Appreciable increase in Tn levels was also observed when most of the hits were depleted in Skov3 cells (Figure 4-3B), substantiating that the phenotype is not cell-type specific and is a biological phenomenon.

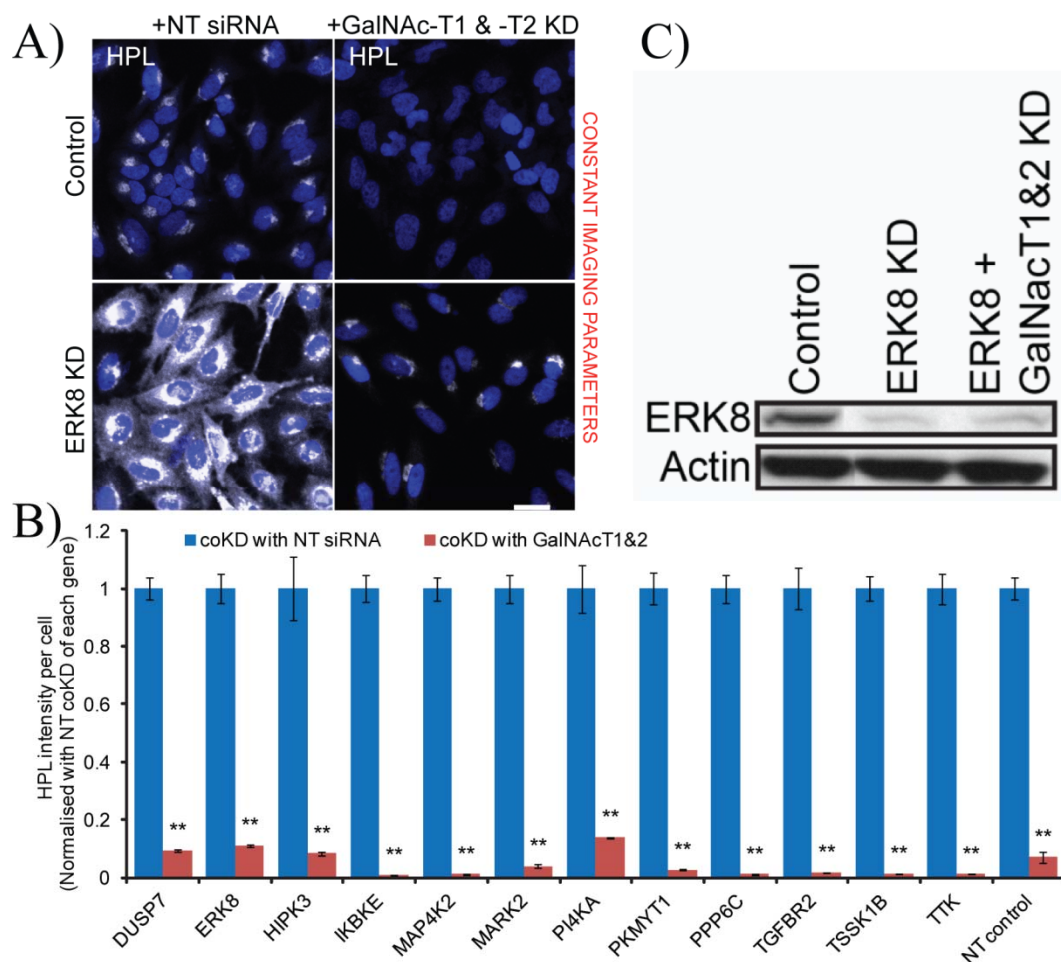


**Figure 4-3: Upregulation of Tn in ERK8 depletion and most hits is conserved across cell lines.** (A) ERK8 knockdown in Skov3 cells induced a similar phenotype as that in HeLa cells. HPL staining in ERK8 knockdown cells appeared diffuse- looking and cytoplasmic with multiple punctuate structures. The Golgi (MannII-GFP) showed some signs of fragmentation in some cells. (B) Tn levels were significantly elevated when most of the hits were depleted, validating that the phenotype is not cell-type specific. Values on graphs indicate mean±SEM. \* $p < 0.05$  by two-tailed unpaired t-test, relative to NT siRNA-treated cells.

In addition, to further validate that the genes control the GalNAc O-glycosylation of proteins, I next sought to downregulate the responsible enzymes. Although GalNAc-Ts represent a large family of enzymes, the -T1 and -T2 isoforms are by far the most prevalent and represent most of the activity in HeLa cells [241]. This is apparent in the almost completely abolished Tn levels when GalNAc-T1 and -T2 are depleted (Figure 4-4A and B). Not surprisingly, co-depletion of the two

enzymes also reduced significantly the Tn increase from the knockdown of ERK8 as well as the other Tn regulators (Figure 4-4A and B). This effect was not due to inefficient protein knockdown as ERK8 levels were still significantly reduced in the triple knockdown configuration (Figure 4-4C).

Overall, the screen revealed a number of negative regulators of Tn levels which highlighted that the O-GalNAc glycosylation process appears to be tightly controlled by signaling mechanisms.



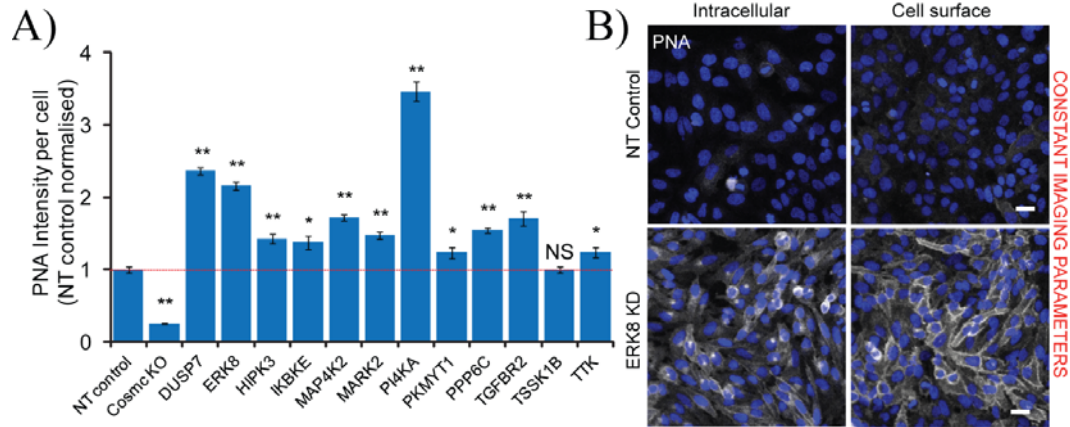
**Figure 4-4: Tn increases are predominantly due to GalNAc-T1 and -T2 activity.** (A) Co-knockdown with GalNAc-T1 and -T2 significantly reduced the increased Tn levels from ERK8 depletion. Scale bar: 30 $\mu$ m. (B) Co-knockdown of each of the 12 Tn regulators with GalNAc-T1 and -T2 resulted in substantial rescues of Tn expression. (C) SDS-PAGE analysis of ERK8 expression levels in single and co-knockdown with GalNAc-T1 and -T2 validated the efficiencies in a triple knockdown configuration. Values on graphs indicate mean $\pm$ SEM. \*\* $p < 0.0001$ , \* $p < 0.05$  by two-tailed unpaired t-test, relative to NT siRNA-treated cells.

#### **4.2.2 Negative regulators of Tn expression are not required for O-glycan extension.**

I next sought to establish the mechanism by which signaling genes control O-GalNAc glycosylation. As mentioned in Section 4.1, two mechanisms are known to increase Tn levels: inhibition of O-GalNAc glycan chain extension [266, 267] or relocation of GalNAc-Ts from the Golgi apparatus to the ER [193]. However, different phenotypes were found to arise from the two mechanisms: for instance, loss of expression of C1GalT or its molecular chaperone Cosmc resulted in failure to generate the subsequent Core 1 glycan structure, also known as the Thomsen-Friedenreich (TF antigen), which can be detected with the PNA lectin [445]. By contrast, our group has previously reported that relocation of GalNAc-Ts from the Golgi to ER induces a modest but measurable increase in PNA staining [194].

To distinguish between the two possibilities responsible for Tn expression, I first tested if C1GalT activity is perturbed. Each of the 12 Tn regulators were depleted and the fluorescence staining intensity of PNA in the cells was quantified. I also measured the PNA staining in Cosmc knockout cells, which lack C1GalT activity, as the positive control. As expected, loss of Cosmc almost completely abolished PNA staining (Figure 4-5A). On the other hand, there was either no significant decrease or some increases in PNA staining levels when each of the 12 Tn regulators were depleted (Figure 4-5A). Similar trends were observed when the genes were depleted with single siRNAs from the pooled version shown in Figure 4-5A, verifying the phenotype observed (not depicted). Increase in PNA levels seemed to correlate with Tn increases and was one of the most significant with ERK8 knockdown. Staining intensities of PNA on the cell surfaces of ERK8 depleted cells (non-permeabilised) paralleled the increases in intracellular staining, suggesting that a large proportion of O-glycan chains remain unextended during their passage through the Golgi (Figure 4-5B). Supporting this, ERK8 depleted cells displayed pronounced reduction in extended O-glycan structures as marked by the *Datura stramonium* lectin (DSL) that was shown in the previous

chapter (Table 3.2). Finally, my results indicate that none of the Tn regulating genes that was identified appear to be required for core 1 forming activity.



**Figure 4-5: The identified Tn regulators do not control O-glycan extension.** (A) Knockdown of each of the 12 Tn regulators did not reduce PNA lectin staining intensities significantly as shown with Cosmc knockout cells. This suggests that C1GalT activity was not affected when the genes were depleted, hence Tn increases were not due to lack of core 1 forming activity. Values on graphs indicate mean± SEM. \*\*p<0.0001, \*p<0.05 by two-tailed unpaired t-test, relative to non- targeting siRNA treated cells. (B) ERK8 depleted cells displayed increases in intracellular and cell surface peanut agglutinin lectin ( PNA) staining. Scale bar: 30µm.

#### 4.2.3 Tn levels depend on GalNAc-Ts subcellular localization.

The other phenotypic difference between the two regulatory mechanisms is the intracellular distribution of the Tn antigen. In cases of C1GalT activity loss, Tn is mostly localized at the cell surface and Golgi, and not the ER, whereas it is mostly in the ER when GalNAc-Ts are relocated [194]. I next probed if the increase in Tn expression was due to the latter case by evaluating the subcellular distribution of GalNAc-Ts using specific antibodies for immunofluorescence staining. In control cells, GalNAc-T1 localised exclusively in the perinuclear region and co-localizes with Golgi marker MannII (Figure 4-6A). Upon ERK8 depletion, GalNAc-T1 localisation was shifted from a perinuclear location to a

diffuse distribution, which co-localizes with ER marker Calreticulin (Figure 4-6A). This was also observed in GalNAc-T2 staining (not depicted). By contrast, the medial Golgi N-glycosylation enzyme MannII-GFP remained mostly perinuclear, suggesting that the relocation event was specific to GalNAc-Ts in ERK8 depletion. MannII-GFP positive structures appeared more fragmented than in untreated cells, reminiscent of the effects of Src activation. Indeed, active Src induces GalNAc-Ts relocation to the ER with limited fragmentation of the rest of the Golgi [193]. Depletion of another major regulator of Tn, the phosphatidylinositol (PI) 4-kinase (PIK4CA), also resulted in redistribution of GalNAc-Ts from a perinuclear localization (Figure 4-6A). Hence, high Tn levels appear to derive from the ER relocation of the GalNAc-T enzymes in these two cases. However, in contrast with ERK8, MannII-GFP appeared to also redistribute to a cytoplasmic pattern upon PIK4CA depletion (Figure 4-6A). In fact, the entire content of the Golgi apparatus was redistributed to the ER in PIK4CA knockdown as a similar pattern was observed with trans Golgi marker TGN46 and general protein secretion was blocked (Table 3.2).

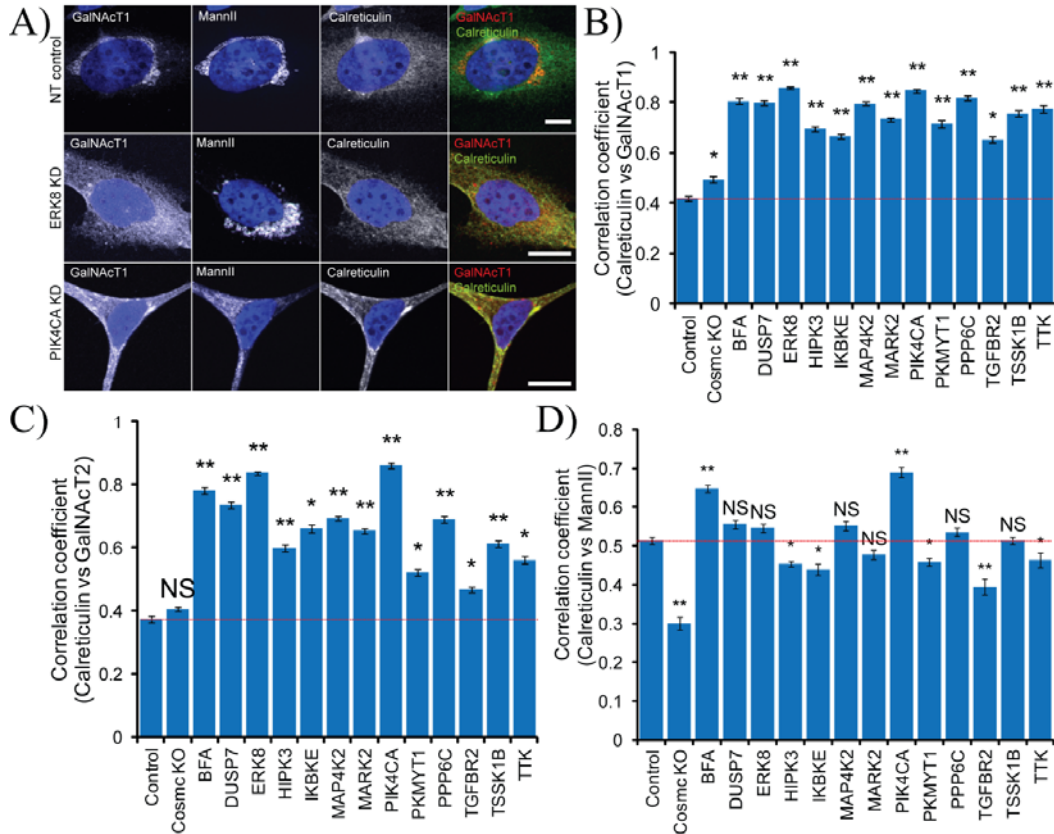
I extended the analysis to the other Tn regulating genes using a quantitative approach. To measure the extent of ER relocation, the colocalisation between GalNAc-T1 and Calreticulin staining was measured. Mean Pearson's correlation coefficient (MPCC) between the two markers was significantly increased in the knockdown of each of the 12 genes (Figure 4-6B). Similar trends were observed in the depletions with single siRNAs from the siRNA pools used in Figure 4-6B, further verifying the phenotype observed (not depicted). Most gene depletions exhibited similar MPCC levels as Brefeldin A (BFA) treatment which have been shown to redistribute Golgi proteins to the ER [446]. In contrast, GalNAc-T1 localisation in the Cosmc knockout cell appeared similar to non-targeting siRNA treated cells (Figure 4-6B). Similar trends were also observed for GalNAc-T2 staining (Figure 4-6C). In addition, high Tn levels in each of the gene depletions was not due to increased expression levels of GalNAc-Ts. This is based on the



quantification of total cellular GalNAc-T1 and -T2 staining intensities in each gene knockdowns (data not shown).

Next, I determined if GalNAc-Ts are specifically relocated in the knockdown of the other Tn regulators ie. if the phenotype is similar to ERK8 depletion. I probed for the integrity of the MannII-GFP staining by measuring the co-localization between MannII-GFP and Calreticulin. As expected from visual observations in Figure 4-6A, PIK4CA depletion resulted in significant co-localisation between the two markers, similar to, if not stronger than, BFA treatment (Figure 4-6D). In contrast, depletion of the other Tn regulators did not affect MannII-GFP localisation as dramatically as PIK4CA.

Collectively, the results suggest that GalNAc-Ts subcellular distribution plays a central role in how signaling cascades can influence Tn staining levels. Other factors may also be at play, but the down-regulation of C1GalT activity does not appear to be a major hub regulated by the identified signaling genes. Finally, it appears that most genes that were identified, with the exception of PIK4CA, control specifically the subcellular distribution of GalNAc-Ts.



**Figure 4-6: Tn regulators control Tn expression through GalNAc-T subcellular localisation.** (A) Immunofluorescence staining for endogenous GalNAc-T1 with Golgi (MannII-GFP) and ER (Calreticulin) markers revealed that the enzyme appeared to localise at the ER in ERK8- and PIK4CA-depleted cells. Medial Golgi MannII enzyme remained predominantly at the perinuclear region when ERK8 is depleted while it was diffused and appeared more cytoplasmic in PIK4CA knockdown. Scale bar: 10  $\mu$ m. (B) Colocalisation between the GalNAc-T1 and Calreticulin was measured using Mean Pearson's correlation coefficient (MPCC) of the staining intensities of the two staining. Cells were analysed using MetaXpress Translocation-Enhanced analysis module. (C) Quantification of MPCC between GalNAc-T2 and Calreticulin staining revealed significant increases in GalNAc-T2 co-localisation with ER marker upon depletion of each of the 12 genes. (D) Quantification of MPCC between MannII and Calreticulin staining revealed that MannII localisation in cells depleted with each of the hit genes were not as perturbed as PIK4CA depletion, suggesting that ER relocation was specific to the GalNAc-Ts in these gene knockdowns. Values on graphs indicate the mean $\pm$ SEM. \*\* $p$ <0.0001, \* $p$ <0.05 by two-tailed unpaired t-test, relative to control untreated cells.

#### **4.2.4 Bioinformatics analyses reveal a putative complex network of Tn regulators acting at the Golgi apparatus.**

To explore how the identified genes might be functioning, I retrieved data pertaining to their subcellular localisation and protein-protein interactions from Protein Atlas, GeneCards and STRING [447-452]. Three proteins—PIK4CA, PKMYT1 and MAP4K2—have previously been reported to be localized at least partially at the Golgi apparatus [453-455]. While the role of MAP4K2 at the Golgi is not completely understood, PIK4CA has been proposed to generate phosphoinositol-4-phosphate (PI4P) at the Golgi (Figure 3-9). PI4P is essential for recruiting membrane trafficking effectors to the Golgi [144], including Vps74/GOLPH3 that is required to retain various glycosyltransferases at the Golgi through retrograde trafficking [456]. Although GalNAc-Ts have not been known to be regulated by Vps74/GOLPH3, it represents a potential mechanism for their retention at the Golgi. PKMYT1, on the other hand, is required for the reassembly of the Golgi during telophase [457, 458]. In addition, ERK8 has been reported to localize perinuclearly in A431 cells by the Protein Atlas database [449], suggesting potential Golgi localisation.

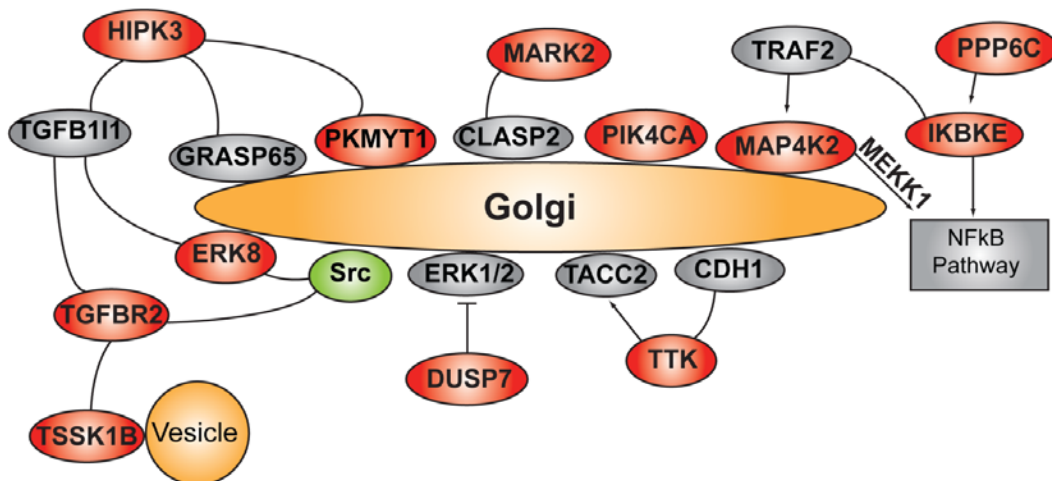
Four other kinases, HIPK3, TTK, MARK2 and DUSP7, have been found to interact with Golgi associated proteins through genetic and large scale proteomics studies with yeast two-hybrid or anti-tag co-immunoprecipitation assays [459-463]. Though extensive protein interaction mapping of human signaling proteins, HIPK3 was found to interact with Golgin GRASP65, Golgi localised LIM kinase and ERK8 interactor TGFB111 [460]. HIPK3 was also found interact with PKMYT1 [464].

The MARK2 protein controls microtubule stability through phosphorylation of microtubule-associated proteins [465] and its interaction with microtubule tracking protein CLASP2 [462] suggests CLASP2 as a potential substrate. CLASP2 is involved in microtubule nucleation at the Golgi for post Golgi

trafficking [68] and also forms a distinct microtubule subsets at the cis Golgi [74]. In addition, Golgi to ER retrograde traffic is known to depend on microtubules tracks [466, 467] suggesting that GalNAc-T relocation could depend on CLASP2 associated microtubules.

Two proteins ERK8 and TGFBR2 have been shown to interact with Src, a positive Tn regulator [444, 468]. ERK8 activity was reported to increase in the presence of active Src [444] and TGFBR2 is phosphorylated by Src [468], suggesting roles in pathways involving Src. In addition, MAP4K2, IKBKE and PPP6C are linked to the canonical NFkB pathway, suggesting that this pathway might control GalNAc-T localisation [469-472]. Finally, several other interactions, either direct or with one intermediate, were found between the Tn regulating genes.

Altogether, this analysis suggests that the Tn-regulating genes are acting at the Golgi level, perhaps part of a regulatory network controlling the subcellular localization of GalNAc-Ts (Figure 4-7). Further experiments are required to confirm the reality of this network and its precise connectivity.



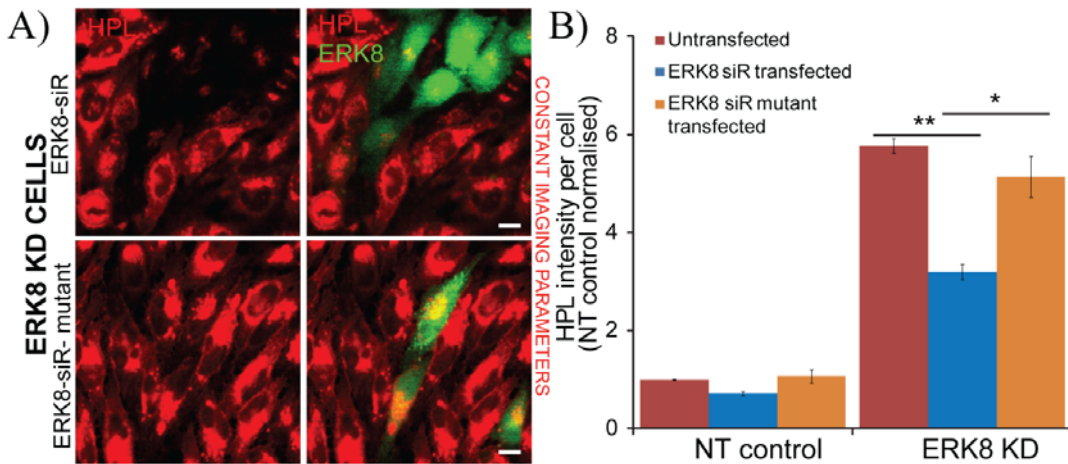
**Figure 4-7: A potential regulatory network of signaling proteins regulating GalNAc-T localisation at the Golgi apparatus.**

#### **4.2.5 ERK8 kinase activity is required for O-glycosylation regulation.**

I next sought to better understand the mechanistic basis of the regulation of Tn levels and focused my efforts on the top hit, ERK8. In contrast with the classical MAP kinases ERK1/2, ERK8 displays high basal activity in resting cells and is not stimulated by growth factor stimulation [444, 473]. Although ERK8 possesses a typical Thr-X-Tyr (T-E-Y) activation motif at residues 175 to 177, it does not appear to be activated by the classical, three-tiered MAP kinase cascade as the other MAP kinases. Conversely, activation of ERK8 occurs by auto-phosphorylation on the TEY motif. These properties suggest that its constitutive kinase activity could be important for ERK8 to function as a constant brake on GalNAc-Ts trafficking in the cell.

To test this notion, I selected the siRNA dERK8-4 for its potency and knockdown efficiency (Figure 4-2B) and designed an siRNA resistant ERK8 construct tagged with GFP (GFP-ERK8siR). A kinase inactive version mutated at the TEY activation motif (GFP-ERK8-siR-T175A-Y177F/ ERK8-siR-mutant) was generated in parallel to test the importance of its kinase activity on GalNAc-T trafficking. Gene replacement with either wild type or kinase mutant ERK8 was performed by transfecting each construct into ERK8 depleted cells at 48 hours after dERK8-4 siRNA treatment (Figure 4-8A). The HPL intensity was quantified for transfected (GFP expressing) and non-transfected (non-GFP expressing) cell populations, each comprising hundreds of cells. While the ERK8 depleted cells that were not transfected (non-GFP expressing) displayed a marked increase in HPL staining, there was significantly lower HPL staining in cells transfected with wild type GFP-ERK8siR construct (Figure 4-8B).

More importantly, HPL intensities remained almost similar to non-GFP expressing cells when transfected with the kinase inactive mutant (GFP-ERK8-siR-T175A-Y177F/ ERK8-siR-mutant) (Figure 4-8B). This suggests that the kinase activity of ERK8 is important for the negative regulation of Tn expression.



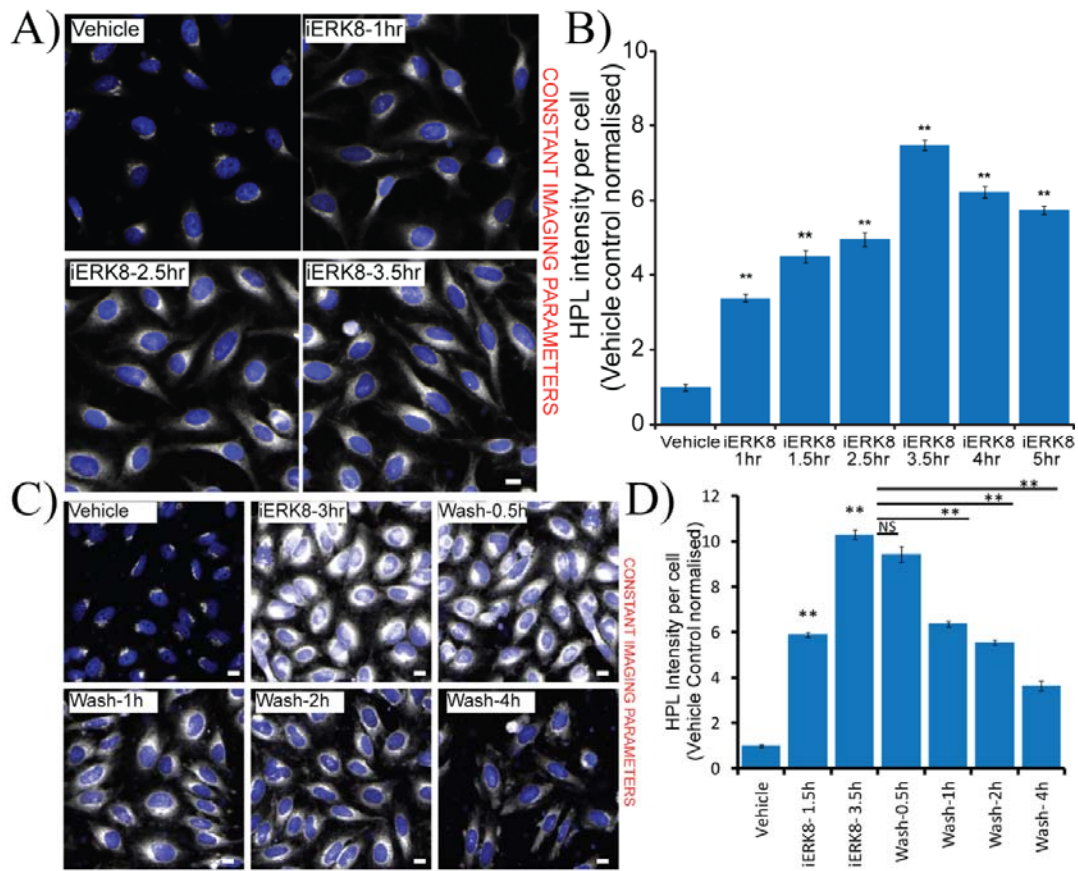
**Figure 4-8: Kinase activity of ERK8 is required to block Tn expression.** (A) Gene replacement by expressing of siRNA resistant wild-type ERK8 (ERK8-siR) in ERK8 depleted (dERK8-4 siRNA treated) cells resulted in a significant rescue of HPL intensity levels (top panels) while expression of the kinase inactive mutant (ERK8-siR-mutant) showed little effect (bottom panels). Scale bar: 30 $\mu$ m. (B) Tn levels of NT siRNA treated and ERK8 depleted cells that were untransfected (red), transfected with wild type ERK8 (*blue bars*) or kinase inactive mutant ERK8 (*orange*). Values on graph indicate the mean  $\pm$  SEM. \*\* $p < 0.0001$ , \* $p < 0.05$  by two-tailed unpaired t- test, relative to untransfected or ERK8 wildtype transfected cells.

#### 4.2.6 ERK8 inhibitor induces a rapid and reversible increase in Tn levels.

Indoyl bismaleimide Ro-31-8220 has been reported to inhibit the kinase activity of ERK8 by blocking its auto-phosphorylation [473]. The compound has been active only on ERK8 and not other MAP kinases such as ERK2, JNK1 or p38 isoforms. I next seek to determine if this compound could recapitulate ERK8 depletion and to evaluate its kinetics of action by treating cells with 5 $\mu$ M Ro-31-8220 for various durations before fixing and staining for Tn levels. 5 $\mu$ M Ro-31-8220 was found to effectively abolish ERK8 phosphorylation levels within one hour of treatment [473]. Strikingly, a significant increase in Tn level was also observed as early as one hour and peaked at eight- to ten-folds from basal levels

after 3.5 hours of Ro-31-8220 treatment (Figure 4-9A and B). Consistent with the levels of phosphorylated ERK8 [473], treatment with a lower concentration of Ro-31-8220 at 1 $\mu$ M resulted in slower increases in Tn levels, rising to only three-fold after four to five hours of treatment (not depicted). Similar to ERK8 depletion, visual observations revealed that cells treated with Ro-31-8220 also displayed a diffused HPL staining. Tn levels were observed to decrease after 3.5 hours of treatment, which was likely due to the effect on cell mortality. In addition, the effects of ERK8 inhibition were rapidly reversible. Inhibitor washout after three hours of treatment began to rescue the Tn levels as early as one hour and significantly by 40% and 65% after two and four hours respectively (Figure 4-9C and D).

Thus, these evidences substantiate that the kinase activity of ERK8 is important for negative regulation of O-glycosylation initiation whereby its constitutive activity provides a continual brake to GalNAc-T relocation. Rescue of Tn expression upon the inhibitor washout demonstrated that reactivation of ERK8 was able to rapidly block GalNAc-T redistribution to the ER, which was most likely relocated back to the Golgi by anterograde traffic, thus accounting for the rescue in Tn expression. Given the rapidity of changes in Tn levels, ERK8 appears to inhibit the process quite directly.

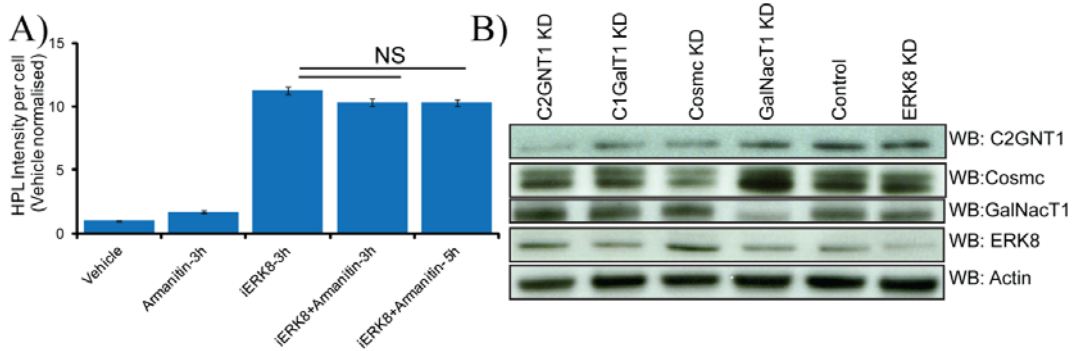


**Figure 4-9: ERK8 inhibition led to rapid and reversible changes in Tn expression.** (A) Treatment with 5  $\mu$ M ERK8 inhibitor Ro-31-8220 (iERK8) induced increases in Tn staining over time compared to the vehicle control (water). The diffused HPL staining recapitulated the phenotype observed in ERK8 depletion and was more apparent with time. (B) Quantification of Tn expression dynamics of 5  $\mu$ M iERK8 over time revealed significant increases within one hour of treatment. (C) Compound washout of 5 $\mu$ M iERK8 Ro-31-8220 over various durations revealed the reversibility of Tn expression levels. (D) Quantification of Tn expression dynamics upon iERK8 treatment followed by compound washout highlighted the short duration required for Tn levels to reduce significantly. Values on graphs indicate the mean $\pm$ SEM. \*\* $p$ <0.0001, \* $p$ <0.05 by two-tailed unpaired t- test, relative to vehicle treated cells unless indicated by a line above the bars of the compared treatments.

The rapid increase in Tn levels also suggests that accumulation of O-GalNAc glycosylated proteins can be achieved in a few hours and it is not likely to be due to expression changes of these O-glycoproteins or the O-glycosylation machinery. Indeed, co-treatment of Ro-31-8220 with transcriptional inhibitor  $\alpha$ -armanitin



[474] did not reduce Tn levels over time (Figure 4-10A). Protein levels of the O-glycosylation enzymes and molecular chaperones were also found to be unaffected in ERK8 depleted cells (Figure 4-10B).



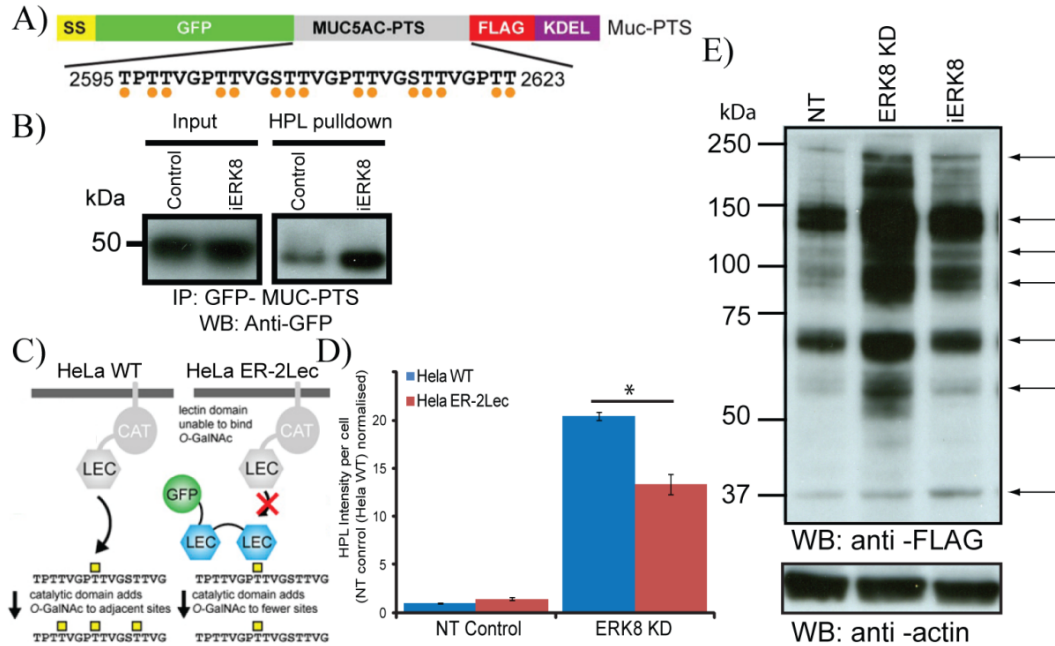
**Figure 4-10: Tn increase in ERK8 inhibition was not due to expression changes in the O-glycoproteins and O-glycosylation machinery.** (A) Co-treatment of cells 10 $\mu$ g/ml transcription inhibitor  $\alpha$ -armanitin and 5 $\mu$ M iERK8 Ro-31-8220 for three and five hours did not reduce high Tn levels brought by iERK8, indicating that Tn increases was not due to transcriptional upregulation. (B) SDS-PAGE analysis of protein expression levels of O-glycosylation initiating enzymes and molecular chaperones in ERK8 depleted cells appeared unchanged compared to control. siRNA knockdown of these O-glycosylation proteins also verified the specificities of the antibodies. Values on graphs indicate the mean  $\pm$  SEM. \*\*p<0.0001, \*p<0.05 by two-tailed unpaired t-test, relative iERK8 treated cells for three hours.

#### 4.2.7 O-glycosylation is initiated in the ER and several proteins are hyperglycosylated when ERK8 is inhibited.

Staining of GalNac-T1 and -T2 strongly suggested their relocation to the ER upon ERK8 depletion (Figure 4-6A). In addition, the dramatic increases in Tn levels suggested that the enzymes are more active in the ER (Figure 4-2 and 4-9). To further confirm this, I used an ER-specific glycosylation reporter (GFP-Muc-PTS) (Figure 4-11A). This reporter construct is specifically targeted to the ER and contains a proline, threonine, serine (PTS)-rich sequence that is prone to O-glycosylation whereby it contains up to 15 sites of GalNac addition [193]. The

glycosylation status of the reporter was evaluated by immunoprecipitation with HPL-conjugated beads. This confirmed a significant increase in ER-localized O-glycosylation upon ERK8 inhibition with Ro-31-8220 for 3.5 hours (Figure 4-11B). ER localization of GalNAc-Ts was further verified using an ER-trapped GalNAc-T inhibitor (ER-2Lec) that is stably and homogeneously expressed in HeLa cells [194]. ER-2Lec contains two lectin domains from GalNAc-T2 in tandem fused together with an ER-targeting sequence and GFP at the N-terminus and a KDEL sequence at the C-terminus. Both ER-targeting and KDEL sequences ensure inhibitor targeting and retention in the ER. Normally, the lectin domain of GalNAc-Ts would recognize O-GalNAc on glycoproteins and add more GalNAc to adjacent sites, increasing the density of GalNAc addition. Presence of ER-2Lec would compete with endogenous GalNAc-Ts by binding to the O-glycosylated substrates in the ER, hence reducing GalNAc density (Figure 4-11C). In line with the results from the Muc-PTS reporter, expression of this inhibitor reduced significantly the increase in Tn levels observed upon ERK8 knockdown (Figure 4-11D), substantiating ER localised activity.

It has recently been proposed that several ER resident proteins are O-glycosylated [436]. To test the extent of modification of the proteome upon ERK8 depletion, I metabolically labeled cells with FLAG-GalNAz, a GalNAc sugar analogue that is covalently conjugated with a FLAG epitope [475]. After 24 hours of incorporation, cells depleted of ERK8 or inhibited with Ro-31-8220 exhibited substantial increases in GalNAz incorporation in several bands as revealed by SDS-PAGE analysis (Figure 4-11E). This suggests that ERK8 controls the O-glycosylation status of a number of different proteins.

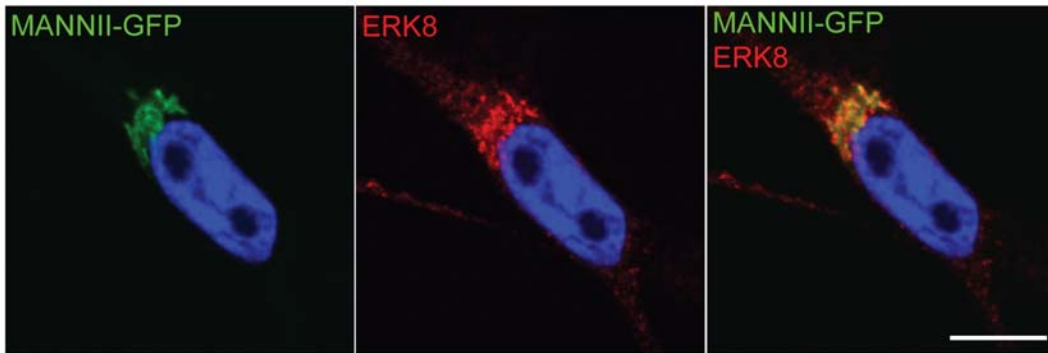


**Figure 4-11: ERK8 inhibited cells displayed increased ER- localized O-glycosylation.** (A) A schematic of ER-trapped Muc-PTS GalNAc-T activity reporter. The reporter contains a secretion signal sequence (SS) fused with GFP at the N-terminus and a KDEL motif at the C-terminus to ensure delivery and retention in the ER. Orange dots represent sites for O-GalNAc addition. (B) SDS-PAGE analysis of Muc-PTS expressed in HEK293T cells treated with vehicle or with 5 $\mu$ M iERK8 Ro-31-8220 for 3.5 hours. Muc-PTS was immunoprecipitated using HPL-conjugated agarose. (C) A schematic of the effect of the ER-specific GalNAc-T inhibitor (ER-2Lec). ER-2Lec comprise of two isolated GalNAc-T lectin domains in tandem tagged with GFP for visualization. ER-2Lec would compete with the lectin domain of endogenous GalNAc-Ts and prevents further addition of GalNAc to substrates. (D) The level of ERK8 depleted cells was significantly lower in cells expressing ER localised 2Lec (ER-2Lec) compared to wild type HeLa cells. (E) SDS-PAGE analysis of control, ERK8 depleted and inhibitor (iERK8) treated cell lysate metabolically labeled using GalNAz-FLAG revealed increased GalNAz addition to multiple proteins in ERK8 depleted or inhibited cells [476].

#### 4.2.8 ERK8 localizes at the Golgi and is displaced upon growth factor stimulation.

GalNAc-Ts have been proposed to regularly cycle between the ER and the Golgi apparatus [477]. Thus, the relocation of these enzymes to the ER upon ERK8

depletion could result either from an enhanced export from the Golgi or an inhibition of exit from the ER. To address this alternative, I first analyzed the subcellular localization of ERK8 protein. Regular immunofluorescence staining of ERK8 in wild type HeLa cells produced a predominantly cytosolic staining pattern. However, prolonged permeabilization with 0.2% triton-X detergent for two hours revealed an obvious Golgi staining, suggesting that a fraction of ERK8 is associated with this organelle (Figure 4-12). This is consistent with the perinuclear pattern observed in A-431 cells by the Protein Atlas project [449].

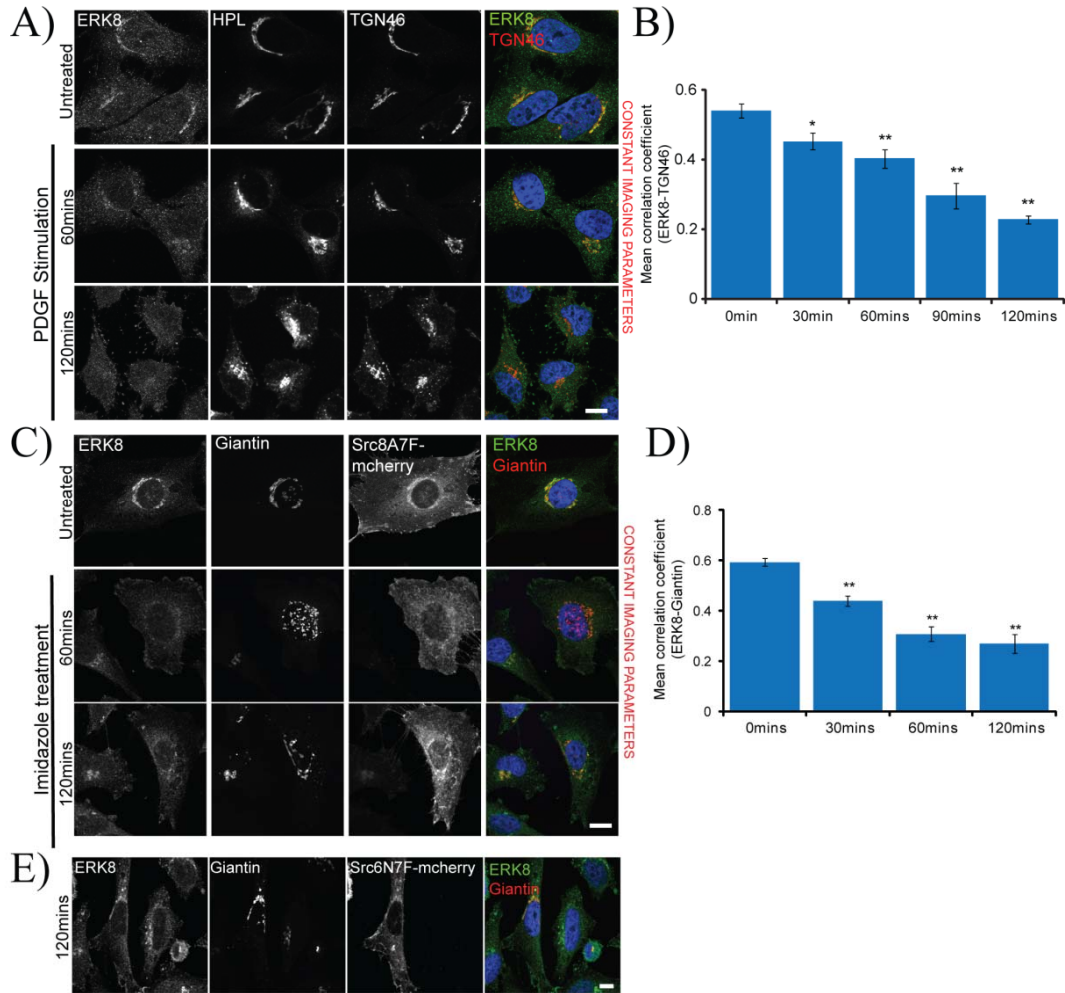


**Figure 4-12: Endogenous ERK8 is enriched at the Golgi.** Image was acquired on 100x magnification. Scale bar: 10 $\mu$ m.

To test how dynamic is this pattern and to understand how ERK8 is regulated when GalNAc-Ts are induced to relocate, HeLa cells were stimulated with 50 ng/ $\mu$ l of growth factor platelet- derived growth factor (PDGF) for various durations. Reported previously, stimulation with PDGF induced significant increases of HPL staining intensity between 30 minutes and two hours [193]. Interestingly, I found that during this period, there was a constant decrease of ERK8 at the Golgi apparatus (Figure 4-13A). The mean Pearson Correlation coefficient of ERK8 and Golgi marker TGN46 staining was quantified to assess localisation of ERK8. Consistent with the visual observations, it revealed significant reductions of the Golgi fraction of ERK8 within 30 minutes and about 60% decrease after two hours of PDGF stimulation (Figure 4-13B).

Tyrosine kinase Src is a key signal transducer that relays growth factor stimulation (PDGF and EGF) at the cell surface to regulate GalNAc-Ts traffic at the Golgi [193]. An inactivated mutant construct of Src (Src-8A7F) has been shown to be inducible by small molecule imidazole [478]. This provided a useful tool to measure the kinetic effects of Src activation. I have generated a HeLa cell line stably expressing Src-8A7F-mcherry and another expressing Src-6N7F-mcherry, a catalytically defective mutant that is insensitive to imidazole. Induction with 5mM imidazole resulted in a gradual decrease of ERK8 at the Golgi, similar to PDGF stimulation (Figure 4-13C and D). Akin to the constitutively active Src expression observed previously [193], longer durations of imidazole treatment also resulted in a fragmented Golgi with multiple punctuate structures. Conversely, as a negative control, cells expressing Src-6N7F had little effect after two hours of imidazole addition (Figure 4-13E). This data suggests that Src activity regulates ERK8 localization at the Golgi.

Overall, the data suggests that ERK8 is dynamically localized at the Golgi apparatus where it could control GalNAc-Ts export.



**Figure 4-13: ERK8 is dynamically localized at the Golgi.** (A) The Golgi fraction of ERK8 was displaced over PDGF (50ng/ml) stimulation time. Scale bar: 10 $\mu$ m. (B) Mean Pearson's correlation coefficient (MPCC) between ERK8 and Golgi marker TGN46 in cells treated with PDGF for the indicated times. (C) The Golgi fraction of ERK8 was displaced over the duration of induction of Src-8A7F activation with 5mM imidazole treatment. Scale bar: 10 $\mu$ m. (D) MPCC between ERK8 and Golgi marker Giantin in Src-8A7F expressing cells treated with imidazole for the indicated times. (E) The Golgi fraction of ERK8 remained unperturbed after two hours of imidazole treatment in cells expressing kinase inactive mutant Src-6N7F. Scale bar: 10 $\mu$ m. Images were acquired on 100x magnification. More than 30 cells were quantified in each treatment duration. Values on graphs indicate the mean $\pm$ SEM. \*\*p<0.0001, \*p<0.05 by two-tailed unpaired t-test, relative to vehicle treated cells.

#### **4.2.8 ERK8 regulates COPI-dependent GalNAc-Ts traffic.**

Upon Src activation, export of GalNAc-Ts to the ER is dependent on the COPI coatomer and the Arf small GTPases family [193]. The activity of these Arf GTPases is regulated by GTP exchange factors which replace GDP to GTP. The key GTP exchange factor that is essential for the Golgi to ER retrograde traffic is GBF1 which is likely to regulate COPI mediated GalNAc-T relocation to the ER [442, 479].

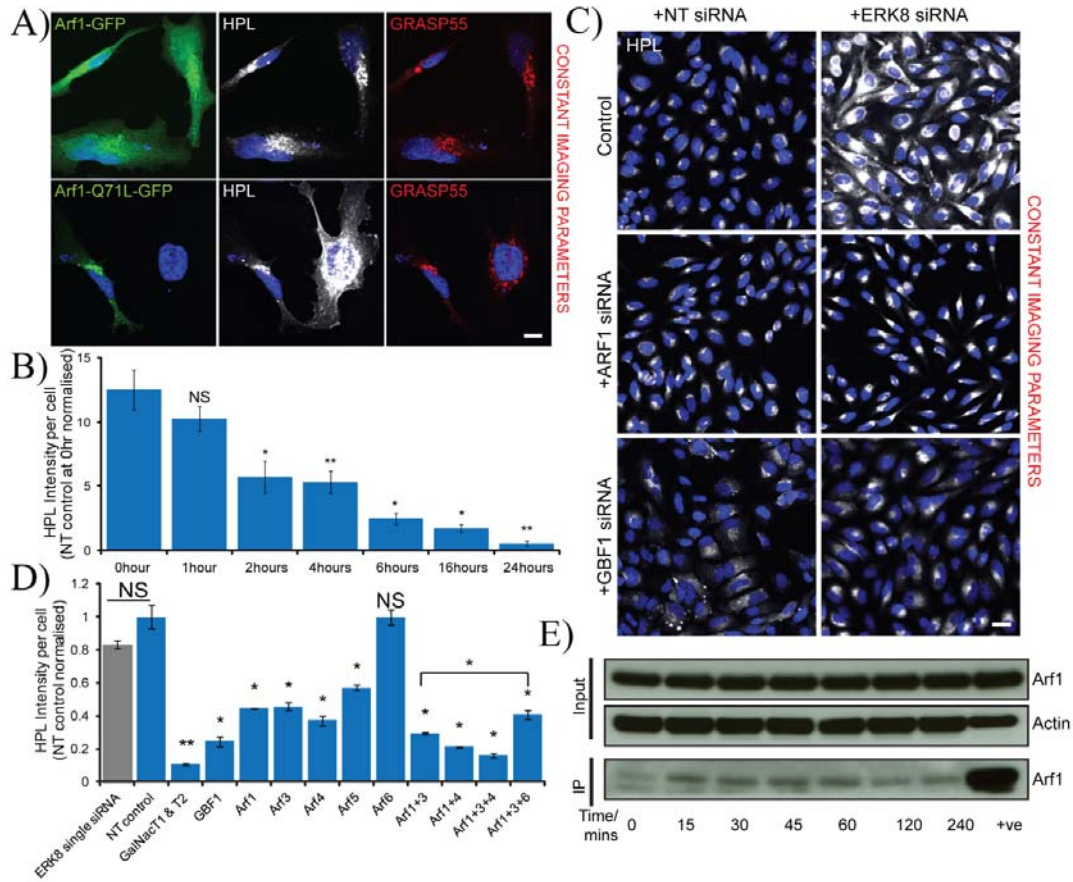
To test if the relocation of GalNAc-Ts upon ERK8 depletion relies on the COPI machinery, wild type Arf1 and the dominant negative mutant Arf1(Q71L) were separately expressed in ERK8 depleted cells. Arf1(Q71L) is unable to hydrolyze bound GTP (Dascher and Balch, 1994). Similar to Src activation [193], Tn levels in Arf (Q71L) expressing ERK8 depleted cells appeared significantly reduced compared to the neighbouring untransfected cells and those expressing wild type Arf1 (Figure 4-14A). I also tested if GBF1 is required for GalNAc-T traffic by treating ERK8 depleted cells with 50nM GBF1 inhibitor Golgicide [480] over various durations. Quantification of Tn levels revealed significant rescue of more than 50% after two hours and 80% by six hours (Figure 4-14B). These results imply that both Arf1 GTPase and its GTP exchange factor GBF1 and hence, COPI-dependent retrograde traffic is required for GalNAc-T trafficking to the ER.

To further establish the specificity of these results, ERK8 was co-depleted with the various COPI regulators to evaluate the effects on Tn levels. The combined knockdown of ERK8 and GBF1 almost completely reversed high HPL staining from ERK8 depletion, further indicating that GBF1 is required for relocation of GalNAc-Ts from Golgi to ER (Figure 4-14C). Co-knockdown of GBF1 with ERK8 reduced HPL staining intensity by about 80% whereas a non-targeting siRNA had almost no effect (Figure 4-14D). Interestingly, co-knockdown of ERK8 with Arf1, the primary Arf involved in Golgi to ER trafficking [481], did not reduce Tn levels as dramatically as GBF1 co-knockdown but produced about

60% reduction (Figure 4-14C and D). Similar decreases were observed in co-knockdown with other Arfs, Arf3, -4 and -5, all potential regulators of COPI at the Golgi [482], suggesting functional redundancy amongst the Arf proteins. By contrast, co-knockdown with Arf6, which is not involved in COPI vesicle formation but regulates endosomal traffic at the plasma membrane, did not affect Tn levels (Figure 4-14D). Consistently, combined double or triple knockdowns of the Arf GTPases in ERK8 depleted cells resulted in more extensive rescue, with the exception of Arf6 inclusion (Figure 4-14D). For instance, co-knockdown with Arf1 and 3 (Arf1+3) or Arf1, 3 and 4 (Arf1+3+4) with ERK8 led to 71% and 84% decrease in Tn levels respectively. These reductions in HPL levels were not due to reduced knockdown efficiencies of ERK8, as similar effects were observed with increasing amounts of NT siRNA added to the transfection mix (not depicted). The efficiency and specificity was also verified by assaying protein expression of each gene (not depicted). Collectively, these data indicate that the COPI trafficking machinery is essential for the ER relocation of GalNAc-Ts and suggest that ERK8 represses constitutively the activity of this transport system.

A key activation step for the COPI coatomer is the exchange of GDP for GTP of the Arf1 family small GTPases [442, 479, 483]. Therefore, I assessed Arf1-GTP loading after ERK8 inhibition using Ro-31-8220. This is by the specific pulldown of Arf1-GTP in cell lysates using the binding domain of an Arf1 effector coupled to agarose beads [484]. ERK8 inhibition over various time points revealed activation of Arf1 as early as 15 minutes after treatment and sustained for over two hours (Figure 4-14E).





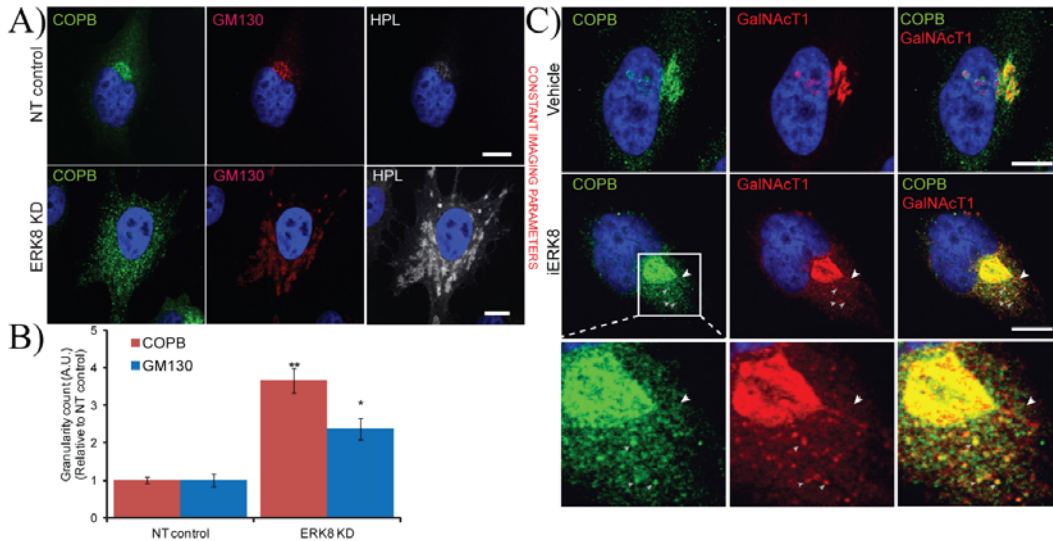
**Figure 4-14: COPI machinery is required for GalNAc-T relocation in ERK8 depleted cells.** (A) Rescue of Tn levels was observed in ERK8 depleted cells expressing dominant negative mutant Arf1 (Q71L) but not in wildtype Arf1 expressing cells. Scale bar: 10  $\mu$ m. (B) Quantification of Tn expression dynamics upon 50nM GBF1 inhibitor Golgicide treatment. (C) Co-knockdown of ERK8 with small GTPase Arf1 or its GEF GBF1, but not NT siRNA, rescued increased Tn levels from ERK8 depletion. Scale bar: 30 $\mu$ m. (D) Quantification of Tn expression upon ERK8 co-knockdown with the Arf proteins and GBF1. (E) SDS-PAGE analysis of total Arf1 and actin, as well as, immunoprecipitated Arf1-GTP from lysate of cells treated with 5  $\mu$ M of iERK8 Ro-31-8220 at the indicated times. Values on graphs indicate the mean  $\pm$  SEM. \*\* $p$ <0.0001, \* $p$ <0.05 by two-tailed unpaired t-test, relative to vehicle treated cells in (B) and NT siRNA-treated cells in (D), unless indicated by a line above the bars of the compared treatments.

To evaluate the effect of ERK8 depletion on COPI, I next stained cells for the Golgi marker GM130 and the COPI subunit beta-COP (COPB). As observed previously with MannII-GFP, GM130 staining revealed significant Golgi

fragmentation after ERK8 depletion. Interestingly, COPB staining was significantly more affected and found on small structures in the cytoplasm, suggesting enrichment on transport intermediates (Figure 4-15A). Using a granularity measurement algorithm, I found a nearly four-fold increase in distribution for COPB but only slightly more than two-fold increase for GM130 (Figure 4-15B), suggesting that depletion of ERK8 induces the activation of COPI transport carriers that export GalNAc-Ts from the Golgi apparatus. This data suggests that depletion of ERK8 induces the activation of COPI transport carriers that export GalNAc-Ts from the Golgi apparatus.

To visualize this process, cells were treated with the ERK8 inhibitor Ro-31-8220 for 15 minutes then fixed and processed for staining. In inhibitor-treated cells specifically, numerous COPI positive vesicular structures could be detected near the Golgi apparatus (Figure 4-15C). Some of these structures were also clearly stained with an antibody against GalNAc-T1 (Figure 4-15C), supporting my hypothesis. Interestingly, in several instances, I could detect tubular structures emanating from the Golgi apparatus and stained for GalNAc-T1 (Figure 4-15C bottom panel). These structures were also stained for COPB, although usually not as homogeneously on their whole length as for GalNAc-T1 (Figure 4-15C bottom panel).

Taken together, these results strongly support the notion that ERK8 specifically inhibits the formation of COPI transport intermediates at the Golgi apparatus, thus preventing the retrograde movement of GalNAc-Ts enzymes to the ER.



**Figure 4-15: ERK8 regulates the formation of COPI transport carriers.** (A) Staining of beta-COP (COPB) revealed significant increase in COPI transport carriers in ERK8-depleted compared to NT siRNA treated cells. The Golgi marked by GM130 also appeared significantly fragmented in ERK8 depletion but not as strongly perturbed as COPB staining. Scale bar: 10 $\mu$ m. (B) Quantification of the relative numbers of COPI transport carriers (red bars) and number of Golgi fragments in GM130 staining (blue bars) using granularity measurement module in MetaXpress software in NT and ERK8 siRNA treated cells. Cells were imaged under 100x magnification and more than 30 cells were quantified for each treatment. Values on graphs indicate the mean  $\pm$  SEM. \*\* $p < 0.0001$ , \* $p < 0.05$  by two-tailed unpaired t- test, relative to NT siRNA treated cells. (C) Co-staining of COPB and GalNAc-T1 in cells treated with 5  $\mu$ M iERK8 Ro-31-8220 for 15 minutes revealed that a number of COPI transport intermediates co-localize with GalNAc-T1. Transient tubular structures were observed in GalNAc-T1 and less homogeneously COPI staining in some cells. Scale bars: 10  $\mu$ m.

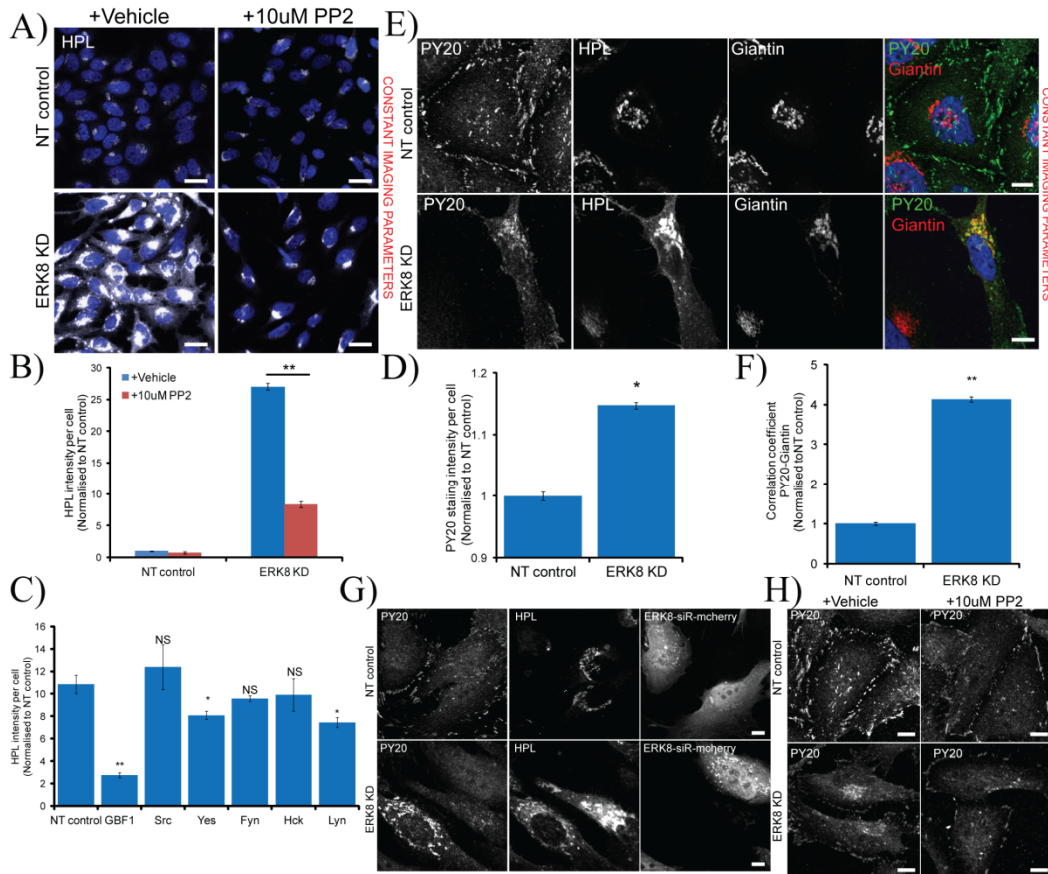
#### 4.2.9 ER relocation of GalNAc-Ts in ERK8 depletion is dependent on tyrosine phosphorylation of Golgi proteins.

Redistribution of GalNAc-Ts to the ER was previously reported to be induced by Src activation [193]. To test if ER relocation of GalNAc-Ts in ERK8 depletion is dependent on Src activity, HeLa cells knockdown with ERK8 were treated with 10 $\mu$ M Src family kinase (SFK) inhibitor PP2 for 16 hours. Interestingly, PP2 addition resulted in a dramatic reduction of HPL staining intensity by 70% (Figure 4-16A and B). However, none of the members of the SFK family

dramatically rescued Tn levels with ERK8 depletion (Figure 4-16C), suggesting that there is likely to be redundancy among the SFKs or PP2-inhibited tyrosine kinase are involved in regulating GalNAc-T trafficking, given that the drug has some effects on other tyrosine kinases [485].

I further investigated if GalNAc-T trafficking was dependent on the activity of SFKs or other tyrosine kinases by immunofluorescence staining of phosphotyrosine in ERK8 depleted cells. Interestingly, the general cellular phosphotyrosine intensities appeared to increase slightly only by about 1.2-fold in ERK8 depleted cells (Figure 4-16D). This was also validated by western blotting of total phosphotyrosine levels of cell lysates (data not shown). However, strikingly, while phosphotyrosine staining in non-targeting siRNA treated cells was predominantly at the cytoplasm and cell membrane, there was a significant upregulation of phosphotyrosine levels at the perinuclear region in ERK8 depleted cells (Figure 4-16E). This perinuclear pool of phosphotyrosine proteins was observed to colocalise with Golgi marker Giantin. Indeed, when I quantified the mean Pearson's correlation coefficient between PY20 and Giantin staining, there was about four-fold increase in phospho-tyrosine levels at the Golgi region (Figure 4-16F) This suggested that a pool of Golgi localised proteins that are tyrosine phosphorylated. The effect is specific to ERK8 as the expression of siRNA-resistant ERK8 construct reduced the high perinuclear phosphotyrosine staining to a cytoplasmic staining, similar to NT-siRNA treated cells (Figure 4-16G). Addition of PP2 also abolished the perinuclear phospho-tyrosine staining (Figure 4-16H), suggesting that SFKs or PP2-inhibited tyrosine kinases are the primary mediators of the tyrosine phosphorylation.

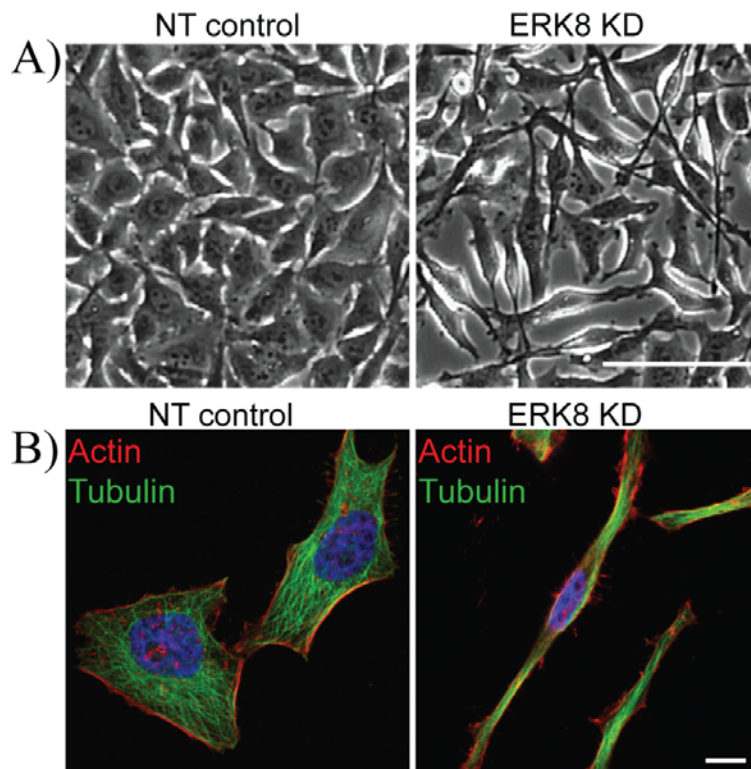
Collectively, the results have shown that ERK8 controls tyrosine phosphorylation of a pool of Golgi or Golgi-associated proteins. Tyrosine phosphorylation is likely to depend on the activities of several SFKs or PP2-inhibited tyrosine kinase. These phosphorylated Golgi proteins are likely to participate in GalNAc-T traffic.



**Figure 4-16: ERK8 regulates Golgi-localized phosphotyrosine levels.** (A) Treatment with 10µM Src inhibitor PP2 for 16 hours rescued Tn levels in ERK8 depleted cells significantly. Scale bar: 30µm. (B) Quantification of Tn levels of NT-siRNA treated or ERK8 depleted cells treated with PP2 or vehicle over 16 hours. (C) Quantification of Tn expression upon ERK8 co-knockdown with several members of SFK family revealed that none of the SFKs was specifically involved in GalNAc-T relocation in ERK8 depleted cells. (D) Quantification of total phospho-tyrosine immunofluorescence staining intensities revealed mild overall increase in phospho-tyrosine levels in ERK8 depletion. (E) Immunofluorescence staining with phospho-tyrosine specific antibody (PY20) revealed spatial upregulation of phospho-tyrosine levels at Golgi regions when ERK8 is depleted. Images acquired at 60x magnification. Scale bar: 10µm. (F) MPCC between PY20 and Golgi marker Giantin staining in NT siRNA-treated and ERK8 depleted cells. (G) Expression of siRNA resistant ERK8 (ERK8-siR-mcherry) reduced the upregulated PY20 staining in ERK8 depleted cells. Scale bar: 10µm. (H) Treatment of ERK8 depleted cells with 10µM Src inhibitor PP2 for 16 hours abolished phospho-tyrosine levels at the Golgi region. Scale bar: 10µm. Values on graphs indicate the mean  $\pm$  SEM. \*\* $p < 0.0001$ , \* $p < 0.05$  by two-tailed unpaired t- test, relative to NT siRNA treated cells.

#### 4.2.10 ERK8 regulates cell migratory ability through control of O-glycosylation.

I previously reported that O-glycosylation in the ER stimulates cell adhesion and cell migration and tends to induce spindle-shaped cell morphology [194]. Interestingly, this morphology was also apparent in ERK8 depleted HeLa cells under phase contrast microscopy (Figure 4-17A) and after staining for the actin and tubulin cytoskeleton (Figure 4-17B).



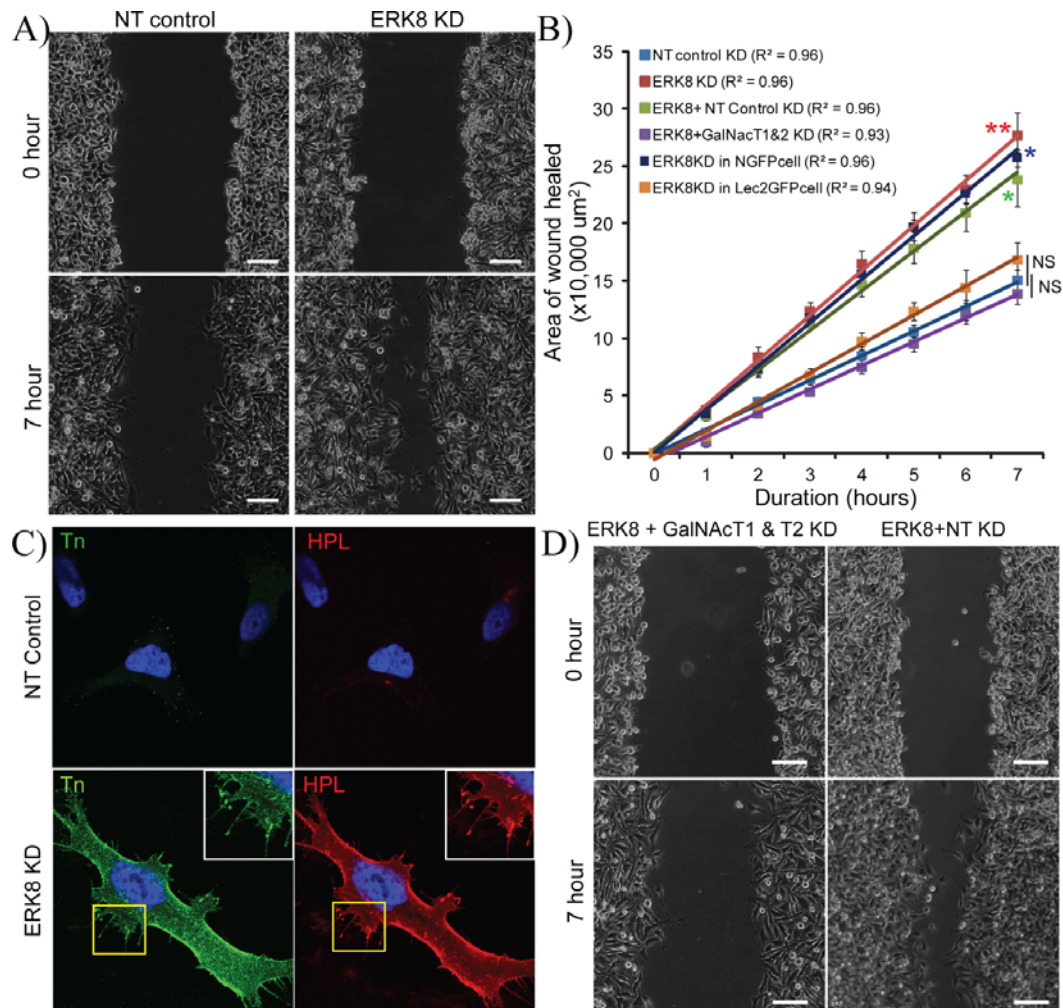
**Figure 4-17: Loss of ERK8 result in spindle- shaped cells.** (A) Phase contrast images and (B) actin and tubulin staining of NT siRNA- treated (NT control) and ERK8- depleted (ERK8 KD) cells. Scale bar: 100  $\mu\text{m}$  in (A) and 10  $\mu\text{m}$  in (B).

I next tested if ERK8 depleted cells also display enhanced cell motility. When tested on fibronectin-coated plates in a scratch-wound healing assay, ERK8

depleted cells migrated about two-fold faster into the denuded area compared with NT siRNA-treated cells (Figure 4-18A). This faster rate was constant over seven hours (Figure 4-18B), indicating that the faster wound closure is caused by faster cell migration and not enhanced reactivity to the initial wound. ERK8 knockdown also led to a dramatically higher cell surface Tn staining, with numerous Tn-positive protrusion structures (Figure 4-18C). These Tn-bearing glycoproteins are likely to promote increased cell adhesion, as shown previously [194].

However, ERK8 has also been implicated in various other cellular processes. To verify that the increased cell motility was due to enhanced O-glycosylation, the scratch-wound healing assay was repeated in ERK8 and GalNAc-T1 and -T2 knocked down cells (ERK8+GalNAcT1&2 KD). I found that these cells migrated significantly slower than ERK8 and ERK8+NT knockdown cells and were in fact similar to NT control cells (Figure 4-18B and D). To further confirm the importance of ER O-glycosylation, I used the ER-localised GalNAc-T inhibitor, Lec2GFP. Cell migration rates induced by ERK8 depletion in Lec2GFP cells were significantly reduced compared with cells expressing only GFP (NGFP cells) (Figure 4-18B) and again rather similar to non-targeting control cell migration. It is important to note that the Lec2GFP construct itself did not significantly slow cell migration in the absence of ERK8 depletion.

Thus, collectively, these results indicate that ERK8 is a negative regulator of cell migration through inhibition of protein O-glycosylation in the ER.



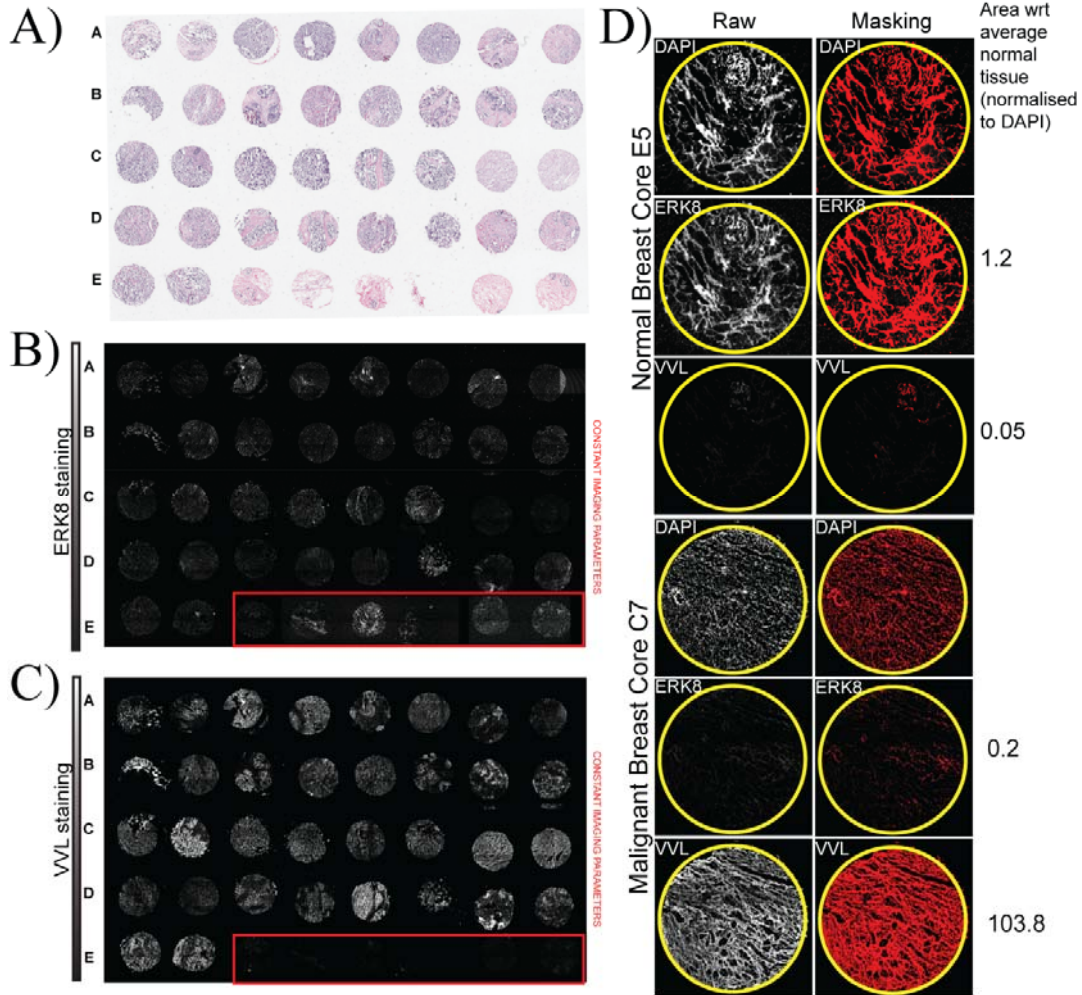
**Figure 4-18: ERK8 regulates cell migration through ER O-glycosylation.** (A) Migration assay using scratch wound of cellular monolayer on fibronectin coated plates revealed significantly faster migratory rates of ERK8-depleted cells compared to NT siRNA treated cells. Scale bars: 100  $\mu\text{m}$ . (B) Rate of wound closure (area) measured over seven hours ( $n = 4$  experiments). Values on graphs indicate mean  $\pm$  SEM. \*\* $p < 0.001$ , \* $p < 0.05$  by two-tailed unpaired t-test. Red asterisk indicates t-test between NT siRNA-treated and ERK8-depleted cells. Green asterisk indicates t-test between cells co-knockdown with ERK8 and GalNAc-T1 and -T2 (ERK8+GalNAc-T1 & -T2 KD) and cells co-knockdown with ERK8 and NT siRNA (ERK8+NT control KD). Blue asterisk indicates t-test between ERK8 knockdown in NGFP-expressing and ER-localised GalNAc-T inhibitor Lec2GFP cells. NS, not significant (black vertical lines). (C) Cell surface staining using a specific Tn antibody (green) and *Helix Pomatia* Lectin (HPL) (red) on non-permeabilised cells revealed a dramatic upregulation in Tn levels in ERK8-depleted cells with localised increases in multiple protrusion structures. Scale bar: 10  $\mu\text{m}$ . (D) Cells co-knockdown with ERK8 and GalNAc-T1 and -T2 (ERK8+GalNAcT1 & T2) migrated dramatically slower than cells co-knockdown with ERK8 and non-targeting (NT) siRNA (ERK8+NT). Scale bars: 100  $\mu\text{m}$ .



#### **4.2.11 ERK8 expression is frequently downregulated in breast and lung carcinoma.**

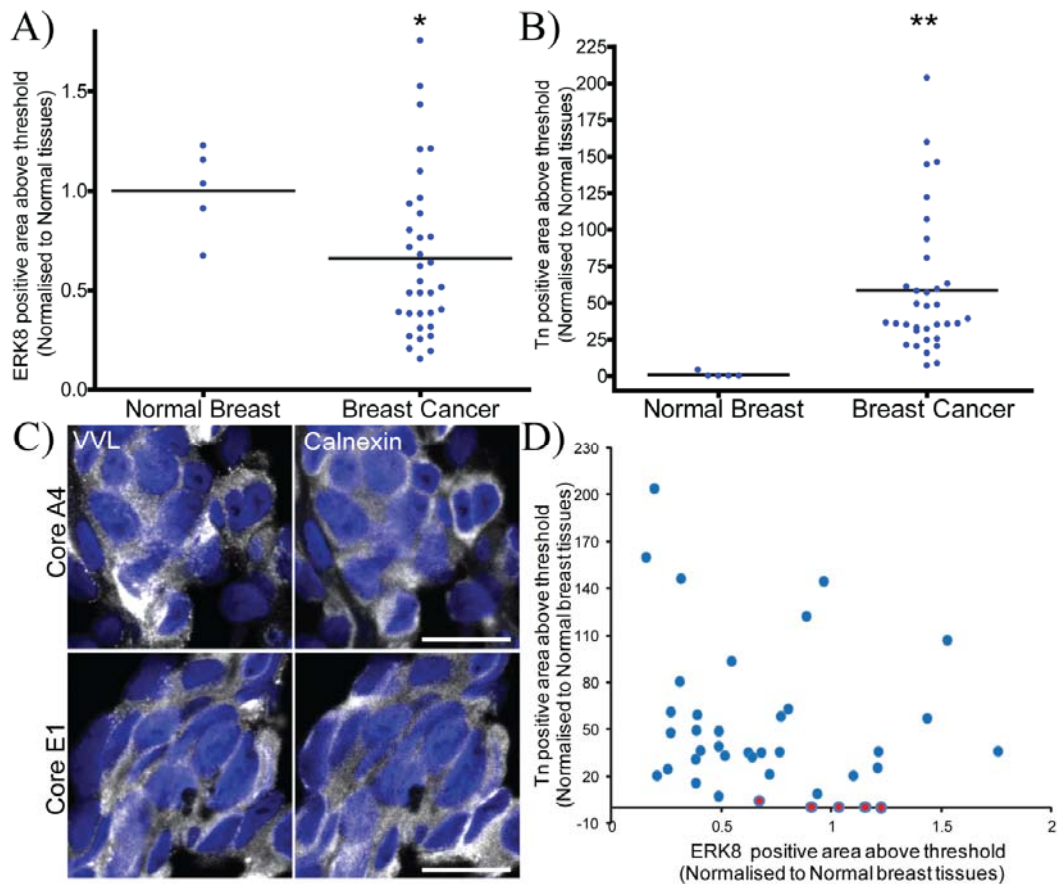
Tn levels were found to be frequently upregulated in tumours of multiple tissue types [438] and my initial goal was to elucidate mechanisms for this frequent increase. Interestingly, on the other hand, ERK8 protein levels was reported to be fairly constant in normal breast tissue and benign tumours but decline significantly in malignant tumours, with a loss in about 50, 80 and 100% of grade 1, 2 and 3 tumours, respectively [486]. The authors proposed that ERK8 stimulates the degradation of Oestrogen Receptor-alpha, suggesting a possible selective advantage for the loss of this MAPK [486]. Interestingly, this trend is also consistent with the increased frequency and intensity of Tn staining as our group had previously reported in breast carcinomas [194].

To further examine the relationship between ERK8 and Tn levels in breast cancer, both ERK8 and Tn (stained with VVL) were co-labelled in a panel of 39 human frozen tissue arrays comprising five normal breast tissues and 34 invasive ductal breast carcinoma (Figure 4-19A-C). Visually, recapitulating previous reports, VVL staining in the normal cores was observed to be significantly lower than the tumour cores. Conversely, ERK8 levels appeared higher in the normal cores. Hence, to compare their expression levels, ERK8 and VVL levels of each tissue core were quantified by measuring the area of the tissue core with staining intensity above a fixed threshold and normalised to the total area of the core represented by nuclei staining (DAPI) (Figure 4-19D). The thresholds for ERK8 and VVL staining were selected based on the masking of the brightest and dimmest core, such that the masking on the brightest core covered the entire core while little or absence of masking could be seen in the dimmest ones (Figure 4-19D).



**Figure 4-19: Quantification of ERK8 and Tn expression levels in human breast carcinomas.** (A) Hematoxylin and eosin stain (H&E) staining of 40 human breast biopsies on BRF404 slides purchased from US Biomax, Inc. Image is from Biomax website (<http://www.biomax.us/>). (B) ERK8 and (C) *Vicia Villosa* Lectin (VVL) were co-stained on the breast tissue arrays. Red boxes indicate the positions of normal breast tissue cores. Note: Core E6 was absent on the slide, hence only 39 of the original 40 biopsies were included in the analysis. (D) Method of quantification of ERK8 and VVL staining in the tissue cores. The area of tissue core with intensity above a fixed threshold, highlighted by the masking (red), was measured. This was then normalised to the total core area represented by the nuclei (DAPI) staining. The fold change of ERK8 and VVL staining area with respect to (wrt) the average of all normal cores is presented on the right of each example image.

Although the levels varied considerably, more than half of the carcinoma cores (18/34) showed at least 50% reduction of ERK8 (Figure 4-20A). In line with previous reports, Tn levels also varied significantly in the carcinoma cores but in the large majority of samples, they were significantly upregulated compared to the normal tissue cores (Figure 4-20B). The subcellular pattern of VVL staining in many carcinoma cores also displayed an ER pattern, verifying that Tn expression in these carcinomas are likely due to ER relocation of GalNAc-Ts (Figure 4-20C). When I compared both ERK8 and Tn levels, their levels appeared to show opposing trends in most cores, suggesting that loss of ERK8 could partially drive high Tn expression. Several cores displayed increased Tn levels, yet high ERK8 levels, indicating that Tn expression in these cores are likely due to other mechanisms. Hence, there was no clear correlation between the levels of both antigens (Figure 4-20D).



**Figure 4-20: ERK8 is downregulated in human breast carcinomas.** (A) Quantification of ERK8 staining in 39 human breast biopsies reveals significantly reduced levels in carcinomas compared normal tissues. Each point represents the staining of one tissue core and normalised to the average staining of the normal tissue cores. (B) Quantification of Tn (VVL) staining in human breast biopsies illustrates upregulated Tn levels in carcinomas. \* $p < 0.05$ , \*\* $p < 0.01$ , by two-tailed unpaired t-test. (C) Co-staining VVL and ER marker Calnexin revealed extensive ER localisation of Tn in two different malignant breast carcinoma samples. Scale bar: 20  $\mu\text{m}$ .

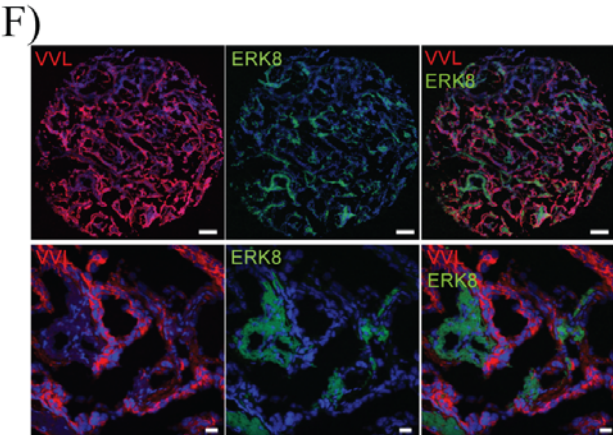
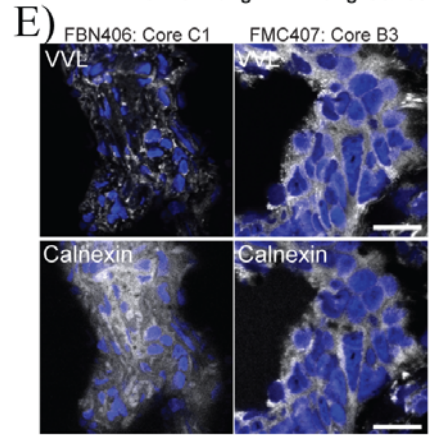
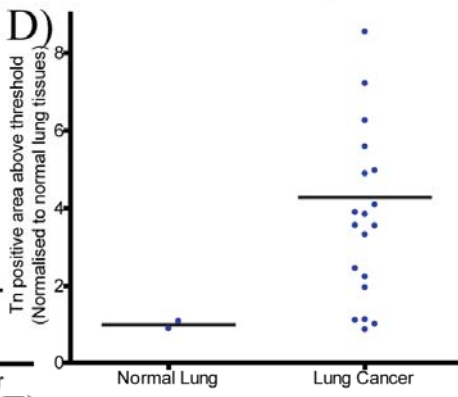
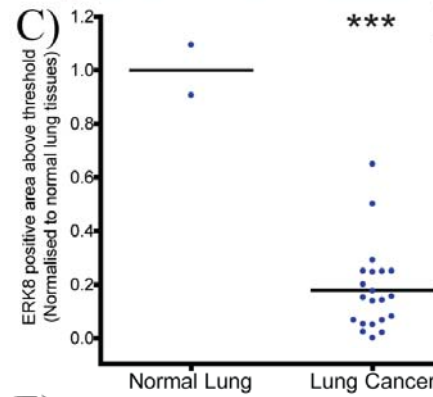
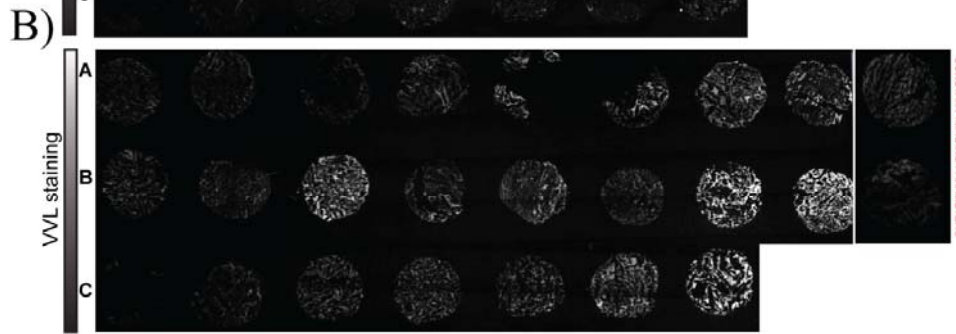
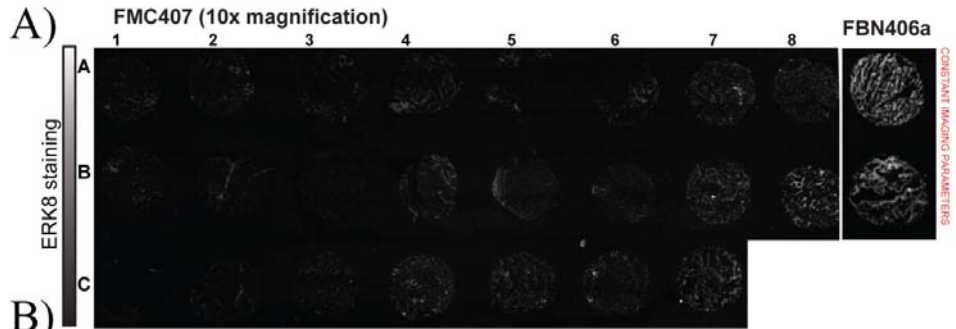
High Tn has also been reported in other tumour types, where Oestrogen regulation is not thought to be critical. As ERK8 was previously found to be highly expressed in the lung [444], I explored the link between ERK8 and Tn levels in lung cancer with 23 lung biopsies containing two normal lung tissues, 14 squamous cell carcinomas, six adenocarcinomas and one small cell carcinoma.

Visually, ERK8 staining appeared clearly detectable in normal tissues but markedly reduced in all lung carcinomas (Figure 4-21A). On the other hand, Tn staining appeared upregulated a number of carcinoma cores (Figure 4-21B). Strikingly, when I quantified ERK8 levels, the reduction was ~80% on average with a range of 40 to 90% reduction (Figure 4-21C). No specific trend in regards to cancer type was noticed. Quantification of Tn levels revealed a significant increase in a majority of samples, with on average more than four-fold increase. This increase ranged from two- to ten-fold, with 18 cores (86%) displayed higher than normal levels of Tn (Figure 4-21D).

I also investigated if high Tn was linked to ER O-glycosylation as observed in breast carcinomas. Indeed, Tn staining co-localised extensively with the ER marker calnexin in lung carcinoma samples. By contrast, Tn staining in the normal lung tissue was clearly more punctuate and reminiscent of a Golgi localization (Figure 4-21E).

Thus, in most lung carcinoma tumours, ERK8 expression is downregulated while Tn levels are increased. However, similar to the breast carcinomas, anti-correlation between ERK8 and Tn levels was not observed in the lung carcinomas. Interestingly, I noticed an anti-correlation between ERK8 and Tn staining in samples with heterogeneous staining for Tn (Figure 4-21F).

The lack of direct correlation indicates that, in human lung and breast tumours, ERK8 levels do not strictly control the levels of Tn. Given the number of Tn regulators that have been identified in the screen (Figure 4-1) and in previous studies, this is not very surprising. Notwithstanding, our analysis indicates that ERK8 is frequently downregulated in lung and breast carcinomas, which probably facilitates the relocation of GalNAc-Ts to the ER when other biochemical or genetic perturbations, such as Src activation, are engaged.



**Figure 4-21: ERK8 is downregulated in human lung carcinomas.** (A) ERK8 and (B) VVL staining of 23 lung biopsies on FBN406a and FMC407 slides purchased from US Biomax, Inc. Note: Core B1 of FMC407 was absent on the slide, hence only 23 of the original 24 biopsies were included in the analysis. (C) Quantification of ERK8 staining in human lung biopsies. (D) Quantification of Tn staining in human lung biopsies. \* $p < 0.05$ , \*\* $p < 0.01$ , \*\*\* $p < 0.0001$  by two-tailed unpaired t-test. (E) Co-staining VVL and ER marker Calnexin revealed extensive ER co-localisation of Tn in lung carcinoma (FMC407: Core B3) while Tn appeared as punctuate structures in the normal lung (FBN406: Core C1). Scale bar: 20 $\mu$ m. (F) Top panel: ERK8 and Tn staining appear anti-correlated in some regions of a lung adenocarcinoma core (FMC407: Core B8). Scale bar: 200 $\mu$ m. Bottom panel: A close-up acquired at 40 $\times$  magnification. Scale bar: 20 $\mu$ m.

### 4.3 DISCUSSION

Several hallmarks of neoplastic transformation in cells, including metastatic potential, have been linked with the expression tumour-associated carbohydrate antigens (TACA). Hence, multiple studies attempted to understand the molecular basis of their expression, with the aim of generating antitumor therapy [487-490]. Among the most common TACAs is the Tn antigen, that is expressed in more than 80% of human carcinomas of multiple tissue origins [252, 254, 491]. In contrast, the corresponding normal tissues exhibit little or no expression. Given the dramatic variations of Tn levels in cancer cells, it suggests that O-glycosylation initiation and/or elongation is highly regulated. Indeed, through an RNAi screen on signalling and related proteins, I identified 12 proteins that exert significant control over O-glycosylation initiation. In addition to the Src tyrosine kinase which our group have previously reported [492], the identification of novel regulators helps in expanding the current limited knowledge on the molecular mechanisms involved in Tn expression in cancer.

The mechanisms of linking Tn antigen to cancer progression are just beginning to be understood. High Tn levels were initially found to arise from a loss or inhibition of the elongation of the O-GalNAc and was attributed primarily through loss of activity of the elongating enzyme, C1GalT or its specific chaperone, Cosmc. Consequently, this has been proposed to underlie the high Tn cancer phenotype [251, 267]. However, the loss of C1GalT activity has only been in a limited set of cancer cell lines and human tumors [216, 251, 267]. In recent years, our group have reported that O-glycosylation initiation can be regulated through trafficking of the GalNAc-Ts between the ER and the Golgi [492] and that marked ER localisation of these enzymes explains the high Tn phenotype of at least 60% of human breast tumours [194].

In our secondary screens, it appears that most, if not all, signalling proteins affecting Tn levels regulate the subcellular localisation of GalNAc-Ts and not the



expression levels of the enzymes or the O-GalNAc elongation process. This obviously does not preclude C1GalT or Cosmc from being regulated in some conditions but a significant inhibition of the activity of these proteins was not observed in our screen conditions.

By contrast, the subcellular localisation of GalNAc-Ts appears to be a nodal point of control in a complex signalling network. Indeed, at least 12 independent negative regulators that were identified and at least as many positive regulators, including the Src family tyrosine kinases, are likely to be involved. This regulatory complexity suggests that perhaps signals of different origins are being integrated at the level of GalNAc-Ts traffic.

ERK8 is one of the most potent regulators that was identified in the screen. The extent of Tn expression and GalNAc-T relocation with ERK8 depletion and the spontaneous Tn increases upon drug inhibition provided an initial hint to its directness on regulating GalNAc-T localisation. This is further substantiated by the findings that a fraction of ERK8 localises to the Golgi region in resting cells, suggesting that ERK8 is constantly present to control the rate of GalNAc-T trafficking. How ERK8 localises to the Golgi is a question worth to pursue and would further clarify its regulatory mechanisms. Several MAPKs have been shown to localise at the Golgi where they spatially direct specific signals [493]. For instance, ERK and MEK are tethered to Golgi membranes by scaffold proteins interleukin-17 receptor D (Sef) [155] or peptidyl-tRNA hydrolase 2 (BIT1) [329]. ERK3, on the other hand, localises to Golgi membranes by its C-terminal residues that are reminiscent to the dilysine (KKXX) motif for targeting to early secretory apparatus [494]. It is possible ERK8 could adopt any of these mechanisms for its Golgi localisation, although a C-terminal dilysine motif could not be observed in ERK8 sequence. Yet, there are other possibilities including post-translational myristoylation [495] or palmitoylation [496] that are involved in membrane targeting of kinases.

Furthermore, I showed for the first time that the localisation of ERK8 at the Golgi is dynamic and appears to be controlled by growth factor (PDGF) and Src-mediated signalling. These findings present a regulatory mechanism for ERK8 activity at the Golgi. Since ERK8 is constitutively active by autophosphorylation in the cell [444], spatially limiting access to Golgi substrates would make sense to regulate its activity. In line with this, classical MAP kinases ERK1/2 also display dynamic localisation upon stimulation and they act on different sets of substrates at different locations. For instance, in resting cells, ERK1/2 is localised in the cytoplasm where it phosphorylates multiple cytoplasmic targets. Upon mitogen stimulation, it translocates to the nucleus and acts on nuclear proteins [497]. ERK1/2 was also found to accumulate at the Golgi during G2/M phase of the cell cycle and was proposed to act on golgi proteins to induce Golgi fragmentation during mitosis [135, 498, 499]. In addition, what could be the underlying mechanisms that coordinate ERK8 translocation from the Golgi during growth factor stimulation/Src activation? Changes in subcellular localisation of ERK1/2 have been known to be mediated by various mechanisms such as phosphorylation in and outside the activation motif [497, 500] and distorting scaffold interactions [501]. ERK8 could also be controlled by similar mechanisms and the process is likely to be mediated by Src signalling. Nevertheless, the findings highlight the dynamicity of the system in controlling GalNAc-T trafficking whereby the “brake” by ERK8 can be spontaneously regulated by extracellular signals.

Various lines of evidence indicate that ERK8 control GalNAc-T localisation by inhibiting the formation of GalNAc-Ts containing COPI vesicles and this is a signalling-dependent mechanism. While it is found that some kinases that localise at the secretory pathway have non-signalling roles [502], my findings that activity of ERK8 is essential to block GalNAc-T relocation supports that it is a signalling event (Figure 4-8). However, one of the important questions that remained open in this study is what could be the downstream substrate(s) of ERK8 involved in GalNAc-T trafficking? Given the fact that ERK8 was only discovered a decade

ago [444], direct substrates of ERK8 are still not identified while it is only known to exhibit distinct substrate specificities from the classical ERK1/2 [473].

The observations that loss of ERK8 promotes Golgi localised upregulation of phosphotyrosine levels, and not general cellular levels, indicates that ERK8 specifically inhibits tyrosine phosphorylation at the Golgi. As demonstrated by our previous results that Src activity at the Golgi regulates GalNAc-T trafficking [193], it substantiates that tyrosine phosphorylation of a pool of Golgi proteins is important for GalNAc-T ER relocation. Supporting this, ERK8 was found to directly interact with Src by binding to its SH3 domains [444], implying that both proteins could carry out similar biological functions, although direct phosphorylation between both proteins is not known. Thus, the rescue of GalNAc-T ER relocation with Src inhibitor PP2 initially supports the view that ERK8 could act by inhibiting Src which mediates tyrosine phosphorylation of the pool of Golgi proteins involved in GalNAc-T trafficking. However, the assumption is refuted by the lack of rescue of HPL intensities when ERK8 is co-depleted with Src or other SFKs. In addition, it is known that PP2 is not specific to Src but affects the activities of other members of SFK, particularly Lck and Hck. More recently, it was also found to affect several other tyrosine kinases [485]. Taken together, the results imply that tyrosine phosphorylation of Golgi proteins for GalNAc-T traffic could involve multiple SFKs or a PP2-inhibited non-SFK tyrosine kinase. It is possible that there is functional redundancy among the SFKs in regulating GalNAc-T traffic as several members of the SFKs have been found to localise and act at the Golgi [129]. ERK8 could interact and act with other SFKs/non-SFK tyrosine kinase through their SH3 domains like Src. However, whether there is any direct phosphorylation and activity inhibition between ERK8 and other SFKs/non-SFK tyrosine kinase is not known.

Given the current results, three scenarios could be postulated. Firstly, in normal cells, ERK8 directly acts and inhibits the hyperactivation of SFKs or non-SFK tyrosine kinase (PP2-inhibited) that phosphorylates Golgi proteins involved in

GalNAc-T traffic (Figure 4-22). Secondly, ERK8 acts on a phosphotyrosine phosphatase that dephosphorylates tyrosines on the SFKs or Golgi protein(s) involved in GalNAc-T trafficking. Thirdly, ERK8 could directly act on phosphorylated Golgi proteins involved in COPI biogenesis and block their activities. For instance, several Golgi proteins involved in ER-Golgi traffic have been found to be phosphorylated for regulation of membrane traffic [392, 484, 503, 504]. However, with the lack of information of ERK8 substrates, the mechanisms of this signalling event such as the order of ERK8 and SFKs/non-SFK tyrosine kinase remains elusive. It can only be concluded at this point that both ERK8 and SFK or tyrosine kinase act in antagonistic pathways on GalNAc-T trafficking. Hence, my findings demonstrate that ERK8 acts by specifically inhibiting tyrosine phosphorylation of a pool of Golgi proteins involved in targeting GalNAc-Ts for Golgi to ER trafficking. Future studies should encompass the elucidation of the precise signalling events that regulate GalNAc-T traffic and the identification of ERK8 substrates at the Golgi should shed more light to this aspect. Identification of the subset of tyrosine phosphorylated Golgi proteins would also uncover how GalNAc-Ts are specifically targeted to COPI carriers.

Based on the genetic interaction profile, the other negative regulators appear to act at the same level as ERK8. Consistently, two of these proteins, PKMYT1 and MAP4K2, are also reported to localize at the Golgi [454, 455], and several other regulators interact with Golgi localized proteins. Together, this suggest that the incorporation of GalNAc-Ts in COPI vesicles is the key point of regulation of this potential regulatory network.

The trafficking of GalNAc-Ts to the ER results in the glycosylation of multiple different substrates, as indicated by the metabolic labelling results. The precise identity of these substrates, as well as the functional effects of their glycosylation, remains to be established. Notwithstanding, the outcome of the relocation at the cellular level is clearly a significant stimulation of cell migration. Indeed, the

stimulatory effect of ERK8 depletion is dependent on ER-localized O-glycosylation. These results are also consistent with our previous data based on the expression of an exogenous, ER-targeted form of GalNAc-T2 [194]. Thus, an interesting hypothesis is that the intensity of packaging of GalNAc-Ts into Golgi-derived COPI-coated vesicles could be a signalling integration point that sets the “motility potential” of cells.

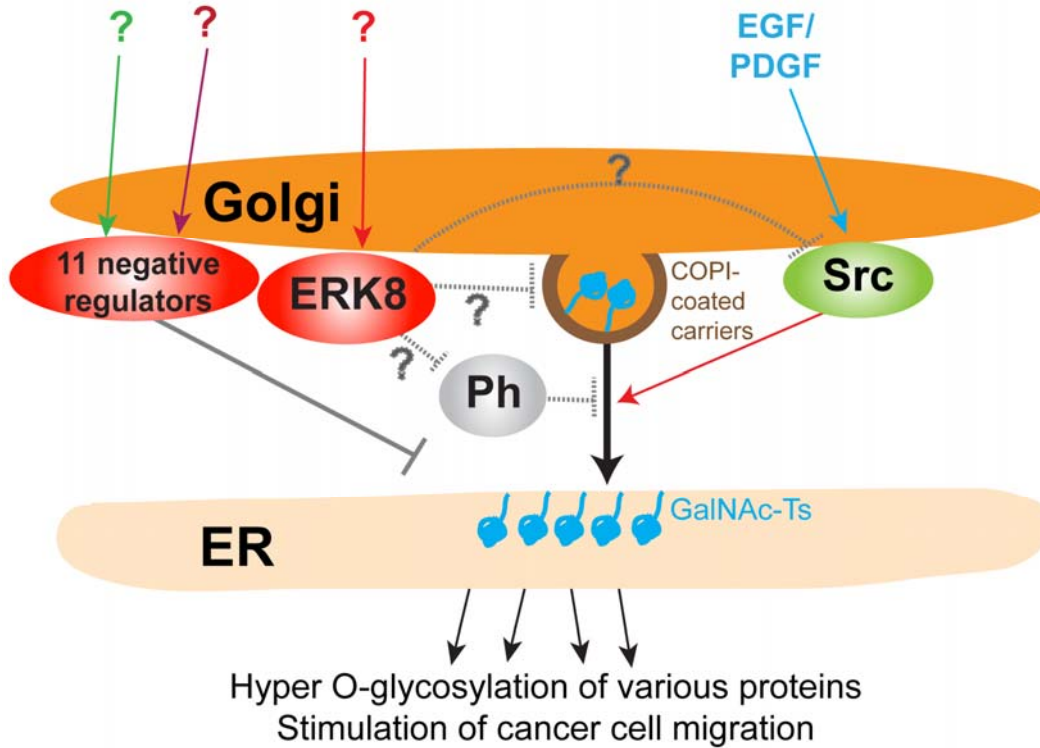
In breast and lung cancer cells, this set-point appears constitutively high, as the relocation of GalNAc-Ts is extensive and frequent. The promotion of cell motility associated with ER-localized O-glycosylation appeared to favour the formation of lung metastases in a tail-vein injection-based assay [194]. Thus, how GalNAc-T relocation is stimulated in cancer cells probably has important medical implications.

My analyses suggest that multiple mechanisms are possible, including a decrease in ERK8 protein levels. However, the actual level of decrease required to stimulate relocation is not known and is anyway probably dependent on other cellular parameters. Additionally, Tn levels are not likely to depend only on the intracellular distribution of GalNAc-Ts. For instance, normal tissues with high levels of mucin expression, such as stomach, colon or kidney, tend to have higher endogenous Tn levels without clear evidence for relocation. This complexity probably contributes to the lack of direct correlation between ERK8 and Tn levels.

In addition to promoting O-glycosylation, ERK8 depletion could also have other beneficial advantages for cancer cells. Indeed, ERK8 has been implicated in multiple, apparently unrelated, molecular processes, such as maintenance of genomic integrity [505], regulation of telomerase activity [506], autophagy [507] and inhibition of nuclear receptor activity [486, 508, 509]. Recently, the *Drosophila* homolog ERK7 and human ERK8 were also shown to participate in the regulation of protein secretion during starvation through disassembly of ER

exit sites [413]. Whether these different processes are somewhat linked through ERK8 or whether ERK8 is simply moonlighting in different, independent functions constitute an interesting challenge for the future.

In sum, my results suggest that initiation of O-glycosylation in the ER is under an elaborate regulatory control system of which ERK8 is a key player. This regulation sets the level of cellular motility and is frequently perturbed in cancer cells of breast and lung origins.



**Figure 4-22: A model illustrating signaling regulation of O-glycosylation initiation at the Golgi that influences cellular motility and cancer invasiveness.** Golgi to ER relocation of GalNAc-T is dependent on tyrosine phosphorylation of a pool of Golgi proteins. ERK8 could regulate tyrosine phosphorylation in three potential scenarios: inhibiting activation of SFKs/tyrosine kinases, activating an unidentified phosphotyrosine phosphatase or inhibiting the activity of tyrosine phosphorylated Golgi protein(s) involve in GalNAc-T traffic. Src represents multiple SFKs and non-SFK tyrosine kinase. Ph represents a potential phosphotyrosine phosphatase that acts downstream of ERK8. Src

## **CHAPTER FIVE: CONCLUSIONS AND FUTURE DIRECTIONS**



## **5.1 RNAI SCREENING REVEALS A LARGE SIGNALING NETWORK CONTROLLING THE GOLGI APPARATUS IN HUMAN CELLS**

### **5.1.1 Main conclusions**

To investigate the mechanisms that regulate Golgi architecture, I utilised RNAi screening coupled with high-throughput imaging and quantitative image analysis to identify its molecular regulators in an unbiased fashion. Golgi organization was probed with three markers specific for different Golgi compartments to assess cisternal specific effects. A pilot screen on membrane traffic regulators revealed three visually observable Golgi morphologies in human cells. Based on these reference Golgi phenotypes, a support vector machine was successfully developed to automatically classify and quantify the three different Golgi morphologies. The screen on 948 kinases and phosphatases uncovered 159 signalling genes, which constitutes nearly 20% of genes assayed. The signalling gene depletions induced strong and varied Golgi morphological perturbations that were comparable, if not stronger, than that of the membrane trafficking regulators. Using bioinformatics data, a large regulatory network on Golgi morphology could be constructed. Specific sub-networks involving phosphoinositides regulation, acto-myosin dynamics, and MAPK signalling provided further understanding to Golgi regulatory mechanisms. Depletions of most Golgi organization regulators also affected Golgi functions of secretion and glycan biosynthesis, suggesting that signalling cascades can control these processes directly at the Golgi level. Collectively, our data provides a genetic overview of the signalling pathways that control the Golgi physiology in human cells.

### **5.1.2 Future directions: towards better Golgi morphological classification**

Our RNAi screen identified numerous signalling proteins, both known and novel, regulating Golgi organization and its secretory and glycosylation functions. The data was further supported by our bioinformatics study which found an

unexpectedly large number of phosphoproteins associated with the Golgi whereby many interact with the identified hits, suggesting the direct impact of the signalling proteins on the Golgi. However, for most of these signalling regulators, what regulates them, as well as how and when they are activated are still not completely known. It is not known if the connections in the large regulatory network that we derived are direct phosphorylation events, given that the direct substrates of these signalling proteins are mostly not clear. Furthermore, the precise functional and physiological meaning of this signalling regulation to the cell and organism are not well-understood.

The functions are only beginning to be elucidated for a few of them. For instance, ERK phosphorylates GRASP65 to remodel and re-orientate the Golgi towards the leading edge for cell migration [116] and MEK1 and several signalling proteins phosphorylate GRASP65 to unlink the Golgi ribbon for mitosis which also serves as a mitotic checkpoint [124, 125, 510, 511]. Our secondary screens demonstrated that most of our hits also strongly affected Golgi functions, particularly glycan synthesis. The functional implications of most of this glycan regulation are not known, apart from the regulation of cell adhesion and motility by O-glycans as shown in Chapter 4. Given the vast number of glycosylated proteins in the proteome (more than 50% of the proteome), it suggests the critical importance of glycans to cell and organism physiology and hence, understanding the regulation of glycan biosynthesis is essential. Based on our data, it can be speculated that the downstream functions of the identified signaling regulators could also be executed from changes in glycan expression. For example, the ERK-regulated remodelling of the Golgi during cell migration [116] could also lead to changes in glycan structures of adhesive and migratory factors transported to the cell leading edge.

Thus, future efforts should be placed on elucidating the mechanistic basis and physiological relevance of Golgi organisation and glycan regulation by the identified signalling regulators. This will advance our understanding on the long-standing questions of how the Golgi maintains and changes its structure under

different conditions. It will also aid comprehension on the role of this organelle in various cellular processes and ultimately, its importance in organism physiology and pathology. In recent years, various human diseases are increasingly linked to the Golgi and its associated proteins, suggesting its critical role in organism homeostasis [308]. For instance, mutations and loss of the vesicle tethering COG complex leads to defects in Golgi organization and glycosylation and result in genetic diseases known as the congenital disorders of glycosylation (CDG) [301]. Loss of ubiquitin-protein ligase UBE3A results in altered Golgi morphology and protein sialylation, causing the neurodisorder known as Angelman syndrome [512]. However, the molecular origins of most disease etiology remain to be established. Hence, the study of the molecular basis of Golgi regulation provides more complete knowledge of the disease-causing mechanisms and ultimately, aid in the development of appropriate therapies.

The study of Golgi regulatory mechanisms can be initiated by more in-depth classification of Golgi morphologies. Although the current screen methodology is efficient in identifying and distinguishing between the three visually observable Golgi perturbations, the approach is constrained by the limits of human vision. There are actually different shades of perturbations within each phenotypic category and they may arise from very different underlying mechanisms. For instance, a fragmented Golgi may or may not involve the loss of perinuclear positioning of the Golgi mini-stacks. The latter could arise from loss of lateral linking of the Golgi ribbon and the former from perturbations of the microtubule cytoskeleton. Therefore, by establishing a more refined classification of Golgi phenotypes from our hit gene depletions, it would further distinguish gene depletions with similar phenotypes which are most likely acting in common pathways and functions. This can be executed through computer-based classification and clustering algorithms that are independent of human vision [513]. The refined Golgi classification method would greatly improve the detection, classification and deciphering of genetic networks in Golgi regulation. Subsequent expansion to a genome-wide screen could also reveal putative Golgi

targets of the signalling proteins. Signalling proteins that give similar phenotypes to known Golgi proteins could represent potential signalling cascades. This could generate hypotheses and verified by experimental testing to uncover novel regulatory mechanisms on the Golgi

## **5.2 ERK8 IS A NEGATIVE REGULATOR OF O-GALNAC GLYCOSYLATION AND CELL MIGRATION**

### **5.2.1 Main conclusions**

The Tn antigen is an O-GalNAc glycan that is frequently up-regulated in tumors and its expression correlates with metastasis and poor prognosis. Tn is generated during O-glycosylation initiation of secreted and cell surface proteins. Our group has previously reported that O-glycosylation initiation can be up-regulated by the redistribution of GalNAc-Ts to the ER. The process markedly increases cell motility and was found to be activated in more than 60% of human breast carcinomas. To better understand the mechanistic basis of Tn expression in cancer, I screened 948 signaling and related genes using RNAi and imaging that revealed 12 negative regulators of Tn expression. All 12 regulators do not appear to regulate Tn levels through inhibition of O-GalNAc elongation but through the subcellular localisation of the GalNAc-Ts. Based on their genetic interaction and cellular localisation profiles, most of them act at the Golgi level and constitute a regulatory network controlling GalNAc-T subcellular localisation. Among the most potent regulators was atypical MAP kinase ERK8 whose depletion induced dramatic increases in Tn levels. ERK8 partially localise at the Golgi where its constitutive kinase activity is required to inhibit COPI-dependent GalNAc-T trafficking to the ER. Drug inhibition with Ro-31-8220 induced rapid and reversible increases in Tn levels, further demonstrating the directness of ERK8 on the process. ERK8 spatially inhibits tyrosine phosphorylation at the Golgi that controls GalNAc-T traffic. Growth factor stimulation spontaneously perturbs the Golgi fraction of ERK8, thus presenting a dynamic mechanism for the system to

control GalNAc-T trafficking according to extracellular signals. Regulation of ERK8 on O-GalNAc glycosylation, in turn, inhibits cell motility. In human breast and lung carcinomas, ERK8 expression is frequently downregulated while O-glycosylation initiation is hyperactivated. In sum, my results demonstrate a novel role of ERK8 as a constitutive brake on GalNAc-T relocation and loss of its expression could drive cancer aggressivity through increased cell motility.

### **5.2.2 Future directions: more in-depth studies of the regulatory mechanisms of GalNAc-T localisation**

The focused study on the regulation of Tn expression revealed negative regulators that all control GalNAc-T subcellular localisation. Bioinformatics analysis indicate that they are likely to act at the level of the Golgi and form a potential regulatory network controlling GalNAc-T trafficking. Further experiments will be required to confirm this network and its connectivity. In-depth characterization of how each of the Tn regulators and their associated pathways regulate GalNAc-T trafficking would gain further insights to the mechanisms of signaling control on the process. In addition, determining the physiological changes *in vivo* upon loss/mutations of these proteins will enrich our understanding of mechanisms involved in the progression of Tn-related cancers. Extensions of these studies can lead to potential therapeutic opportunities.

Among the Tn regulators, my findings highlighted that ERK8 is an important node with implications in cancer metastasis. Future efforts should be placed on identifying the molecular mechanism of how ERK8 inhibit GalNAc-T relocation. Investigations on how and what modulates ERK8 at the Golgi will further enrich our understanding on how the system coordinates this brake on GalNAc-T relocation. This could be first addressed by identifying ERK8 interactors and substrates which could be approached by proteomic techniques such as SILAC/mass spectrometry [514] or genetically engineered kinase mutants that utilize ATP analogs [515]. The list can be filtered using bioinformatics analyses

for Golgi-associated proteins which could constitute the potential upstream regulators and substrates involved in GalNAc-T trafficking. Subsequent molecular and biochemical validations will be required to confirm the protein-protein relationships.

The mechanisms involved in the specific targeting GalNAc-T into COPI carriers to the ER also require further study. Like most glycosyltransferases, GalNAc-Ts are type II integral membrane proteins with a short cytoplasmic tail, transmembrane domain and luminal stem, catalytic and lectin domain [241]. Localisation signals of most glycosyltransferases mainly reside in the N-terminal cytoplasmic tail, transmembrane and stem regions [516-519]. Mechanisms that influence the localisation of Golgi glycosyltransferases include direct or indirect links through adaptor proteins with the COPI coat [213, 520]. While the mechanisms are well-studied in several glycosyltransferases, it is not elucidated for GalNAc-Ts. Hence, future efforts should be placed on how GalNAc-Ts maintain their Golgi localisation and targeting into COPI carriers. This can be addressed by generating substitution and/or chimeric mutants of GalNAc-T to determine the essential COPI targeting domains. Immunoprecipitation studies with COPI components would verify if they directly interact with the coatomer. These experiments should be performed in cells when the ER relocation pathway is activated, such as an ERK8-depleted cell line. Identification of the players that target GalNAc-Ts to COPI carriers will also aid in the mechanistic study which could be addressed by an RNAi screen for genes that promote GalNAc-T trafficking to the ER, for instance, by co-RNAi screening with ERK8 depletion for genes that rescue high Tn levels.

### 5.3 THE GOLGI: A HIGHLY REGULATED SORTING AND PROCESSING MACHINE

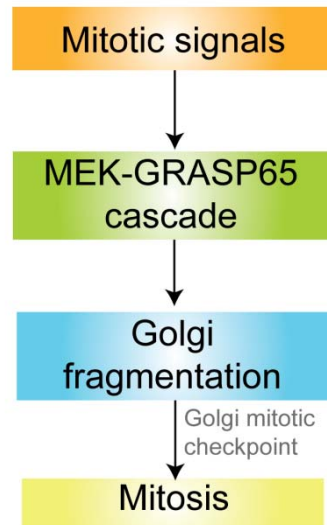
Central in the secretory pathway, the Golgi is a dynamic organelle that constantly exchanges proteins and lipids with other organelles and cell surface. This together with its role as the primary protein and lipid processing station in the cell indicate that its structure and functions must be correctly coordinated and tightly controlled under different physiological contexts for cellular growth, survival, communication and homeostasis. Dysregulation of these processes can initiate pathological conditions.

In recent years, various signaling components that are involved in key cellular processes are increasingly discovered to reside at the Golgi and regulate its functional organization according to intracellular and extracellular cues [127-129]. The Golgi was found to be highly responsive to endogenous and exogenous stimuli and its functional organization is deeply integrated to various signaling events in order to accommodate cellular requirements and modulate homeostasis.

#### *Mitosis regulates Golgi and Golgi regulates mitosis*

Perhaps the best studied to date is its critical involvement in mitosis. During mitosis, the Golgi ribbon progressively fragments into dispersed elements to allow correct partitioning into the two daughter cells. Several signaling players including CDK1, RAF/MEK1/ERK1c, Plk1 and Plk3 [130-135] have been found to be involved and they phosphorylate Golgi proteins including GRASPs and golgins to mediate Golgi fragmentation. Unexpectedly, Golgi fragmentation at the G2 phase is also required for mitotic entry, suggesting the existence of a novel 'Golgi mitotic checkpoint' that links the state of Golgi disassembly to mitotic progression (Figure 5-1). Failure of Golgi fragmentation would arrest the cell cycle at the G2 stage [124, 125, 325]. The exact mechanisms of this checkpoint

remain elusive currently but it suggests that the Golgi at G2 phase might initiate signaling cascades to regulate mitotic entry.



**Figure 5-1. Schematic of the involvement of the Golgi apparatus in mitosis.** Stimulus for mitosis (*orange box represents stimulus*) promotes intracellular signaling pathways (e.g. phosphorylation of GRASP65 by MEK) (*green box represents signaling event*) which lead to Golgi structural remodeling and subsequent breakdown (*blue box represents effects on the Golgi*). Golgi fragmentation at G2 phase also serves as a mitotic checkpoint. Upon Golgi fragmentation, mitosis results (*yellow box represents cellular process*).

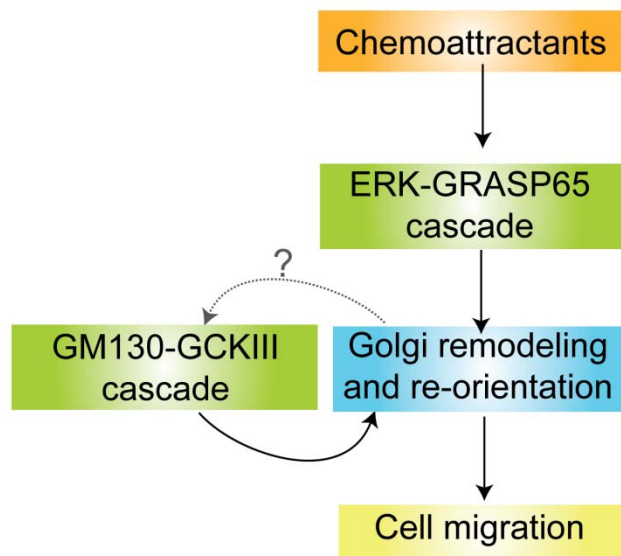
#### *Golgi re-orientation and cell migration*

Another well-established example revolves around directional cell migration in response to chemoattractants. The process requires reorientation and structural remodeling of the Golgi to the leading edge of the migrating cell [121] so as to establish cell polarity and ensure delivery of new membrane and secretory cargo to the leading cell periphery. Mechanisms for Golgi remodeling and orientation are starting to be elucidated whereby ERK phosphorylation of GRASP65 at serine residue 277 have been shown to be crucial (Figure 5-2) [116]. The mechanisms



involved in the downstream events in cell polarity and specific trafficking to the leading edge of the cell are still unknown, but the current knowledge implies that these events could also depend on signaling-based regulation.

The Golgi also generates signaling for its own reorientation during cell migration. Binding of germinal-centre kinases III (GCKIII), MST4 and YSK1, to GM130 recruits them to the Golgi and leads to their activation. This, in turn, phosphorylates 14-3-3 $\zeta$  that might recruit the Par complex for cell polarity and migration (Figure 5-2) [117, 148, 326]. This could represent an additional regulatory mechanism to the ERK-GRASP65 signaling to ensure alignment of the Golgi to the leading edge for cell migration.

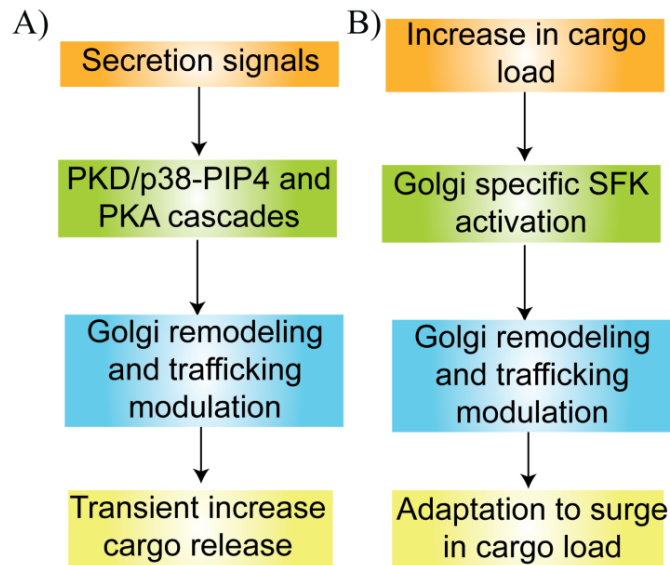


**Figure 5-2: Schematic of the involvement of the Golgi apparatus in cell migration.** Cell migration stimulus by chemoattractants activates intracellular signaling pathways involving ERK phosphorylation on GRASP65. GRASP65 phosphorylation leads to Golgi remodeling and re-orientation to the leading edge of the migrating cell. Recruitment and binding of GM130 activates GCKIII kinases which participate in establishing Golgi polarity and re-enforces the leading edge alignment of the Golgi for cell migration.

### *Regulation of cargo flow and regulation of Golgi by cargo*

Signaling regulation is also important for controlling general secretion at the Golgi level. Golgi PIP4 regulation by protein kinase D (PKD) and p38 MAPK [138-141] and protein kinase A (PKA) activation [142, 143] were found to remodel the Golgi structure and facilitate cargo flux from the TGN (Figure 5-3A). Although the physiological stimuli of these signaling events are still unknown, they highlight the involvement of signaling cascades in Golgi functional regulation.

One of the most interesting instances of regulation of cargo flow is the initiation of signaling by the Golgi to modulate its functional organization. This is highlighted by the local activation of the SFKs by the Golgi in response to variable cargo load (Figure 5-3B) [145]. This local SFK activation is mediated by KDEL receptor binding to the incoming luminal chaperones which enter the Golgi with the cargo wave [145]. SFK activation promotes secretion and facilitates intra-Golgi trafficking, likely through Golgi organisation remodeling. The functional significance of this regulatory mechanism is proposed to maintain Golgi homeostasis so as to prevent functional and structural disruption and dynamically adapt to the amount of cargo that needs to be processed and trafficked.



**Figure 5-3: Schematic of the regulatory mechanisms of secretion at the Golgi.** (A) Stimuli for secretion such as activation of G-protein coupled receptor (GPCR) promote signaling pathways involving PKD, p38 MAPK and PKA which remodel the Golgi and supports post-Golgi trafficking to increase cargo secretion. (B) In contrast, increased cargo wave from the ER activates SFKs at the Golgi which regulates intra-Golgi trafficking and promotes secretion.

#### *Regulation of Golgi glycosylation*

These various examples imply that the complex structure and functions of the Golgi are under the control of multiple signaling regulations. Current studies mainly examine the effects of one or a few genes but this could only provide partial information on the complex regulation of the Golgi given the highly integrated and dynamic nature of the mammalian Golgi. Moreover, different studies vary in experimental setups and biological models used. These shortcomings highlighted the importance of studying Golgi regulation in a more coordinated and large-scale fashion and this can be resolved by RNAi screening. Pioneering RNAi screens have been used to study various aspects of secretory pathway regulation such as endocytosis [521, 522], secretion [523, 524] and ER-Golgi trafficking [392]. To date, a comprehensive study on Golgi morphological

regulation has not been attempted. In this study, shown in Chapter 3, I reported the utilization of RNAi screening to uncover signaling genes involved in Golgi regulation in an unbiased fashion.

The screen results demonstrate significant importance of signaling cascades on Golgi organisation regulation with a relatively large proportion (20%) of signaling proteins involved. In addition to identifying several known regulators of Golgi organisation that validated our approach, the screen also yielded multiple novel Golgi regulators which deserve further characterization for their roles at the Golgi in the future. The morphological diversity and the extensive morphological perturbations from the various gene knockdowns imply that multiple regulatory mechanisms are involved. This supported by the unexpectedly high proportion of Golgi associated phosphoproteins (413 out of 854) and many interact with the signaling hits, forming a large interconnected regulatory network. However, at the moment, it remains unknown if the signaling protein-Golgi phosphoprotein interaction represents a direct phosphorylation event as the network is built on protein-protein interaction information. How this network is regulated, what it regulates and its physiological functions in the cell and organism also remain mostly unknown, although it has been uncovered for some of the subnetworks that I found i.e. PIP4, actomyosin and MAPK subnetworks. Future studies will be required to further understand the exact regulatory mechanisms involved and their functional implications. Nevertheless, the data obtained from this screen study present a global overview of the genetic regulation of signaling regulation on the intricate morphology of the mammalian Golgi and hence, provided a rich dataset to further explore this question.

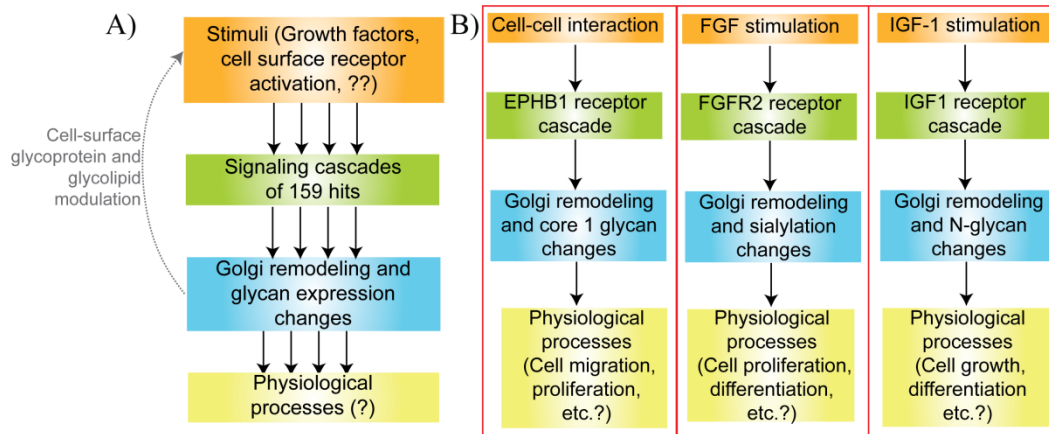
On top of the previous examples of functional regulation by signaling cascades, our findings propose an additional instance of regulation, which is the regulation of Golgi cargo glycosylation, and perhaps also encompassing general cargo processing events. We show that a large proportion of signaling proteins affect glycan synthesis strongly and variably, indicating that there might be many

different glycosylation pathways that are being regulated, presumably by different signaling pathways. The massive co-occurrence of glycan and Golgi morphological changes implies that the glycosylation perturbations occur through Golgi organisational modifications (Figure 5-4A). Overall, it suggests an exquisite regulation by the different signaling pathways impacting on the Golgi that finely modulates its organization, under different physiological contexts, to generate the diversity of glycans patterns expressed.

Each of these glycan patterns has a unique and specific role in mediating cellular processes. For instance, the ephrin receptors (e.g. EPHB1) are activated by membrane-associated ligands expressed on neighboring cells [525] and cell-cell contact promotes ephrin signaling. As reflected by our screen results that EPHB1 depletion perturbs the Golgi and dramatically influences the expression of the truncated Core 1 O-glycan, it indicates that ephrin signaling would regulate Golgi structure and O-glycan expression. These effects on glycan synthesis could, in turn, control various biological processes downstream of ephrin signaling (Figure 5-4B). Similarly, growth factor stimulation of the FGF and IGF receptors remodel the Golgi and affects glycosylation which could ultimately, influence the plethora of physiological processes that are regulated by these receptors [526-528]. Supporting this, our data show that FGF and IGF-1 stimulation affect Golgi structure within a short duration, indicating that these signaling pathways can rapidly regulate Golgi organization and functions (Figure 5-4B). Furthermore, the changes in Golgi organization could affect glycan expression patterns on these cell surface receptors and in turn, further impact on signaling cascades and cellular physiology.

As opposed to gene expression changes of the glycosylation machinery, Golgi remodeling would provide a faster mechanism to modulate glycan changes for example during stem cell differentiation [430]. Glycan changes could also occur to aid progression of spontaneous cellular events such as cell migration [116] and mitosis [319]. For instance, modulation of glycans on the glycoproteins and

glycolipids that are transported to the leading edge of the cell during cell migration could rapidly mediate cell-matrix adhesion and cell-cell communication. Indeed, cell adhesive and migratory factors, such as integrins [529] and cadherins [530], are known to be heavily glycosylated proteins and the glycans expressed modulate their conformation and activities.

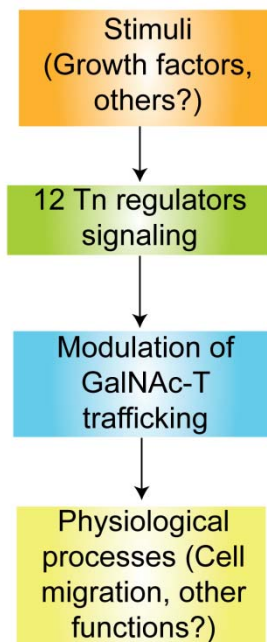


**Figure 5-4: Schematics of Golgi organization and glycosylation regulation.** (A) Multiple signaling cascades involving the identified 159 Golgi organization regulators are activated by different stimuli. These different signaling pathways regulate the Golgi organization and affect different glycosylation pathway. This generates a diversity of glycan expressed and each having a unique, distinct role in mediating various physiological processes. (B) Examples of regulation of Golgi organization and glycosylation by our hits EPHB1, FGFR2 and IGF1R.

#### *Signaling regulation of O-glycosylation initiation*

Signaling mechanisms can affect the Golgi glycosylation in multiple ways, such as modulating the luminal pH, as well as network and cisternal distribution of glycosylation enzymes. The latter mechanism is exemplified by the findings of a subset of signaling genes that specifically control the cisternal localisation of O-glycosylation enzymes GalNAc-Ts, and not mannosidase II. This was examined in further detail in Chapter 4. Relocation of GalNAc-Ts from the Golgi to the ER

was previously shown to be rapidly induced by growth factor stimulation and Src activation [193]. Redistribution to the ER increases O-GalNAc glycosylation on multiple glycoproteins, leading to an increased expression of the Tn antigen, a tumor-associated glycan structure. Tn expression increases cell motility and invasiveness of cancer cells and ER O-glycosylation occurs in at least 60% of breast carcinomas [194]. My screen identified the molecular players that negatively regulate this glycosylation pathway (Figure 5-5). Most of them were found to act at the Golgi level, thus validating the dataset. It suggests that many signals from various origins impinge at the Golgi to regulate GalNAc-T traffic. The precise mechanisms for each of these regulators would require further study to gain insights to the progression of Tn-related cancers and aid future development of therapies.



**Figure 5-5: Schematic of the regulation of O-glycosylation initiation.** Various stimuli impact on multiple signaling cascades involving the 12 Tn regulators which control GalNAc-T trafficking at the Golgi. This, in turn, modulates different cellular processes including cell adhesion and migration that I have identified.

### *Regulation of ER O-glycosylation initiation by ERK8*

I have examined the atypical MAPK ERK8 in greater detail. ERK8 was previously found to interact with Src through its SH3 domains [444], suggesting that it could act in Src regulated pathways. Inhibition of ERK8 resulted in rapid increases in O-glycosylation of multiple proteins, suggesting that the kinase acts relatively directly on the pathway. This was reconciled by the fact that ERK8 partially localizes at the Golgi, further indicating that it inhibits trafficking at the Golgi (Golgi-to-ER retrograde trafficking) and not at the ER (blocking anterograde trafficking to the Golgi). The notion was further substantiated by the acute increases in COPI transport carriers containing GalNAc-Ts upon ERK8 inhibition. How ERK8 selectively inhibits the GalNAc-T COPI trafficking to the ER is an interesting aspect to pursue in the future and this can be addressed by identifying its Golgi substrates.

Unlike the classical MAPKs that require multiple tiers of activation, ERK8 is a constitutively active kinase by autophosphorylation. Rescue experiments with an inactive ERK8 mutant demonstrated that the inhibition of GalNAc-T trafficking is a kinase activity-dependent event. It indicates that ERK8 phosphorylation on an unknown Golgi substrate(s) provides a constant “brake” to this trafficking pathway in normal resting cells. In line with this, ERK8 activity is reduced in at least two breast cancer cell lines: MCF-7 and T47D [505] which we have also found upregulated ER O-glycosylation [194]. This further substantiates that ERK8 kinase activity required to inhibit this pathway.

Surprisingly, the ERK8 “brake” is dynamically regulated and is released in times when GalNAc-Ts are induced to relocate as observed by the loss of Golgi localisation upon growth factor stimulation. Indeed, it makes sense to spatially regulate ERK8 given its constitutive kinase activity. Supporting this, the classical MAPKs are also dynamically localised to different subcellular locations upon stimulation where they act on different substrates [497]. This could also be the



case for ERK8. Hence, the underlying mechanisms involved in regulating ERK8 localisation at the Golgi and its activity when it is relocated should be established in the future to gain further insights on ERK8's functions in the cell. Taken together, these results suggest that the ER O-glycosylation pathway is under constant, yet dynamic, repression by a constitutively active kinase.

This model presents an interesting alternative mechanism to our current knowledge of signaling cascades. Signal transduction pathways are typically conceived to be “switch on” by upstream molecule activating a downstream effector or by inactivating an inhibitory molecule through phosphorylation events. The former being the central dogma of signal transduction pathways, is commonly occurring as in the classical MAPK pathway [531], PI3K-Akt [532] pathway, and many others. On the other hand, the latter can be observed in the NFkB pathway where NFkB is constantly sequestered and inhibited in the cytoplasm by the Ikb proteins. Phosphorylation of Ikb proteins by the IKK complex releases NFkB into the nucleus for transcriptional activation, thus activating the pathway [533]. Our findings, hence, presents a novel alternative regulatory mechanism of a signaling event. Finally, our findings have increased the current knowledge on the poorly characterized functions of ERK8.

#### **5.4 FINAL REMARKS**

Protein glycosylation is an essential post-translational modification process for numerous different proteins in the cell. The process has profound effects on protein functions and controls numerous biological processes, and ultimately cell and organism physiology. Most glycosylation reactions occur at the Golgi apparatus and depend on its intricate and compartmentalized organization for proper glycan synthesis. In recent years, the complex Golgi organization was found to be controlled by an increasing number of signaling proteins. For a few of them, their effects on Golgi functions and implications in cell physiology are only beginning to be elucidated. The regulation of glycosylation at the Golgi and how

it relates to health and disease have not been well-studied. Therefore, the findings reported in this dissertation had contributed to further understanding to this complex field of the regulation of Golgi organization and glycosylation by signaling cascades.

## BIBLIOGRAPHY

1. Lopez-Garcia P, M.D. (1999). "Metabolic symbiosis at the origin of eukaryotes." *Trends in biochemical sciences* 24(3): 88-93.
2. Kirschner M, G.J. (1998). "Evolvability." *Proceedings of the National Academy of Sciences of the United States of America* 95(15): 8420-8427.
3. Warren, G. (1990). "Intracellular transport. Vesicular consumption." *Nature* 345(6274): 382-383.
4. Pryer, N.K., L.J. Wuestehube, et al. (1992). "Vesicle-mediated protein sorting." *Annual Review of Biochemistry* 61: 471-516.
5. Golgi, C. (1898). "Sur la structure des cellules nerveuses des ganglions spinaux." *Arch Ital Biologie* 30: 278-286.
6. Klumperman, J. (2011). "Architecture of the Mammalian Golgi." *Cold Spring Harbor perspectives in biology* 3(7): a005181-a005181.
7. Gillin, F.D., D.S. Reiner, et al. (1996). "Cell biology of the primitive eukaryote *Giardia lamblia*." *Annual review of microbiology* 50: 679-705.
8. Preuss, D., J. Mulholland, et al. (1992). "Characterization of the *Saccharomyces* Golgi complex through the cell cycle by immunoelectron microscopy." *Mol Biol Cell* 3(7): 789-803.
9. Rambourg, A., C.L. Jackson, et al. (2001). "Three dimensional configuration of the secretory pathway and segregation of secretion granules in the yeast *Saccharomyces cerevisiae*." *J Cell Sci* 114(Pt 12): 2231-2239.
10. Pelletier, L., C.A. Stern, et al. (2002). "Golgi biogenesis in *Toxoplasma gondii*." *Nature* 418(6897): 548-552.
11. Rabouille, C., T. Misteli, et al. (1995). "Reassembly of Golgi stacks from mitotic Golgi fragments in a cell-free system." *The Journal of Cell Biology* 129(3): 605-618.
12. Ladinsky, M.S., D.N. Mastronarde, et al. (1999). "Golgi structure in three dimensions: functional insights from the normal rat kidney cell." *The Journal of Cell Biology* 144(6): 1135-1149.
13. Glick, B.S. and A. Nakano (2009). "Membrane traffic within the Golgi apparatus." *Annual review of cell and developmental biology* 25: 113-132.
14. Rambourg A, C.Y. (1997). "Three-dimensional structure of the Golgi apparatus in mammalian cells." In *The Golgi Apparatus* (ed. E.G. Berger, J. Roth) Birkhauser Verlag, Basel.: 37-61.
15. Mollenhauer, H.H. (1974). "Distribution of microtubules in the golgi apparatus of *Euglena gracilis*." *Journal of Cell Science* 15(1): 89-97.
16. Rambourg, A. and Y. Clermont (1990). "Three-dimensional electron microscopy: structure of the Golgi apparatus." *Eur J Cell Biol* 51(2): 189-200.
17. Glick, B.S. and A. Luini (2011). "Models for Golgi Traffic: A Critical Assessment." *Cold Spring Harbor perspectives in biology* 3(11): a005215-a005215.
18. Goldfischer, S., E. Essner, et al. (1964). "The Localization of Phosphatase Activities at the Level of Ultrastructure." *The journal of histochemistry and cytochemistry : official journal of the Histochemistry Society* 12: 72-95.
19. Novikoff, P.M., A.B. Novikoff, et al. (1971). "Golgi apparatus, GERL, and lysosomes of neurons in rat dorsal root ganglia, studied by thick section and thin section cytochemistry." *The Journal of Cell Biology* 50(3): 859-886.
20. Grove, S.N., C.E. Bracker, et al. (1968). "Cytomembrane differentiation in the endoplasmic reticulum-Golgi apparatus-vesicle complex." *Science* 161(3837): 171-173.

21. Sprong, H., P. van der Sluijs, et al. (2001). "How proteins move lipids and lipids move proteins." *Nat Rev Mol Cell Biol* 2(7): 504-513.
22. Orci, L., R. Montesano, et al. (1981). "Heterogeneous distribution of filipin--cholesterol complexes across the cisternae of the Golgi apparatus." *Proceedings of the National Academy of Sciences of the United States of America* 78(1): 293-297.
23. Cluett, E.B., E. Kuismanen, et al. (1997). "Heterogeneous distribution of the unusual phospholipid semilyso-bisphosphatidic acid through the Golgi complex." *Molecular Biology of the Cell* 8(11): 2233-2240.
24. Mobius, W., E. van Donselaar, et al. (2003). "Recycling compartments and the internal vesicles of multivesicular bodies harbor most of the cholesterol found in the endocytic pathway." *Traffic* 4(4): 222-231.
25. Banfield, D.K. (2011). "Mechanisms of Protein Retention in the Golgi." *Cold Spring Harbor perspectives in biology* 3(8): a005264-a005264.
26. Paroutis, P., N. Touret, et al. (2004). "The pH of the secretory pathway: measurement, determinants, and regulation." *Physiology (Bethesda)* 19: 207-215.
27. Carnell, L. and H.P. Moore (1994). "Transport via the regulated secretory pathway in semi-intact PC12 cells: role of intra-cisternal calcium and pH in the transport and sorting of secretogranin II." *The Journal of Cell Biology* 127(3): 693-705.
28. Chanat, E. and W.B. Huttner (1991). "Milieu-induced, selective aggregation of regulated secretory proteins in the trans-Golgi network." *The Journal of Cell Biology* 115(6): 1505-1519.
29. Chapman, R.E. and S. Munro (1994). "Retrieval of TGN proteins from the cell surface requires endosomal acidification." *The EMBO journal* 13(10): 2305-2312.
30. Dunphy, W.G., E. Fries, et al. (1981). "Early and late functions associated with the Golgi apparatus reside in distinct compartments." *Proc Natl Acad Sci U S A* 78(12): 7453-7457.
31. Farquhar, M.G. and H.P. Hauri (1997). *Protein sorting and vesicular traffic in the Golgi apparatus*. Birkhauser, Basel, Switzerland.
32. Wang, Y., J.-H. Wei, et al. (2008). "Golgi cisternal unstacking stimulates COPI vesicle budding and protein transport." *PloS one* 3(2): e1647.
33. Mowbray K, D.J. (2009). "Evolution and diversity of the Golgi body." *FEBS Letters* 583(23): 3738-3745.
34. Lees, J.A., C.K. Yip, et al. (2010). "Molecular organization of the COG vesicle tethering complex." *Nature structural & molecular biology* 17(11): 1292-1297.
35. Marsh, B.J., N. Volkmann, et al. (2004). "Direct continuities between cisternae at different levels of the Golgi complex in glucose-stimulated mouse islet beta cells." *Proceedings of the National Academy of Sciences of the United States of America* 101(15): 5565-5570.
36. Trucco, A., R.S. Polishchuk, et al. (2004). "Secretory traffic triggers the formation of tubular continuities across Golgi sub-compartments." *NATURE CELL BIOLOGY* 6(11): 1071-1081.
37. Boevink, P., K. Oparka, et al. (1998). "Stacks on tracks: the plant Golgi apparatus traffics on an actin/ER network." *The Plant journal : for cell and molecular biology* 15(3): 441-447.
38. Nebenfuhr, A., L.A. Gallagher, et al. (1999). "Stop-and-go movements of plant Golgi stacks are mediated by the acto-myosin system." *Plant physiology* 121(4): 1127-1142.
39. Kondylis, V. and C. Rabouille (2009). "The Golgi apparatus: lessons from *Drosophila*." *FEBS Lett* 583(23): 3827-3838.

40. Brigrance, W.T., C. Barlowe, et al. (2000). "Organization of the yeast Golgi complex into at least four functionally distinct compartments." *Molecular Biology of the Cell* 11(1): 171-182.
41. Dacks, J.B., L.A. Davis, et al. (2003). "Evidence for Golgi bodies in proposed 'Golgi-lacking' lineages." *Proceedings. Biological sciences / The Royal Society* 270 Suppl 2: S168-171.
42. Mollenhauer, H.H. (1965). "An Intercisternal Structure in the Golgi Apparatus." *J Cell Biol* 24(3): 504-511.
43. Franke, W.W., J. Kartenbeck, et al. (1972). "Inter- and intracisternal elements of the Golgi apparatus. A system of membrane-to-membrane cross-links." *Z Zellforsch Mikrosk Anat* 132(3): 365-380.
44. Cluett, E.B. and W.J. Brown (1992). "Adhesion of Golgi cisternae by proteinaceous interactions: intercisternal bridges as putative adhesive structures." *J Cell Sci* 103 ( Pt 3): 773-784.
45. Slusarewicz, P., T. Nilsson, et al. (1994). "Isolation of a matrix that binds medial Golgi enzymes." *J Cell Biol* 124(4): 405-413.
46. Xiang, Y. and Y. Wang (2011). "New components of the Golgi matrix." *Cell Tissue Res* 344(3): 365-379.
47. Barr, F.A., M. Puype, et al. (1997). "GRASP65, a protein involved in the stacking of Golgi cisternae." *Cell* 91(2): 253-262.
48. Shorter, J., R. Watson, et al. (1999). "GRASP55, a second mammalian GRASP protein involved in the stacking of Golgi cisternae in a cell-free system." *EMBO J* 18(18): 4949-4960.
49. Sutterlin, C., R. Polishchuk, et al. (2005). "The Golgi-associated protein GRASP65 regulates spindle dynamics and is essential for cell division." *Mol Biol Cell* 16(7): 3211-3222.
50. Puthenveedu, M.A., C. Bachert, et al. (2006). "GM130 and GRASP65-dependent lateral cisternal fusion allows uniform Golgi-enzyme distribution." *Nat Cell Biol* 8(3): 238-248.
51. Feinstein, T.N. and A.D. Linstedt (2008). "GRASP55 regulates Golgi ribbon formation." *Molecular Biology of the Cell* 19(7): 2696-2707.
52. Xiang, Y. and Y. Wang (2010). "GRASP55 and GRASP65 play complementary and essential roles in Golgi cisternal stacking." *J Cell Biol* 188(2): 237-251.
53. Kondylis, V., K.M. Sporendonk, et al. (2005). "dGRASP localization and function in the early exocytic pathway in *Drosophila* S2 cells." *Mol Biol Cell* 16(9): 4061-4072.
54. Levi, S.K., D. Bhattacharyya, et al. (2010). "The yeast GRASP Grh1 colocalizes with COPII and is dispensable for organizing the secretory pathway." *Traffic* 11(9): 1168-1179.
55. Behnia, R., F.A. Barr, et al. (2007). "The yeast orthologue of GRASP65 forms a complex with a coiled-coil protein that contributes to ER to Golgi traffic." *J Cell Biol* 176(3): 255-261.
56. Schotman, H., L. Karhinen, et al. (2008). "dGRASP-mediated noncanonical integrin secretion is required for *Drosophila* epithelial remodeling." *Dev Cell* 14(2): 171-182.
57. Staehelin, L.A. and B.H. Kang (2008). "Nanoscale architecture of endoplasmic reticulum export sites and of Golgi membranes as determined by electron tomography." *Plant physiology* 147(4): 1454-1468.
58. Faso, C., A. Boulaflois, et al. (2009). "The plant Golgi apparatus: last 10 years of answered and open questions." *FEBS Lett* 583(23): 3752-3757.

59. Sengupta, D., S. Truschel, et al. (2009). "Organelle tethering by a homotypic PDZ interaction underlies formation of the Golgi membrane network." *J Cell Biol* 186(1): 41-55.
60. Tang, D., H. Yuan, et al. (2010). "The role of GRASP65 in Golgi cisternal stacking and cell cycle progression." *Traffic* 11(6): 827-842.
61. Vinke, F.P., A.G. Grieve, et al. (2011). "The multiple facets of the Golgi reassembly stacking proteins." *Biochem J* 433(3): 423-433.
62. Barr, F.A., N. Nakamura, et al. (1998). "Mapping the interaction between GRASP65 and GM130, components of a protein complex involved in the stacking of Golgi cisternae." *EMBO J* 17(12): 3258-3268.
63. Short, B., C. Preisinger, et al. (2001). "A GRASP55-rab2 effector complex linking Golgi structure to membrane traffic." *J Cell Biol* 155(6): 877-883.
64. Lowe, M. (2011). "Structural organization of the Golgi apparatus." *Current Opinion in Cell Biology* 23(1): 85-93.
65. Ramirez, I.B. and M. Lowe (2009). "Golbins and GRASPs: holding the Golgi together." *Seminars in cell & developmental biology* 20(7): 770-779.
66. Shorter, J. and G. Warren (1999). "A role for the vesicle tethering protein, p115, in the post-mitotic stacking of reassembling Golgi cisternae in a cell-free system." *J Cell Biol* 146(1): 57-70.
67. Rambourg, A., Y. Clermont, et al. (1987). "Tridimensional structure of the Golgi apparatus of nonciliated epithelial cells of the ductuli efferentes in rat: an electron microscope stereoscopic study." *Biology of the cell / under the auspices of the European Cell Biology Organization* 60(2): 103-115.
68. Miller, P.M., A.W. Folkmann, et al. (2009). "Golgi-derived CLASP-dependent microtubules control Golgi organization and polarized trafficking in motile cells." *Nat Cell Biol* 11(9): 1069-1080.
69. Wei, J.H. and J. Seemann (2009). "The mitotic spindle mediates inheritance of the Golgi ribbon structure." *J Cell Biol* 184(3): 391-397.
70. Pelletier, L., E. Jokitalo, et al. (2000). "The effect of Golgi depletion on exocytic transport." *Nat Cell Biol* 2(11): 840-846.
71. Chabin-Brion, K., J. Marceiller, et al. (2001). "The Golgi complex is a microtubule-organizing organelle." *Mol Biol Cell* 12(7): 2047-2060.
72. Efimov, A., A. Kharitonov, et al. (2007). "Asymmetric CLASP-dependent nucleation of noncentrosomal microtubules at the trans-Golgi network." *Developmental cell* 12(6): 917-930.
73. Rios, R.M., A. Sanchis, et al. (2004). "GMAP-210 recruits gamma-tubulin complexes to cis-Golgi membranes and is required for Golgi ribbon formation." *Cell* 118(3): 323-335.
74. Rivero, S., J. Cardenas, et al. (2009). "Microtubule nucleation at the cis-side of the Golgi apparatus requires AKAP450 and GM130." *The EMBO journal* 28(8): 1016-1028.
75. Cole, N.B., N. Sciaky, et al. (1996). "Golgi dispersal during microtubule disruption: regeneration of Golgi stacks at peripheral endoplasmic reticulum exit sites." *Mol Biol Cell* 7(4): 631-650.
76. Wehland, J., M. Henkart, et al. (1983). "Role of microtubules in the distribution of the Golgi apparatus: effect of taxol and microinjected anti-alpha-tubulin antibodies." *Proc Natl Acad Sci U S A* 80(14): 4286-4290.
77. Burkhardt, J.K., C.J. Echeverri, et al. (1997). "Overexpression of the dynamitin (p50) subunit of the dynactin complex disrupts dynein-dependent maintenance of membrane organelle distribution." *J Cell Biol* 139(2): 469-484.

78. Liang, Y., W. Yu, et al. (2004). "Nudel functions in membrane traffic mainly through association with Lis1 and cytoplasmic dynein." *J Cell Biol* 164(4): 557-566.
79. Cortesy-Theulaz, I., A. Pauloin, et al. (1992). "Cytoplasmic dynein participates in the centrosomal localization of the Golgi complex." *J Cell Biol* 118(6): 1333-1345.
80. Hurtado, L., C. Caballero, et al. (2011). "Disconnecting the Golgi ribbon from the centrosome prevents directional cell migration and ciliogenesis." *J Cell Biol* 193(5): 917-933.
81. Vinogradova, T., R. Paul, et al. (2012). "Concerted effort of centrosomal and Golgi-derived microtubules is required for proper Golgi complex assembly but not for maintenance." *Mol Biol Cell* 23(5): 820-833.
82. Goldfischer, S., Y. Kress, et al. (1981). "Primary fixation in osmium-potassium ferrocyanide: the staining of glycogen, glycoproteins, elastin, an intranuclear reticular structure, and intercisternal trabeculae." *J Histochem Cytochem* 29(9): 1105-1111.
83. Duran, J.M., M. Kinseth, et al. (2008). "The role of GRASP55 in Golgi fragmentation and entry of cells into mitosis." *Molecular Biology of the Cell* 19(6): 2579-2587.
84. Wang, Y., J. Seemann, et al. (2003). "A direct role for GRASP65 as a mitotically regulated Golgi stacking factor." *The EMBO journal* 22(13): 3279-3290.
85. Nilsson, T., M.H. Hoe, et al. (1994). "Kin recognition between medial Golgi enzymes in HeLa cells." *EMBO J* 13(3): 562-574.
86. Yadav, S., S. Puri, et al. (2009). "A primary role for Golgi positioning in directed secretion, cell polarity, and wound healing." *Molecular Biology of the Cell* 20(6): 1728-1736.
87. Sutterlin, A., M. Sutterlin, et al. (2005). "Normalization of a severely abnormal ductus venosus Doppler flow velocity waveform in the presence of normal arterial flow parameters." *J Perinat Med* 33(1): 83-86.
88. Schoenenberger, C.A., S. Buchmeier, et al. (2005). "Conformation-specific antibodies reveal distinct actin structures in the nucleus and the cytoplasm." *J Struct Biol* 152(3): 157-168.
89. Honig, A., L. Rieger, et al. (2005). "Brain metastases in breast cancer--an in vitro study to evaluate new systemic chemotherapeutic options." *Anticancer Res* 25(3A): 1531-1537.
90. Kristen, P., R. Lorenz, et al. (2005). "Axillary recurrences after sentinel node (SLN) biopsy without complete axillary dissection in breast cancer patients." *Br J Cancer* 92(5): 981; author reply 982.
91. Frambach, T., T. Muller, et al. (2005). "Self-limitation of intravenous tocolysis with beta2-adrenergic agonists is mediated through receptor G protein uncoupling." *J Clin Endocrinol Metab* 90(5): 2882-2887.
92. Stroud, W.J., S. Jiang, et al. (2003). "Persistence of Golgi matrix distribution exhibits the same dependence on Sar1p activity as a Golgi glycosyltransferase." *Traffic* 4(9): 631-641.
93. Ward, T.H., R.S. Polishchuk, et al. (2001). "Maintenance of Golgi structure and function depends on the integrity of ER export." *The Journal of Cell Biology* 155(4): 557-570.
94. Mardones, G.A., C.M. Snyder, et al. (2006). "Cis-Golgi matrix proteins move directly to endoplasmic reticulum exit sites by association with tubules." *Molecular Biology of the Cell* 17(1): 525-538.
95. Altan-Bonnet, N., R. Sougrat, et al. (2006). "Golgi inheritance in mammalian cells is mediated through endoplasmic reticulum export activities." *Molecular Biology of the Cell* 17(2): 990-1005.

96. Puri, S., H. Telfer, et al. (2004). "Dispersal of Golgi matrix proteins during mitotic Golgi disassembly." *Journal of Cell Science* 117(Pt 3): 451-456.
97. Bechler, M.E., P. de Figueiredo, et al. (2012). "A PLA1-2 punch regulates the Golgi complex." *Trends in Cell Biology* 22(2): 116-124.
98. Schmidt, J.A. and W.J. Brown (2009). "Lysophosphatidic acid acyltransferase 3 regulates Golgi complex structure and function." *J Cell Biol* 186(2): 211-218.
99. Brown, W.J., K. Chambers, et al. (2003). "Phospholipase A2 (PLA2) enzymes in membrane trafficking: mediators of membrane shape and function." *Traffic* 4(4): 214-221.
100. Baumgart, T., S.T. Hess, et al. (2003). "Imaging coexisting fluid domains in biomembrane models coupling curvature and line tension." *Nature* 425(6960): 821-824.
101. Zimmerberg, J. and M.M. Kozlov (2006). "How proteins produce cellular membrane curvature." *Nature reviews. Molecular cell biology* 7(1): 9-19.
102. Manneville, J.B., J.F. Casella, et al. (2008). "COPI coat assembly occurs on liquid-disordered domains and the associated membrane deformations are limited by membrane tension." *Proceedings of the National Academy of Sciences of the United States of America* 105(44): 16946-16951.
103. Bard, F. and V. Malhotra (2006). "The formation of TGN-to-plasma-membrane transport carriers." *Annual review of cell and developmental biology* 22: 439-455.
104. Ha, K.D., B.A. Clarke, et al. (2012). "Regulation of the Golgi complex by phospholipid remodeling enzymes." *Biochim Biophys Acta* 1821(8): 1078-1088.
105. Bechler, M.E., A.M. Doody, et al. (2010). "The phospholipase complex PAFAH Ib regulates the functional organization of the Golgi complex." *J Cell Biol* 190(1): 45-53.
106. Bechler, M.E., A.M. Doody, et al. (2011). "The phospholipase A(2) enzyme complex PAFAH Ib mediates endosomal membrane tubule formation and trafficking." *Mol Biol Cell* 22(13): 2348-2359.
107. San Pietro, E., M. Capestrano, et al. (2009). "Group IV phospholipase A(2)alpha controls the formation of inter-cisternal continuities involved in intra-Golgi transport." *PLoS Biol* 7(9): e1000194.
108. Yang, J.S., C. Valente, et al. (2011). "COPI acts in both vesicular and tubular transport." *Nat Cell Biol* 13(8): 996-1003.
109. Dorner, C., T. Ciossek, et al. (1998). "Characterization of KIF1C, a new kinesin-like protein involved in vesicle transport from the Golgi apparatus to the endoplasmic reticulum." *J Biol Chem* 273(32): 20267-20275.
110. Dippold, H.C., M.M. Ng, et al. (2009). "GOLPH3 bridges phosphatidylinositol-4-phosphate and actomyosin to stretch and shape the Golgi to promote budding." *Cell* 139(2): 337-351.
111. Zilberman, Y., N.O. Alieva, et al. (2011). "Involvement of the Rho-mDia1 pathway in the regulation of Golgi complex architecture and dynamics." *Mol Biol Cell* 22(16): 2900-2911.
112. Campellone, K.G., N.J. Webb, et al. (2008). "WHAMM is an Arp2/3 complex activator that binds microtubules and functions in ER to Golgi transport." *Cell* 134(1): 148-161.
113. Diao, A., D. Rahman, et al. (2003). "The coiled-coil membrane protein golgin-84 is a novel rab effector required for Golgi ribbon formation." *J Cell Biol* 160(2): 201-212.
114. Cole, N.B., C.L. Smith, et al. (1996). "Diffusional mobility of Golgi proteins in membranes of living cells." *Science* 273(5276): 797-801.
115. Marra, P., L. Salvatore, et al. (2007). "The biogenesis of the Golgi ribbon: the roles of membrane input from the ER and of GM130." *Mol Biol Cell* 18(5): 1595-1608.
116. Bisel, B., Y. Wang, et al. (2008). "ERK regulates Golgi and centrosome orientation towards the leading edge through GRASP65." *J Cell Biol* 182(5): 837-843.



117. Preisinger, C. (2004). "YSK1 is activated by the Golgi matrix protein GM130 and plays a role in cell migration through its substrate 14-3-3." *The Journal of Cell Biology* 164(7): 1009-1020.
118. Stinchcombe, J.C., E. Majorovits, et al. (2006). "Centrosome polarization delivers secretory granules to the immunological synapse." *Nature* 443(7110): 462-465.
119. Jaffe, A.B. and A. Hall (2005). "Rho GTPases: biochemistry and biology." *Annu Rev Cell Dev Biol* 21: 247-269.
120. Horton, A.C., B. Racz, et al. (2005). "Polarized secretory trafficking directs cargo for asymmetric dendrite growth and morphogenesis." *Neuron* 48(5): 757-771.
121. Yadav, S., S. Puri, et al. (2009). "A primary role for Golgi positioning in directed secretion, cell polarity, and wound healing." *Mol Biol Cell* 20(6): 1728-1736.
122. Magdalena, J., T.H. Millard, et al. (2003). "Microtubule involvement in NIH 3T3 Golgi and MTOC polarity establishment." *J Cell Sci* 116(Pt 4): 743-756.
123. Noske, A.B., A.J. Costin, et al. (2008). "Expedited approaches to whole cell electron tomography and organelle mark-up in situ in high-pressure frozen pancreatic islets." *J Struct Biol* 161(3): 298-313.
124. Sutterlin, C., P. Hsu, et al. (2002). "Fragmentation and dispersal of the pericentriolar Golgi complex is required for entry into mitosis in mammalian cells." *Cell* 109(3): 359-369.
125. Yoshimura, S., K. Yoshioka, et al. (2005). "Convergence of cell cycle regulation and growth factor signals on GRASP65." *J Biol Chem* 280(24): 23048-23056.
126. Rabouille, C. and V. Kondylis (2007). "Golgi ribbon unlinking: an organelle-based G2/M checkpoint." *Cell cycle* 6(22): 2723-2729.
127. Farhan, H. and C. Rabouille (2011). "Signalling to and from the secretory pathway." *J Cell Sci* 124(Pt 2): 171-180.
128. Cancino, J. and A. Luini (2013). "Signaling circuits on the Golgi complex." *Traffic* 14(2): 121-134.
129. Mayinger, P. (2011). "Signaling at the Golgi." *Cold Spring Harb Perspect Biol* 3(5).
130. Colanzi, A., C. Suetterlin, et al. (2003). "Cell-cycle-specific Golgi fragmentation: how and why?" *Curr Opin Cell Biol* 15(4): 462-467.
131. Misteli, T. and G. Warren (1994). "COP-coated vesicles are involved in the mitotic fragmentation of Golgi stacks in a cell-free system." *J Cell Biol* 125(2): 269-282.
132. Acharya, U., A. Mallabiabarrena, et al. (1998). "Signaling via mitogen-activated protein kinase kinase (MEK1) is required for Golgi fragmentation during mitosis." *Cell* 92(2): 183-192.
133. Sutterlin, C., C.Y. Lin, et al. (2001). "Polo-like kinase is required for the fragmentation of pericentriolar Golgi stacks during mitosis." *Proc Natl Acad Sci U S A* 98(16): 9128-9132.
134. Xie, S., Q. Wang, et al. (2004). "MEK1-induced Golgi dynamics during cell cycle progression is partly mediated by Polo-like kinase-3." *Oncogene* 23(21): 3822-3829.
135. Shaul, Y.D. and R. Seger (2006). "ERK1c regulates Golgi fragmentation during mitosis." *J Cell Biol* 172(6): 885-897.
136. Colanzi, A., C. Hidalgo Carcedo, et al. (2007). "The Golgi mitotic checkpoint is controlled by BARS-dependent fission of the Golgi ribbon into separate stacks in G2." *EMBO J* 26(10): 2465-2476.
137. Bard, F. and V. Malhotra (2006). "The formation of TGN-to-plasma-membrane transport carriers." *Annu Rev Cell Dev Biol* 22: 439-455.

138. Hausser A, S.P., Märtens S, Link G, Toker A, Pfizenmaier K. (2005). "Protein kinase D regulates vesicular transport by phosphorylating and activating phosphatidylinositol-4 kinase IIIbeta at the Golgi complex." *Nat Cell Biol* 7(9): 880-886.
139. Liljedahl, M., Y. Maeda, et al. (2001). "Protein kinase D regulates the fission of cell surface destined transport carriers from the trans-Golgi network." *Cell* 104(3): 409-420.
140. Bossard, C., D. Bresson, et al. (2007). "Dimeric PKD regulates membrane fission to form transport carriers at the TGN." *J Cell Biol* 179(6): 1123-1131.
141. Blagoveshchenskaya, A., F.Y. Cheong, et al. (2008). "Integration of Golgi trafficking and growth factor signaling by the lipid phosphatase SAC1." *J Cell Biol* 180(4): 803-812.
142. Muniz, M., M.E. Martin, et al. (1997). "Protein kinase A activity is required for the budding of constitutive transport vesicles from the trans-Golgi network." *Proc Natl Acad Sci U S A* 94(26): 14461-14466.
143. Mavillard, F., J. Hidalgo, et al. (2010). "PKA-mediated Golgi remodeling during cAMP signal transmission." *Traffic* 11(1): 90-109.
144. De Matteis, M.A., A. Di Campli, et al. (2005). "The role of the phosphoinositides at the Golgi complex." *Biochim Biophys Acta* 1744(3): 396-405.
145. Pulvirenti, T., M. Giannotta, et al. (2008). "A traffic-activated Golgi-based signalling circuit coordinates the secretory pathway." *Nat Cell Biol* 10(8): 912-922.
146. Wang, Y., J. Seemann, et al. (2003). "A direct role for GRASP65 as a mitotically regulated Golgi stacking factor." *EMBO J* 22(13): 3279-3290.
147. Preisinger, C., B. Short, et al. (2004). "YSK1 is activated by the Golgi matrix protein GM130 and plays a role in cell migration through its substrate 14-3-3zeta." *J Cell Biol* 164(7): 1009-1020.
148. Hurd, T.W., S. Fan, et al. (2003). "Phosphorylation-dependent binding of 14-3-3 to the polarity protein Par3 regulates cell polarity in mammalian epithelia." *Curr Biol* 13(23): 2082-2090.
149. Kodani, A., I. Kristensen, et al. (2009). "GM130-dependent control of Cdc42 activity at the Golgi regulates centrosome organization." *Mol Biol Cell* 20(4): 1192-1200.
150. Inder, K., A. Harding, et al. (2008). "Activation of the MAPK module from different spatial locations generates distinct system outputs." *Mol Biol Cell* 19(11): 4776-4784.
151. Inder, K. and J.F. Hancock (2008). "System output of the MAPK module is spatially regulated." *Commun Integr Biol* 1(2): 178-179.
152. Choy, E., V.K. Chiu, et al. (1999). "Endomembrane trafficking of ras: the CAAX motif targets proteins to the ER and Golgi." *Cell* 98(1): 69-80.
153. Matallanas, D., V. Sanz-Moreno, et al. (2006). "Distinct utilization of effectors and biological outcomes resulting from site-specific Ras activation: Ras functions in lipid rafts and Golgi complex are dispensable for proliferation and transformation." *Mol Cell Biol* 26(1): 100-116.
154. Chiu, V.K., T. Bivona, et al. (2002). "Ras signalling on the endoplasmic reticulum and the Golgi." *Nat Cell Biol* 4(5): 343-350.
155. Torii, S., K. Nakayama, et al. (2004). "Regulatory mechanisms and function of ERK MAP kinases." *Journal of biochemistry* 136(5): 557-561.
156. Kairouz-Wahbe, R., H. Biliran, et al. (2008). "Anoikis effector Bit1 negatively regulates Erk activity." *Proc Natl Acad Sci U S A* 105(5): 1528-1532.
157. Haltiwanger, R.S. and J.B. Lowe (2004). "Role of glycosylation in development." *Annu Rev Biochem* 73: 491-537.
158. Paulson, J.C., O. Blixt, et al. (2006). "Sweet spots in functional glycomics." *Nat Chem Biol* 2(5): 238-248.

159. Ohtsubo, K. and J.D. Marth (2006). "Glycosylation in cellular mechanisms of health and disease." *Cell* 126(5): 855-867.
160. Raman, R., S. Raguram, et al. (2005). "Glycomics: an integrated systems approach to structure-function relationships of glycans." *Nat Methods* 2(11): 817-824.
161. Nairn, A.V., W.S. York, et al. (2008). "Regulation of glycan structures in animal tissues: transcript profiling of glycan-related genes." *J Biol Chem* 283(25): 17298-17313.
162. Cummings, R.D. (2009). "The repertoire of glycan determinants in the human glycome." *Mol Biosyst* 5(10): 1087-1104.
163. Nairn, A.V. and K.W. Moremen "Handbook of Glycomics." (eds Cummings, R. & Pierce, J.M.): 95–136.
164. Schachter, H. (2000). "The joys of HexNAc. The synthesis and function of N- and O-glycan branches." *Glycoconj J* 17(7-9): 465-483.
165. Yan, A. and W.J. Lennarz (2005). "Unraveling the mechanism of protein N-glycosylation." *J Biol Chem* 280(5): 3121-3124.
166. Cao, R., Y. Liu, et al. (2010). "Improvement of hydrophobic integral membrane protein identification by mild performic acid oxidation-assisted digestion." *Analytical biochemistry* 407(2): 196-204.
167. Kinoshita, T., K. Ohishi, et al. (1997). "GPI-anchor synthesis in mammalian cells: genes, their products, and a deficiency." *J Biochem* 122(2): 251-257.
168. Esko, J.D. and S.B. Selleck (2002). "Order out of chaos: assembly of ligand binding sites in heparan sulfate." *Annu Rev Biochem* 71: 435-471.
169. Maccioni, H.J., C.G. Giraud, et al. (2002). "Understanding the stepwise synthesis of glycolipids." *Neurochem Res* 27(7-8): 629-636.
170. Weigel, P.H., V.C. Hascall, et al. (1997). "Hyaluronan synthases." *J Biol Chem* 272(22): 13997-14000.
171. Munro, S. (2001). "What can yeast tell us about N-linked glycosylation in the Golgi apparatus?" *FEBS Lett* 498(2-3): 223-227.
172. Varki, A., H.H. Freeze, et al. (2009). "Evolution of Glycan Diversity." *Essentials of Glycobiology*.
173. Moremen, K.W., M. Tiemeyer, et al. (2012). "Vertebrate protein glycosylation: diversity, synthesis and function." *Nat Rev Mol Cell Biol* 13(7): 448-462.
174. Freeze, H.H. (2006). "Genetic defects in the human glycome." *Nat Rev Genet* 7(7): 537-551.
175. Varki, A. (1995). "Oligosaccharides in vertebrate development." *Seminars Dev Biol* 6: 127–138.
176. Takeuchi, M., Kobata, A. (1991). "Structures and functional roles of the sugar chains of human erythropoietins." *Glycobiology* 1(4): 337-346.
177. Marino, K., Bones, J., Kattla, J. J., Rudd, P. M. (2010). "A systematic approach to protein glycosylation analysis: a path through the maze." *Nat Chem Biol* 6(10): 713-723.
178. Varki, A. and J.B. Lowe (2009). "Biological Roles of Glycans." *Essentials of Glycobiology*.
179. Brockhausen, I., H. Schachter, et al. (2009). "O-GalNAc Glycans." *Essentials of Glycobiology*.
180. Padera, R., G. Venkataraman, et al. (1999). "FGF-2/fibroblast growth factor receptor/heparin-like glycosaminoglycan interactions: a compensation model for FGF-2 signaling." *FASEB J* 13(13): 1677-1687.
181. Sakata, H., S.J. Stahl, et al. (1997). "Heparin binding and oligomerization of hepatocyte growth factor/scatter factor isoforms. Heparan sulfate glycosaminoglycan requirement for Met binding and signaling." *J Biol Chem* 272(14): 9457-9463.

182. Varki, A. (1993). "Biological roles of oligosaccharides: all of the theories are correct." *Glycobiology* 3(2): 97-130.
183. Rosen, S.D. (2004). "Ligands for L-selectin: homing, inflammation, and beyond." *Annu Rev Immunol* 22: 129-156.
184. Shur, B.D., M.A. Ensslin, et al. (2004). "SED1 function during mammalian sperm-egg adhesion." *Curr Opin Cell Biol* 16(5): 477-485.
185. Surani, M.A. (1979). "Glycoprotein synthesis and inhibition of glycosylation by tunicamycin in preimplantation mouse embryos: compaction and trophoblast adhesion." *Cell* 18(1): 217-227.
186. Akama, T.O., A.K. Misra, et al. (2002). "Enzymatic synthesis in vitro of the disulfated disaccharide unit of corneal keratan sulfate." *J Biol Chem* 277(45): 42505-42513.
187. Dennis, J.W., Granovsky, M., Warren, C. E. (1999). "Protein glycosylation in development and disease." *Bioessays* 21(5): 412-421.
188. Partridge, E.A., C. Le Roy, et al. (2004). "Regulation of cytokine receptors by Golgi N-glycan processing and endocytosis." *Science* 306(5693): 120-124.
189. Hoseki, J., R. Ushioda, et al. (2010). "Mechanism and components of endoplasmic reticulum-associated degradation." *J Biochem* 147(1): 19-25.
190. Kollmann, K., S. Pohl, et al. (2010). "Mannose phosphorylation in health and disease." *Eur J Cell Biol* 89(1): 117-123.
191. Bax, M., J.J. Garcia-Vallejo, et al. (2007). "Dendritic cell maturation results in pronounced changes in glycan expression affecting recognition by siglecs and galectins." *J Immunol* 179(12): 8216-8224.
192. Lau, K.S., E.A. Partridge, et al. (2007). "Complex N-glycan number and degree of branching cooperate to regulate cell proliferation and differentiation." *Cell* 129(1): 123-134.
193. Gill, D.J., J. Chia, et al. (2010). "Regulation of O-glycosylation through Golgi-to-ER relocation of initiation enzymes." *J Cell Biol* 189(5): 843-858.
194. Gill, D.J., K.M. Tham, et al. (2013). "Initiation of GalNAc-type O-glycosylation in the endoplasmic reticulum promotes cancer cell invasiveness." *Proc Natl Acad Sci U S A* 110(34): E3152-3161.
195. Ohtsubo, K., S. Takamatsu, et al. (2005). "Dietary and genetic control of glucose transporter 2 glycosylation promotes insulin secretion in suppressing diabetes." *Cell* 123(7): 1307-1321.
196. Fuster, M.M., Esko, J. D. (2005). "The sweet and sour of cancer: glycans as novel therapeutic targets." *Nat Rev Cancer* 5(7): 526-542.
197. Brockhausen, I. (2006). "Mucin-type O-glycans in human colon and breast cancer: glycodynamics and functions." *EMBO Rep* 7(6): 599-604.
198. Marth, J.D., Grewal, P. K. (2008). "Mammalian glycosylation in immunity." *Nat Rev Immunol* 8(11): 874-887.
199. Schulz BL, S.A., Robinson LJ, Prasad SS, Lindner RA, Robinson M, Bye PT, Nielson DW, Harry JL, Packer NH, Karlsson NG. (2007). "Glycosylation of sputum mucins is altered in cystic fibrosis patients." *Glycobiology* 17(7): 698-712.
200. Van Beek, W.P., L.A. Smets, et al. (1975). "Changed surface glycoprotein as a marker of malignancy in human leukaemic cells." *Nature* 253: 457-460.
201. Julien S, A.E., Ottenberg K, Furlan A, Courtand G, Vercoutter-Edouart AS, Hanisch FG, Delannoy P, Le Bourhis X. (2006). "ST6GalNAc I expression in MDA-MB-231 breast cancer cells greatly modifies their O-glycosylation pattern and enhances their tumorigenicity." *Glycobiology* 16(1): 54-64.
202. Gabius, H.J. (2011). "Glycobiomarkers by glycoproteomics and glycan profiling (glycomics): emergence of functionality." *Biochem Soc Trans* 39(1): 399-405.

203. Li, M., Song, L., Qin, X. (2010). "Glycan changes: cancer metastasis and anti-cancer vaccines." *J Biosci* 35(4): 665-673.
204. Kang, J.G., Ko, J. H., Kim, Y. S. (2011). "Pros and cons of using aberrant glycosylation as companion biomarkers for therapeutics in cancer." *BMB Rep* 44(12): 765-771.
205. Takashima, S. (2008). "Characterization of mouse sialyltransferase genes: their evolution and diversity." *Biosci Biotechnol Biochem* 72(5): 1155-1167.
206. Koles, K., K.D. Irvine, et al. (2004). "Functional characterization of *Drosophila* sialyltransferase." *J Biol Chem* 279(6): 4346-4357.
207. Tian, E. and K.G. Ten Hagen (2009). "Recent insights into the biological roles of mucin-type O-glycosylation." *Glycoconj J* 26(3): 325-334.
208. Kitazume, S., R. Oka, et al. (2009). "Molecular insights into beta-galactoside alpha2,6-sialyltransferase secretion in vivo." *Glycobiology* 19(5): 479-487.
209. Shifley, E.T. and S.E. Cole (2008). "Lunatic fringe protein processing by proprotein convertases may contribute to the short protein half-life in the segmentation clock." *Biochim Biophys Acta* 1783(12): 2384-2390.
210. Nilsson, T., P. Slusarewicz, et al. (1993). "Kin recognition. A model for the retention of Golgi enzymes." *FEBS Lett* 330(1): 1-4.
211. Nilsson, T., C. Rabouille, et al. (1996). "The role of the membrane-spanning domain and stalk region of N-acetylglucosaminyltransferase I in retention, kin recognition and structural maintenance of the Golgi apparatus in HeLa cells." *J Cell Sci* 109 ( Pt 7): 1975-1989.
212. Opat, A.S., F. Houghton, et al. (2000). "Medial Golgi but not late Golgi glycosyltransferases exist as high molecular weight complexes. Role of luminal domain in complex formation and localization." *J Biol Chem* 275(16): 11836-11845.
213. Tu, L., W.C. Tai, et al. (2008). "Signal-mediated dynamic retention of glycosyltransferases in the Golgi." *Science* 321(5887): 404-407.
214. Tu, L. and D.K. Banfield (2010). "Localization of Golgi-resident glycosyltransferases." *Cell Mol Life Sci* 67(1): 29-41.
215. Sen, J., J.S. Goltz, et al. (2000). "Windbeutel is required for function and correct subcellular localization of the *Drosophila* patterning protein Pipe." *Development* 127(24): 5541-5550.
216. Ju, T. and R.D. Cummings (2002b). "A unique molecular chaperone Cosmc required for activity of the mammalian core 1 beta 3-galactosyltransferase." *Proceedings of the National Academy of Sciences of the United States of America* 99(26): 16613-16618.
217. Aryal, R.P., T. Ju, et al. (2010). "The endoplasmic reticulum chaperone Cosmc directly promotes in vitro folding of T-synthase." *J Biol Chem* 285(4): 2456-2462.
218. Zielinska, D.F., F. Gnad, et al. (2010). "Precision mapping of an in vivo N-glycoproteome reveals rigid topological and sequence constraints." *Cell* 141(5): 897-907.
219. Kornfeld, R. and S. Kornfeld (1985). "Assembly of asparagine-linked oligosaccharides." *Annu Rev Biochem* 54: 631-664.
220. Kelleher, D.J. and R. Gilmore (2006). "An evolving view of the eukaryotic oligosaccharyltransferase." *Glycobiology* 16(4): 47R-62R.
221. Lederkremer, G.Z. (2009). "Glycoprotein folding, quality control and ER-associated degradation." *Curr Opin Struct Biol* 19(5): 515-523.
222. Helenius, A. and M. Aebi (2004). "Roles of N-linked glycans in the endoplasmic reticulum." *Annu Rev Biochem* 73: 1019-1049.
223. An, H.J., P. Gip, et al. (2012). "Extensive determination of glycan heterogeneity reveals an unusual abundance of high mannose glycans in enriched plasma membranes of human embryonic stem cells." *Mol Cell Proteomics* 11(4): M111 010660.

224. Stanley, P., H. Schachter, et al. (2009). "N-Glycans."
225. Koles, K., J.M. Lim, et al. (2007). "Identification of N-glycosylated proteins from the central nervous system of *Drosophila melanogaster*." *Glycobiology* 17(12): 1388-1403.
226. Aoki, K., M. Perlman, et al. (2007). "Dynamic developmental elaboration of N-linked glycan complexity in the *Drosophila melanogaster* embryo." *J Biol Chem* 282(12): 9127-9142.
227. Cipollo, J.F., A.M. Awad, et al. (2005). "N-Glycans of *Caenorhabditis elegans* are specific to developmental stages." *J Biol Chem* 280(28): 26063-26072.
228. Lau, K.S. and J.W. Dennis (2008). "N-Glycans in cancer progression." *Glycobiology* 18(10): 750-760.
229. Lowe, J.B. and J.D. Marth (2003). "A genetic approach to Mammalian glycan function." *Annual Review of Biochemistry* 72: 643-691.
230. Hart, G.W. (1997). "Dynamic O-linked glycosylation of nuclear and cytoskeletal proteins." *Annu Rev Biochem* 66: 315-335.
231. Wopereis, S., D.J. Lefeber, et al. (2006). "Mechanisms in protein O-glycan biosynthesis and clinical and molecular aspects of protein O-glycan biosynthesis defects: a review." *Clin Chem* 52(4): 574-600.
232. Luther, K.B. and R.S. Haltiwanger (2009). "Role of unusual O-glycans in intercellular signaling." *Int J Biochem Cell Biol* 41(5): 1011-1024.
233. Hashimoto, K., T. Tokimatsu, et al. (2009). "Comprehensive analysis of glycosyltransferases in eukaryotic genomes for structural and functional characterization of glycans." *Carbohydr Res* 344(7): 881-887.
234. Hanisch, F.G. (2001). "O-glycosylation of the mucin type." *Biol Chem* 382(2): 143-149.
235. Hang, H.C. and C.R. Bertozzi (2005). "The chemistry and biology of mucin-type O-linked glycosylation." *Bioorg Med Chem* 13(17): 5021-5034.
236. Halim, A., G. Brinkmalm, et al. (2011). "Site-specific characterization of threonine, serine, and tyrosine glycosylations of amyloid precursor protein/amyloid beta-peptides in human cerebrospinal fluid." *Proc Natl Acad Sci U S A* 108(29): 11848-11853.
237. Halim, A., J. Nilsson, et al. (2012). "Human urinary glycoproteomics; attachment site specific analysis of N- and O-linked glycosylations by CID and ECD." *Mol Cell Proteomics* 11(4): M111 013649.
238. Steentoft, C., S.Y. Vakhrushev, et al. (2011). "Mining the O-glycoproteome using zinc-finger nuclease-glycoengineered SimpleCell lines." *Nat Methods* 8(11): 977-982.
239. Schjoldager, K.T. and H. Clausen (2012). "Site-specific protein O-glycosylation modulates proprotein processing - deciphering specific functions of the large polypeptide GalNAc-transferase gene family." *Biochim Biophys Acta* 1820(12): 2079-2094.
240. Gill, D.J., H. Clausen, et al. (2011). "Location, location, location: new insights into O-GalNAc protein glycosylation." *Trends Cell Biol* 21(3): 149-158.
241. Bennett, E.P., U. Mandel, et al. (2012). "Control of mucin-type O-glycosylation: a classification of the polypeptide GalNAc-transferase gene family." *Glycobiology* 22(6): 736-756.
242. Tran, D.T. and K.G. Ten Hagen (2013). "Mucin-type O-glycosylation during development." *J Biol Chem* 288(10): 6921-6929.
243. Schwientek, T., E.P. Bennett, et al. (2002). "Functional conservation of subfamilies of putative UDP-N-acetylgalactosamine:polypeptide N-acetylgalactosaminyltransferases in *Drosophila*, *Caenorhabditis elegans*, and mammals. One subfamily composed of I(2)35Aa is essential in *Drosophila*." *J Biol Chem* 277(25): 22623-22638.

244. ten Hagen, K.G., L. Zhang, et al. (2009). "Glycobiology on the fly: developmental and mechanistic insights from *Drosophila*." *Glycobiology* 19(2): 102-111.
245. Hassan, H., C.A. Reis, et al. (2000). "The lectin domain of UDP-N-acetyl-D-galactosamine: polypeptide N-acetylgalactosaminyltransferase-T4 directs its glycopeptide specificities." *J Biol Chem* 275(49): 38197-38205.
246. Bennett, E.P., H. Hassan, et al. (1999). "Cloning and characterization of a close homologue of human UDP-N-acetyl-alpha-D-galactosamine:Polypeptide N-acetylgalactosaminyltransferase-T3, designated GalNAc-T6. Evidence for genetic but not functional redundancy." *J Biol Chem* 274(36): 25362-25370.
247. Rottger, S., J. White, et al. (1998). "Localization of three human polypeptide GalNAc-transferases in HeLa cells suggests initiation of O-linked glycosylation throughout the Golgi apparatus." *J Cell Sci* 111 ( Pt 1): 45-60.
248. Kato, K., C. Jeanneau, et al. (2006). "Polypeptide GalNAc-transferase T3 and familial tumoral calcinosis. Secretion of fibroblast growth factor 23 requires O-glycosylation." *J Biol Chem* 281(27): 18370-18377.
249. Schjoldager, K.T., M.B. Vester-Christensen, et al. (2010). "O-glycosylation modulates proprotein convertase activation of angiopoietin-like protein 3: possible role of polypeptide GalNAc-transferase-2 in regulation of concentrations of plasma lipids." *J Biol Chem* 285(47): 36293-36303.
250. Miwa, H.E., T.A. Gerken, et al. (2010). "Isoform-specific O-glycosylation of osteopontin and bone sialoprotein by polypeptide N-acetylgalactosaminyltransferase-1." *J Biol Chem* 285(2): 1208-1219.
251. Ju, T., V.I. Otto, et al. (2011). "The Tn antigen-structural simplicity and biological complexity." *Angew Chem Int Ed Engl* 50(8): 1770-1791.
252. Springer, G. (1984). "T and Tn, general carcinoma autoantigens." *Science* 224(4654): 1198-1206.
253. Springer, G.F. (1997). "Immunoreactive T and Tn epitopes in cancer diagnosis, prognosis, and immunotherapy." *Journal of molecular medicine (Berlin, Germany)* 75(8): 594-602.
254. Desai, P. (2000). "Immunoreactive T and Tn antigens in malignancy: role in carcinoma diagnosis, prognosis, and immunotherapy." *Transfus Med Rev* 14(4): 312-325.
255. Saeland, E., S.J. van Vliet, et al. (2007). "The C-type lectin MGL expressed by dendritic cells detects glycan changes on MUC1 in colon carcinoma." *Cancer Immunol Immunother* 56(8): 1225-1236.
256. Kozarsky, K., D. Kingsley, et al. (1988). "Use of a mutant cell line to study the kinetics and function of O-linked glycosylation of low density lipoprotein receptors." *Proc Natl Acad Sci U S A* 85(12): 4335-4339.
257. Kuwano, M., T. Seguchi, et al. (1991). "Glycosylation mutations of serine/threonine-linked oligosaccharides in low-density lipoprotein receptor: indispensable roles of O-glycosylation." *J Cell Sci* 98 ( Pt 2): 131-134.
258. Byrne, S.L., R. Leverence, et al. (2006). "Effect of glycosylation on the function of a soluble, recombinant form of the transferrin receptor." *Biochemistry* 45(21): 6663-6673.
259. Liu, W., V. Ramachandran, et al. (1998). "Identification of N-terminal residues on P-selectin glycoprotein ligand-1 required for binding to P-selectin." *J Biol Chem* 273(12): 7078-7087.
260. Endo, T. (2007). "Dystroglycan glycosylation and its role in alpha-dystroglycanopathies." *Acta Myol* 26(3): 165-170.
261. Marcos, N.T., S. Pinho, et al. (2004). "Role of the human ST6GalNAc-I and ST6GalNAc-II in the synthesis of the cancer-associated sialyl-Tn antigen." *Cancer Res* 64(19): 7050-7057.

262. Julien, S., E. Adriaenssens, et al. (2006). "ST6GalNAc I expression in MDA-MB-231 breast cancer cells greatly modifies their O-glycosylation pattern and enhances their tumorigenicity." *Glycobiology* 16(1): 54-64.
263. Brockhausen, I., J. Yang, et al. (1998). "Enzymatic basis for sialyl-Tn expression in human colon cancer cells." *Glycoconj J* 15(6): 595-603.
264. Ju, T., K. Brewer, et al. (2002a). "Cloning and expression of human core 1 beta1,3-galactosyltransferase." *J Biol Chem* 277(1): 178-186.
265. Xia, L., T. Ju, et al. (2004). "Defective angiogenesis and fatal embryonic hemorrhage in mice lacking core 1-derived O-glycans." *J Cell Biol* 164(3): 451-459.
266. Ju, T., R.P. Aryal, et al. (2008). "Regulation of protein O-glycosylation by the endoplasmic reticulum-localized molecular chaperone Cosmc." *J Cell Biol* 182(3): 531-542.
267. Ju, T., G.S. Lanneau, et al. (2008a). "Human tumor antigens Tn and sialyl Tn arise from mutations in Cosmc." *Cancer Res* 68(6): 1636-1646.
268. Lee, Y.C., M. Kaufmann, et al. (1999). "Molecular cloning and functional expression of two members of mouse NeuAcalpha2,3Galbeta1,3GalNAc GalNAcalpha2,6-sialyltransferase family, ST6GalNAc III and IV." *J Biol Chem* 274(17): 11958-11967.
269. Bierhuizen, M.F. and M. Fukuda (1992). "Expression cloning of a cDNA encoding UDP-GlcNAc:Gal beta 1-3-GalNAc-R (GlcNAc to GalNAc) beta 1-6GlcNAc transferase by gene transfer into CHO cells expressing polyoma large tumor antigen." *Proc Natl Acad Sci U S A* 89(19): 9326-9330.
270. Carlow, D.A., S.Y. Corbel, et al. (2001). "IL-2, -4, and -15 differentially regulate O-glycan branching and P-selectin ligand formation in activated CD8 T cells." *J Immunol* 167(12): 6841-6848.
271. Mitoma, J. and M. Fukuda (2010). "Core O-glycans required for lymphocyte homing gene knockout mice of core 1 beta1,3-N-acetylglucosaminyltransferase and core 2 N-acetylglucosaminyltransferase." *Methods Enzymol* 479: 257-270.
272. Brockhausen, I., W. Kuhns, et al. (1991). "Biosynthesis of O-glycans in leukocytes from normal donors and from patients with leukemia: increase in O-glycan core 2 UDP-GlcNAc:Gal beta 3 GalNAc alpha-R (GlcNAc to GalNAc) beta(1-6)-N-acetylglucosaminyltransferase in leukemic cells." *Cancer Res* 51(4): 1257-1263.
273. Lanteri, M., V. Giordanengo, et al. (2003). "Altered T cell surface glycosylation in HIV-1 infection results in increased susceptibility to galectin-1-induced cell death." *Glycobiology* 13(12): 909-918.
274. Vavasseur, F., J.M. Yang, et al. (1995). "Synthesis of O-glycan core 3: characterization of UDP-GlcNAc: GalNAc-R beta 3-N-acetyl-glucosaminyltransferase activity from colonic mucosal tissues and lack of the activity in human cancer cell lines." *Glycobiology* 5(3): 351-357.
275. Iwai, T., N. Inaba, et al. (2002). "Molecular cloning and characterization of a novel UDP-GlcNAc:GalNAc-peptide beta1,3-N-acetylglucosaminyltransferase (beta 3Gn-T6), an enzyme synthesizing the core 3 structure of O-glycans." *J Biol Chem* 277(15): 12802-12809.
276. Byrd, J.C. and R.S. Bresalier (2004). "Mucins and mucin binding proteins in colorectal cancer." *Cancer metastasis reviews* 23(1-2): 77-99.
277. Iwai, T., T. Kudo, et al. (2005). "Core 3 synthase is down-regulated in colon carcinoma and profoundly suppresses the metastatic potential of carcinoma cells." *Proc Natl Acad Sci U S A* 102(12): 4572-4577.
278. Garner, B., A.H. Merry, et al. (2001). "Structural elucidation of the N- and O-glycans of human apolipoprotein(a): role of o-glycans in conferring protease resistance." *J Biol Chem* 276(25): 22200-22208.



279. Kim, Y.S. and S.B. Ho (2010). "Intestinal goblet cells and mucins in health and disease: recent insights and progress." *Curr Gastroenterol Rep* 12(5): 319-330.
280. Skelton, T.P., C. Zeng, et al. (1998). "Glycosylation provides both stimulatory and inhibitory effects on cell surface and soluble CD44 binding to hyaluronan." *J Cell Biol* 140(2): 431-446.
281. Stone, E.L., M.N. Ismail, et al. (2009). "Glycosyltransferase function in core 2-type protein O glycosylation." *Mol Cell Biol* 29(13): 3770-3782.
282. Ugorski, M. and A. Laskowska (2002). "Sialyl Lewis(a): a tumor-associated carbohydrate antigen involved in adhesion and metastatic potential of cancer cells." *Acta Biochim Pol* 49(2): 303-311.
283. Comelli, E.M., S.R. Head, et al. (2006). "A focused microarray approach to functional glycomics: transcriptional regulation of the glycome." *Glycobiology* 16(2): 117-131.
284. Lanctot, P.M., Gage, F. H., Varki, A. P. (2007). "The glycans of stem cells." *Curr Opin Chem Biol* 11(4): 373-380.
285. Gawlitzek, M., Ryll, T., Lofgren, J., Sliwowski, M. B. (2000). "Ammonium alters N-glycan structures of recombinant TNFR-IgG: degradative versus biosynthetic mechanisms." *Biotechnol Bioeng* 68(6): 637-646.
286. McCaffrey, G. and J.C. Jamieson (1993). "Evidence for the role of a cathepsin D-like activity in the release of Gal beta 1-4GlcNAc alpha 2-6sialyltransferase from rat and mouse liver in whole-cell systems." *Comp Biochem Physiol B* 104(1): 91-94.
287. Nilsson, T., C.E. Au, et al. (2009). "Sorting out glycosylation enzymes in the Golgi apparatus." *FEBS Lett* 583(23): 3764-3769.
288. Axelsson, M.A., N.G. Karlsson, et al. (2001). "Neutralization of pH in the Golgi apparatus causes redistribution of glycosyltransferases and changes in the O-glycosylation of mucins." *Glycobiology* 11(8): 633-644.
289. Rivinoja, A., A. Hassinen, et al. (2009). "Elevated Golgi pH impairs terminal N-glycosylation by inducing mislocalization of Golgi glycosyltransferases." *J Cell Physiol* 220(1): 144-154.
290. Hassinen, A., F.M. Pujol, et al. (2011). "Functional organization of Golgi N- and O-glycosylation pathways involves pH-dependent complex formation that is impaired in cancer cells." *J Biol Chem* 286(44): 38329-38340.
291. Maeda, Y., T. Ide, et al. (2008). "GPHR is a novel anion channel critical for acidification and functions of the Golgi apparatus." *Nat Cell Biol* 10(10): 1135-1145.
292. Maeda, Y. and T. Kinoshita (2010). "The acidic environment of the Golgi is critical for glycosylation and transport." *Methods Enzymol* 480: 495-510.
293. Waldman, B.C. and G. Rudnick (1990). "UDP-GlcNAc transport across the Golgi membrane: electroneutral exchange for dianionic UMP." *Biochemistry* 29(1): 44-52.
294. Rivinoja, A., N. Kokkonen, et al. (2006). "Elevated Golgi pH in breast and colorectal cancer cells correlates with the expression of oncofetal carbohydrate T-antigen." *J Cell Physiol* 208(1): 167-174.
295. Berninsone, P.M. and C.B. Hirschberg (2000). "Nucleotide sugar transporters of the Golgi apparatus." *Curr Opin Struct Biol* 10(5): 542-547.
296. Lubke, T., T. Marquardt, et al. (2001). "Complementation cloning identifies CDG-IIc, a new type of congenital disorders of glycosylation, as a GDP-fucose transporter deficiency." *Nat Genet* 28(1): 73-76.
297. Schwarzkopf, M., K.P. Knobloch, et al. (2002). "Sialylation is essential for early development in mice." *Proc Natl Acad Sci U S A* 99(8): 5267-5270.

298. Xu, Y.X., L. Liu, et al. (2010). "Inhibition of Golgi apparatus glycosylation causes endoplasmic reticulum stress and decreased protein synthesis." *J Biol Chem* 285(32): 24600-24608.
299. Huang, H.-H. and P. Stanley (2010). "A testis-specific regulator of complex and hybrid N-glycan synthesis." *The Journal of Cell Biology* 190(5): 893-910.
300. Yamaji, T., K. Nishikawa, et al. (2010). "Transmembrane BAX inhibitor motif containing (TMBIM) family proteins perturbs a trans-Golgi network enzyme, Gb3 synthase, and reduces Gb3 biosynthesis." *J Biol Chem* 285(46): 35505-35518.
301. Smith, R.D. and V.V. Lupashin (2008). "Role of the conserved oligomeric Golgi (COG) complex in protein glycosylation." *Carbohydr Res* 343(12): 2024-2031.
302. Podos, S.D., P. Reddy, et al. (1994). "LDLC encodes a brefeldin A-sensitive, peripheral Golgi protein required for normal Golgi function." *J Cell Biol* 127(3): 679-691.
303. Zeevaert, R., F. Foulquier, et al. (2008). "Deficiencies in subunits of the Conserved Oligomeric Golgi (COG) complex define a novel group of Congenital Disorders of Glycosylation." *Mol Genet Metab* 93(1): 15-21.
304. Lubbehusen, J., C. Thiel, et al. (2010). "Fatal outcome due to deficiency of subunit 6 of the conserved oligomeric Golgi complex leading to a new type of congenital disorders of glycosylation." *Hum Mol Genet* 19(18): 3623-3633.
305. Foulquier, F. (2009). "COG defects, birth and rise!" *Biochim Biophys Acta* 1792(9): 896-902.
306. Wu, X., Steet, R. A., Bohorov, O., Bakker, J., Newell, J., Krieger, M., Spaapen, L., Kornfeld, S., Freeze, H. H. (2004). "Mutation of the COG complex subunit gene COG7 causes a lethal congenital disorder." *Nat Med* 10(5): 518-523.
307. Freeze, H.H. and B.G. Ng (2011). "Golgi glycosylation and human inherited diseases." *Cold Spring Harb Perspect Biol* 3(9): a005371.
308. Bexiga, M.G. and J.C. Simpson (2013). "Human diseases associated with form and function of the Golgi complex." *Int J Mol Sci* 14(9): 18670-18681.
309. Moreau, D., P. Kumar, et al. (2011). "Genome-wide RNAi screens identify genes required for Ricin and PE intoxications." *Dev Cell* 21(2): 231-244.
310. Swamy MJ, G.D., Mahanta SK, Surolia A (1991). "Further characterization of the saccharide specificity of peanut (*Arachis hypogaea*) agglutinin." *Carbohydr Res* 213: 59-67.
311. Sen, B.H., B.G. Akdeniz, et al. (2000). "The effect of ethylenediamine-tetraacetic acid on *Candida albicans*." *Oral Surg Oral Med Oral Pathol Oral Radiol Endod* 90(5): 651-655.
312. Debray, H., D. Decout, et al. (1981). "Specificity of twelve lectins towards oligosaccharides and glycopeptides related to N-glycosylproteins." *Eur J Biochem* 117(1): 41-55.
313. Schwarz, R.E., D.C. Wojciechowicz, et al. (1996). "Phytohemagglutinin-L (PHA-L) lectin surface binding of N-linked beta 1-6 carbohydrate and its relationship to activated mutant ras in human pancreatic cancer cell lines." *Cancer Lett* 107(2): 285-291.
314. Cummings, R.D. and S. Kornfeld (1982). "Characterization of the structural determinants required for the high affinity interaction of asparagine-linked oligosaccharides with immobilized *Phaseolus vulgaris* leucoagglutinating and erythroagglutinating lectins." *J Biol Chem* 257(19): 11230-11234.
315. Kaladas, P.M., E.A. Kabat, et al. (1982). "Immunochemical studies on the combining site of the D-galactose/N-acetyl-D-galactosamine specific lectin from *Erythrina cristagalli* seeds." *Arch Biochem Biophys* 217(2): 624-637.
316. Sun, Q., X. Kang, et al. (2009). "DSA affinity glycoproteome of human liver tissue." *Arch Biochem Biophys* 484(1): 24-29.

317. Crowley, J.F., I.J. Goldstein, et al. (1984). "Carbohydrate binding studies on the lectin from *Datura stramonium* seeds." *Arch Biochem Biophys* 231(2): 524-533.
318. Geisler, C. and D.L. Jarvis (2011). "Effective glycoanalysis with *Maackia amurensis* lectins requires a clear understanding of their binding specificities." *Glycobiology* 21(8): 988-993.
319. Colanzi, A. and D. Corda (2007). "Mitosis controls the Golgi and the Golgi controls mitosis." *Curr Opin Cell Biol* 19(4): 386-393.
320. Hicks, S.W. and C.E. Machamer (2005). "Golgi structure in stress sensing and apoptosis." *Biochim Biophys Acta* 1744(3): 406-414.
321. Hicks SW, M.C. (2005). "Golgi structure in stress sensing and apoptosis." *Biochim Biophys Acta* 1744(3): 406-414.
322. Efimov, A., A. Kharitonov, et al. (2007). "Asymmetric CLASP-dependent nucleation of noncentrosomal microtubules at the trans-Golgi network." *Dev Cell* 12(6): 917-930.
323. Missiaen, L., L. Dode, et al. (2007). "Calcium in the Golgi apparatus." *Cell Calcium* 41(5): 405-416.
324. Dolman, N.J. and A.V. Tepikin (2006). "Calcium gradients and the Golgi." *Cell Calcium* 40(5-6): 505-512.
325. Hidalgo Carcedo, C., M. Bonazzi, et al. (2004). "Mitotic Golgi partitioning is driven by the membrane-fissioning protein CtBP3/BARS." *Science* 305(5680): 93-96.
326. Fidalgo, M., M. Fraile, et al. (2010). "CCM3/PDCD10 stabilizes GCKIII proteins to promote Golgi assembly and cell orientation." *J Cell Sci* 123(Pt 8): 1274-1284.
327. Mor, A., G. Campi, et al. (2007). "The lymphocyte function-associated antigen-1 receptor costimulates plasma membrane Ras via phospholipase D2." *Nat Cell Biol* 9(6): 713-719.
328. Perez de Castro, I., T.G. Bivona, et al. (2004). "Ras activation in Jurkat T cells following low-grade stimulation of the T-cell receptor is specific to N-Ras and occurs only on the Golgi apparatus." *Mol Cell Biol* 24(8): 3485-3496.
329. Yi, P., D.T. Nguyen, et al. (2010). "MAPK scaffolding by BIT1 in the Golgi complex modulates stress resistance." *Journal of Cell Science* 123(Pt 7): 1060-1072.
330. Shorter, J. and G. Warren (2002). "Golgi architecture and inheritance." *Annu Rev Cell Dev Biol* 18: 379-420.
331. Yang, W. and B. Storrie (1998). "Scattered Golgi elements during microtubule disruption are initially enriched in trans-Golgi proteins." *Mol Biol Cell* 9(1): 191-207.
332. Gleeson, P.A., J.G. Lock, et al. (2004). "Domains of the TGN: coats, tethers and G proteins." *Traffic* 5(5): 315-326.
333. Gleeson PA, L.J., Luke MR, Stow JL. (2004). "Domains of the TGN: coats, tethers and G proteins." *Traffic* 5(5): 315-326.
334. Wilson, C. and A. Ragnini-Wilson (2010). "Conserved molecular mechanisms underlying homeostasis of the Golgi complex." *Int J Cell Biol* 2010: 758230.
335. Munro, S. (2005). "The Golgi apparatus: defining the identity of Golgi membranes." *Curr Opin Cell Biol* 17(4): 395-401.
336. Malsam, J. and T.H. Sollner (2011). "Organization of SNAREs within the Golgi stack." *Cold Spring Harb Perspect Biol* 3(10): a005249.
337. Rabouille, C., N. Hui, et al. (1995). "Mapping the distribution of Golgi enzymes involved in the construction of complex oligosaccharides." *J Cell Sci* 108 ( Pt 4): 1617-1627.
338. Shima, D.T., K. Haldar, et al. (1997). "Partitioning of the Golgi apparatus during mitosis in living HeLa cells." *J Cell Biol* 137(6): 1211-1228.
339. Martinez-Alonso, E., M. Tomas, et al. (2013). "Golgi tubules: their structure, formation and role in intra-Golgi transport." *Histochem Cell Biol* 140(3): 327-339.

340. Elbashir, S.M., J. Harborth, et al. (2001). "Duplexes of 21-nucleotide RNAs mediate RNA interference in cultured mammalian cells." *Nature* 411(6836): 494-498.
341. Roth, J., Y. Wang, et al. (1994). "Subcellular localization of the UDP-N-acetyl-D-galactosamine: polypeptide N-acetylgalactosaminyltransferase-mediated O-glycosylation reaction in the submaxillary gland." *Proceedings of the National Academy of Sciences of the United States of America* 91(19): 8935-8939.
342. Pavelka, M. and A. Ellinger (1985). "Localization of binding sites for concanavalin A, Ricinus communis I and Helix pomatia lectin in the Golgi apparatus of rat small intestinal absorptive cells." *J Histochem Cytochem* 33(9): 905-914.
343. Storrie, B., J. White, et al. (1998). "Recycling of golgi-resident glycosyltransferases through the ER reveals a novel pathway and provides an explanation for nocodazole-induced Golgi scattering." *The Journal of Cell Biology* 143(6): 1505-1521.
344. Ghosh, R.N., W.G. Mallet, et al. (1998). "An endocytosed TGN38 chimeric protein is delivered to the TGN after trafficking through the endocytic recycling compartment in CHO cells." *The Journal of Cell Biology* 142(4): 923-936.
345. Hong, W. (2005). "SNAREs and traffic." *Biochimica et biophysica acta* 1744(2): 120-144.
346. Hutagalung AH, N.P. (2011). "Role of Rab GTPases in membrane traffic and cell physiology." *Physiol Rev* 91(1): 119-149.
347. Dinter, A., Berger, E. G. (1998). "Golgi-disturbing agents." *Histochem Cell Biol* 109(5-6): 571-590.
348. Thyberg, J., Moskalewski, S. (1999). "Role of microtubules in the organization of the Golgi complex." *Exp Cell Res* 246(2): 263-279.
349. Puthenveedu, M.A., C. Bachert, et al. (2006). "GM130 and GRASP65-dependent lateral cisternal fusion allows uniform Golgi-enzyme distribution." *NATURE CELL BIOLOGY* 8(3): 238-248.
350. Duran JM, K.M., Bossard C, Rose DW, Polishchuk R, Wu CC, Yates J, Zimmerman T, Malhotra V (2008). "The role of GRASP55 in Golgi fragmentation and entry of cells into mitosis." *Mol Biol Cell* 19(6): 2579-2587.
351. Valderrama, F., J.M. Durán, et al. (2001). "Actin microfilaments facilitate the retrograde transport from the Golgi complex to the endoplasmic reticulum in mammalian cells." *Traffic* 2(10): 717-726.
352. Young, J., Stauber, T., del Nery, E., Vernos, I., Pepperkok, R., Nilsson, T. (2005). "Regulation of microtubule-dependent recycling at the trans-Golgi network by Rab6A and Rab6A'." *Mol Biol Cell* 16(1): 162-177.
353. Bard, F., L. Mazelin, et al. (2003). "Src regulates Golgi structure and KDEL receptor-dependent retrograde transport to the endoplasmic reticulum." *J Biol Chem* 278(47): 46601-46606.
354. Racine, V., M. Sachse, et al. (2007). "Visualization and quantification of vesicle trafficking on a three-dimensional cytoskeleton network in living cells." *J Microsc* 225(Pt 3): 214-228.
355. Boser, B.E., I.M. Guyon, et al. (1992). "A training algorithm for optimal margin classifiers." 5th Annual ACM Workshop on COLT.
356. Moreau, D., P. Kumar, et al. (2011). "Genome-Wide RNAi Screens Identify Genes Required for Ricin and PE Intoxications." *Developmental cell*: 1-14.
357. Manning, G., D.B. Whyte, et al. (2002). "The protein kinase complement of the human genome." *Science (New York, NY)* 298(5600): 1912-1934.
358. Vicinanza M, D.A.G., Di Campli A, De Matteis MA. (2008). "Function and dysfunction of the PI system in membrane trafficking." *The EMBO journal* 27(19): 2457-2470.

359. Weixel KM, B.-P.A., Watkins SC, Aridor M, Weisz OA. (2005). "Distinct Golgi populations of phosphatidylinositol 4-phosphate regulated by phosphatidylinositol 4-kinases." *The Journal of biological chemistry* 280(11): 10501-10508.
360. Santiago-Tirado FH, B.A. (2011). "Membrane-trafficking sorting hubs: cooperation between PI4P and small GTPases at the trans-Golgi network." *Trends in Cell Biology* 21(9): 515-525.
361. Farhan, H., M. Weiss, et al. (2008). "Adaptation of endoplasmic reticulum exit sites to acute and chronic increases in cargo load." *The EMBO journal* 27(15): 2043-2054.
362. Godi, A., P. Pertile, et al. (1999). "ARF mediates recruitment of PtdIns-4-OH kinase-beta and stimulates synthesis of PtdIns(4,5)P2 on the Golgi complex." *NATURE CELL BIOLOGY* 1(5): 280-287.
363. Siddhanta, A., J.M. Backer, et al. (2000). "Inhibition of phosphatidic acid synthesis alters the structure of the Golgi apparatus and inhibits secretion in endocrine cells." *The Journal of biological chemistry* 275(16): 12023-12031.
364. Jones, D.H. (2000). "Type I Phosphatidylinositol 4-Phosphate 5-Kinase Directly Interacts with ADP-ribosylation Factor 1 and Is Responsible for Phosphatidylinositol 4,5-Bisphosphate Synthesis in the Golgi Compartment." *Journal of Biological Chemistry* 275(18): 13962-13966.
365. Sweeney, D.A., A. Siddhanta, et al. (2002). "Fragmentation and re-assembly of the Golgi apparatus in vitro. A requirement for phosphatidic acid and phosphatidylinositol 4,5-bisphosphate synthesis." *J Biol Chem* 277(4): 3030-3039.
366. Wu, Y., D. Dowbenko, et al. (2001). "PTEN 2, a Golgi-associated testis-specific homologue of the PTEN tumor suppressor lipid phosphatase." *The Journal of biological chemistry* 276(24): 21745-21753.
367. Roth, M.G. (2004). "Phosphoinositides in constitutive membrane traffic." *Physiological reviews* 84(3): 699-730.
368. De Matteis, M.A., A. Di Campli, et al. (2005). "The role of the phosphoinositides at the Golgi complex." *Biochimica et biophysica acta* 1744(3): 396-405.
369. Lindmo, K. and H. Stenmark (2006). "Regulation of membrane traffic by phosphoinositide 3-kinases." *Journal of Cell Science* 119(Pt 4): 605-614.
370. Low, P.C., R. Misaki, et al. (2010). "Phosphoinositide 3-kinase  $\delta$  regulates membrane fission of Golgi carriers for selective cytokine secretion." *The Journal of Cell Biology* 190(6): 1053-1065.
371. Jin, T.-G. (2001). "Role of the CDC25 Homology Domain of Phospholipase Cepsilon in Amplification of Rap1-dependent Signaling." *Journal of Biological Chemistry* 276(32): 30301-30307.
372. Blayney, L., P. Gapper, et al. (1998). "Identification of phospholipase C beta isoforms and their location in cultured vascular smooth muscle cells of pig, human and rat." *Cardiovascular research* 40(3): 564-572.
373. Orlando, K.A. and R.N. Pittman (2006). "Rho kinase regulates phagocytosis, surface expression of GlcNAc, and Golgi fragmentation of apoptotic PC12 cells." *Experimental cell research* 312(17): 3298-3311.
374. Foletta, V.C., N. Moussi, et al. (2004). "LIM kinase 1, a key regulator of actin dynamics, is widely expressed in embryonic and adult tissues." *Experimental cell research* 294(2): 392-405.
375. Miserey-Lenkei, S., G. Chalancon, et al. (2010). "Rab and actomyosin-dependent fission of transport vesicles at the Golgi complex." *NATURE CELL BIOLOGY* 12(7): 645-654.
376. Bard, F., L. Casano, et al. (2006). "Functional genomics reveals genes involved in protein secretion and Golgi organization." *Nature* 439(7076): 604-607.

377. von Blume, J., J.M. Duran, et al. (2009). "Actin remodeling by ADF/cofilin is required for cargo sorting at the trans-Golgi network." *The Journal of Cell Biology* 187(7): 1055-1069.
378. Salvarezza, S.B., S. Deborde, et al. (2009). "LIM kinase 1 and cofilin regulate actin filament population required for dynamin-dependent apical carrier fission from the trans-Golgi network." *Molecular Biology of the Cell* 20(1): 438-451.
379. Egea, G., F. Lázaro-Diéguez, et al. (2006). "Actin dynamics at the Golgi complex in mammalian cells." *Current Opinion in Cell Biology* 18(2): 168-178.
380. Sanders, L.C., F. Matsumura, et al. (1999). "Inhibition of myosin light chain kinase by p21-activated kinase." *Science (New York, NY)* 283(5410): 2083-2085.
381. Even-Faitelson, L., M. Rosenberg, et al. (2005). "PAK1 regulates myosin II-B phosphorylation, filament assembly, localization and cell chemotaxis." *Cellular Signalling* 17(9): 1137-1148.
382. Deacon, S.W., A. Beeser, et al. (2008). "An isoform-selective, small-molecule inhibitor targets the autoregulatory mechanism of p21-activated kinase." *Chemistry & Biology* 15(4): 322-331.
383. Cayrol, C., C. Cougoule, et al. (2002). "The beta2-adaptin clathrin adaptor interacts with the mitotic checkpoint kinase BubR1." *Biochemical and biophysical research communications* 298(5): 720-730.
384. Simmen, T., S. Höning, et al. (2002). "AP-4 binds basolateral signals and participates in basolateral sorting in epithelial MDCK cells." *NATURE CELL BIOLOGY* 4(2): 154-159.
385. Fingerhut, A., K. von Figura, et al. (2001). "Binding of AP2 to sorting signals is modulated by AP2 phosphorylation." *The Journal of biological chemistry* 276(8): 5476-5482.
386. Vollert, C.S. (2004). "The Phox Homology (PX) Domain Protein Interaction Network in Yeast." *Molecular & cellular proteomics : MCP* 3(11): 1053-1064.
387. Kanehisa, M., S. Goto, et al. (2010). "KEGG for representation and analysis of molecular networks involving diseases and drugs." *Nucleic acids research* 38(Database issue): D355-360.
388. Qi, W., Z. Tang, et al. (2006). "Phosphorylation- and polo-box-dependent binding of Plk1 to Bub1 is required for the kinetochore localization of Plk1." *Molecular Biology of the Cell* 17(8): 3705-3716.
389. Wang, Y., J. Seemann, et al. (2003). "A direct role for GRASP65 as a mitotically regulated Golgi stacking factor." *The EMBO journal* 22(13): 3279-3290.
390. Bandyopadhyay, S., C.-Y. Chiang, et al. (2010). "A human MAP kinase interactome." *Nature Methods* 7(10): 801-805.
391. Plotnikov, A., E. Zehorai, et al. (2011). "The MAPK cascades: Signaling components, nuclear roles and mechanisms of nuclear translocation." *BBA - Molecular Cell Research* 1813(9): 1619-1633.
392. Farhan, H., M.W. Wendeler, et al. (2010). "MAPK signaling to the early secretory pathway revealed by kinase/phosphatase functional screening." *The Journal of Cell Biology* 189(6): 997-1011.
393. Zacharogianni, M., V. Kondylis, et al. (2011). "ERK7 is a negative regulator of protein secretion in response to amino-acid starvation by modulating Sec16 membrane association." *The EMBO journal* 30(18): 3684-3700.
394. Bisel, B., Y. Wang, et al. (2008). "ERK regulates Golgi and centrosome orientation towards the leading edge through GRASP65." *The Journal of Cell Biology* 182(5): 837-843.

395. Harada, T., O. Matsuzaki, et al. (2003). "AKRL1 and AKRL2 activate the JNK pathway." [Some factors, with an impact on the outcome of the Hungarian Liver Transplant Program, with special consideration of the hepatitis C virus]. 8(5): 493-500.
396. Akhmanova, A. and J.A.H. Iii (2010). "Linking molecular motors to membrane cargo." *Current Opinion in Cell Biology* 22(4): 479-487.
397. Shaywitz DA, E.P., Gimeno RE, Kaiser CA. (1997). "COPII subunit interactions in the assembly of the vesicle coat." *J Biol Chem* 272(41): 25413-25416.
398. Galli T, C.T., Mundigl O, Binz T, Niemann H, De Camilli P. (1994). "Tetanus toxin-mediated cleavage of cellubrevin impairs exocytosis of transferrin receptor-containing vesicles in CHO cells." *J Cell Biol* 125(5): 1015-1024.
399. Kean MJ, W.K., Skalski M, Myers D, Burtnik A, Foster D, Coppolino MG. (2009). "VAMP3, syntaxin-13 and SNAP23 are involved in secretion of matrix metalloproteinases, degradation of the extracellular matrix and cell invasion." *J Cell Sci* 122(Pt 22): 4089-4098.
400. Holt, M., F. Varoqueaux, et al. (2006). "Identification of SNAP-47, a novel Qbc-SNARE with ubiquitous expression." *The Journal of biological chemistry* 281(25): 17076-17083.
401. Mallard, F., B.L. Tang, et al. (2002). "Early/recycling endosomes-to-TGN transport involves two SNARE complexes and a Rab6 isoform." *The Journal of Cell Biology* 156(4): 653-664.
402. Amessou, M., A. Fradagrada, et al. (2007). "Syntaxin 16 and syntaxin 5 are required for efficient retrograde transport of several exogenous and endogenous cargo proteins." *Journal of Cell Science* 120(Pt 8): 1457-1468.
403. Gromada J, B.C., Smidt K, Efanov AM, Janson J, Mandic SA, Webb DL, Zhang W, Meister B, Jeromin A, Berggren PO. (2005). "Neuronal calcium sensor-1 potentiates glucose-dependent exocytosis in pancreatic beta cells through activation of phosphatidylinositol 4-kinase beta." *Proc Natl Acad Sci U S A* 102(29): 10303-10308.
404. Routt SM, R.M., Tyeryar K, Rizzieri KE, Mousley C, Roumanie O, Brennwald PJ, Bankaitis VA. (2005). "Nonclassical PITPs activate PLD via the Stt4p PtdIns-4-kinase and modulate function of late stages of exocytosis in vegetative yeast." *Traffic* 6(12): 1157-1172.
405. Wenk MR, D.C.P. (2004). "Protein-lipid interactions and phosphoinositide metabolism in membrane traffic: insights from vesicle recycling in nerve terminals." *Proc Natl Acad Sci U S A* 101(22): 8262-8269.
406. Zilberstein, A., M.D. Snider, et al. (1980). "Mutants of vesicular stomatitis virus blocked at different stages in maturation of the viral glycoprotein." *Cell* 21(2): 417-427.
407. Stanley, P. (2011). "Golgi glycosylation." *Cold Spring Harbor perspectives in biology* 3(4).
408. Sciaky, N., J. Presley, et al. (1997). "Golgi tubule traffic and the effects of brefeldin A visualized in living cells." *J Cell Biol* 139(5): 1137-1155.
409. Sengupta, D. and A.D. Linstedt (2011). "Control of organelle size: the Golgi complex." *Annu Rev Cell Dev Biol* 27: 57-77.
410. Altan-Bonnet, N., R. Sougrat, et al. (2004). "Molecular basis for Golgi maintenance and biogenesis." *Curr Opin Cell Biol* 16(4): 364-372.
411. Pfeffer, S.R. (1996). "Transport vesicle docking: SNAREs and associates." *Annu Rev Cell Dev Biol* 12: 441-461.
412. Jahn, R. and R.H. Scheller (2006). "SNAREs--engines for membrane fusion." *Nat Rev Mol Cell Biol* 7(9): 631-643.
413. Zacharogianni, M., V. Kondylis, et al. (2011). "ERK7 is a negative regulator of protein secretion in response to amino-acid starvation by modulating Sec16 membrane association." *EMBO J* 30(18): 3684-3700.

414. Simpson, J.C., B. Joggerst, et al. (2012). "Genome-wide RNAi screening identifies human proteins with a regulatory function in the early secretory pathway." *Nat Cell Biol* 14(7): 764-774.
415. Burman, J.L., J.N.R. Hamlin, et al. (2010). "Scyl1 regulates Golgi morphology." *PloS one* 5(3): e9537.
416. Burman, J.L., L. Bourbonniere, et al. (2008). "Scyl1, mutated in a recessive form of spinocerebellar neurodegeneration, regulates COPI-mediated retrograde traffic." *J Biol Chem* 283(33): 22774-22786.
417. Duwel, M. and E.J. Ungewickell (2006). "Clathrin-dependent association of CVAK104 with endosomes and the trans-Golgi network." *Mol Biol Cell* 17(10): 4513-4525.
418. Nakamura, N., J.H. Wei, et al. (2012). "Modular organization of the mammalian Golgi apparatus." *Curr Opin Cell Biol* 24(4): 467-474.
419. Cheong, F.Y., V. Sharma, et al. (2010). "Spatial regulation of Golgi phosphatidylinositol-4-phosphate is required for enzyme localization and glycosylation fidelity." *Traffic* 11(9): 1180-1190.
420. Miserey-Lenkei, S., G. Chalancon, et al. (2010). "Rab and actomyosin-dependent fission of transport vesicles at the Golgi complex." *Nat Cell Biol* 12(7): 645-654.
421. Ron, D. and P. Walter (2007). "Signal integration in the endoplasmic reticulum unfolded protein response." *Nat Rev Mol Cell Biol* 8(7): 519-529.
422. Pulvirenti, T., M. Giannotta, et al. (2008). "A traffic-activated Golgi-based signalling circuit coordinates the secretory pathway." *NATURE CELL BIOLOGY* 10(8): 912-922.
423. Sumara, G., I. Formentini, et al. (2009). "Regulation of PKD by the MAPK p38delta in insulin secretion and glucose homeostasis." *Cell* 136(2): 235-248.
424. Stanley, P. (2011). "Golgi glycosylation." *Cold Spring Harb Perspect Biol* 3(4).
425. Yamaguchi, N. and M.N. Fukuda (1995). "Golgi retention mechanism of beta-1,4-galactosyltransferase. Membrane-spanning domain-dependent homodimerization and association with alpha- and beta-tubulins." *The Journal of biological chemistry* 270(20): 12170-12176.
426. Wassler, M.J., C.I. Foote, et al. (2001). "Functional interaction between the SSeCKS scaffolding protein and the cytoplasmic domain of beta1,4-galactosyltransferase." *J Cell Sci* 114(Pt 12): 2291-2300.
427. Quintero, C.A., J. Valdez-Taubas, et al. (2008). "Calsenilin and CALP interact with the cytoplasmic tail of UDP-Gal:GA2/GM2/GD2 beta-1,3-galactosyltransferase." *Biochem J* 412(1): 19-26.
428. Schmitz, K.R., J. Liu, et al. (2008). "Golgi localization of glycosyltransferases requires a Vps74p oligomer." *Dev Cell* 14(4): 523-534.
429. Lauc, G., I. Rudan, et al. (2010). "Complex genetic regulation of protein glycosylation." *Mol Biosyst* 6(2): 329-335.
430. Lanctot, P.M., F.H. Gage, et al. (2007). "The glycans of stem cells." *Curr Opin Chem Biol* 11(4): 373-380.
431. Orlando, K.A. and R.N. Pittman (2006). "Rho kinase regulates phagocytosis, surface expression of GlcNAc, and Golgi fragmentation of apoptotic PC12 cells." *Exp Cell Res* 312(17): 3298-3311.
432. Kellokumpu, S., R. Sormunen, et al. (2002). "Abnormal glycosylation and altered Golgi structure in colorectal cancer: dependence on intra-Golgi pH." *FEBS Lett* 516(1-3): 217-224.
433. Wollscheid, B., D. Bausch-Fluck, et al. (2009). "Mass-spectrometric identification and relative quantification of N-linked cell surface glycoproteins." *Nat Biotechnol* 27(4): 378-386.



434. Narimatsu, H., H. Sawaki, et al. (2010). "A strategy for discovery of cancer glyco-biomarkers in serum using newly developed technologies for glycoproteomics." *FEBS J* 277(1): 95-105.
435. Boscher, C., J.W. Dennis, et al. (2011). "Glycosylation, galectins and cellular signaling." *Curr Opin Cell Biol* 23(4): 383-392.
436. Steentoft, C., S.Y. Vakhrushev, et al. (2013). "Precision mapping of the human O-GalNAc glycoproteome through SimpleCell technology." *EMBO J* 32(10): 1478-1488.
437. Kato K, J.C., Tarp MA, Benet-Pagès A, Lorenz-Depiereux B, Bennett EP, Mandel U, Strom TM, Clausen H. (2006). "Polypeptide GalNAc-transferase T3 and familial tumoral calcinosis. Secretion of fibroblast growth factor 23 requires O-glycosylation." *The Journal of biological chemistry* 281(27): 18370-18377.
438. Springer, G.F. and H. Tegtmeier (1983). "Tn, a universal carcinoma (CA) marker, frequently strongly expressed in anaplastic, aggressive CA." *Die Naturwissenschaften* 70(12): 621-622.
439. Newman, R.A. and G.G. Uhlenbruck (1977). "Investigation into the occurrence and structure of lectin receptors on human and bovine erythrocytes milk fat globule and lymphocyte plasma-membrane glycoproteins." *European journal of biochemistry / FEBS* 76(1): 149-155.
440. Egea, G., C. Franci, et al. (1993). "cis-Golgi resident proteins and O-glycans are abnormally compartmentalized in the RER of colon cancer cells." *J Cell Sci* 105 ( Pt 3): 819-830.
441. Beck, R., M. Rawet, et al. (2009). "The COPI system: molecular mechanisms and function." *FEBS Letters* 583(17): 2701-2709.
442. Szul, T. and E. Sztul (2011). "COPII and COPI traffic at the ER-Golgi interface." *Physiology (Bethesda)* 26(5): 348-364.
443. Chia, J., G. Goh, et al. (2012). "RNAi screening reveals a large signaling network controlling the Golgi apparatus in human cells." *Mol Syst Biol* 8: 629.
444. Abe, M.K., M.P. Saelzler, et al. (2002). "ERK8, a new member of the mitogen-activated protein kinase family." *J Biol Chem* 277(19): 16733-16743.
445. Swamy, M.J., D. Gupta, et al. (1991). "Further characterization of the saccharide specificity of peanut (*Arachis hypogaea*) agglutinin." *Carbohydr Res* 213: 59-67.
446. Fujiwara T, O.K., Yokota S, Takatsuki A, Ikehara, Y. (1988). "Brefeldin A causes disassembly of the Golgi complex and accumulation of secretory proteins in the endoplasmic reticulum." *J Biol Chem* 263(34): 18545-18552.
447. Jensen, L.J., M. Kuhn, et al. (2009). "STRING 8--a global view on proteins and their functional interactions in 630 organisms." *Nucleic Acids Res* 37(Database issue): D412-416.
448. Safran, M., I. Dalah, et al. (2010). "GeneCards Version 3: the human gene integrator." *Database (Oxford)* 2010: baq020.
449. Uhlen, M., P. Oksvold, et al. (2010). "Towards a knowledge-based Human Protein Atlas." *Nat Biotechnol* 28(12): 1248-1250.
450. Jensen LJ, K.M., Stark M, Chaffron S, Creevey C, Muller J, Doerks T, Julien P, Roth A, Simonovic M, Bork P, von Mering C. (2009). "STRING 8--a global view on proteins and their functional interactions in 630 organisms." *Nucleic Acids Res* 37(Database issue): D412-416.
451. Safran M, D.I., Alexander J, Rosen N, Iny Stein T, Shmoish M, Nativ N, Bahir I, Doniger T, Krug H, Sirota-Madi A, Olender T, Golan Y, Stelzer G, Harel A, Lancet D. (2010). "GeneCards Version 3: the human gene integrator." *Database (Oxford)* 2010: baq020.

452. Uhlen M, O.P., Fagerberg L, Lundberg E, Jonasson K, Forsberg M, Zwahlen M, Kampf C, Wester K, Hober S, Wernerus H, Björling L, Ponten F (2010). "Towards a knowledge-based Human Protein Atlas." *Nat Biotechnol* 28(12): 1248-1250.
453. Nakagawa, T. (1996). "Cloning, expression and localization of 230 kDa phosphatidylinositol 4-kinase." *J. Biol. Chem* 271: 12088–12094.
454. Ren, M., J. Zeng, et al. (1996). "In its active form, the GTP-binding protein rab8 interacts with a stress-activated protein kinase." *Proc Natl Acad Sci U S A* 93(10): 5151-5155.
455. Liu, F., J.J. Stanton, et al. (1997). "The human Myt1 kinase preferentially phosphorylates Cdc2 on threonine 14 and localizes to the endoplasmic reticulum and Golgi complex." *Mol Cell Biol* 17(2): 571-583.
456. Wood, C.S., K.R. Schmitz, et al. (2009). "PtdIns4P recognition by Vps74/GOLPH3 links PtdIns 4-kinase signaling to retrograde Golgi trafficking." *J Cell Biol* 187(7): 967-975.
457. Nakajima, H., S. Yonemura, et al. (2008). "Myt1 protein kinase is essential for Golgi and ER assembly during mitotic exit." *J Cell Biol* 181(1): 89-103.
458. Nakajima H, Y.S., Murata M, Nakamura N, Piwnica-Worms H, Nishida E. (2008). "Myt1 protein kinase is essential for Golgi and ER assembly during mitotic exit." *J Cell Biol* 181(1): 89-103.
459. Dowd, S., A.A. Sneddon, et al. (1998). "Isolation of the human genes encoding the pyst1 and Pyst2 phosphatases: characterisation of Pyst2 as a cytosolic dual-specificity MAP kinase phosphatase and its catalytic activation by both MAP and SAP kinases." *J Cell Sci* 111 ( Pt 22): 3389-3399.
460. Colland, F., X. Jacq, et al. (2004). "Functional proteomics mapping of a human signaling pathway." *Genome Res* 14(7): 1324-1332.
461. Dou, Z., X. Ding, et al. (2004). "TTK kinase is essential for the centrosomal localization of TACC2." *FEBS Lett* 572(1-3): 51-56.
462. Sowa, M.E., E.J. Bennett, et al. (2009). "Defining the human deubiquitinating enzyme interaction landscape." *Cell* 138(2): 389-403.
463. Cui, Y., X. Cheng, et al. (2010). "Degradation of the human mitotic checkpoint kinase Mps1 is cell cycle-regulated by APC-cCdc20 and APC-cCdh1 ubiquitin ligases." *J Biol Chem* 285(43): 32988-32998.
464. Wells, N.J., N. Watanabe, et al. (1999). "The C-terminal domain of the Cdc2 inhibitory kinase Myt1 interacts with Cdc2 complexes and is required for inhibition of G(2)/M progression." *J Cell Sci* 112 ( Pt 19): 3361-3371.
465. Yoshimura, Y. and H. Miki (2011). "Dynamic regulation of GEF-H1 localization at microtubules by Par1b/MARK2." *Biochem Biophys Res Commun* 408(2): 322-328.
466. Palmer, K.J., P. Watson, et al. (2005). "The role of microtubules in transport between the endoplasmic reticulum and Golgi apparatus in mammalian cells." *Biochemical Society symposium*(72): 1-13.
467. Spang, A. (2013). "Retrograde traffic from the Golgi to the endoplasmic reticulum." *Cold Spring Harbor perspectives in biology* 5(6).
468. Galliher, A.J. and W.P. Schiemann (2007). "Src phosphorylates Tyr284 in TGF-beta type II receptor and regulates TGF-beta stimulation of p38 MAPK during breast cancer cell proliferation and invasion." *Cancer Res* 67(8): 3752-3758.
469. Chadee, D.N., T. Yuasa, et al. (2002). "Direct activation of mitogen-activated protein kinase kinase kinase MEKK1 by the Ste20p homologue GCK and the adapter protein TRAF2." *Mol Cell Biol* 22(3): 737-749.
470. Eddy SF, G.S., Demicco EG, Romieu-Mourez R, Landesman-Bollag E, Seldin DC, and Sonenshein GE (2005). "Inducible IkappaB kinase/IkappaB kinase epsilon

expression is induced by CK2 and promotes aberrant nuclear factor-kappaB activation in breast cancer cells." *Cancer Res* 65(24): 11375-11383.

471. Shimada, T., T. Kawai, et al. (1999). "IKK-i, a novel lipopolysaccharide-inducible kinase that is related to IkappaB kinases." *Int Immunol* 11(8): 1357-1362.

472. Stefansson, B. and D.L. Brautigan (2006). "Protein phosphatase 6 subunit with conserved Sit4-associated protein domain targets IkappaBepsilon." *J Biol Chem* 281(32): 22624-22634.

473. Klevernic, I.V., M.J. Stafford, et al. (2006). "Characterization of the reversible phosphorylation and activation of ERK8." *Biochem J* 394(Pt 1): 365-373.

474. Chafin, D.R., H. Guo, et al. (1995). "Action of alpha-amanitin during pyrophosphorolysis and elongation by RNA polymerase II." *J Biol Chem* 270(32): 19114-19119.

475. Laughlin, S.T. and C.R. Bertozzi (2007). "Metabolic labeling of glycans with azido sugars and subsequent glycan-profiling and visualization via Staudinger ligation." *Nat Protoc* 2(11): 2930-2944.

476. Sessions, O.M., N.J. Barrows, et al. (2009). "Discovery of insect and human dengue virus host factors." *Nature* 458(7241): 1047-1050.

477. Rhee, S.W., T. Starr, et al. (2005). "The steady-state distribution of glycosyltransferases between the Golgi apparatus and the endoplasmic reticulum is approximately 90:10." *Traffic* 6(11): 978-990.

478. Qiao, Y., H. Molina, et al. (2006). "Chemical rescue of a mutant enzyme in living cells." *Science* 311(5765): 1293-1297.

479. Beck, R., M. Rawet, et al. (2009). "The COPI system: molecular mechanisms and function." *FEBS Lett* 583(17): 2701-2709.

480. Saenz, J.B., W.J. Sun, et al. (2009). "Golgicide A reveals essential roles for GBF1 in Golgi assembly and function." *Nat Chem Biol* 5(3): 157-165.

481. D'Souza-Schorey, C. and P. Chavrier (2006). "ARF proteins: roles in membrane traffic and beyond." *Nat Rev Mol Cell Biol* 7(5): 347-358.

482. Popoff, V., J.D. Langer, et al. (2011). "Several ADP-ribosylation factor (Arf) isoforms support COPI vesicle formation." *J Biol Chem* 286(41): 35634-35642.

483. Antonny, B., J. Bigay, et al. (2005). "Membrane curvature and the control of GTP hydrolysis in Arf1 during COPI vesicle formation." *Biochem Soc Trans* 33(Pt 4): 619-622.

484. Morohashi, Y., Z. Balklava, et al. (2010). "Phosphorylation and membrane dissociation of the ARF exchange factor GBF1 in mitosis." *Biochem J* 427(3): 401-412.

485. Brandvold, K.R., M.E. Steffey, et al. (2012). "Development of a highly selective c-Src kinase inhibitor." *ACS chemical biology* 7(8): 1393-1398.

486. Henrich, L.M., J.A. Smith, et al. (2003). "Extracellular signal-regulated kinase 7, a regulator of hormone-dependent estrogen receptor destruction." *Mol Cell Biol* 23(17): 5979-5988.

487. Hakomori, S. (2001). "Tumor-associated carbohydrate antigens defining tumor malignancy: basis for development of anti-cancer vaccines." *Advances in experimental medicine and biology* 491: 369-402.

488. Feizi, T. (1985). "Carbohydrate antigens in human cancer." *Cancer surveys* 4(1): 245-269.

489. Xu, Y., A. Sette, et al. (2005). "Tumor-associated carbohydrate antigens: a possible avenue for cancer prevention." *Immunology and cell biology* 83(4): 440-448.

490. Dube, D.H. and C.R. Bertozzi (2005). "Glycans in cancer and inflammation--potential for therapeutics and diagnostics." *Nature reviews. Drug discovery* 4(6): 477-488.

491. Springer, G. (1997). "Immunoreactive T and Tn epitopes in cancer diagnosis, prognosis, and immunotherapy." *J Mol Med (Berl)* 75(8): 594-602.
492. Gill, D.J., J. Chia, et al. (2010). "Regulation of O-glycosylation through Golgi-to-ER relocation of initiation enzymes." *The Journal of cell biology* 189(5): 843-858.
493. Wortzel, I. and R. Seger (2011). "The ERK Cascade: Distinct Functions within Various Subcellular Organelles." *Genes Cancer* 2(3): 195-209.
494. Bind, E., Y. Kleyner, et al. (2004). "A novel mechanism for mitogen-activated protein kinase localization." *Molecular Biology of the Cell* 15(10): 4457-4466.
495. Patwardhan, P. and M.D. Resh (2010). "Myristoylation and membrane binding regulate c-Src stability and kinase activity." *Mol Cell Biol* 30(17): 4094-4107.
496. Lu, D., H.Q. Sun, et al. (2012). "Phosphatidylinositol 4-kinase IIalpha is palmitoylated by Golgi-localized palmitoyltransferases in cholesterol-dependent manner." *J Biol Chem* 287(26): 21856-21865.
497. Chuderland, D., A. Konson, et al. (2008). "Identification and characterization of a general nuclear translocation signal in signaling proteins." *Mol Cell* 31(6): 850-861.
498. Cha, H. and P. Shapiro (2001). "Tyrosine-phosphorylated extracellular signal-regulated kinase associates with the Golgi complex during G2/M phase of the cell cycle: evidence for regulation of Golgi structure." *J Cell Biol* 153(7): 1355-1367.
499. Aebersold, D.M., Y.D. Shaul, et al. (2004). "Extracellular signal-regulated kinase 1c (ERK1c), a novel 42-kilodalton ERK, demonstrates unique modes of regulation, localization, and function." *Mol Cell Biol* 24(22): 10000-10015.
500. Bendetz-Nezer, S. and R. Seger (2007). "Role of non-phosphorylated activation loop residues in determining ERK2 dephosphorylation, activity, and subcellular localization." *J Biol Chem* 282(34): 25114-25122.
501. Formstecher, E., J.W. Ramos, et al. (2001). "PEA-15 mediates cytoplasmic sequestration of ERK MAP kinase." *Dev Cell* 1(2): 239-250.
502. Burman, J.L., L. Bourbonniere, et al. (2008). "Scyl1, mutated in a recessive form of spinocerebellar neurodegeneration, regulates COPI-mediated retrograde traffic." *The Journal of biological chemistry* 283(33): 22774-22786.
503. Muppitala, M., V. Gupta, et al. (2012). "Tyrosine phosphorylation of a SNARE protein, syntaxin 17: implications for membrane trafficking in the early secretory pathway." *Biochim Biophys Acta* 1823(12): 2109-2119.
504. Dirac-Svejstrup, A.B., J. Shorter, et al. (2000). "Phosphorylation of the vesicle-tethering protein p115 by a casein kinase II-like enzyme is required for Golgi reassembly from isolated mitotic fragments." *The Journal of Cell Biology* 150(3): 475-488.
505. Groehler, A.L. and D.A. Lannigan (2010). "A chromatin-bound kinase, ERK8, protects genomic integrity by inhibiting HDM2-mediated degradation of the DNA clamp PCNA." *J Cell Biol* 190(4): 575-586.
506. Cerone, M.A., D.J. Burgess, et al. (2011). "High-throughput RNAi screening reveals novel regulators of telomerase." *Cancer Res* 71(9): 3328-3340.
507. Colecchia, D., A. Strambi, et al. (2012). "MAPK15/ERK8 stimulates autophagy by interacting with LC3 and GABARAP proteins." *Autophagy* 8(12): 1724-1740.
508. Saelzler, M.P., C.C. Spackman, et al. (2006). "ERK8 down-regulates transactivation of the glucocorticoid receptor through Hic-5." *J Biol Chem* 281(24): 16821-16832.
509. Rossi, M., D. Colecchia, et al. (2011). "Extracellular signal-regulated kinase 8 (ERK8) controls estrogen-related receptor alpha (ERRalpha) cellular localization and inhibits its transcriptional activity." *J Biol Chem* 286(10): 8507-8522.
510. Duran, J.M., M. Kinseth, et al. (2008). "The role of GRASP55 in Golgi fragmentation and entry of cells into mitosis." *Mol Biol Cell* 19(6): 2579-2587.

511. Preisinger, C., R. Korner, et al. (2005). "Plk1 docking to GRASP65 phosphorylated by Cdk1 suggests a mechanism for Golgi checkpoint signalling." *EMBO J* 24(4): 753-765.
512. Condon, K.H., J. Ho, et al. (2013). "The Angelman syndrome protein Ube3a/E6AP is required for Golgi acidification and surface protein sialylation." *J Neurosci* 33(9): 3799-3814.
513. Tjhi, W.C., K.K. Lee, et al. (2011). "Exploratory analysis of cell-based screening data for phenotype identification in drug-siRNA study." *Int J Comput Biol Drug Des* 4(2): 194-215.
514. Ibarrola, N., D.E. Kalume, et al. (2003). "A proteomic approach for quantitation of phosphorylation using stable isotope labeling in cell culture." *Anal Chem* 75(22): 6043-6049.
515. Kumar, N.V., S.T. Eblen, et al. (2004). "Identifying specific kinase substrates through engineered kinases and ATP analogs." *Methods* 32(4): 389-397.
516. Aoki D, L.N., Yamaguchi N, Dubois C, Fukuda MN. (1992). "Golgi retention of a trans-Golgi membrane protein, galactosyltransferase, requires cysteine and histidine residues within the membrane-anchoring domain." *Proc Natl Acad Sci U S A*.
517. Burke J, P.J., Humphris D, Gleeson PA. (1994). "Medial-Golgi retention of N-acetylglucosaminyltransferase I. Contribution from all domains of the enzyme." *J Biol Chem* 269(16): 12049-12059.
518. El-Battari (2006). "Autofluorescent proteins for monitoring the intracellular distribution of glycosyltransferases." *Methods Enzymol* 416: 102-120.
519. Nilsson T, R.C., Hui N, Watson R, Warren G. (1996). "The role of the membrane-spanning domain and stalk region of N-acetylglucosaminyltransferase I in retention, kin recognition and structural maintenance of the Golgi apparatus in HeLa cells." *J Cell Sci* 109 ( Pt 7): 1975-1989.
520. Uemura, S., S. Yoshida, et al. (2009). "The cytoplasmic tail of GM3 synthase defines its subcellular localization, stability, and in vivo activity." *Mol Biol Cell* 20(13): 3088-3100.
521. Pelkmans, L., E. Fava, et al. (2005). "Genome-wide analysis of human kinases in clathrin- and caveolae/raft-mediated endocytosis." *Nature* 436(7047): 78-86.
522. Collinet, C., M. Stoter, et al. (2010). "Systems survey of endocytosis by multiparametric image analysis." *Nature* 464(7286): 243-249.
523. Bard, F., L. Casano, et al. (2006). "Functional genomics reveals genes involved in protein secretion and Golgi organization." *Nature* 439(7076): 604-607.
524. Wendler, F., A.K. Gillingham, et al. (2010). "A genome-wide RNA interference screen identifies two novel components of the metazoan secretory pathway." *EMBO J* 29(2): 304-314.
525. Pasquale, E.B. (2005). "Eph receptor signalling casts a wide net on cell behaviour." *Nat Rev Mol Cell Biol* 6(6): 462-475.
526. Riedemann, J. and V.M. Macaulay (2006). "IGF1R signalling and its inhibition." *Endocr Relat Cancer* 13 Suppl 1: S33-43.
527. Taniguchi, C.M., B. Emanuelli, et al. (2006). "Critical nodes in signalling pathways: insights into insulin action." *Nat Rev Mol Cell Biol* 7(2): 85-96.
528. Beenken, A. and M. Mohammadi (2009). "The FGF family: biology, pathophysiology and therapy." *Nat Rev Drug Discov* 8(3): 235-253.
529. Janik, M.E., A. Litynska, et al. (2010). "Cell migration-the role of integrin glycosylation." *Biochim Biophys Acta* 1800(6): 545-555.
530. Guo, H.B., H. Johnson, et al. (2009). "Regulation of homotypic cell-cell adhesion by branched N-glycosylation of N-cadherin extracellular EC2 and EC3 domains." *J Biol Chem* 284(50): 34986-34997.

531. Cargnello, M. and P.P. Roux (2011). "Activation and function of the MAPKs and their substrates, the MAPK-activated protein kinases." *Microbiol Mol Biol Rev* 75(1): 50-83.
532. Bozulic, L. and B.A. Hemmings (2009). "PIKKing on PKB: regulation of PKB activity by phosphorylation." *Curr Opin Cell Biol* 21(2): 256-261.
533. Perkins, N.D. (2012). "The diverse and complex roles of NF-kappaB subunits in cancer." *Nat Rev Cancer* 12(2): 121-132.